PREPARATION ET MANIPULATION DES ATOMES ET DES MOLECULES DE CESIUM

Dimitris Sofikitis

Dimitris Sofikitis. PREPARATION ET MANIPULATION DES ATOMES ET DES MOLECULES DE CESIUM. Physique Atomique [physics.atom-ph]. Université Paris Sud - Paris XI, 2009. Français. NNT : . tel-00444057

HAL Id: tel-00444057
https://theses.hal.science/tel-00444057
Submitted on 5 Jan 2010

Orsay
N° d'ordre:

UNIVERSITE PARIS XI
U.F.R SCIENTIFIQUE D'ORSAY

THESE

présentée pour obtenir

le TITRE de DOCTEUR EN SCIENCES

par

Dimitrios SOFIKITIS

Sujet

PREPARATION ET MANIPULATION DES ATOMES ET DES MOLECULES DE CESIUM

Soutenue le 11-12-2009 à Orsay devant la commission d'examen:

Mme	M. LEDUC	Rapporteur
M	N.BIGELOW	Rapporteur
Mme	M. ALLEGRINI	
M	A. HUETZ	
M	D. CHARALAMBIDIS	
M	D. COMPARAT	
M	P. PILLET	Directeur de thèse

Orsay
N° d'ordre:

PARIS UNIVERSITY XI
U.F.R SCIENTIFIC ORSAY

THESIS

presented to obtain

the TITLE of DOCTEUR EN SCIENCES

by

Dimitrios SOFIKITIS

Subject

PREPARATION AND MANIPULATION OF CESIUM ATOMS AND MOLECULES

Defented the 11-12-2009 at Orsay before the jury:

Mme	M. LEDUC	Rapporteur
Mr	N.BIGELOW	Rapporteur
Mme	M. ALLEGRINI	
Mr	A. HUETZ	
Mr	D. CHARALAMBIDIS	
Mr	D. COMPARAT	
Mr	P. PILLET	Directeur de these

οὔτε λέγει οὔτε κρύπτει ἀλλὰ σημαίνει

ACKNOWLEDGMENTS

Initially I would like to express my gratitude to my supervisor, Dr. Pierre Pillet, for the opportunity to work in his group, as well as for his support through these three years. Similarly, for Daniel Comparat, with whom I collaborated closely during the experimental work and the reduction of this document. Additionally, the help of more members of the group 'Molecules Froides' at Laboratoire Aimé Cotton, and in particularly of Andrea Fioretti, Guillame Stern, Emilia Dimova, Matthieu Viteau, Amodsen Chotia, Manabendra Bera is gratefully acknowledged. I also received great help from the group's theoreticians, and in particularly by Olivier Dulieu, Nadia Balufa and Viatcheslav Kokoouline and Vladimir Akouline. I would also like to thank Maria Allegrini and Marin Pichler, for their collaboration and support in a very difficult period. I also thank our scientific collaborators Beatrice Chatel and Christian Webe. Finally, I thank my friends and family for their help and support through all these years.

ABSTRACT

At the time of my arrival in Laboratoire Aimé Cotton (LAC) in November 2006, the activity of the experimental group of cold molecules in LAC was, on one hand on the formation and manipulation of cold molecules in a Magneto-Optical Trap (MOT), and on the other, in the realization of a dipole trap for cesium atoms. The preparation of a dipole trap of Cs atoms aimed both in the preparation of Bose-Einstein Condensation (BEC) of atomic Cs, and in the study of preparation and manipulation of Cs dimers in ultra-low temperatures. My enrollment in the activity of the experimental group of cold molecules in LAC was both in the preparation of the dipole trap, and in the study of cold molecule's creation and manipulation.

In the first part of my thesis, I describe the studies conducted in the period November 2006 to October 2008. In this period, I focused my efforts on the study of different techniques for the loading of a dipole trap with Cs atoms, using a pre-existing set-up. The target was the creation of a cold and dense trapped atomic sample, in which the evaporation technique could be applied, to further cool the sample down to the critical temperature for the creation of a Cs BEC. At the beginning of the experiment, a Cs BEC had been reported only once [Web03], after years of unsuccessful efforts by many groups [Sod98, Boir98, Thom04]. Despite the difficulty of the subject, the interest in preparing samples of ultra-cold Cs atoms remained high, especially due to experiments related to ultra-cold molecules, as the creation of a molecular BEC [Herb03], or the formation of Cs trimers and the observation of Efimov states [Lee07, Knoo08].

The strategy upon which the dipole trap experiment was based, is theoretically studied in a previous publication of the group [Comp06], which considers rapid evaporation of a dense atomic sample in a crossed, deep dipole trap. This dense dipole trap, is provided by superimposing the dipole laser to a much larger trapped atomic sample, the so-called *atomic reservoir*. Collisions in this atomic reservoir can thermalize the sample and lead to the transfer of atoms in the dipole trap. Since this process can last for relatively large time intervals, it can result to higher loading efficiencies with comparison to alternative, *instantaneous* loading methods. This approach is very different to the one used in the only successful BEC experiment at that time [Web03], in which a shallow, very cold, but not so dense dipole trap, is prepared with the use of Raman Sideband Cooling.

In the theoretical proposal reported in [Comp06], a magnetic trap was considered for the realization of the atomic reservoir, while the initial experimental study of this approach is the subject of a previous thesis in our group [Stern08]. However, the general ideas considered in this approach, allowed for the substitution of this magnetic reservoir, by several atomic traps. Thus, the experimental studies discussed in the first part of my thesis, are the continuation of the work made during the thesis of G. Stern [Stern08], with whom I collaborated in the beginning of my thesis. In particular, I studied the loading a dipole trap from a magnetic trap reservoir, and compared it to the loading obtained when the magnetic reservoir is replaced by a Dark-SPOT and a Compressed MOT (C-MOT). Furthermore, all these reservoir-loading methods are compared to a simpler, instantaneous-loading method which involves optical molasses.

By June 2008, it was made clear that our experimental approach to the dipole trap loading, could not lead to the preparation of a sufficiently cold and dense atomic sample, in which evaporating cooling could be applied for the preparation of cesium atoms in ultra-low temperatures. In the same time, the approach considered in the first successful realization of a Cs BEC [Web03] gained ground, since the experiments reported in [Hung08] showed that it could provide with a Cs BEC with a fast and relatively simple experimental sequence. Thus, we also attempted the preparation of an ultra-cold Cs sample with the use of a shallow, not very dense, but very cold

dipole trap provided by Raman Sideband Cooling. Unfortunately, a series of experimental problems related to the old vacuum system used in our experiment, prevented us from creating an ultra-cold atomic cesium sample with such an approach, despite the encouraging preliminary results.

On the same period, the studies of the manipulation of cold molecules created in a MOT, conducted by members of the experimental group of cold molecules in LAC, advanced considerably, leading to the demonstration of the vibrational cooling technique reported in [Vit08]. The operating principle of the vibrational cooling technique is similar to the one of optical pumping in atoms [Kast66]. In this process, molecules that initially lie in different vibrational levels, are simultaneously excited by shaped broadband light and are accumulated to a single vibrational level via spontaneous emission. The accumulation to a single vibrational level, is accomplished by choosing to remove from the shaped pulse, all frequencies resonant to transitions from this level and thus turn it to a *dark state*. The technique enjoys simplicity and generality, and its demonstration opened the way for many interesting extensions, some of which are the subject of the second part of my thesis.

More particularly, my activity in the cold molecule experiment which is discussed in the second part of my thesis, considered several extensions and generalizations of the vibrational cooling technique. The first extension to be considered, was the transfer of the molecular population to any pre-selected vibrational level, via optical pumping induced by more sophisticated, shaped femptosecond pulses, and is also discussed in [Sof09]. Another extension, considered the realization of vibrational cooling and molecular population transfer with the use of a broadband, non-coherent, diode light source, instead of a femptosecond laser and is reported in [Sof09b]. Another extension was considered to be the vibrational cooling of Cs molecules in their ground triplet electronic state, in addition to the ground singlet state, that was so far manipulated. Despite the optimistic initial predictions, the experimental study did not led to considerable results. However, this 'failed' experimental study, provides with an opportunity to revisit the various key elements of the vibrational cooling technique, and to consider the possible reasons that can lead to its failure. Such a discussion is particularly useful for the following study of the extension of the vibrational cooling technique to heteronuclear molecules through the example of NaCs. Finally, the generalization of the vibrational cooling technique to include rotation, which is theoretically considered in various publications of the group in which I participated [Vit09, Sof09, Sof09c], is discussed. In addition to these theoretical considerations, I discuss the preliminary experiments considered for rotational cooling, which involve the preparation of rotationally resolved depletion spectroscopy, and which are also discussed in [Fio09].

ABSTRACT (*fr*)

Au début de mon travail de thèse dans l'équipe Atomes et Molécules Froides du Laboratoire Aimé Cotton, l'intérêt du groupe était, d'un côté, la préparation et la manipulation des molécules de Césium créées via photoassociation, et de l'autre, à la préparation d'un échantillon de Césium à basse température et de grande densité dans un piége dipolaire. Initialement, j'ai participé aux études de realization du piége dipolaire atomique, et ensuite aux études de préparation et de manipulation des molécules.

Dans la période entre Novembre 2006 jusqu'a Octobre 2008 j'ai développé une série de techniques différentes pour le chargement d'un piége dipolaire à partir d'un réservoir atomique, réalisé soit par un piége magnétique, soit par un piége du type 'Dark-SPOT', soit par C-MOT (piége magnéto-optique comprimé) et un mêlasse optique. Au commencement du mon travail, un BEC de Césium a été rapporté un seule fois [Web03], après des années des efforts de plusieurs équipes [Sod98, Boir98, Thom04]. De plus, l'intérêt sur l'atome de Césium a augmenté à cause des expériences liées à la formation de trimères de Césium et des résonances du type 'Efimof' [Lee07, Knoo08].

La stratégie sur laquelle notre approche pour le chargement du piége dipolaire était basée, est discutée dans une publication rédigée avant mon intégration au sein d'équipe Atomes et Molécules Froides du Laboratoire Aimé Cotton [Comp06]. Il s'agit d'un chargement à partir d'un réservoir obtenu par un piége magnétique. L'objectif de cette proposition était la préparation d'un échantillon ultra froid avec un dispositif expérimental beaucoup plus simple que celui de la référence [Web03]. De plus, la proposition [Comp06] prédit la préparation d'un condensat de Césium en un temps beaucoup plus court que les temps de préparation rapportée dans la référence [Web03].

L'étude de la réalisation expérimentale de cette proposition théorique a déjà commencé, dans le cadre de la thèse de G.Stern [Stern08]. J'ai continué cette étude et j'ai réalisé plusieurs études avec différents types de réservoir (Dark-SPOT, C-MOT) et aussi de un type de chargement différent qui est basé sur le refroidissement par bandes latérales (Raman-Sideband Cooling). Toutes les piéges préparés par ces méthodes, avait une densité inférieure a celle nécessaire pour la réalisation d'un processus de refroidissement évaporatif, qui est nécessaire pour la réalisation d'un condensat. Les problèmes techniques que nous avons rencontrés vers Mai 2008 (destruction de vide), nous ont conduit d'arrêter les études de refroidissement des atomes, et de s'orienter vers les études de manipulation des molécules de Césium.

Pendant cette période, l'équipe avait beaucoup progressé dans manipulation des molécules de Césium, et plus spécifiquement sur la réalisation du refroidissement du degré de liberté qui correspond à la vibration des molécules. La nouvelle technique que l'équipe avait introduit et qui est rapporté à la référence [Vit08], permet le refroidissement de la vibration des molécules de Césium par un laser femtoseconde faconné, avec un processus de pompage optique [Kast66]. Mon objectif dans la thématique de la manipulation des molécules froides, était d'étudier la généralisation de cette technique. Par example le transfert de la population moléculaire dans un seul état vibrationnel pré – sélectionné a été observé. Ce résultat est discuté dans la référence [Sof09]. Une autre généralisation est la réalisation du refroidissement vibrationnel et du transfert de la population moléculaire avec une source de lumière non cohérente, résultat qui est discuté dans la référence [Sof09b]. Une autre généralisation importante est le refroidissement de la rotation moléculaire. Cette étude théorique est discutée dans les articles de l'équipe auxquels j'ai participé [Vit09, Sof09,

Sof09c], et les études expérimentales préliminaires dans la référence [Fio09]. Finalement, la généralisation de la technique pour le refroidissement vibrationnel des molécules heteronucleaires est discuté dans le dernière chapitre de ma thèse.

Le document de ma thèse est donc divisé en deux parties, dans chacune d'elles je discute en détails ma contribution scientifique dans l'équipe Atomes et Molécules Froides du Laboratoire Aimé Cotton.

Table of Contents

Part I – Abstract 15
- I.1. INTRODUCTION....19
  - I.1.1. Basic description of a BEC....19
  - I.1.2. Atom cooling techniques 22
    - I.1.2.a. Laser cooling and trapping 23
    - I.1.2.b. Evaporating Cooling....27
  - I.1.4. Previous approaches to the Cs BEC....32
    - I.1.4.a. The magnetic trap approaches....33
    - I.1.4.b. The optical dipole and hybrid approaches....33
- I.2. OUR APPROACH TO THE BEC....39
  - I.2.1. Basic parameters and geometry of the dipole trap....39
  - I.2.2. Loading the dipole trap from an atomic reservoir....42
  - I.2.3. Evaporation in the dipole trap 46
  - I.2.4. Conclusion 49
- I.3. EXPERIMENTAL SET-UP....53
  - I.3.1. Chamber architecture and vacuum system....53
  - I.3.2. Magneto-optic and dipole trap....55
    - I.3.2.a. Diode laser set-up and magneto-optical traps....55
    - I.3.2.b. Atom transfer and pushing beam....58
  - I.3.3. Magnetic trap....59
  - I.3.4. Dipole trap laser and dynamic modification of its dimensions....60
  - I.3.5. Data acquisition and thermometry....65
    - I.3.5.a. Fluorescence imaging and Time of Flight temperature determination....65
    - I.3.5.b. Absorption imaging and in-situ temperature determination....67
    - I.3.5.c. Non destructive imaging based on diffraction....69
  - I.3.6. Piloting program with LabVIEW....70
- I.4. EXPERIMENTAL WORK....75
  - I.4.1. Loading the dipole trap from a magnetic trap reservoir....76
    - I.4.1.a. Preparation of the magnetic trap 'reservoir'....77
    - I.4.1.b. Polarization....80
    - I.4.1.c. Loading a crossed dipole trap from a magnetic trap reservoir....83
  - I.4.2. Loading the dipole trap from a Dark-SPOT....90
    - I.4.2.a. The Dark-SPOT and its realization in LAC....90
    - I.4.2.b. Loading the dipole trap by the Dark-SPOT....91
  - I.4.3. Loading the dipole trap from a C-MOT and molasses....93
    - I.4.3.a. The C-MOT and molasses phase....93
  - I.4.4. Loading the dipole trap from the C-MOT and molasses....95
  - I.4.5. Loading the dipole trap via Raman Sideband Cooling....98
    - I.4.5.a. The Raman -Sideband Cooling in LAC....99
    - I.4.5.b. Stray magnetic field compensation....99
    - I.4.5.c. Loading a 600 μm dipole trap....102
  - I.4.6. Summary....104
- I.5. DISCUSSION ON THE EXPERIMENTAL RESULTS....107
  - I.5.1. Phenomenological approach for the description of the loading process....108
  - I.5.2. Fitting the experimental data 110

I.5.3. Conclusion....113
I.6. CONCLUSION & PERSPECTIVES....115
Part II - Abstract....119
II. PREPARATION AND MANIPULATION OF COLD MOLECULES....125
II.1. INTRODUCTION....125
II.1.1. The cold molecules as a separate field of scientific research....125
II.1.2. Atoms and molecules in the context of laser cooling....125
II.1.3. Some elements of of molecular physics....127
II.1.3.a. The cases of Hund....127
II.1.3.b. Cases (a) and (c) and corresponding notation. 128
II.1.3.c. Interactions with light....129
II.1.4. Conclusion....130
II.2. TECHNIQUES FOR THE STUDY OF COLD MOLECULES....135
II.2.1. General description of the various methods for the study of cold molecules. 135
II.2.2. Methods for molecular cooling....137
II.2.3. Methods for the preparation of cold molecules by association 141
II.2.4. Recent developments in the area of cold molecules 145
II.2.4.a. Photo-association....145
II.2.4.b. Magneto-association....147
II.2.5. Conclusion 148
II.3. VIBRATIONAL COOLING WITH BROADBAND LIGHT....151
II.3.1. Vibrational Cooling technique 151
II.3.1.a. Operating principle 151
II.3.1.b. Broadband detection of deeply bound Cs dimers....153
II.3.1.c. Cooling the molecular vibration with the use of shaped broadband lasers....155
II.3.2. Experimental set-up....158
II.3.2.a. Photoassociation in the MOT....158
II.3.2.b. Shaped femtosecond laser for optical pumping....159
II.3.2.c. Dye lasers and ionization detection....160
II.3.3. Conclusion 163
II.4. MOLECULAR POPULATION TRANSFER TO A GIVEN VIBRATIONAL STATE....167
II.4.1. Introduction....167
II.4.2. The Spacial Light Modulator....168
II.4.3. Simulation of the vibrational cooling method....169
II.4.4. Molecular population transfer via the creation of dark states....170
II.4.5. Improved optical pumping via optimized pulses....173
II.4.6. Perspectives for direct laser cooling of molecules....176
II.4.7. Conclusion....177
II.5. NON-COHERENT SELECTIVE POPULATION TRANSFER IN Cs2 MOLECULES. 181
II.5.1. Vibrational cooling with the use of a non coherent broadband source....181
II.5.2. Population transfer to vX = 0....181
II.5.3. Population transfer to vX = 1....184
II.5.4. Conclusion....186
II.6. GENERALIZATION OF VIBRATIONAL COOLING 191
II.6.1. Key parameters for optical pumping of molecules....191
II.6.1.a. 'Toy model' for molecular potentials....192
II.6.2. Study for the cooling of molecules in the a3Σu+ triplet state....195
II.6.2.a. Motivation....196
II.6.2.b. Experimental study 200

II.6.2.c. Interpretation of the results 201
II.6.3. Study of the applicability of vibrational cooling to heteronuclear molecules............206
II.6.3.a. Choice of electronic transition...206
II.6.3.b. Production of the FC-dipole parabola...208
II.6.3.c. Simulations of optical pumping 211
II.6.4. Conclusion & Perspectives 215
II.7. TOWARDS COOLING THE MOLECULAR ROTATION 220
II.7.1. Rotational cooling with broadband radiation...220
II.7.2. Rotational cooling with narrowband radiation...223
II.7.3. Preliminary experiments and depletion spectroscopy...231
II.7.4. Conclusions...233
II.8. CONCLUSION& PERSPECTIVES 235
III. GENERAL CONCLUSION 239
ANNEX I.1...243
ANNEX I.2...247
ANNEX I.3...259
ANNEX II.1..263
ANNEX II.2..267

Part I – Abstract

Realization a dipole trap for Cs atoms; towards a Cs BEC

In this first part of my thesis I describe the experiment of the Cs atom dipole trap, which is is the experiment in which I was involved from November 2006 to October 2008. The description is organized in four chapters.

In the first chapter, the introduction, a basic description of a BEC is initially given. Then, I give a brief description of the major atom-cooling techniques used in the experiments described in this part of my my thesis. These include the operating principle of the Magneto-Optical traps, the molasses and finally the Raman-Sideband cooling. Only the operating principles are discussed here; the details of the experimental realization of these techniques in our laboratory are discussed in the chapter I4. Next, I present the special characteristics of the Cs atom, the reasons of the particular interest for this atom and finally, the previous approaches for Cs BEC followed by several groups [Perr98, Web03, Thom04, Hung08].

The second chapter is devoted to revisit the theoretical proposition in which the experiment was based [Comp06], and to explain our motivation on the particular method. This approach considers rapid evaporation of a very dense but not very cold atomic sample in a dipole trap. The evaporation is predicted to be fast enough to overcome the collision losses and to result to a condensation in less than one second. The dense dipole trap is obtained by overlapping it to a much larger trapped atomic sample, the so-called *atomic reservoir*. The atomic collisions in the combined dipole-reservoir trapping potential result to the sample's re-thermalization and eventually to the transfer of atoms in the dipole trap in high densities. The first paragraph of this chapter, describes the basic characteristics and the geometry of our reservoir and dipole trap; the second paragraph outlines the theoretical study of reservoir loading and the third paragraph, refers to the predicted evaporation performance.

The third chapter, describes the experimental set up and the basic experimental sequences used in the experiment. The experimental set up description starts with the vacuum system and the mechanical parts. Then, I describe the laser set-ups and the two Magneto Optical traps, the atom transfer between them and the magnetic and dipole traps. I also describe the data acquisition techniques: the fluorescence imaging, the absorption imaging, as well as an additional imaging technique which is based on diffraction. Finally, I describe the piloting program with which the experimental sequences were executed.

The fourth chapter, contains the most important experimental results for the loading of a dipole trap. The role of the reservoir, played by a magnetic trap both in the theoretical proposal [Comp06] and in the previous work [Stern08], was played also by a Dark- SPOT and a compressed MOT[1]. Additionally, these loading strategies are compared to simpler loading methods, like loading by molasses. Finally, the realization of Raman-Sideband Cooling (RSC) is also considered. The RSC is a necessary element in both the so-far successful Cs BEC experiments [Web03, Hung08]. Its realization and use for the dipole trap loading, was decided as an alternative to the 'reservoir' loading methods that were found to be insufficient.

---

[1] There has been a large discussion on what should be called 'reservoir' and what not, with most of my collaborators believing that this name should be strictly used only for the case of conservative traps. However, I consider a much less strict definition and I use the term 'reservoir loading' to describe all the loading methods that operate for an important time interval (superior to some tens of ms), thus distinguishing two main approaches: the 'reservoir' and the 'instantaneous' loading methods.

In the fifth chapter, the results for the several types of the reservoir loading are discussed. In this chapter, I search for an explanation for a striking common characteristic of the 'reservoir' loading techniques: the short duration of the loading process that is inevitably connected to the technique's poor performance.

A great part of the experimental work has been left out of this thesis main part, for the sake of economy and continuity. This work is mostly related to evaporating cooling and it is presented in Annexes I1 and I2. In particularly, in Annex I1 I discuss the observed lifetime of the dipole traps prepared in the laboratory. With the exception of the large (~700μm) and shallow dipole traps prepared with the use of Raman-Sideband cooling, the dipole traps obtained with the reservoir loading techniques (~100μm) were all very short lived. The time in which the number of atoms trapped was decreased in half of its initial value, which we call 'lifetime' of the dipole trap, was almost common for all these traps, around half a second. In Annex I1 I describe a simplified analysis in the dipole trap lifetime data inspired by the analysis presented in [Web03b]. Then, in Annex I2, I describe our attempts to perform evaporating cooling to these traps, as well as to 'compress' them, with the use of an optical 'zoom' configuration installed in the dipole laser and described in I.3.4. Finally, in Annex I3, I present some experimental tests on the quality of the spatial profile of the laser used for the realization of the dipole trap, as well as a study on the possibility of interferences.

CHAPTER I1: INTRODUCTION

I.1. INTRODUCTION

The introduction is organized in four paragraphs. The first paragraph gives the basic description of what is a BEC and a BEC transition. It presents the basic description via the Gross-Pitaevskii equation, aiming to describe the BEC phase transition signature, when this is realized in dilute gases, and which consists of an anisotropic expansion of the atoms once released from their trapping potential.

The second paragraph describes the basic principles of laser cooling, the operating principle of the Magneto-Optical traps (MOTs), the molasses and the Raman-Sideband cooling, as well as the evaporation cooling. The MOT, is probably the most widespread laser cooling technique in our days. In the same time, it's relatively simple operating principle gives an opportunity to introduce the basic concepts of laser cooling. Based in this introduction, I can proceed in the descriptions of particular laser cooling techniques which I employed during my thesis, which are the molasses and the Raman-Sideband cooling. Evaporation is also discussed in an oversimplified example. Again, I return to a more detailed description of the evaporation process in Chapter I2, where the theoretical predictions for the applicability and the efficiency of our technique are discussed.

In the following paragraph, I discuss the special characteristics of the Cs atom and the particular interest on it. The goal here is to explain the group's investment in time and resources in the Cs atom experiment. In the period where this experiment was in progress, Cs was in the center of interest in the area of cold molecules, where LAC is very active. In particular, for LAC, the great interest emerged from the resent breakthrough of optical pumping and laser cooling of vibration achieved in the laboratory [Vit08]. As far as Cs BEC is concerned, shortly after the first Cs BEC reported in [Web03], and while this experiment was in progress, various developments related to cold molecules, Feshbach resonances and Efimov trimer states were reported [Herb03, Lee07, Vit08].

In the last part of the introduction, we revisit some of the most important approaches to Cs condensation [Perr98, Hung08, Thom04, Web03]. This is probably the easiest way to present the particular difficulties that are involved in Cs condensation. As the Cs collision properties where getting explored, the experiments that were trying to achieve Cs condensation evolved, passing from magnetic to optical and hybrid traps. Additionally, this historical review of the Cs condensation gives the opportunity to explain the reasons why our approach towards the BEC was such. It also points out the particular difficulty that is involved in Cs condensation, in comparison to other atoms, which are simpler to condense like for example Rb.

I.1.1. Basic description of a BEC

One of the biggest goals in the domain of cold atom physics has been the observation of the Bose- Einstein condensation (BEC), as its accomplishment led to the observation of a variety of exciting phenomena [Deng99, Den00, Grein02, Abo01, Gret06, Billy08, Corn02], as well as to the development of new theoretical tool work for it’s description, to the extend that it is considered today an almost separate, and very widespread field of scientific research.

As predicted in 1925, the fundamental differences between the two different groups of particles, the bosons which have integer spin, and the fermions which have semi-integer spin, lead to very different behavior in low temperatures. Bose-Einstein condensation is actually a separate phase of matter, additional to the gas, the liquid, the solid and the plasma phase, that can be observed when a sample of bosons is cooled bellow a ‘critical temperature’, the value of which depends on the cooled species. It is a phase of matter that allows for the observation of various exotic phenomena that can be explained only in the context of quantum mechanics[1].

Quantum mechanics points out the existence of 'wave- matter' duality in nature. For example, light that classical mechanics and electromagnetism consider as a wave, is viewed as a particle in quantum mechanics, the 'photon', without which, commonly observed phenomena like the photoelectric phenomena, find no explanation. For what is considered by classic mechanics as 'matter', quantum mechanics appoints wave properties. For a collection of particles the 'wave' qualities are embodied in the so-called *de Broglie* wavelength, λ_{dB}

$$\lambda_{dB}=\sqrt{\frac{2\pi\hbar^2}{m k_B T}} \tag{1.1}$$

This *de Broglie* wavelength is inversely proportional to the temperature and the mass, a fact which explains why the wave qualities of matter are not evident in everyday life. In a sample consisted of bosonic particles, when the temperature is very low, and the density is very high, the *de Broglie* wavelength can become comparable to the inter-atomic distances. The product of λ_{dB} with the density of the atomic sample, the so-called 'phase-space density' increases with decreasing temperature and increasing density. In conditions of ultra low temperature the sample is best described as a wave, rather than a sum of many particles, and many phenomena related to wave properties have been observed [And97].

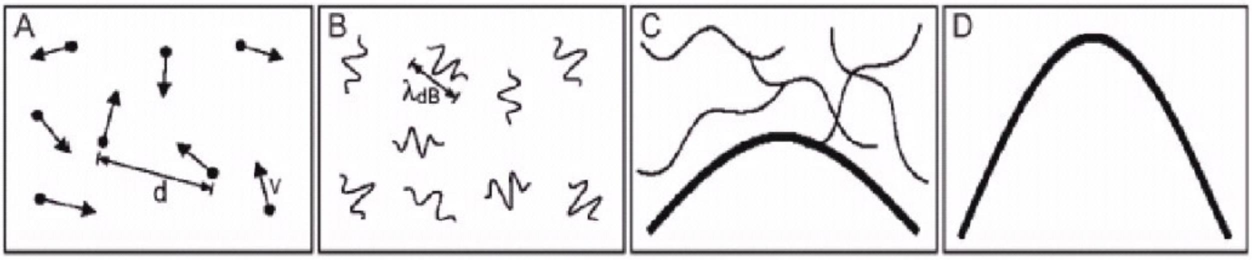

Fig.I.1.1: The transition from a classical gas to a BEC. Initially (A) the sample behaves as a collection of particles, but as the temperature decreases and the density increases or remains constant (B), the *de Broglie* wavelength increases, and gradually becomes comparable to the inter-atomic distances (C). Finally, the sample is best described as by a singe wave function as all the atoms participate to the condensate (D). Figure adapted from [Web03b]

The picture that is presented in Fig.I.1.1 gives the impression that the BEC is a phenomenon that occurs gradually as phase-space density increases, where actually it appears as a distinct phase transition. To understand why this happens we have to take a look to boson statistics and how these are transformed to describe BECs.

For a sample of bosonic atoms in a trapping potential, with a mean occupation number N_v of a single particle v with energy ε_v, the maximum numbers of atoms that lie in any excited state is given by

$$N_{\varepsilon_v}=\sum_{v=1}^{\infty}\frac{1}{e^{(\varepsilon_v-\mu)/k_B T}-1} \tag{1.2}$$

where μ is the chemical potential that is calculated upon the normalization condition $N=\sum_{v=0} N_{\varepsilon_v}$. As the temperature lowers, μ increases in order to preserve the normalization condition. The chemical potential cannot exceed ε_0 the energy of the ground state since in this case the expression 1.2 would take an infinite value for $v = 0$. Thus, equation's 1.2 limiting form for low temperature is

---

[1] The behavior of fermions in ultra-low temperatures, although similarly exotic and interesting, is not related to this thesis and will not be analyzed here.

$$N_{\text{ex.max}} = \sum_{\nu=1}^{\infty} \frac{1}{e^{(\varepsilon_\nu - \varepsilon_0)/k_B T} - 1} \qquad (1.3)$$

giving the maximum number of the particles that can occupy all excited states. Relation 1.3 is useful in order to derive a qualitative criterion for the BEC phase transition, and for the critical temperature Tc for which this occurs. BEC occurs when the number of particles that occupy all excited states, $N_{ex,max}$ becomes comparable to the number of particles in the ground state N_0, and the onset of this transition can be defined as the point where $N_{ex,max} = N_0$. The critical temperature can by calculated according to this criterion and is found to be [Peth02]

$$T_C = \frac{N^{1/a}}{k_B}[C_a \Gamma(a)\zeta(a)]^{1/a} \qquad (1.4)$$

where C_α is a constant, $\zeta(\alpha)$ is the Riemann zeta function, $\Gamma(\alpha)$ is the gamma function and a is a constant that depends on the trapping potential geometry, and takes the value 3 for harmonic traps. We note that k_BT_c is usually much higher than the energy difference between the ground and the first excited state; for this reason BEC does not result to a gradual ‘washing out’ of motion in the trapping potential, but as a distinct phase transition.

In the BEC experiments that are realized with neutral atoms, this phase transition has an experimental ‘signature’, which is the anisotropic expansion of the BEC when it is released from the trapping potential and falls under the influence of gravity. To explain this anisotropic expansion, we need to take a look of the thermodynamic properties of the BEC in the trapping potential. The mathematical description necessary for the derivation of the basic thermodynamic properties of a BEC, can be done in the context of many-particle theory. However, this complicated process is usually avoided and most basic properties of condensates are derived with the use of the Gross-Pitaevskii (GP) equation:

$$i\hbar\frac{\partial}{\partial t}\Phi(r) = (\frac{-\hbar^2\nabla^2}{2m} + U_{ext}(r) + g|\Phi(r)|^2)\Phi(r) \qquad (1.5)$$

The GP equation resembles to the Schrödinger equation. Nevertheless, an important point is that it is an equation written not for an atomic wavefunction, but for the so-called “order parameter” $\Phi(r)$, which is a complex quantity which if risen in square gives the condensate's density[1]. Apart from the order parameter, $U_{ext}(r)$ is the external trapping potential and $g = 4\pi\, h2a/m$ with a being the scattering length. The scattering length is a very important quantity, since in low temperatures, all collision properties can be parametrized with respect to this single parameter [Kohl07]. Its value controls the nature and magnitude of the inter-atomic interactions, since when it takes positive values, the interactions of the sample are repulsive and when it takes negative values the interactions are attractive. Moreover, the value of the scattering length depends on the magnetic field, a fact that gives rise to a very important ultra-cold atom phenomenon, the Feshbach resonance in which we will refer to in the following paragraphs.

Equation 1.5 can be solved to give the density profile of the condensate. In the case of repulsive interactions, the interactions creates a virtual potential, the mean-field potential, which cancels out the trapping potential and stabilizes temporally the BEC’s density profile. If the kinetic energy term in the GP equation is neglected, (this is widely known as the Tomas-Fermi approximation), the cancellation of these potentials gives rise to a flat effective potential and results to an inverted parabola shape for the density of the condensate, which reflects the shape of the trapping potential.

---

[1] However, the order parameter is often refereed to as 'condensate' wavefunction.

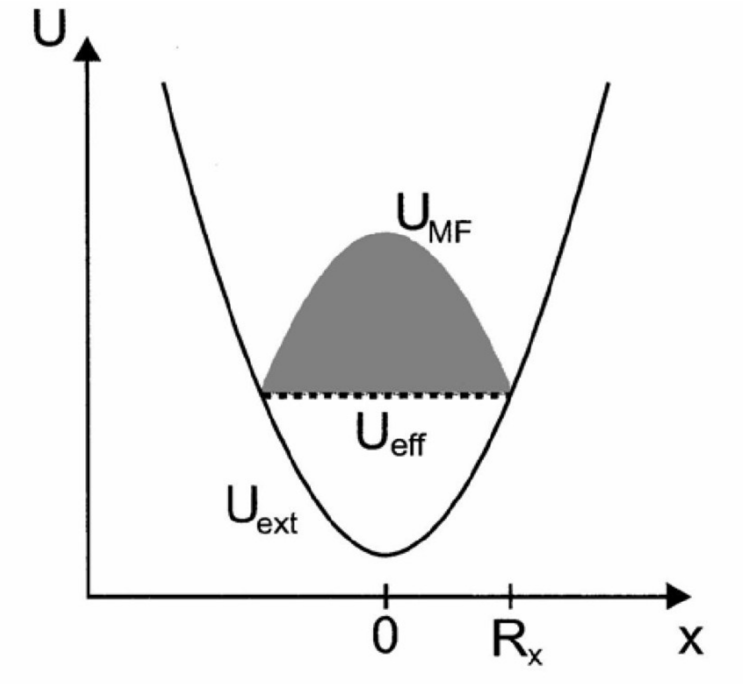

Fig.I.1.2: A condensate in the Thomas-Fermi limit. The trapping potential is canceled by the mean-field potential, in a way that a flat effective potential is created. The BEC's density profile is an inverted parabola that reflects the shape of trapping potential.

After the trapping potential is turned off, the mean field energy, that results from the interaction and that follows the same inverted parabola shape as the density of the BEC, is converted to kinetic energy and leads to an asymmetric ballistic expansion for the condensate. This asymmetric ballistic expansion is an experimental ‘signature’ for condensation and helps to distinguish BECs from dense but not condensed atomic samples.

The creation of BECs with negative scattering length and thus attractive inter-atomic interactions is also possible. In such condensates the attractive interaction is usually balanced by the kinetic energy a fact that can lead to a dynamic stabilization of the BEC. That puts an upper limit to the number of atoms that can participate to negative scattering length BECs [Peth02].

I.1.2. Atom cooling techniques

The combination of laser cooling and evaporation is the dominating technology for the preparation of a BEC, not only due to its use in the pioneering experiments, but also due to the fact that it still remains the most popular experimental approach in the field. Exceptions exist only for the case of condensation of spin-polarized hydrogen [Fried98], and for the case of condensation of exciton polaritrons in the solid phase [Kasp06], where cryogenic methods were used. With the general term ‘laser cooling’ I intend to enclose various techniques like the magneto-optical trap and the various molasses cooling. The magneto-optical trap (MOT) is the most widespread laser cooling technique, and even though it was not the first to be developed among the ones mentioned, the description of its basic principle opens the way for a more economical and comprehensive description of laser cooling. Similarly for evaporating cooling, evaporation in magnetic traps will be used as the paradigm over which the basic principle of evaporation is going to be discussed. Evaporation in optical dipole traps will be discussed after the properties of the Cs atom are presented in the following paragraph, and the need for such a trap becomes clear.

I.1.2.a. Laser cooling and trapping

Magneto-Optical traps

Laser cooling is based in the fact that the spontaneous emission is homogenous in its direction, which means that when an atom emits a photon spontaneously, this photon can be emitted towards any direction with the same probability. When an atom absorbs or emits a photon, light transfers momentum to the atom, or away from it, which equals

$$p=\hbar k \tag{1.6}$$

where k is the wave-vector associated to the photon. Let us consider an atom traveling in a direction opposite to the propagation direction of a laser beam resonant to one of its transitions. As the laser radiation is directional, while spontaneous emission is homogenous in space, a repetition of absorption - spontaneous emission circles leads to a constant momentum loss in the direction of the atomic motion. This momentum loss is based to the fact that spontaneous emission is isotropic; if the emission is stimulated by the laser field; the photon emitted is forced to have the direction of the simulating field, leading to zero net momentum exchange.

For the simple one dimensional geometry, let us imagine a counter-propagating pair of beams that are resonant to a particular atomic transition. The force that results such a situation is the sum of the forces F± which correspond to the counter-propagating beams and equals to

$$F_{\pm}=\frac{\hbar k \Gamma}{2}\frac{s_0}{1+s_0+[2(\delta\mp|\omega_D|)/2]^2} \tag{1.7}$$

where Γ is the natural line width of the excited state, ω_D the Doppler shift of the transition frequency and s_0 the saturation factor, as this results from the solution of the excitation of the related two-level system and equals to $2|\Omega|^2/\Gamma^2$ with Ω being the Rabi frequency. The sum of these forces gives the total force

$$F_{tot}\simeq\frac{8\hbar k^2\delta s_0\vec{\upsilon}}{\Gamma(1+s_0+(2\delta/\Gamma)^2)^2} \tag{1.8}$$

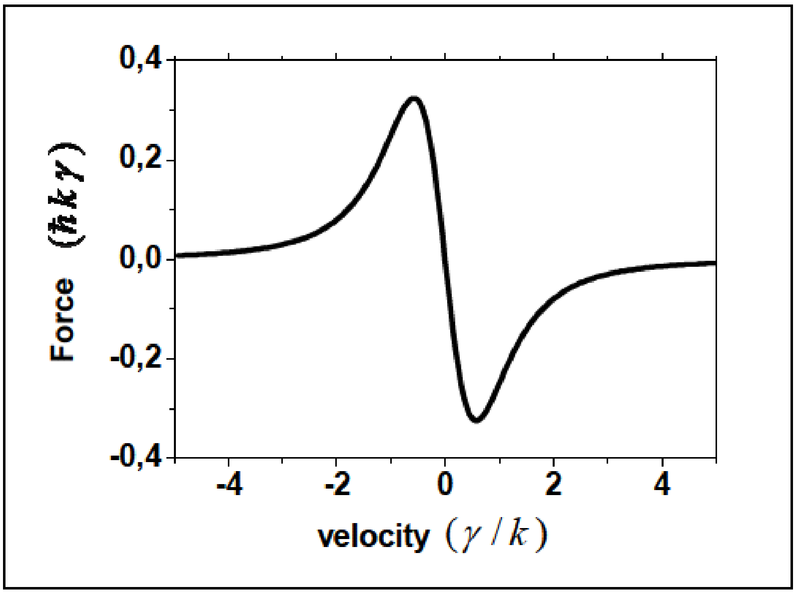

Fig.I.1.3: The radiation force F_{tot} as a function of the atomic velocity, for the convenient choice of $s_0 = 2$ and $\Gamma = 2\ s^{-1}$. We note that there is a maximum velocity after which the force is not attractive and the atoms cannot be cooled.

In Fig.I.1.3 we see a plot of F_{tot} for a convenient choice of parameters. Such a process can lead to more general cooling and trapping if the momentum exchange always opposes atomic motion. In a MOT this is ensured by a simple configuration of laser light polarization and magnetic field gradients. In a MOT there are three pairs of counter-propagating, circularly polarized laser beams lying in the three axis of the Cartesian coordinate system, while the magnetic field gradient configuration that is used is the quadrupole configuration. The magnetic field in a quadrupole trap increases in a linear fashion with respect to the distance from its center. As atoms move in an inhomogeneous magnetic field, they experience a shift in their energy levels which depends in which particular spin projection state m they lie and in the sign of the *Lande* factor g_F. If we consider atoms that lie in the negative *m* state and that have their energy levels lowered for increasing magnetic field, the positive *m* atoms will have the opposite effect. If the polarization of the light is chosen to be circular right σ_R, and is frequency lower with respect to an atomic transition, then negative *m* state atoms will be driven closer to the resonance and will scatter more light, a fact which results to a radiation force that drives the atoms in their original position. A counter-propagating beam with the opposite polarization ensures that the same effect will take place for atoms that lie in the positive *m* states and that move in the opposite direction. To this process, we add the fact that once an atom starts interacting with such a laser geometry, a combination of radiation forces and of optical pumping keeps it to the extreme *m* states, and assures that most of the atoms are found to this situation where a force that opposes their motion is applied to them at all times.

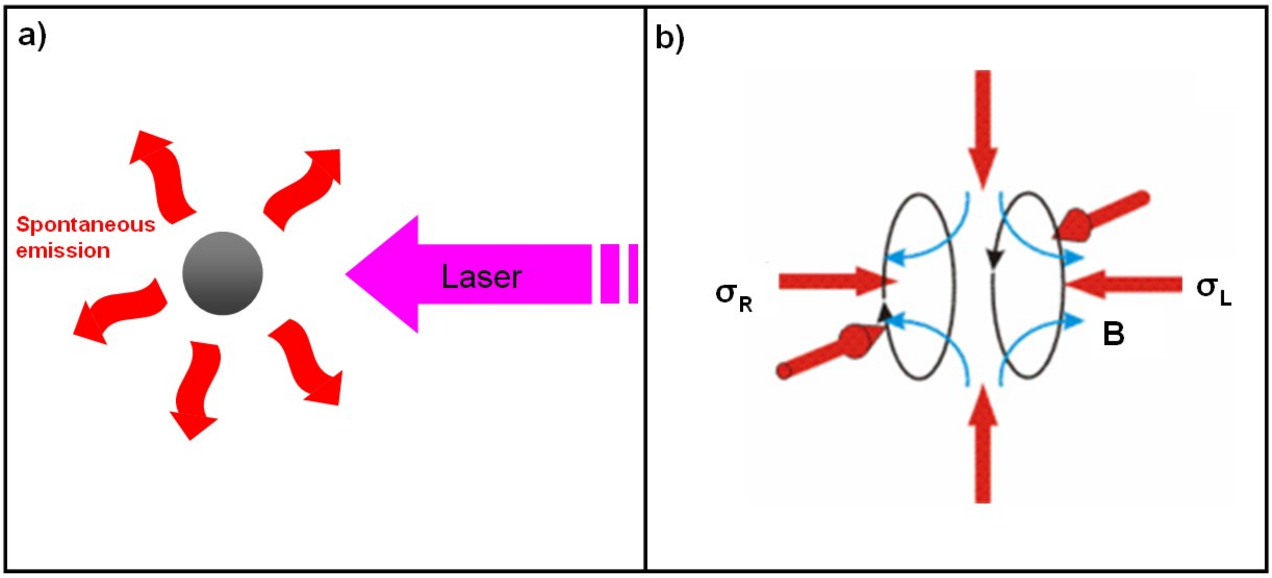

Fig.I.1.4: (a) Schematic representation of laser excitation and spontaneous emission in laser cooling. (b) Configuration of laser beams and coils in a MOT. Two circular coils with counter-propagating currents create a quadrupole field (anti-Helmholtz configuration).

The number of absorption-spontaneous emission circles must be significant, thus atoms must perform transitions between two levels without relaxing to different ones and thus stop being resonant to the laser light. Such isolated, 'closed' transitions, are not easily found in real atoms. Nevertheless, it is possible to find systems, where the losses take place towards states that can be 'connected' to the initial ones with the use of one additional laser, the so-called re-pumper. Although the need of a re-pumper is definitely a complication with respect to the image described above, placing one repumping laser is experimentally realizable. This is not the case for example, in molecules, where the density of states is much larger. Molecules can relax to such a large number of different states that addressing each of them with a different laser is completely impractical. We will return to this interesting aspect in the second part of this thesis, where the difference between atoms and molecules is going to be viewed in more detail, and where we discuss how our research can perhaps give new solutions to related problems.

A detailed analysis of MOTs is beyond the scope of this text as this can be found in many textbooks, like the one referenced here [Metc99]. The physics that are involved for a complete analysis of the MOT is much more complicated than the simplified picture presented here. For example, the given analysis implies that the minimum temperatures that can be achieved coincide with the one photon limit, which is the temperature that corresponds to the kinetic energy acquired by the emission of one photon in a random direction. However, this is not true, since there have been much lower temperatures reported. There are more mechanisms, beyond the photon absorption, that contribute to cooling in a MOT, and that are related to the creation of optical lattices and optical molasses.

Molasses

The operating principle of laser cooling described previously, does not suffice to describe the molasses phase, and additional mechanisms take place as the well known “Sisyphus” mechanism. This mechanism can be considered in two different configurations, which we see in Fig.4.15, (a) the Lin-Lin and (b) the σ+σ- configurations. In both configurations, the counter-propagating laser beams interfere, and the atoms 'see' effective potentials and polarization gradients that depend on their position with respect to the laser's standing wave. In the Lin-Lin configuration, the atoms 'see' the light polarization to change from linear at +45°, σ+, -45 and σ- within one laser wavelength, while the potential they 'see' varies with a sinusoidal fashion. The laser light is resonant with a $m_F \rightarrow m_{F+1}$ transition, which can be realized in the position where the light is σ+ polarized, a position which coincides with the position of the potential 'hill'. After this transition is realized, the atoms are found themselves in a state with increased F, which 'sees' a different potential which has a phase shift of π, and which is shown dotted in the figure. Thus, the atoms are found in the potential 'valley' and loose kinetic energy. This process goes on until the atoms have less kinetic energy than the one that would allow them to 'climb' the potential 'hill'. They cannot then perform any transitions and stay trapped in the 'lattice' produced by the laser beams.

In the σ+σ- configuration, the atoms 'see' the light polarization rotate by 90° in each wavelength. The light is now resonant to a $F \rightarrow F\text{-}1$ transition and not all transitions are allowed by the angular momentum selection rules, leading to the preparation of coupled Ψ_C and non coupled Ψ_{NC} states. The effect of the light on the atoms is that it gradually transfers all atoms to a non coupled state by optical pumping. Kinetic energy can couple the two states, so the atomic population cycles between the two states, until the kinetic energy cannot further couple them and the process terminates.

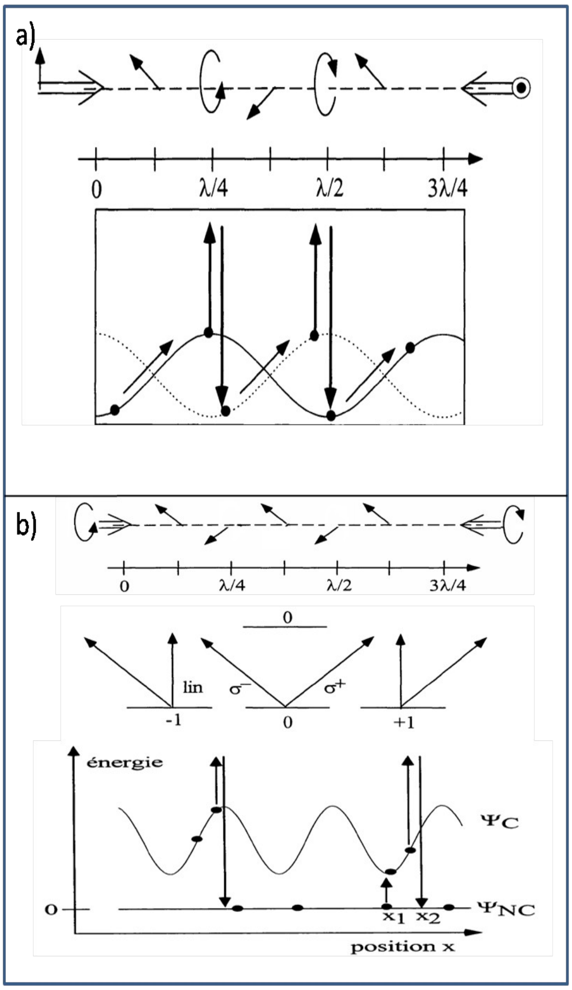

Fig. I.1.5: Schematic diagram concerning 'Sisyphus' effect in (a) Lin-Lin and (b) a σ+σ- configuration. Figure composed by parts adapted from [Boir98].

In Fig. I.1.5 we see a schematic diagram concerning 'Sisyphus' effect in the Lin-Lin and σ+σ- configuration. In part (a) which concerns the Lin-Lin configuration, the polarization of the standing wave produced by the counter propagating linearly polarized trapping beams turns from linear to circular and in a distance equal to ¼ of the wavelength. The atoms are excited when they are found in the potential “hill” and relax to the “valley” of the phase shifted potential. In part (a) which concerns the 'Sisyphus' effect in a σ+σ- configuration, the polarization of the standing wave produced by the counter propagating linearly polarized trapping beams is linear and rotates 45° in a distance equal to ¼ of the wavelength. In each of the angular momentum projection states m_J there are two possible polarizations that cannot excite the atom, creating the non coupled states. The coupled state is excited in the potential 'hill' and relaxes to the non coupled state which sees a flat potential. This scheme is a composition of schemes taken by [Boir98].This cooling methods is also called 'dark' or 'gray' molasses, since in the end of the process the atoms do not interact with the light, and there is no fluorescence.

Raman-Sideband Cooling

Raman Sideband cooling is a laser cooling technique that permits the preparation of atomic samples with temperatures as low as several hundred nKs. As in the case of molasses, the RSC operating principle is complicated and cannot be described by the simple picture of momentum exchange between the photons and the cold atoms.

In the RSC technique, light does not interact with free, but with trapped atoms with relatively high 'trapping frequencies' (or small oscillation periods in the trap). The technique succeeds in performing optical transitions between these vibrational states, and transferring the atomic population in the lowest one. The ability to resolve these vibrational states is essential for the realization of the technique, this is why the it requires either enormous resolution or high confinement. RSC was initially used for the cooling of ions [Nago86], where the electrostatic traps achieve the required confinement. For the realization of the technique in neutral atoms, the required confinement can be achieved only by the use of optical lattice traps in one, two or three dimensions. In our experiment we realized RSC in a three dimensional lattice following the work presented in [Treut01].

In figure 4.23 we see a scheme that presents the operating principle of RSC (taken by [Kerm00]). We consider atoms in the vicinity of an optical lattice pumped in the |F =3,m_F= 3,v> ground state, where v = 0,1,2,3.. is the vibrational quantum number. An appropriate magnetic field can bring into resonance this state with the |F =3,m_F= 2,v-1> and |F =3,m_F= 1,v-2> states. Two photon degenerate Raman transitions couple these states, with a result of atomic population to be transferred to lower vibrational states with a simultaneous modification of the polarization. If the atoms are simultaneously polarized, for example by our standard optical pumping scheme described in I.4.1.b, the atoms are pumped again in a state with m_F=3 and lower v. The process is reinitialized and goes on until all atomic population is pumped in the |F =3,m_F= 3,v=0> absolute ground state of the system, which is a dark state and does not interact with the light.

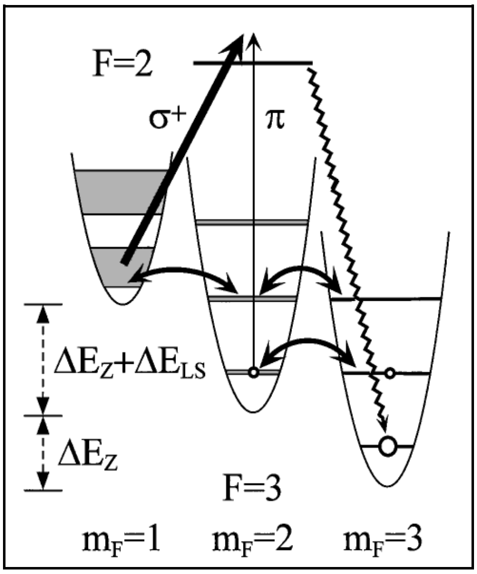

Fig. I.1.6: Operating principle of the RSC technique. A specific magnetic field brings states of vibrational quantum number v into degeneracy with state with vibrational quantum number v – 1. A sequence of Raman transitions between those degenerate states and optical pumping results to the transfer of the atomic population in the |F =3,m_F= 3,v=0> dark state.

The RSC technique demands for three different laser fields, one to provide with the optical lattice, one to induce the degenerate Raman transitions and one to perform polarization. However, the work presented in [Treut01] simplified considerably the technique, to the point that only two lasers are required. One is the polarization laser and another provides the lattice by being in far detuned with respect to the $6^2S_{1/2}$, F=3 → $6^2P_{3/2}$, F'=4 transition, and the Raman transitions shown in Fig. I.1.6 at the same time.

I.1.2.b. Evaporating Cooling

As mentioned above, laser cooling itself cannot lead to the production of a BEC. Perhaps the most serious limitation comes from the fact that for very high densities, like the ones that one needs to obtain a BEC, light that is scattered from one atom is very likely to be absorbed by another causing the atoms to repel each other. An additional reason for which laser cooling cannot lead to the production of BEC, is the fact that in a laser cooled sample, there are always excited atoms, which can collide with ground state atoms in an inelastic and thus exothermic collision.

The technique that carries the second half of the road to condensation is evaporating cooling. It consists of the selective removal of the most energetic (hottest) atoms from the atomic sample and thus lowering the overall temperature, and relies upon elastic collisions in order to bring the system to a new equilibrium.

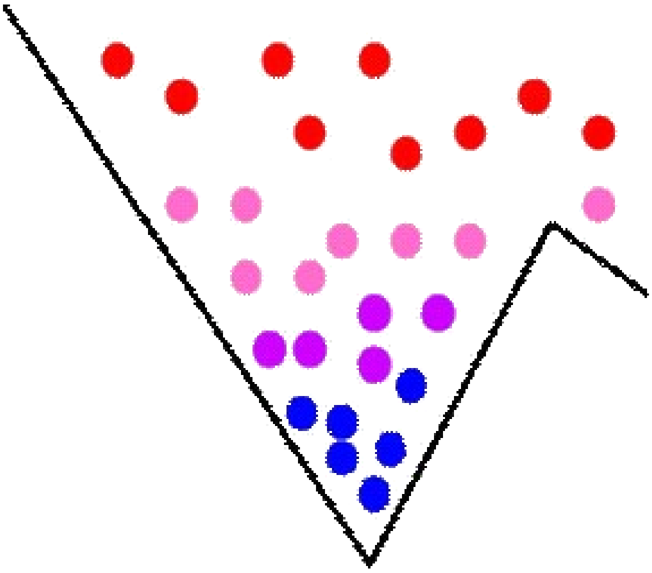

Fig.I.1.7: Schematic representation of the evaporating cooling process. As the trapping barrier is lowered the hottest atoms escape the trap leaving the sample to re-thermalize in a lower temperature.

Evaporation can be realized in any conservative trap. We can choose as example the very simple case of a quadrupole magnetic trap, which is realized with two coils in an anti-Helmholtz configuration, as the ones used to produce the magnetic field of the MOT described in the previous paragraph. Simple quadrupole traps are rarely used in condensation experiments. The reason is that in the center of such a trap, the field becomes zero, which results to spin flipping and atom loss (the so called Majorana losses). Usually in BEC experiments more complicated traps are used, like the Ioffe-Pritchard trap or the Time Averaged Potential (TOP) traps, which manage to create trapping potentials without areas of zero field, and thus without Majorana losses.

Spin flips lead to atom loss, since not all the angular momentum species can be trapped by a magnetic potential. Such a potential can trap only atoms in particular angular momentum projection states, while which state is trapped and which not depends on the atomic species. The condition is that the particular state has to increase its energy with increasing magnetic field, to be a 'low-field seeker'. For the cesium $^6S_{1/2}$ electronic state in particular, such states are the states with negative *m*. High-field seekers like the absolute ground state $F = 3$, $M_F = 3$ of Cs, cannot be magnetically trapped [Wing84]. Such atoms decrease their energy with increasing magnetic field, and thus would be repelled by a local minimum of magnetic field. Thus, if one can trap Cs atoms their $F = 3$, $M_F = -3$ low-field seeking state, he can remove them by exciting them to the high-field seeking $F = 3$, M_F

= 3, for example by means of RF fields. Furthermore, as the coldest atoms are closer to the trap's center, and in lower magnetic field, their energy levels lie somehow lower than the ones of the hottest atoms. Thus, in different RF frequencies, atoms of different temperature can be excited and removed from the trap. Such a technique is often called as an 'RF knife', which one can use to 'cut' the hottest part of the atomic sample's temperature distribution schematically viewed in Fig.I.1.7. This technique has been used for the realization of the pioneering BEC experiments and remains today the most commonly used.

Evaporation can be realized in more types of traps, like the optical dipole traps. Dipole traps are becoming very popular, since they can reduce considerably the loading time. Additionally, dipole traps can be used to trap high field seekers if necessary since, contrary to magnetic traps, they are not state selective. As a consequence, RF knifes can not be used with dipole traps and evaporation can be achieved simply by lowering the trapping potential, which for the case of dipole traps means to lower the power of the trapping laser. However, lowering the power of a dipole laser modifies the trapping potential making it less confining, which effects (slows down) the evaporation process. That's why it is better to hold in mind the magnetic trap picture for the discussion of the evaporation cooling in this paragraph; we will return to evaporation in dipole traps in the chapter I.2. where our approach to evaporation is discussed.

I.1.3. The cesium atom: characteristics and particular interest

Cesium is one of the most studied elements in atomic physics, especially because the SI standard for the definition of the second is based in one of its transitions. The isotope ^{133}Cs, is the only one that is stable, and it is the heaviest stable alkali atom. The structure of the first electronic states, between which the transitions that are used in the laser cooling are performed, are shown in the Fig.I.1.8. The transition from the ground $6^2S_{1/2}$ state and the $6^2P_{3/2}$ (D2 line) is employed for laser cooling and has a natural line width of 5.22 MHz. while the transition between the ground state and the $6^2P_{1/2}$ (D1 line) has a line width of 4.56 MHz. The hyperfine splitting of its ground state, which is used for the definition of the second, equals to 9.2 GHz, while the hyperfine splitting of the $6^2P_{3/2}$ state is 150-250 MHz [Steck02]. Cs was considered to be one of the primer candidates for the achievement of BEC, since its large weight resulted to vary small corresponding temperature for the one photon recoil limit (~200 nK), thus making it very suitable for laser cooling. Another reason for its popularity was the fact that the transitions that are needed for Cs cooling and repumping lies in the infrared region (~852 nm), and can be addressed with cost effective diode lasers.

For our group, as well as for many others, the particular interest on ultra-cold Cs, was due to the fact that this atom is suitable for the study of cold molecules. Indeed some of the first cold [Fio98] and ultra-cold [Herb03] molecule formation where reported with Cs dimers, and prepared with photoassociation and magneto-association respectively.

Photoassociation

Photoassociation is the process in which two atoms are colliding in the presence of a laser field. This laser can bring the atoms into resonance with a long range, but bound molecular state. Because the free-state thermal energy spread is negligibly small, this process leads to a well resolved free-bound absorption spectrum. This "photoassociation spectroscopy" is proving to be a powerful tool for the analysis of atomic interactions at long ranges. It has also shown that these long range molecules can relax to more closely bound states, thus leading to stable cold molecule formation [Fio99]. In our laboratory molecules have also being used to load a magnetic [Vanh02] or a dipole trap [Zahz06]. In a recent development that resulted the efforts of the experimental group of cold molecules in LAC, Cs dimers were optically pumped to their ground vibrational state [Vit08] with the use of shaped femtosecond lasers. Photoassociation is furtherly discussed in the second half of this thesis, were I describe the experiments for the creation and the manipulation of cold Cs molecules.

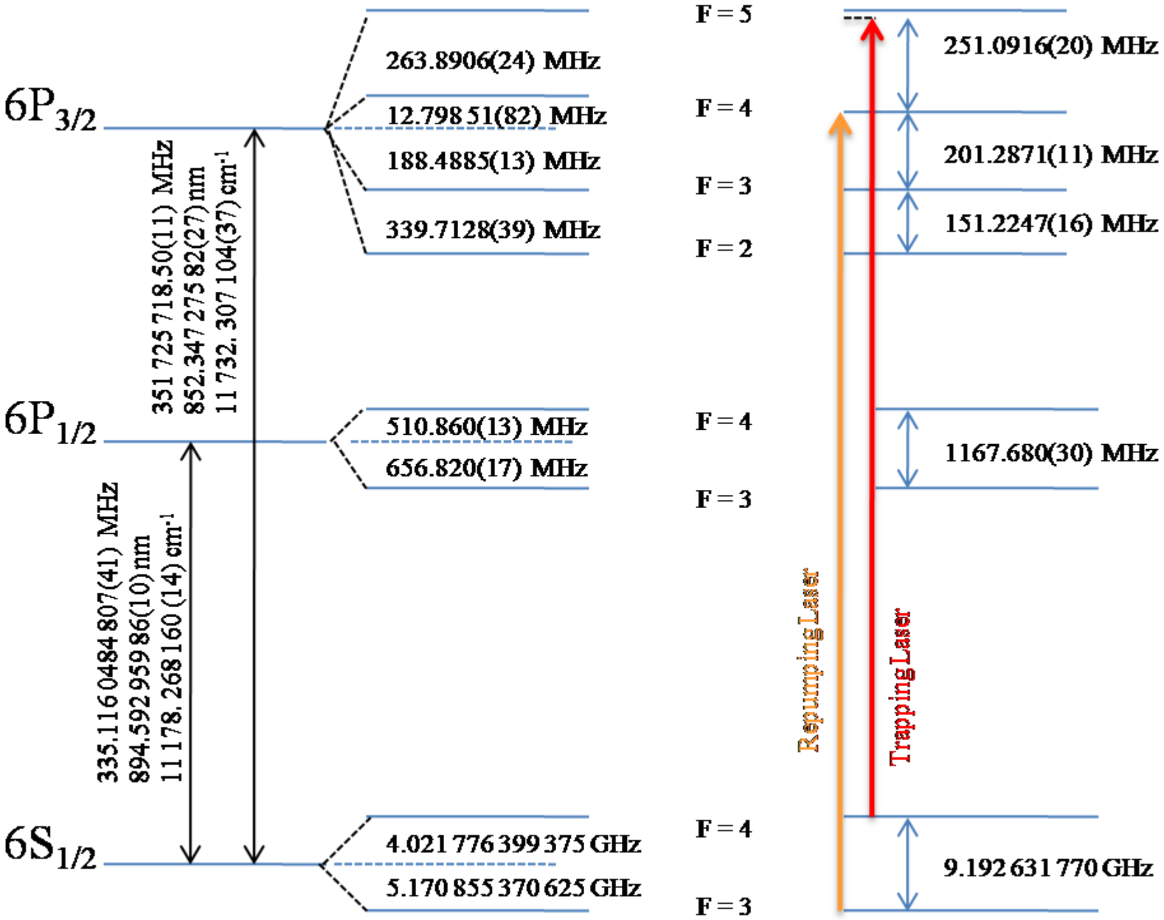

Fig.I.1.8: Diagram of the transitions of Cs atoms which are used for laser cooling and trapping.

Magneto-association

Cold molecules can be formed in ultra cold temperature with the use of magnetic field ramps exploiting the phenomenon known as *Feshbach* resonance [Ties93, Inou98]. The situation in which a Feshbach resonance occurs is schematically represented in Fig. I.1.9. The Feshbach resonance is the result of the coupling between a molecular state in an inter-atomic potential with the threshold of another. Out of the two molecular potentials shown in a), the one which has a threshold close to the collision energy of the free atoms is called the open channel; this potential would not support a bound state for these colliding atoms. A second molecular potential, called the closed channel, has a bind state in the vicinity of the threshold as well. As shown in b), these two molecular states are tuned differently with respect to external magnetic fields, a fact that can lead to the crossing of the two levels and to the production of bound molecular states for particular magnetic field values [Ing07].

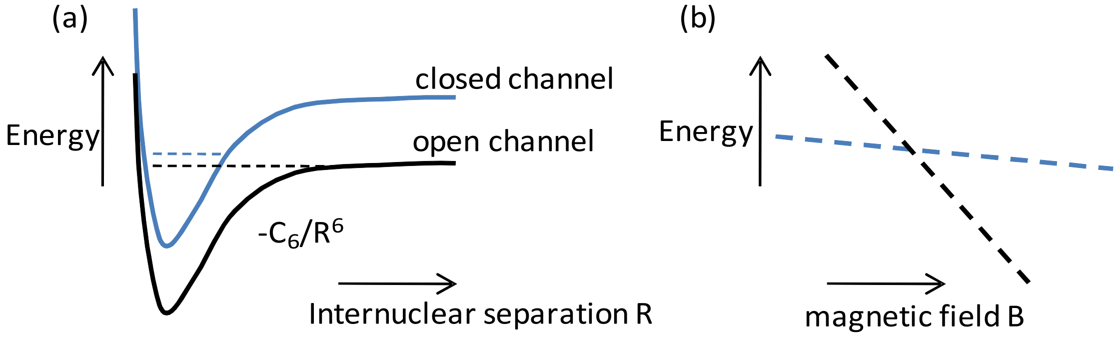

Fig. I.1.9: a) Feshbach resonances is the result of the interaction between a molecular state in an inter-atomic potential with the threshold of another. b) The bare molecular state of the closed channel tunes differently with a magnetic field than the open channel threshold, a fact that can lead to a crossing of the two levels.

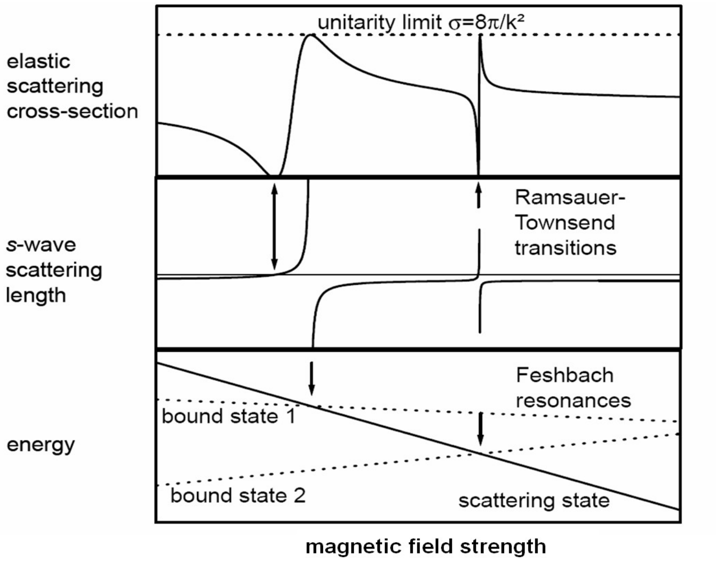

Fig.I.1.10: Dependence of the elastic scattering cross section, the scattering length and the energy of the emerging bound states for the case of Cs atoms. Image takes from [Chin01].

In the vicinity of a Feshbach resonance, the elastic collision cross section takes its extreme values, and moreover the scattering length diverges, as shown in Fig.I.1.10. When the scattering length takes positive values, the inter-atomic interactions are repulsive, and when it takes negative values they are attractive. This fact makes the Feshbach resonance useful not only for the creation of molecules, but for the tuning of the scattering length to values that are convenient for evaporation and for the production of a BEC. The ability to tune the interactions with the magnetic field, can lead to molecule formation under certain conditions [Herb03] and thus can change the nature of the trapped gas from fermionic to bosonic in the case of fermionic atoms [Zwie05].

Magneto-association can result to the production of triatomic molecules, since three colliding atoms can be brought to resonance to a bound trimer state, a case of which are the so-called *Efimov* states. Such a state has an infinite number of energy levels and exists in the absence of corresponding two-body bound states [Efi70, Niel99]. This particularity is schematically presented in Fig. I.1.11, where the binding energy of the trimer states is plotted against the inverse of the scattering length value. The shaded area corresponds to the scattering continuum for free atoms for negative scattering wave values, while it represents an atom and a dimer state for positive scattering length values. In 2006, evidence of Efimov state production where observed, again in ultra-cold cesium atoms [Krae06]. This evidence consisted of a giant recombination loss in conditions where the strength of the two body interaction was varied.

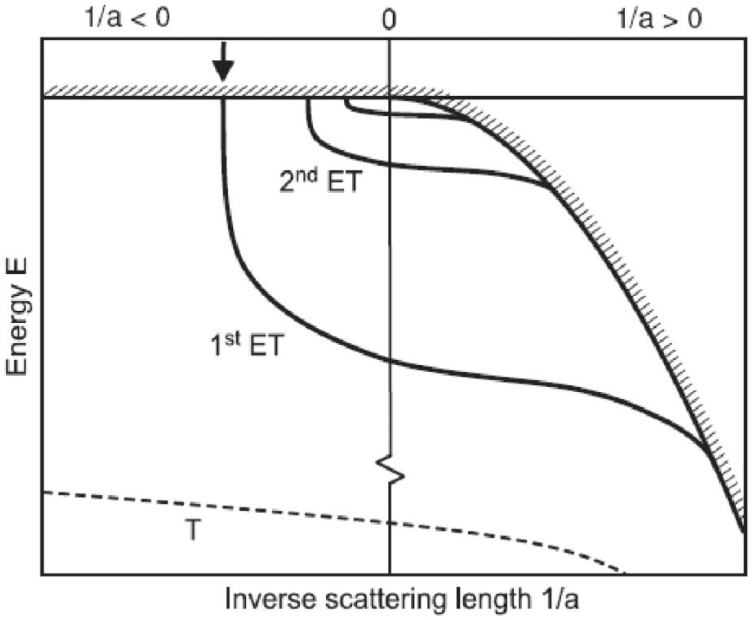

Fig. I.1.11: Binding energy of trimer molecules plotted against the inverse of the scattering length value. The shaded area corresponds to the scattering continuum for free atoms (a < 0) and for one atom and a dimer state (a > 0). The dashed line indicates the existence of a trimer state which does not interact with the scattering continuum and is not considered to be an Efimov state, which are noted as ET [Krae06].

However, these results raised a vivid discussion as a number of groups argued against this interpretation. The argumentation upon which this critics was based, was that the three body recombination rate that was the observable of this experiment does not depend to the magnetic field only by the dependence of the scattering upon the magnetic field, but also through the strongly varying properties of the comparatively tightly bound diatomic molecules [Lee07]. This exciting scientific dialog took place in a period when our team was preparing the BEC experiment in LAC. The fact that in the same period it was proposed theoretically that excited trimer states of Cs can be prepared in the vicinity of 800G [Lee07], contributed to our motivation.

I.1.4. Previous approaches to the Cs BEC

As described earlier, the convenient transitions of Cs in the IR region and its large weight made it one of the most promising elements for the achievement of a BEC. The transitions used in order to perform laser cooling to this element, are easily addressed with the use of laser diodes available in relatively low cost. Additionally, its large mass makes possible the achievement of very low temperatures with the use of laser cooling. Therefore it is not a surprise that many groups worldwide developed experiments to prepare Cs BECs, a route that was proved to be more difficult than expected, but which provided with particular knowledge for the properties of this element that finally led to the creation of a Cs BEC in 2002 [Web03]. In this paragraph I intent to give a comprehensive description of this route; instead of giving a review of each of the experiments realized, I chose to give a qualitative description divided in two categories: the approaches that involved evaporation in magnetic traps and the approaches that involved dipole traps or hybrid dipole-magnetic traps. In these two categories one finds the results of the work of various groups, sorted in a semi-chronological order as each experiment contributed with new important elements for the behavior of the Cs atoms in ultra cold temperatures.

I.1.4.a. The magnetic trap approaches

The early BEC experiments considered evaporation in magnetic traps with the use of the RF knife technique. Since the Cs atoms were initially prepared in the F = 4, M_F = 4 hyperfine states, it was upon the collision properties of this state that the success of these experiments was depended. Therefore, the fact that this state was found to exhibit spin relaxation rates much larger than expected, brought skepticism to the Cs community, as it imposed serious constrains for the trapping methods that could lead to BEC of Cs [Sod98, Gue98]. These large values of the spin relaxation rates were attributed to contribution from second-order spin-orbit interaction, which is generally unimportant for less heavy atoms [Leo98].

The next step for the magnetic trapping approach considered trapping of the F = 3 M_F = -3 state. The hope here was that the absence of hyperfine changing interactions in combination with an optimized evaporation ramp could be sufficient for the production of a BEC; and indeed a sufficient ratio of elastic to inelastic collision rates was predicted at certain magnetic field values [Leo00]. For the experiment sited in [Thom03], which was realized with the F = 3 M_F = -3 state however, there was another surprise. A behavior known as the *hydrodynamic regime* which becomes present in high densities and high values for the scattering length. In the hydrodynamic regime, collision cross sections become so large that atoms collide with each other more than once during one oscillation in the trapping potential. Usually, collisions can favor evaporating cooling, as long as they are elastic. In the hydrodynamic regime though, the atomic motion is somehow collective, a fact that does not favor thermalisation and slows down the evaporation process.

I.1.4.b. The optical dipole and hybrid approaches

Two body inelastic collisions can be avoided if one considers trapping of the F = 3, M_F = 3 state of Cs atoms. This is for Cs the absolute ground state, and thus, it cannot collide inelastically, since none of the colliding particles can loose energy in the collision. On the other hand, this state is not longer magnetically trappable since it is a high field seeker and static magnetic field maxima are forbidden [Wing84]. In fact, trapping of high field seekers with means of dynamic magnetic fields is possible and this has been demonstrated for the case of Cs atoms [Corn91]. But these traps, which create a local maximum by magnetically pushing the atoms with fast varying magnetic fields, did not achieve high enough densities for an evaporation process.

Trapping of Cs atoms in their absolute ground state is possible with the use of dipole trap, which as we said, are not state selective and can be used to trap various types of particles, from atoms to molecules [Zahz06]. Trapping the absolute ground state F = 3, M_F = 3 means that the external magnetic field can be used to tune the inter-atomic interactions, to avoid for example the hydrodynamic regime, since magnetic field depended collisions are now absent. However, an inherit disadvantage of dipole traps, comes from the fact that these traps are not state-selective and thus RF knifes cannot be used for evaporation. Evaporation can be achieved simply by reducing the power of the trapping laser, but this leads to reduction of the trapping potential's confinement and thus to a loss in the trap density. Since confinement is a very important parameter in optical dipole traps, these are usually realized in a crossed configuration, and trapping is realized in the intersection of the two beams. Depending on the choice for the wavelength of the dipole trap laser, it is possible that the potential out of the crossed region, the so called 'arms' of the trap, is deep enough to trap atoms. It is also possible, that atoms that are removed from the trap during the evaporation process, are guided back to it from the weaker, but non zero potential of the trap's arms. An optical dipole trap that was realized in ENS nicely confronted this problem by placing the trap's arms in the vertical plane, thus all atoms that escape the trapping potential are quickly carried away by gravity[Perr98, Boir96]. However, at the times were this experiment was active, the picture of Cs collision properties in the ultra-cold regime was still haze, and this experiment did not result to a Cs BEC.

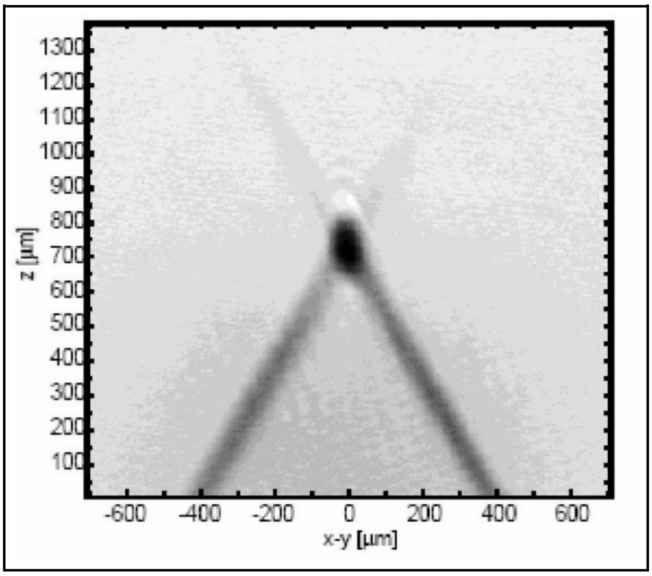

Fig. I.1.12: An optical dipole trap realized in [Perr98]. The vertical configuration of the dipole trap ensures that the atoms that are removed during the evaporation process are carried away by gravity.

A variation of optical dipole traps are the hybrid traps, where magnetic fields are combined to strong, off resonant laser fields. In these traps, magnetic fields are used to compensate gravity, that is to levitate the atoms, while dipole forces confine the atoms in the x-y plane [Bouss04, Hung08]. Dipole forces can compensate gravity, but magnetic levitation provides with some additional advantages. Since the magnetic dipole moment of each spin projection state is different, it can be used to selectively levitate one particular magnetic sub-level and thus ensure the 100% polarization in the sample. Additionally, one can remove atoms from such a trap by performing RF transitions to other magnetic sub-levels and achieve evaporation without lowering the dipole potential and reducing the trap's confinement. The Innsbruck group took advantage of both these properties, while the collision properties of Cs and especially the notorious three body recombination rate, where studied in detail and controlled to all possible extents with the use of magnetic fields. In their experiment, a sample of Cs atoms was cooled down with the use of Raman sideband cooling technique and used to load ~2 10^7 atoms in a temperature of ~1 µK inside a magnetically levitated optical trap. The subsequent evaporation enabled them to create samples of 25000 atoms in a temperature of 60 nK, which was still not enough for BEC. Condensation was achieved only after placing an additional, strongly focalized laser field to create a 'dimple' in their trap, in which the cold atoms where loaded from the magnetically levitated dipole trap during the evaporation process, and which could be further cooled down with plain evaporation. With this process, they were able to create a sample of ~6*10^5 atoms in a temperature of 30 nK, and prepare the first Cs BEC in a process of ~20 seconds [Web03b].

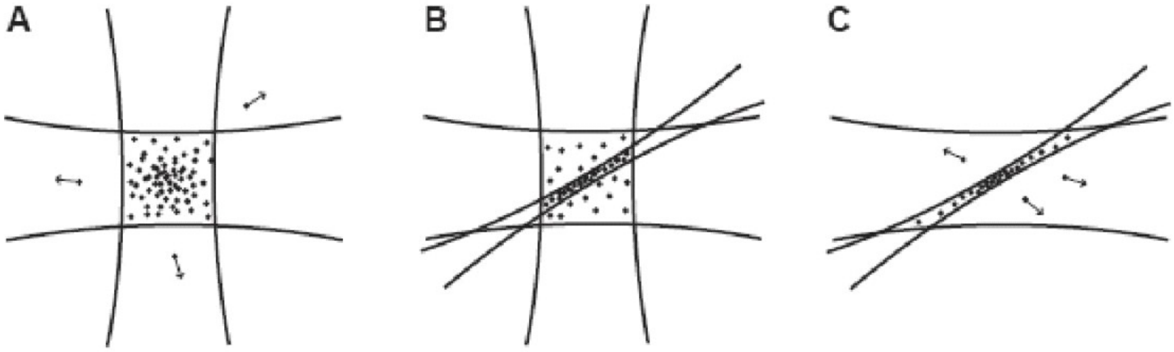

Fig. I.1.13: The Innsbruck experiment dipole trap configuration and the dimple. (A) Initially only the levitated dipole trap is present. The dimple is ramped up during the evaporation process (B) while the levitated trap is gradually removed (C). Figure adapted by [Web03b].

A similar, but improved experiment was performed in 2008 by a different group in Chicago [Hung08]. There, Raman sideband cooling was also employed to provide with a very cold, levitated dipole trap, but did not implement the same evaporation neither used the dimple trick. There, the magnetic field gradient that was used for levitation was increased gradually, in order to expel atoms from the trap region and thus perform evaporation. As shown in the left part of Fig. I.1.14, the combined dipole and magnetic levitation potential appears turned in the vertical direction with respect to the dipole trap potential. This method introduces only weak reductions in confinement strength over a large range of potentials and thus speeds up the evaporation process. An additional advantage of this method is that the atoms are expelled towards all directions (3D evaporation) once they are pulled out of the confinement region of the dipole trap. This runaway evaporation process is much more efficient and allowed for the condensation of Cs atoms in ~2 seconds.

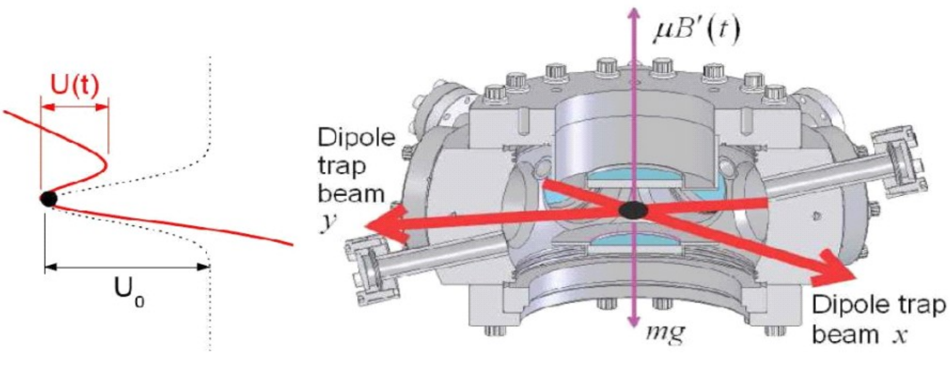

Fig. I.1.14: Configuration of the Cs BEC experiment described in [Hung08]. Right: The dipole trap geometry and the direction of gravity and levitating field in the experiment. Left: Potentials felt by the atoms in the vertical direction; the initial dipole potential (dotted line) and the combined potential of the dipole force and the levitating (red line). Figure adapted by [Hung08].

CHAPTER I2: OUR APPROACH TO THE BEC

I.2. OUR APPROACH TO THE BEC

In this chapter I indent to give a simple but yet precise description of the theoretical analysis upon which our strategy towards the Cs BEC was based. The general ideas of this approach, which has been supported by numeric simulations are reported in [Comp06]. The aim is the preparation of a not so cold, but very dense dipole trap, by loading it from a reservoir of cold atoms consisted of a magnetic trap. In such a dense dipole trap, rapid evaporation could bring the system to degeneracy by outrunning the various losses. The simulations showed that evaporation of a dense atomic sample is very efficient and can lead to the production of a BEC in few seconds, a performance that can be furthermore improved if the geometry of the dipole trap can be varied in real time. However, a summary of this work is essential for this thesis, since I will often refer to [Comp06], either explaining the purpose of the various utilities of the experimental set-up, either when I discuss the experimental results.

In the first paragraph I give the basic relations for the description of dipole traps. My goal is to introduce the relationships which describe the various process involved, as well as to point out how the design of the trap allows to control some of its basic geometrical characteristics. In I.3.4. , where out dipole trap is analyzed from the experimental perspective, we will see an additional utility which allows for the control of the dipole trap's geometrical characteristics.

The main results of [Comp06] which are going to be discussed here are the estimations of the loading of the dipole trap form the magnetic trap reservoir, and the description of the evaporation process. Thus, the two remaining paragraph address each of these issues. Since the part containing the experimental results of this thesis (chapter I.4.), deals mainly with the loading performance of our trap, it is necessary to outline the reasons why we expected such a loading process to be efficient. Finally, the theory discussed on this chapter is useful for the argumentation of chapter I.5. , where the reasons for the inconsistency observed between the theoretical prediction and the experimental realization are discussed.

The second main result of [Comp06] is the predictions on the evaporation process. However, since we never succeeded in preparing a dipole trap with the characteristics (mainly temperature and number of atoms) considered as a good starting point for evaporation in this publication, I do not attempt an analysis of the experimental results of evaporation based in [Comp06]. Instead, a phenomenological (and simpler) treatment is presented in the Annex I, which concerns mostly the an attempt to estimate various collisional losses by fitting the trap's lifetime. However, outlining the theoretical predictions on evaporation of [Comp06] is necessary in order to explain some of the evaporation strategies presented in the Annex.

I.2.1. Basic parameters and geometry of the dipole trap

Even though dipole traps are realized with relatively simple configurations of powerful cw lasers, their characteristics and behavior during evaporation can vary significantly, depending on the wavelength and the chosen geometry. In our experiment, the dipole trap is created with an IPG 100 Ytterbium fiber laser (maximum output power 100 W), but the geometrical characteristics that are needed for the evaporation are achieved with application of magnetic field gradients as well.

An electric field interacts with an atom due to the atoms electric moment, permanent or induced by the field. This can be true for static and for oscillating electric fields as the oscillating field of a laser beam. In this case, the potential of this interaction is

$$U_{dip}=\pm\frac{\langle p E\rangle}{2} \tag{2.1}$$

where p is the electric dipole moment, E the electric field (where the angled brackets stand for *average*). The sign depends on the detuning of the laser light; if the light is detuned at a frequency lower than the nearest transition (red detuned), then the atom minimizes its energy in the area where the electric field is maximized, and the interaction is attractive. In the opposite case of blue detuning the interaction is repulsive. The situation reminds the behavior of atoms in magnetic fields, where atoms either increase (low field seekers) either decrease (high field seekers) their energies with magnetic fields, only that here the creation of a local field maximum is allowed and easily realized. Most of the dipole traps are realized with red detuned lasers, that is they are based on attractive interactions. The electric dipole moment p is proportional to the electric field E

$$p(A) = a(\omega)E \tag{2.2}$$

and $a(\omega)$ is the atomic polarizability, and can be calculated in the context of the classical Lorentz model [Grim00]. The result for the dipole potential is

$$U_{dip}(x,y,z) = -\frac{3\pi c^2}{2\omega^3}\left(\frac{\Gamma}{\omega_0-\omega}+\frac{\Gamma}{\omega_0+\omega}\right)I(x,y,z) \tag{2.3}$$

where is Γ relaxation rate, ω_0 is the atomic transition frequency, ω the laser frequency and I the laser intensity. With x we label the direction in which the beam propagates; as the beam diverges the intensity depends on this dimension. In the case were the dipole trap is realized with a laser that is tuned close to an atomic resonance, as is the case for the traps that are used for Raman Sideband Cooling (see section I.4.4), the rotating wave approximation can be applied and the second part of the sum in the parenthesis of Eq. 2.3 can be omitted. For the case of the Far Off Resonance Traps (FORT) like the one used here, Eq. 2.3 is still valid, only that ω_0 is replaced by $\omega_{eff,}$ which is a 'weighted' average of the transitions that are mainly excited by the far off resonance laser field. Additionally, Γ is substituted by Γ_{eff}, the 'weighted' relaxation rate [Web03b].

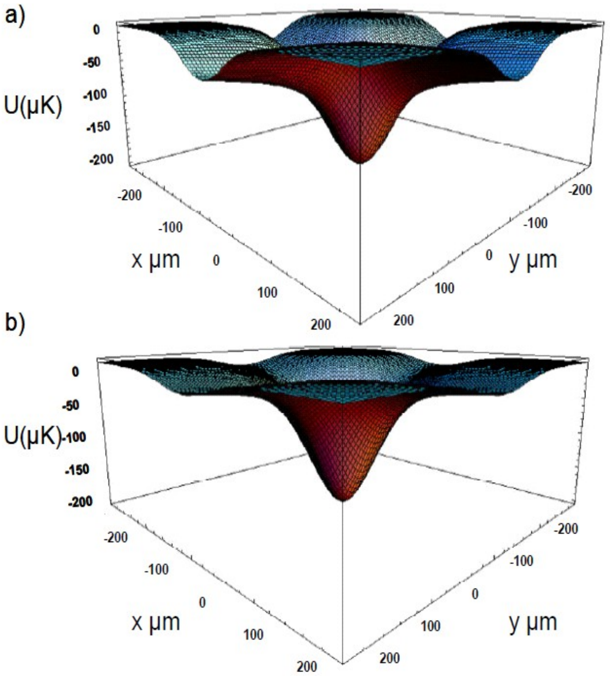

Fig. I.2.1: The potential of a crossed dipole trap of 50 μm realized either with a) an Ytterbium fiber laser or b) by a CO_2 laser. Note that in the second case the ‘arms’ (non-crossed region) of the trap are less profound.

As far as the frequency of the dipole trap is very far detuned with respect to the atomic transitions, the main difference between the use of a CO_2 laser ($\lambda = 10.6$ μm) that has been used in the previous BEC experiment [Web03b] and an Ytterbium fiber laser, is the different beam convergence, which can lead to different evaporation efficiency for the two traps. The dipole trap is usually realized in minimum waist region of a focalized beam, and when crossed dipole traps are discussed, the beams are crossed in this minimum waist region. Convergence becomes important for the evaporation, since it is essential that the dipole potential drops fast outside of the crossed region (arms). If this is not the case, then as the potential depth of the trap is lowered in order for the hottest atoms to be ejected from the trap, some of them are guided back to the trap by the potential that is created by the 'arms', and thus heat the sample. In Fig. I.2.1 we compare two dipole traps of the same potential depth and dimensions, one created with a CO_2 and one created with an Ytterbium fiber laser. We see the 'arms' of the trap for the case Ytterbium fiber laser are much more profound with respect to the crossed region, than the ones for the case of a CO_2 laser. This difference is due to the dependence of the laser waist evolution on the wavelength as this is given by the Gaussian formula

$$w(z)=w_0\sqrt{(1+(\frac{z}{z_R})^2)}\text{ where } z_R=\frac{\pi w_0^2}{\lambda}\text{ the Raleigh range} \tag{2.4}$$

In our experiment, the slow beam divergence is a disadvantage for the evaporation process, due to the possibility of the ejected atoms to be guided back to the trap region by the 'arms'. This problem is confronted with the use of magnetic field gradients. Initially the atoms are found in a low field seeking state, where a quadrupole magnetic field can be used in order to trap the atoms and create the reservoir. After the end of the loading process the atoms are polarized in a high field seeking state, such that the quadrupole field alone would expel them from its center. Thus, by having placed the crossed dipole trap in the center of a quadrupole magnetic field we create a potential which has a local minimum in the crossed region but is repulsive out of it. The combined potentials are shown in Fig. I.2.2.

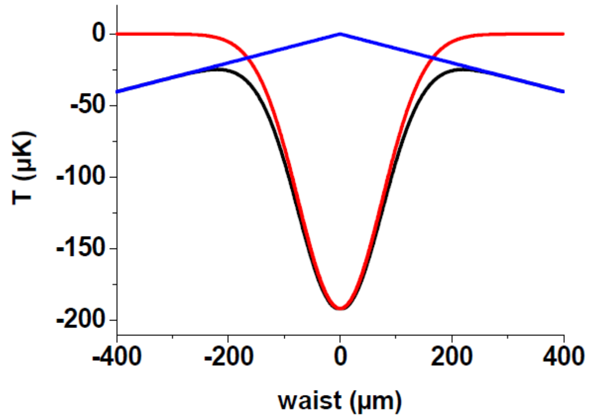

Fig. I.2.2: The trapping potential (black) which is a combination of the dipole (red) and the magnetic (blue) potential for atoms in the F = 3, m_F = 3 high field seeking state. Effects of gravity are not visible in this scale.

A quadrupole magnetic potential is given by

$$U_{magn}=m_F g_F \mu_B B \tag{2.5}$$

where g_F is the *Landé* factor which for the *F = 3* ground cesium state is calculated to be equal to - -¼ [Steck02]; μ_B is *Bohr's magneton*, m_F the spin projection and B the magnetic field. The magnetic field variation in the center of a quadrupole trap varies linearly, thus the potential becomes

$$U_{magn}(r)=-\frac{3}{4}\mu_B \nabla B\, r \tag{2.6}$$

where with ∇B we symbolize the magnetic field gradient. The total potential of the dipole trap is

$$U_{tot}(x,y,z) = -U_{dip}(z)\, e^{\frac{2x^2}{w_x^2} + \frac{2y^2}{w_y^2}} \qquad (2.7)$$

where with w_x, w_y we note the minimum waist for the x and y directions respectively. The geometry of the trap that results the combination of the dipole and the magnetic potential is given in Fig. I.2.2. The laser intensity is 100 Watt and the laser is focalized in 100 μm, while the quadrupole field gradient is 1 mT/cm.

I.2.2. Loading the dipole trap from an atomic reservoir

As previously explained, our strategy is based on a very dense and not so cold initial dipole trap, in which evaporation can be very rapid and can produce a BEC in some seconds, outrunning all relevant losses. Therefore, the first issue to be addressed in the analysis of this strategy is the feasibility of the loading of the dipole trap; that is if the dense dipole trap, which is the initial point of the evaporation, is possible to be prepared.

The loading process consists of superimposing the dipole trap with a larger atomic reservoir which can be maintained for relatively long periods of time (hundreds of μs). During this process, an atom that is moving in the reservoir can cross several times the trap region, and can end up trapped in the dipole potential after loosing kinetic energy due to collisions in this region with other atoms. The fact that this process can be realized for large periods of time, results for important probabilities for atom transfer and thus for increased loading efficiency. In the realization of the experiment, the role of the reservoir was played by several types of traps; in particular Compressed MOT (C-MOT), magnetic trap and Dark SPOT have been used as reservoirs while the experimental results are presented in the chapter I.4. . Nevertheless, magnetic traps are the largest available traps with more than 10^9 atoms at a temperature of ~100 μK directly transferred from a MOT. In the analysis shown here, we consider a magnetic trap as the reservoir without loss of generality, since the basic assumptions remain the same and since all collision losses can been taken into account.

The magnitudes that we need to calculate for the loading process are the number of transferred atoms (or the percentage of the atoms that are transferred on those who are initially found in the reservoir) and the temperature of the atoms in the dipole trap once the loading is finished (saturated), as well as an estimation of the loading time. The estimation of the final atom number and temperature is done with thermodynamic arguments. Initially, a first estimation is done without taking into account any collisional losses. After the production of this first results, the most relevant losses are identified and calculated. Finally, a new estimation is given on the atom number, which is the difference of the initial estimation (without losses) minus the losses calculated in this second step.

The description of the transfer process is done in a thermodynamical context. Usually, the process of loading a dipole trap (as well as many other kinds of manipulations) are done adiabatically. However, the authors of [Comp06] show that the temperature rise associated with non-adiabatic (rapid) loading is small for the usual 'reservoir' temperatures (~100 μK), while the experimental simplifications emerging from such an approach are important. Thus, we assume non-adiabatic loading, that is, we assume that the loading starts with a sudden superposition of the dipole potential to the magnetic trap.

Since no adiabaticity is assumed, the loading dynamics are governed by an equation which expresses conservation of energy. In a case where adiabaticity would be assumed, the starting point would be an equation which expresses entropy conservation. Conservation of energy for our system is expressed by Eq. 2.8

$$E(T_f) + NU_f = E'(T_i) \qquad (2.8)$$

where T_i and T_f are the initial and final temperatures, U_f is the final trapping potential depth and N the number of trapped atoms, while with E and E' we symbolize the energy of the trapped atoms after the end and before the start of the loading process. The term NU_f appears in Eq.2.8 in order to express the fact that the magnetic and the dipole trap do not have the same potential in their centers, since the magnetic potential is zero in the trap center r = 0 and the dipole potential in r = ∞. The energy per atom is given by

$$E(T)=\frac{F(T)+N_{magn}k_B T\,S(T)}{N_{magn}k_B} \tag{2.9}$$

where N_{magn} is the initial atom number in the magnetic trap, *S(T)* and *F(T)* are the entropy and the free Helmholtz energy. The entropy is calculated according to

$$S(T)=\frac{F(T+\delta T)-F(T-\delta T)}{2\delta T\,N_{magn}k_B T} \tag{2.10}$$

where with δT is an infinitesimal temperature modification (in this simulation, this temperature modification equals to 10^{-2} times the initial temperature in the magnetic trap). The free Helmholtz energy is given by

$$F(T)=N_{magn}k_B T(\log(D(T))-1) \tag{2.11}$$

where *D(T)* is the temperature depended phase space density defined as

$$D(T)=\frac{N}{Z(T)} \tag{2.12}$$

The phase-space density is defined in such way that a value of one corresponds to BEC. This is intuitively close to the picture discussed in the introduction chapter, and implies that the point in which the de Broglie wavelength is in the same order of magnitude as the inter-atomic distances has been reached. *Z(T)* is the partition function defined here as

$$Z(T)=\lambda_{dB}(T)^{-3}\int_0^{\infty}4\pi r^2 e^{\frac{U(r)-U(0)}{k_B T}}\,\partial r \tag{2.13}$$

where *U(r)* is here the combined magnetic (reservoir) and dipole potential. More strictly, this potential has a dependence on both the laser intensity and the magnetic field gradient, so that

$$U=U(r,I,\nabla B)\rightarrow U_{\mathrm{in}}=U(r,0,\nabla B) \tag{2.14}$$

A first characterization of the loading process, without taking into account the possible losses is done by numerical computation of the temperature from Eq. 2.8 and from integration of the density from Eq. 2.12 (the integration is done until *r* equals to 100 times the laser waist). The results of the are shown in Fig. I.2.3. The initial temperature for the atoms in the reservoir (magnetic trap) is 150 μK. In this figures, the reservoir loading seems like an excellent scenario, especially because of the very optimistic phase space densities that it predicts for the loading of small (~50 μm) traps. These scenarios are not yet realistic, since there are many types of losses have that have not yet been included. Traps of size smaller than 50 μm are not shown here, even if it seems that this model predicts very good results for small traps; the reason is that the image created for tight traps is going to be reversed as soon as we take into consideration the various losses associated with the loading process and in particularly the hydrodynamical regime, and show that traps of small dimensions (<90 μm) are indeed very bad candidates for this loading process.

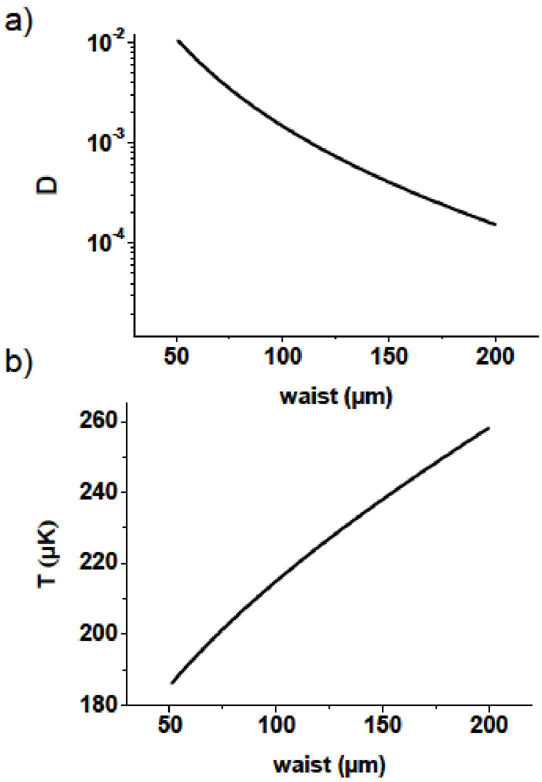

Fig. I.2.3: The dependence on the final atom number (a) and final temperature (b) on the dipole trap's waist during the loading process. The atoms in the reservoir have an initial temperature of 150 μK and the dipole laser total power is 100 W.

In order to study the dynamics during the loading process we make some assumptions that allow us to work with clarity, without loss of generality. One assumption is that the reservoir is much larger than the dipole trap, so that the reservoir stays unaffected in terms of atom number and temperature during the process. Thus, in the context of this study, we can write that $N_f << N_i$ and $T_f \sim T_i$, with the last assumption being not so far away from the prediction shown in figure 2.3. Another simplifying assumption is to consider the factor η, which is the ratio of the dipole trap's potential expressed in units of temperature on the temperature of the atoms, always larger than 4, since this simplifies the analysis and nevertheless this will be the favorable case for the subsequent study of the evaporation process.

The probability to be transferred to or ejected from the dipole trap depends on the energy change during a collision. For an atom that follows the Boltzmann distribution, the probability to acquire energy greater than $\eta k_B T$ after a collision is given by the approximate formula

$$\frac{p(\eta k_B T)}{(E_K)} = \frac{f(\eta)}{f(0)} = 1 + \frac{2e^{-\eta}\sqrt{\eta}}{\sqrt{\pi}} - \text{erf}\,(\sqrt{\eta}) \qquad (2.15)$$

where $E_K \approx 3/2\, k_B T$ the typical kinetic energy of the atom, *erf* the error function and

$$f(n) = \int_{n k_B T}^{+\infty} \sqrt{E'_K}\, e^{\frac{-E'_K}{k_B T}}\, d E'_K \qquad (2.16)$$

[Kett96]. For an atom to remain untrapped in the vicinity of the dipole trap, it has to have kinetic energy bigger than the depth of the dipole trap, so it's energy has to be bigger than $(\eta + 3/2) k_B T$. If a collision of two atoms is to end up with one of them trapped in the dipole potential, then one of the atoms has to have kinetic energy smaller than $\eta k_B T$ leaving the other atom with energy that equals to $(\eta + 3)k_B T$. The probability for such an event to occur equals to

$$p_t = p\left(\frac{(\eta+3)k_B T}{(\eta+3/2)k_B T}\right) \approx 0.5 \tag{2.17}$$

The reverse process, which is the ejection of a trapped atom after a collision is estimated with similar arguments to be ~0.15 [Comp06]. Since such a probability is considered to be very small the process is ignored. Actually, the process of collision between an atom of the reservoir and an atom trapped in the optical potential ends up with the trapping of the reservoir atom as well, with a high probability. This process is again omitted in order to keep this simulation conservative.

Once the probability of each type of collision is calculated, we can consider the atomic flux in the trap region. We note the number of atoms in the dimple region with a common magnitude N_d. In the initial times, it is the atoms from the reservoir that contribute to N_d as $N_d = N_i (r_d / l)^3$ and in the end of the loading process it is the atoms trapped in the dipole potential that contribute to it $N_d = N_f >> N_i (r_d / l)^3$, where r_d is the radius of the dipole and l the radius of the magnetic trap. The radius r_d can be approximately connected to the waist w_0 as $r_d = 2^{1/2} w_0$ while l is considered to be the radius in which 80% of the magnetically trapped atoms are found. The two characteristic times on which the loading depends on, are the oscillation period of the atoms in the magnetic trap t_{osc} and the temporal distance t_{coll} between two atomic collisions

$$t_{osc} = \sqrt{\frac{k_B T}{m l^2}} \text{ and } t_{coll} \approx \frac{1}{n_i \sigma \upsilon_i} \tag{2.18}$$

where n_i the density, σ the elastic collision cross section and υ_i the velocity of the atoms. We assume not to be in the hydrodynamic regime, which means that $t_{coll} > t_{osc}$. An atom oscillates in the reservoir on average t_{coll} / t_{osc} times before colliding with an atom, and the probability that an atom ends up trapped after this collision is given by $p_d \sim p_t r_d (n_d \sigma) t_{coll} / t_{osc}$ with n_d being the density in the dimple region. Thus, the number of atoms finally trapped, can be estimated as the product of the number of atoms passing the dimple area with this probability, leading to the differential equation $dN_d/dt \sim N_d \sigma N_i / 2 t_{osc} l^2$. As a final point of the loading we can consider the point where $N_f = n_{d,0} r_d^3$. With these, the loading time can be estimated to be

$$t_{load} = 2 t_{osc} \frac{l^2}{\sigma N_i} \ln\left(\frac{N_f}{N_i r_d^3 / l^3}\right) \approx 2 t_{coll} \ln\left(\frac{n_f}{n_i}\right) \tag{2.19}$$

The losses that are related to the loading process are the two and three body inelastic losses as well as the Majorana losses. In absence of resonant effects like Feshbach resonances, the heating associated with two body inelastic collisions is proportional to $B^{1/2}$ (due to the dependence of the energy of states on the magnetic field). Thus, the use of a quadrupole field for the realization of the magnetic trap which plays here the role of the reservoir is an advantage, since it provides a large area in its center where the field has small values. The two body inelastic rate for Cs is $K_2 = 410^{-11} B^{1/2}\, mT (\mu K)^{-0.78}$ cm^{3}s^{-1} [Gue98]and the equation for the rate can be written as

$$\dot{N}_2 = K_2 n_d^2 r_d^3 \text{ giving for the lost atoms } N_{2,f} \approx t_{coll} K_2 n_d^2 r_d^3 \tag{2.20}$$

Thus the lost fraction is $N_{2,f} / N_f \sim t_{coll} K_2 n_f$. Similarly for the three body inelastic loss (rate $f \sim L_3 n_d^2$), the lost fraction will be $N_{3,f} / N_f \sim (2/3)\, t_{coll} L_3 n_f^2$. As noted before, the Majorana loss consists of spin flips which occur when atoms pass from an area of small magnetic field, the *Majorana sphere*, with radius $r_{Maj} = (u_d / \mu_B)$ which is in the order of 1μm typically [Comp06], where u_d is the velocity of the atoms in the dimple. The number of spin flipped atoms during time Δt is $N_d (n_d / N_i t_{coll})(r_{Maj} / r_d)^2$ leading to an equation similar to Eq. 2.20 with the factor $(1/n_i\, t_{coll})\,(r_{Maj} / r_d)^2$ replacing K_2. Thus, the total number of lost atoms is thus estimated to be

$$N_{loss} = N_f \left(t_{coll} K_2 n_f + \frac{2}{3} t_{coll} L_3 n_f^2 + \frac{r_{Maj}^2 n_f}{r_d^2 n_i}\right) \tag{2.21}$$

With these considerations for the dynamics of the loading process we can have an estimate of the loading time and the number lost atoms. The final atom number is calculated with the thermodynamic arguments that do not take into account the dynamic losses; nevertheless, a more realistic final number of atoms can be estimated as $N_f - N_{loss}$. In Fig. I.2.4 we give an estimate for the loading time, the lost atom number and the final number of atoms, for a magnetic trap which contains ~ 10^8 atoms in a temperature of 150 μK and for a laser power of 100 Watts.

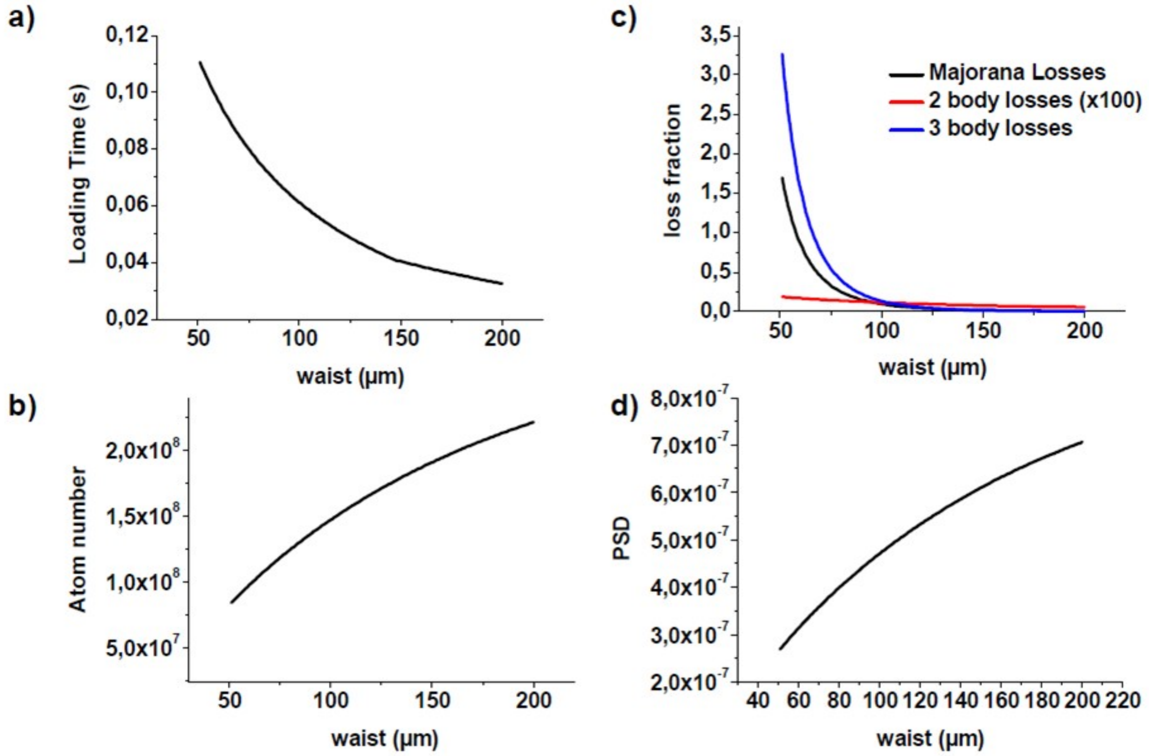

Fig. I.2.4: a) The loading time versus the waist of the dipole trap, b) The final number of atoms trapped in the dimple estimated as N_f,-$N_{loss.}$ c) The loss fraction of atoms due to the two body (red line) and three body (blue line) inelastic collisions as well as due to the Majorana losses (black line). The two body losses are calculated by a factor of 100 in order to be able to show them in the same scale. d) The final phase space density. This calculation is done with the value of α fixed at ~3000 α_0, which is a reasonable value for Cs. In [Comp06] a similar simulation for α ~ 300 (case of Rb) is given.

I.2.3. Evaporation in the dipole trap

The simulation of the evaporation process consists of the solution of two coupled differential equations for the number of atoms and for the energy. Each escaping particle is associated with a decrease in the total energy of the sample. On the other hand, loss of atoms reduces the density, and consequently, the phase space density. Since the objective of the evaporation process is to maximize the phase space density, the evaporation performance results on the relation between the phenomena that reduce the phase-space density, like the atom loss, and the ones that increase it, like the temperature decrease associated with the ejection of hot atoms.

Except from the variation in the atom number caused intentionally during the evaporation process, there are more phenomena on which the final atom number and temperature of the trap depends. These are principally losses related to inelastic collisions. Evaporation relies on elastic collisions in order to redistribute the temperature in the sample during the evaporation. During elastic collisions, the internal energy of the particles does not change, and high elastic collision rates usually favors evaporation. Inelastic collisions on the other hand change the internal energy of the atoms. Usually, atoms are transferred to a lower energy states after the collision, while the excess energy is passed to the system in the form of kinetic energy, thus heating the sample. The lower energy state in which the atoms are transferred after an inelastic collision can be other atomic states like in the case of collision-assisted spin relaxation. It can also be a molecular state, as is the case in the three body recombination, where two out of the three colliding atoms form a molecule and the third escapes after having acquire the reaction's excess energy in the form of kinetic energy.

In this paragraph I try to describe the evaporation process in the dense dipole trap with the use of coupled differential equations for the number of atoms and energy. Each related phenomena is inserted in these equations with its corresponding rate, and contributes either in the increase or the decrease of the energy of the atomic sample. For the sake of clarity the equations are given first and then each of the term's origin is discussed.

The equations for the evolution of the number of atoms and the energy are

$$\dot{N}=-[\Gamma_{ev}+\Gamma_{loss}+\Gamma_3]N \tag{2.22}$$

$$\dot{E}=-[\Gamma_{loss}+\Gamma_3]E-E_{ev}\Gamma_{ev}+E_{pot}\Gamma_{pot}+N\Gamma_{laser}k_BT_{recoil}+\Gamma_3(\frac{2}{3}\delta k_bT+k_BT_hf_{TBR}) \tag{2.23}$$

Starting from Eq.2.22, we see that the number of atoms is decreased at a rate that is the sum of the rates with which the number of atoms is decreased due to the evaporation Γ_{ev}, the three body recombination rate Γ_3 and an additional loss rate $\Gamma_{loss.}$ This final parameter includes both the losses due to collisions between the trapped atoms $\Gamma_{in}=K_2n_{av}$ (where n_{av} is the averaged density) and the background collision rate Γ_{bg}.

Equation 2.23, which describes the evolution of energy appears more complicated. Initially, we see the term proportional to the sum of Γ_3 and Γ_{loss} which describes the energy drop due to the decrease of the atom number. Another source of energy decrease is described by the term E_{ev}, which describes the energy decrease due to the intentionally removed atoms. The evaporation rate Γ_{ev} is related to the elastic collisions that thermalize the sample. The elastic collision rate is $\Gamma_{el}=n_0\sigma u_r$ where $u_r=4(k_BT/\pi m)^{1/2}$ is the average atomic velocity, and $\sigma=8\pi a2/(1+k^2a^2)$ the energy dependent cross section with a being the scattering length. The wavevector $k=mu_r/\hbar$ is modified as $k_{ev}^2=k^2\eta\pi/12$ in order to take into account the energy dependent scattering in the potential. The evaporation rate is related to the elastic collision rate trhough [Perr98]

$$\Gamma_{ev}=\frac{\Gamma_{el}e^{-\eta}}{\sqrt{2}}([\eta-(\frac{5}{2}+\delta)]\frac{e^{a_g}-1}{a_g}-1) \tag{2.24}$$

where α_g is the gravitational field written in temperature scale, equal to mgr_U/k_BT, with r_U being the distance from earth's center. In the actual calculation, the ratio Γ_{ev} is multiplied with the factor $f(p_{coll})$, which is an empirical smoothing function which corrects this rate to take into account the effects of the hydrodynamical regime.

The three body recombination leads to losses at a rate $\Gamma_3=L_3n^23^{-3/2}$ with n being here the density. The three body recombination rate L_3 is [Web03c]

$$L_3\approx 225\frac{\hbar}{m}\frac{a^4}{1+0.1(ka)^4} \tag{2.25}$$

The next two terms in Eq.2.23 describe the energy variation due to the trapping potential's decrease, and the heating rate due to photon absorption by the ultra-cold atoms. The potential during the evaporation process decreases the energy of the sample by $E_{pot}=(3/2)\eta k_BT$ at a rate $\Gamma=dU/dt$. Photon absorption is taken into account in the rate Γ_{laser}. The photon absorption rate is the imaginary part of the polarizability $a(\omega)$ and is equal to

$$\Gamma_{laser}=\frac{3}{2}\frac{\pi c^2}{\hbar\omega^3}(\frac{\Gamma}{\omega_0-\omega}+\frac{\Gamma}{\omega_0+\omega})^2I_{laser} \tag{2.26}$$

The final term in Eq. 2.23 describes the heating associate to three body recombination. An important aspect of the three body recombination is that it leads to “anti-evaporation”, the loss of the coldest atoms in the trap. Thus the average of many of these effects in an atomic sample leads to heating which equal to $2\delta k_BT/3$ per event. Three body recombination leads to the creation of molecules in highly excited rovibrational states. Since these molecules remain in the sample they can relax to a lower lying state after colliding with an atom, releasing their excess energy into the sample and causing a heating equal to k_BT_h . In order to take into account the fact that such a process will not heat the sample if $k_BT_h > \eta k_BT$, but will lead to the expulsion of the atom, we multiply this factor by a smoothing function $f_{TBR}=1-f(_{pcoll})[1-f(k_BT_h/\eta\ k_BT)]$.

With equations 2.22 and 2.23 we can simulate the evaporation process for a variety of conditions, as long as the hydrodynamic regime is avoided. One of the most important parameters to be defined is the value of the scattering length a since most of the collision losses depend on it. In the simulation shown in Fig. I.2.5, the value of the scattering length is considered to be $a \sim 2900a_0$, a value which is close to reality for Cs. Other parameters are the initial number of atoms ~ 10^8, initial temperature 300 μK, laser waist 100 μm and initial laser power 100 Watts. The power is decreased with the criteria to bring the value of η form the initial value of 9 to an asymptotically reached final value of 6.

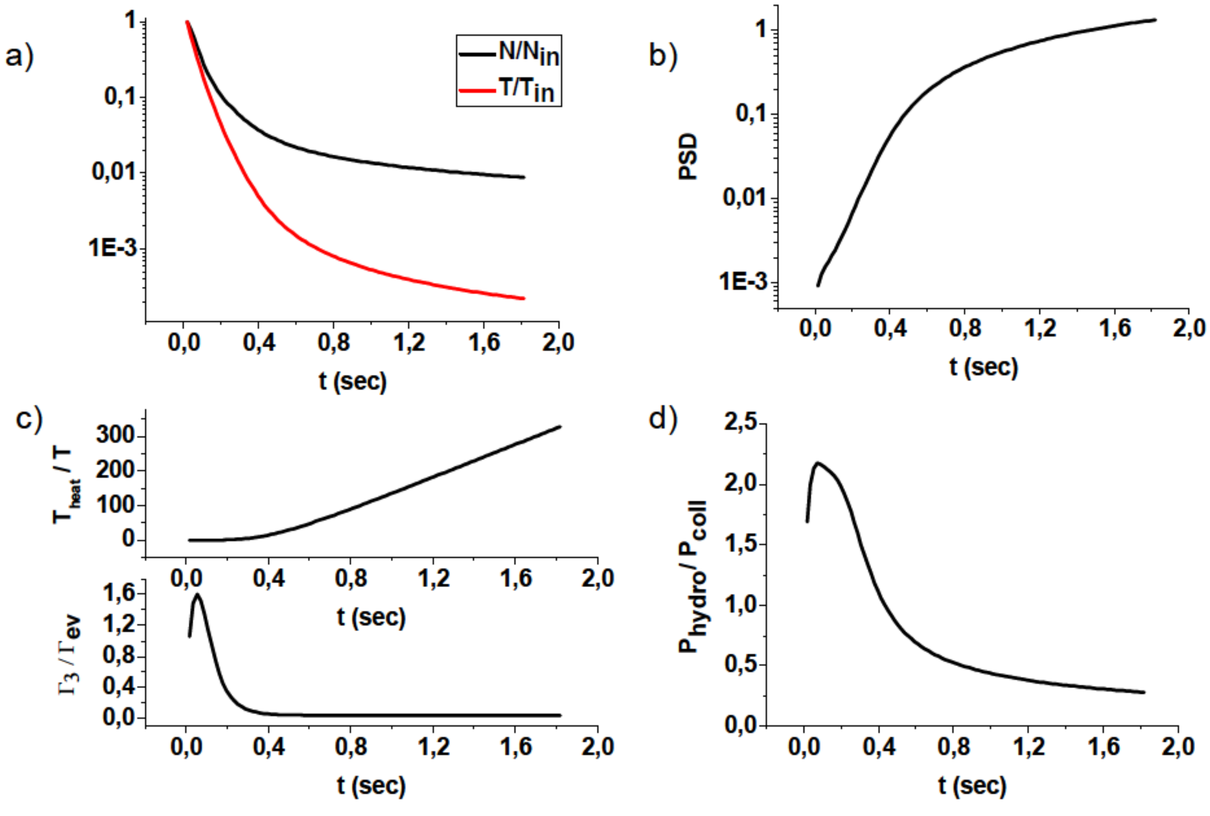

Fig. I.2.5: Simulation results for an evaporation process with constant waist and with η varying from 9 to 6. a) The ratio of number of atoms and temperature with respect to their initial values, b) the phase space density evolution, c) the ratio of three body recombination rate on the elastic collision rate and the associated heating and d) the possibility for collisions on the hydrodynamic regime.

As noticed before, the evaporation in dipole traps is realized by lowering the trapping potential by reducing the trapping laser’s power. This has as an effect that the potential’s shape is modified during the process and become less confining, a fact that reduces the efficiency of the evaporation. As the potential becomes less confining, the frequency of the oscillation of the particles in the trap is lowered, reducing the number of collision and making thermalisation slower. If this effect could be compensated, and the frequency of the trap could be kept constant, the evaporation could be more efficient. In Fig. I.2.6 we simulate a similar situation where the trap's frequency is kept constant during evaporation. Experimentally, a similar situation can be realized since a piezoelectric stage gives us the ability to modify the trapping laser's waist in real time (zoom).

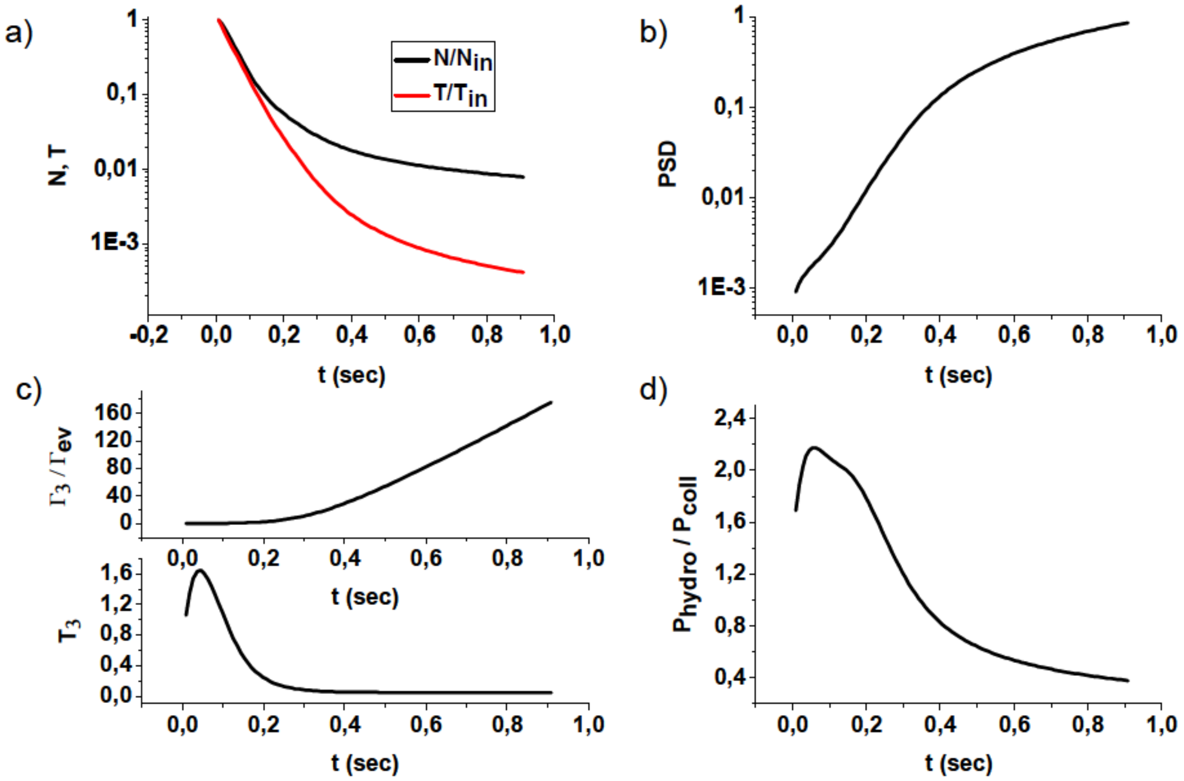

Fig. I.2.6: Simulation results for an evaporation process with constant waist and with η varying from 9 to 6 and with the oscillation frequency of the atoms in the trap kept constant a) The ratio of number of atoms and temperature on their initial values, b) the phase space density evolution, c) the ratio of three body recombination rate on the elastic collision rate and the associated heating and d) the possibility for collisions on the hydrodynamic regime.

I.2.4. Conclusion

In this chapter I have discussed the theoretical proposal upon which our approach to the preparation of a Cs BEC was based. The proposition is reported and explained in detail in [Comp06]. This work can be divided in two parts: one concerning the loading method, which can provide with a not so cold but very dense atomic sample trapped in a dipole potential, and one concerning evaporation of this dense atomic sample. An additional paragraph in which the use of magnetic fields in our experiment is explained is added in the beginning of this chapter.

The method proposed in [Comp06] and outlined here, has important advantages compared to the approach considered in the only experiment that was successful in the creation of a Cs BEC at that time [Web03b]. The most important advantage is the relative simplicity of the experimental set-up, which involves a magnetic trap instead of Raman-Sideband Cooling for the loading, and a simple crossed dipole trap instead of the magnetically levitated dipole trap and the 'dimple trick'. Moreover, the method proposed in [Comp06], predicted the preparation of a Cs in a few seconds, which is considerably improved in comparison to the ~20 seconds required in [Web03b]. Thus, the realization of an experiment based on the approach proposed in [Comp06] was very attractive, both economically and from the perspective's point of view.

CHAPTER I3: EXPERIMENTAL SET-UP

I.3. EXPERIMENTAL SET-UP

The experiments described in the first part of my thesis, were realized in Laboratoire Aimé Cotton, in a set up that was constructed several years ago with the aim to create a Cs BEC. The first experiments involved evaporation in hybrid traps [Hoa02, Bouss04]. This set up undertook subsequent modifications towards the experimental realization of the current approach of the crossed dipole trap. In the following chapter this set-up is presented, with a particular emphasis to those elements that were added for the current approach.

Initially I describe the vacuum set up and the basic mechanical components of the experiment. Then, I describe the laser system and the main traps we realized in the various phases of the experiment. In the first paragraph I describe the diode laser set up, the Magneto-Optical traps and the atom transfer from MOT 1 to MOT 2 with the use of a novel laser pushing system reported in [Dim02]. In the last paragraph I describe the dipole trap and the 'zoom' that allows for real time modification of its geometrical characteristics and the experimental test that verified its performance. The next big part of the experimental set up is the data acquisition systems. These are the fluorescence imaging, the absorption imaging as well as an additional imaging technique that was explored in the laboratory, and which is based on diffraction. Finally, I describe the new piloting system based in LabVIEW, which I developed based on a pre-existing program[1], and which replaced the old RealTimeLinux system.

I.3.1. Chamber architecture and vacuum system

The purpose of the vacuum system was to provide an environment where the losses due to background collisions is not a limiting factor for the dipole trap's loading and evaporation. The most usual configuration for the preparation of a BEC experiment involves a hot alkali source and a Zeeman slower. The Zeeman slower, which principle is described in the references [Phill82, Prod85], consists of the creation of a cold atomic beam starting by atoms that are ejected by an oven. This beam is slowed down by a counter-propagating beam and arrives in an ultra-high vacuum chamber where the atoms are captured in a MOT. However, this technique's implementation remains heavy and was not chosen on this set-up.

The system was consisted of a two MOT chambers connected to each other by a differential pumping tube. In one of them, a MOT is loaded directly by Cs vapor in room temperature and in a pressure of $\sim 10^{-8}$ mbar (MOT 1), and in the other a second MOT (MOT 2) is obtained in pressure of $\sim 10^{-11}$ mbar. MOT 2 is loaded with atoms coming from MOT 1 and the atom transfer is done with the use of a "pushing-guiding" laser system, which will be described in the following paragraph.

---

[1] The piloting program was based on the similar one developed and used by the Cold Atoms group of Laboratoire de Physique des Laser of Universite Paris 13

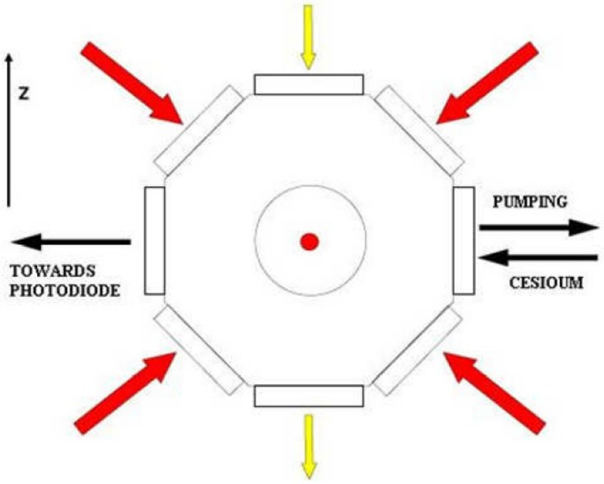

Fig. I.3.1: The higher chamber where MOT 1 is obtained. In red we see the MOT beams, the two counter-propagating pairs in a vertical level, while the superimposed horizontal beams are represented by the red point in the middle. The yellow beam represents the pushing-guiding beam which points towards the lower chamber. Figure adapted from [Stern08].

The higher chamber, in which MOT 1 is obtained, is consisted of an octagonal block of stainless steel equipped with 10 windows of 35 mm diameter. In Fig. I.3.1 we see the use of these different windows. The source of Cs consists of a grammar of Cs deposited in a small glass chamber connected to the main one, and the Cs pressure is controlled by a metal valve. The pumping, in the region of MOT1, is done by a Varian StarCell 45 l/s ionic pump. Estimation for the vacuum can be given by the pump's ionization current and by the gauge of an ultra high vacuum detector, and is in the order of 10^{-9} mbar.

The higher chamber is connected to the lowest by a differential pumping tube. This tube has a length of 18 cm and a conical form, such that its diameter is 3 mm in the peak and 6 mm in the base (see Figure 3.2). A metallic valve permits the isolation of the two chambers and to preserve the vacuum in the lower chamber when the experiment is stopped. The lower chamber is consisted of a square glass cell with a 1 cm side and it is pumped by an ionic pump Riber 140 l/s. Again, the pressure can be estimated by the ionization current of the pump down to 10^{-9} mbar and by the use of an ultra high vacuum detector down to 10^{-11} mbar. Estimation of even lower pressures can by done indirectly, by observing the effect of background collisions to a magnetic trap or a MOT.

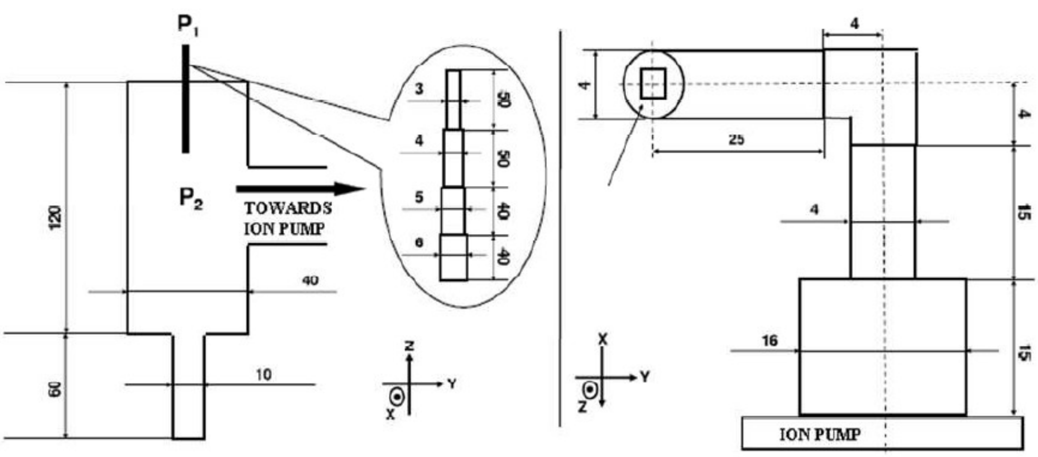

Fig. I.3.2: Left: The lower cell and the differential pumping tube, with the dimensions noted in mm. Right: Connection of the lower cell to the ion pump; here dimensions are in cm. Figure adapted from [Stern08].

With the configuration presented in Fig. I.3.2 we can estimate the vacuum that we can expect. The description is similar to the one of an electrical circuit for which pressure plays the role of the electric potential and the conductance of each of the tubes is played by capacitors of impedance 1/C placed in series with each other. In the molecular regime, where the mean free path between two atomic collisions is greater than the dimensions of the experiment, the conductance of a tube with a length l and a diameter d is given by

$$C=0.1\frac{\pi}{12}\upsilon\frac{d^3}{l}\,\text{with}\,\upsilon=\sqrt{\frac{8k_BT}{\pi m}} \tag{3.1}$$

the average thermal velocity of the background gas. A pump that is pumping in a pumping speed V can be considered as a conductance $C = V$ in units of *l/s* (litters per second). The total conductance of the differential pumping tube C_{tube} and of the total connection to the ionic pump C_{pump} can be calculated with the use of the dimensions showed in Figure 3.2 to be

$$\frac{1}{C_{tube}}=\frac{1}{K}\left(\frac{5}{0.3^3}+\frac{5}{0.4^3}+\frac{4}{0.5^3}+\frac{4}{0.6^3}\right) \tag{3.2}$$

$$\frac{1}{C_{pump}}=\frac{1}{K}\left(\frac{25}{4^3}+\frac{4+27\times4}{0.4^3}+\frac{15}{4^3}+\frac{15}{16^3}\right)+\frac{1}{145} \tag{3.3}$$

If we consider the Cs vapor as the only element responsible for the pressure of the upper chamber, for a temperature equal to 300K we find C_{tube} = 0.02 *l/s* and C_{pump} = 6.6 *l/s*. By the conservation of flux, which plays the role the intensity on the electric circuit analogy, we can estimate the expected pressure P_2

$$P_2=\frac{C_{tube}}{C_{tube}+C_{pump}}P_1\approx2.7\times10^{-11}\,\text{mbar} \tag{3.4}$$

We note that the choice of a pump of 145 *l/s* is not necessary since the result for the final pressure could be attained with a smaller pump as well.

I.3.2. Magneto-optic and dipole trap

I.3.2.a. Diode laser set-up and magneto-optical traps

This experiment involves five diode lasers that realize the trapping in two magneto-optical traps, the repumping, the polarization, the fluorescence and absorption imaging. The basic lasers are distributed Bragg reflection (DBR) lasers, and thus have the advantage that they can be tuned over a large area of frequencies by modulation of their driving current. The trapping lasers are amplified by injection on other laser diodes (SDL). An initial (Master) laser is provided by a DBR SDL 5712-H1 diode and is stabilized with means of saturated absorption spectroscopy in a Cs cell. In particularly the trapping laser is locked to the F = 4→ F' = 4 × F = 4→F' = 5 crossover corresponding to the $^6S_{1/2}$ to $^6P_{3/2}$ transition. Then, the Master laser radiation is divided in two parts and it is detuned further to the red by ~200 MHz by an acousto-optic modulator. It is inserted to the secondary (Slave) SDL 5422-H1 diode lasers by the polarizers contained in the Faraday isolators and then has its frequency shifter by acousto-optic modulators by 80 MHz. Those are the lasers that realize the trapping for the first (Master and Slave 1) and the second MOT (Master and Slave 2), while the repumper laser (SDL 5722- H1), which is not amplified, is divided to two parts and inserted to both MOTs. It is frequency locked to the F = 3→F' = 4 transition and then shifted to the red by 80 MHz by an acousto-optic modulator. Furthermore, a part of the repumper laser is used for the realization of the polarization by having its frequency shifted by 200 MHz by an acousto-optic modulator. A schematic representation of the laser set up is shown in the Fig. I.3.3. An additional laser without any amplification, not shown in the figure, is used to realize the absorption imaging, but we will refer to it when the data acquisition is going to be explained, in a following paragraph.

The current configuration is not the only one that can deliver with the laser radiation necessary for the realization of the magneto-optical traps. Actually, this set up was modified to the one shown in the Fig. I.3.4b, in order to be able to support the realization on the Raman sideband cooling technique. In this configuration, the initial Master radiation is shifted by an acousto-optic modulator by 185 MHz, then divided in two parts and shifted by ~80 MHZ and used to realize trapping for the MOT 1 and 2. Of course, the repumper set-up was not modified for this process.

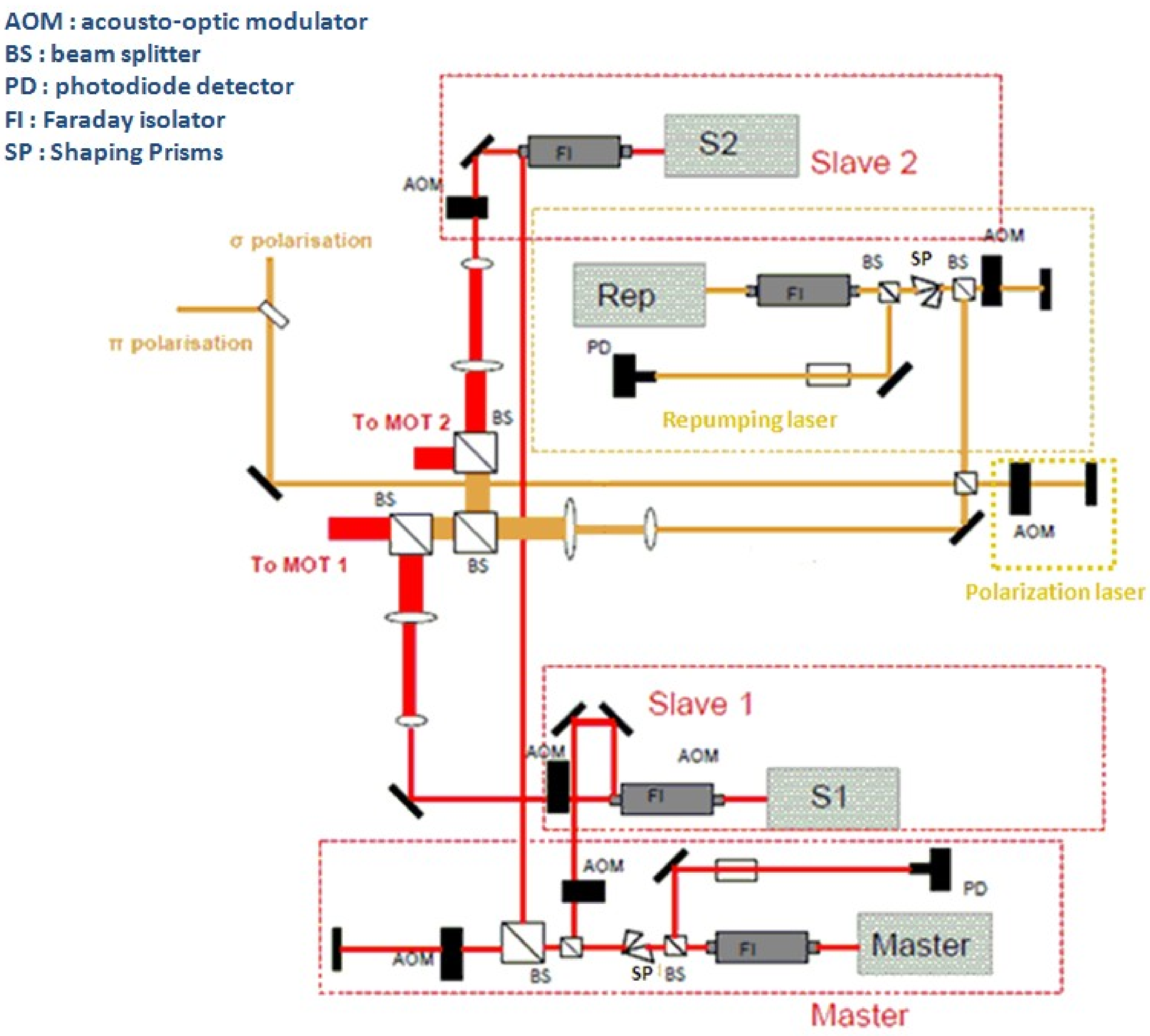

Fig. I.3.3: Schematic representation of the diode laser diagram; see text for details.

The radiation delivered by this laser configuration, is combined with quadrupole magnetic fields to realize the magneto-optical traps. The quadrupole fields are realized simply by inserting current into two circular coils in a counter-propagating fashion (anti-Helmoltz configuration). The opposite, co-propagating configuration is used in order to deliver the bias magnetic field that is used to modulate the scattering properties of the Cs atoms by bringing the system in the vicinity of a Feshbach configuration (Feshbach field). In addition, a Helmoltz configuration field is added in each Cartesian direction in both MOTs in order to compensate stray magnetic fields. This configuration allows for the rapid collection of ~10^9 atoms in the first MOT, and the collection of 10^8 atoms in the second MOT, after a second of loading.

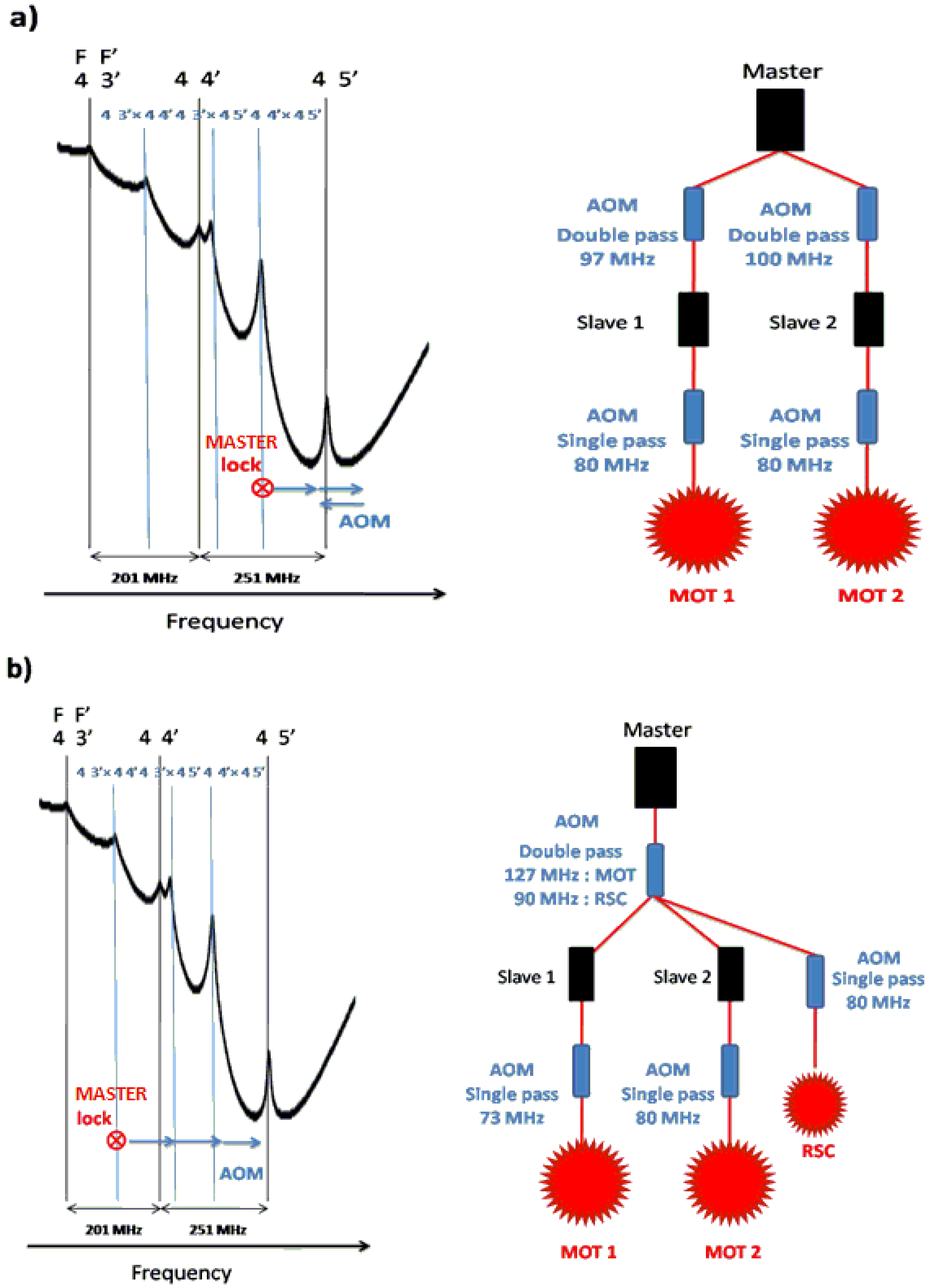

Fig. I.3.4: Two different configurations for the trapping lasers; (a) Initial laser configuration and (b) configuration used for the realization of Raman Sideband Cooling (RSC).

I.3.2.b. Atom transfer and pushing beam

The laser set up that was described in the previous paragraph allows for the preparation of two different magneto-optical traps, in different conditions of pressure. The sufficiently high Cs vapor pressure allows to directly collecting the Cs atoms in a MOT without the use of a dispenser. This of course, imposes that this MOT is created in a non ultra high vacuum enviroment (10^{-10} – 10^{-11} mbar) but rather in high vacuum (10^{-7} in our case). Since the collisions in such an environment would prohibit the preparation of a sufficiently cold sample, the atoms have to be transferred to ultra high vacuum. This in our case is achieved with the use of a "pushing" laser beam that transfers the atoms to a different chamber, which is connected to the first one by a differential pumping tube and where ultra high vacuum is maintained. The Fig. I.3.5 gives a schematic representation of the vacuum system.

The atoms transfer is realized with the use of a pushing beam which is different from the most widely used resonant pushing beams [Roos02], where the pushing beam is a part of the trapping beam. In our case, the pushing beam is much more detuned to the red and much more intense, thus it is able to push via the radiation pressure force and to guide via the dipole force the atoms. The dependence of the transfer efficiency to the detuning and the power is shown in the Fig. I.3.6 and an optimum performance is achieved for a power of ~40 mW and for a detuning of ~1500 MHz from the $F = 4 \rightarrow F' = 5$ transition. As we see in the figure, for those conditions, the transfer efficiency dependence on the detuning slightly varies for a wide range of frequencies. This 'plateau' makes the system less sensitive to detuning, thus the laser needs not to be frequency locked. The pushing beam is focused after the MOT with a 2 m focal lens, and diverges sufficiently until reaching the second MOT, a fact that makes the system less sensitive to alignment [Dim02].

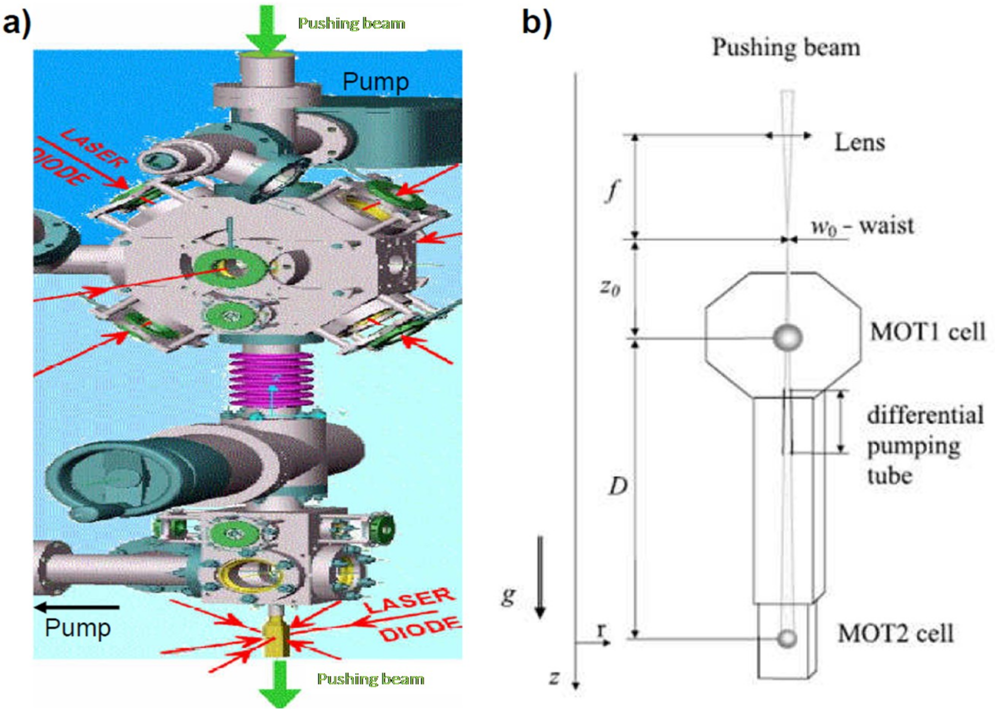

Fig. I.3.5: a) Schematic representation of the vacuum system. In the upper chamber where pressure of ~10^{-7} is maintained, Cs atoms are collected to MOT 1 directly from vapor pressure. The pushing beam transfers atoms through the differential pumping tube to the lower chamber, where pressure of ~10^{-11} is maintained. b) The pushing beam's geometrical characteristics with respect to the several components of the experiment.

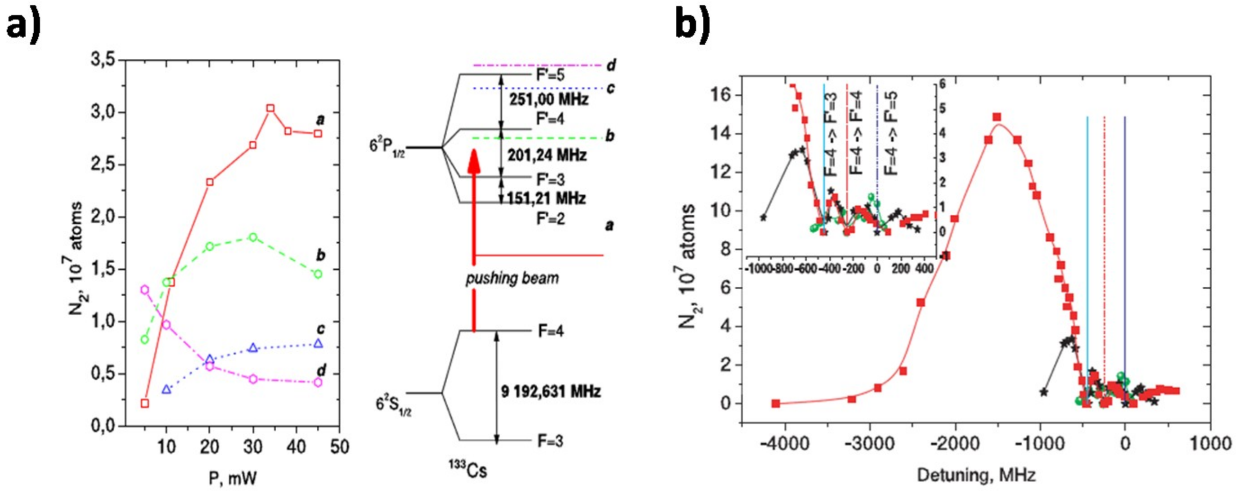

Fig. I.3.6: a) Atom transfer efficiency dependence on the laser power. The four different detunings chosen are shown on the right. b) Dependence on the detuning. The squares correspond to laser power of 46 mW, while the stars to 10 mW and the circles to 2 mW [Dim02].

I.3.3. Magnetic trap

For the realization of the magnetic trap, which has been used as a reservoir for the dipole trap loading, we have used a quadrupole filed available by the same coils that provide the magnetic field for the creation of the MOT 2. These coils are consisted of a cooper cable turned ~63 times giving an overall radius of 3 cm. These wires are supplied with a current up to 160 A, while they are cooled with both an open water circuit and a closed water circuit pumped by an old dye laser circulator. The distance *d* between those coils is adjustable and the maximum magnetic field gradient will depend on the distance *d* and the current *I*. The current is measured by an external Hall effect detector, and it's value can be modified by a circuit which contains a PID controller and a MOSFET switch. The MOSFET switch also gives the ability to modify the coil current in timescales of ~1 ms.

The number of captured atoms in the magnetic trap depends on the gradient and the initial atomic temperature, while the lifetime of the captured atoms depends on the losses due to the Majorana effec and due to the absorption of diffused photons. The Majorana losses for our case are estimated as $t \sim (m/h)l^3$ where t is the time in which the number of atoms in the magnetic trap equals to $1/e$ of the initial atom number and l the radius of the magnetic trap equal to ~100 μm in this case. The time t is estimated to be ~20s. In Fig. I.3.7 we show a characteristic measurement of the magnetic trap lifetime, where the number of atoms is measured for different times after the trap loading, with the use of the fluorescence imaging technique that we will discuss in the following paragraph. As we see, the time in which the initial number of atoms is dropped to the 1/e of its value is smaller than the Majorana lifetime which we estimate. The reasons for the limited lifetime in our magnetic trap can be searched in the quality of vacuum, in terms of particules and photons (absence). Absorption of photons resonant to the transitions F = 3 → F = 2, 3, 4 can lead to population of high field seeking states, and thus to atom loss in the magnetic trap. In order to avoid the presence of stray photons, we cover the MOT 2 chamber with black paper, and we place a mechanical shutter in front of each laser beam.

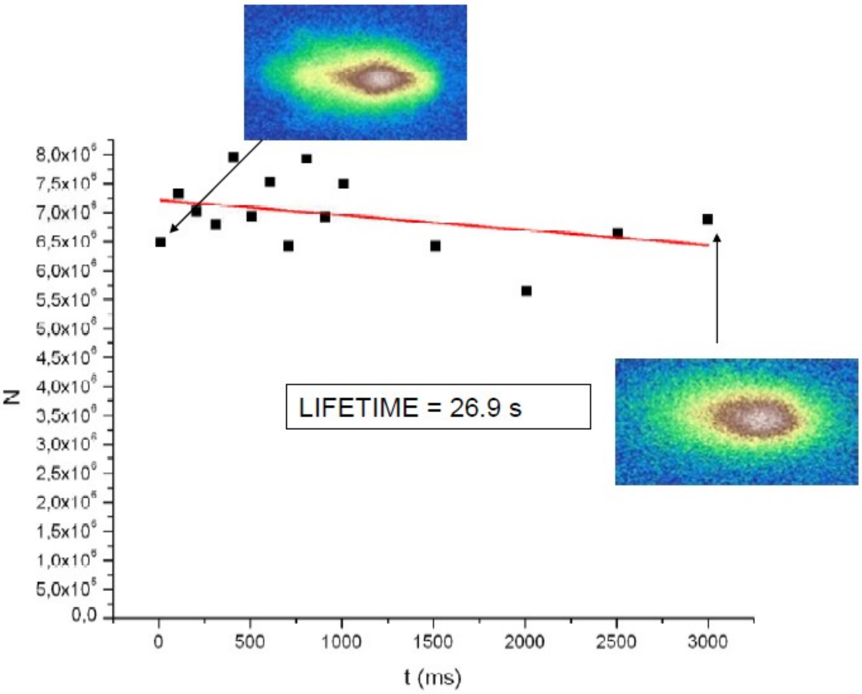

Fig. I.3.7: Measurement of the atom number in the magnetic trap at various times after the magnetic trap loading with the use of the fluorescence imaging technique. The time before the initial number of atoms is reduced to the 1/e of its initial value equals to 26.9 seconds.

I.3.4. Dipole trap laser and dynamic modification of its dimensions

The dipole trap is realized with the use of an 100 W IPG Ytterbium fiber Laser GmbH. This laser generates radiation in 1070 nm with a spectral bandwidth of 5 nm and can deliver up to 100 Watts of power in a beam waist of 2 mm. The laser power is controlled with an acousto-optic modulator (AOM), its power is monitored by a logarithmic photodiode and power-locked with the use of a home-made PID controlling system to avoid power fluctuations due to heating in the acousto-optic crystal. Finally, the laser beam is divided in two parts and is recombined in the MOT region to realize the crossed dipole trap. Additionally, the dimensions of the laser beam is controlled with the use of a M-663.465 PI piezoelectric translation stage which displaces one of the two lens of a telescope with a velocity up to 50 mm/s. A schematic representation of the dipole trap set-up is shown in Fig. I.3.8.

The initial waist of 2 mm is converted to a waist of 550 μm after passing a times 1/3.6 telescope realized with a 360 and a 100 mm lens, in order to optimize the AOM performance. For optimum performance of the AOM, the laser waist has to be well within a particular range of values. When a laser beam passes an AOM, a part of the beam is deflected to a small angle vertical to the direction of the incoming RF field. The relative power of the deflecting beam, which is the part of the beam used for the realization of the dipole trap, depends on the RF power and its frequency is the addition of the initial laser frequency and that of the RF. For the time-of- flight temperature measurements of the atoms trapped in the dipole trap, it is essential that the dipole field is cut sufficiently fast. This speed depends on the dimensions of the laser beam on the acousto-optic crystal, if this is too big, the time in which the RF field is diminished is important. On the other hand the dimensions of the beam cannot be too small, because in this case the power density on the acousto-optic crystal will be too large and the poor deflection efficiency would result to an out coming beam with a degraded spatial profile.

The laser waist modification is done with the use of the piezoelectric stage on which one of the two lenses of the telescope is mounted. This converging lens can move for 10 cm in a speed of 100 cm/s. The resulting dimensions are calculated and compared to the experimental measurement of the laser waist along the optical path. The distance after the lens in which the waist of the beam finds its minimum value is calculated according to the thin lens formula

$$\frac{1}{f}=\frac{1}{s_i+\frac{z_R^2}{s_i-f}}+\frac{1}{s_f} \tag{3.6}$$

where f is the lens focal lens distance, s_f is the focal distance and s_i is the is the distance of the previous focalization point of the, which is infinite for a collimated beam.

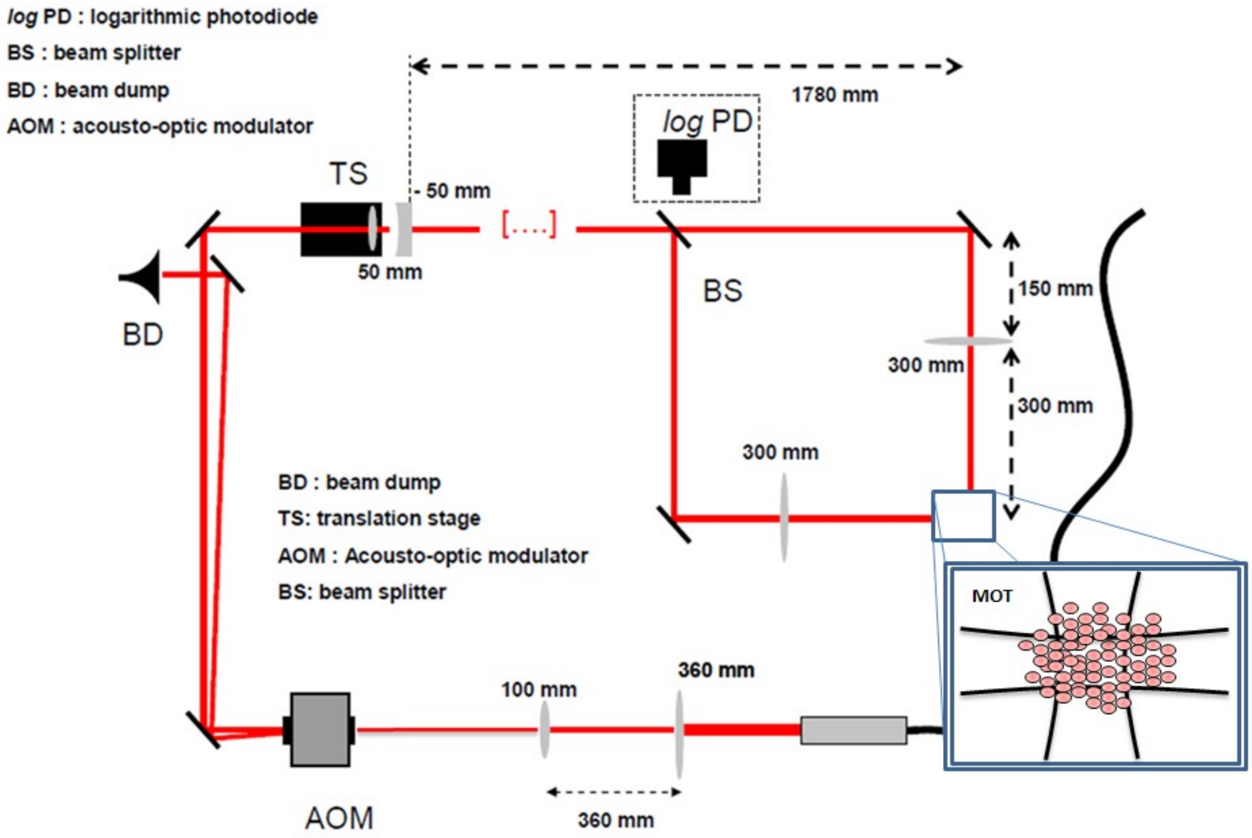

Fig. I.3.8: Schematic diagram of the dipole trap set-up showing the configuration and the relative distances between the various elements. The logarithmic photodiode is squared since it lies in a different level than the one shown here, and monitors the lasers intensity from the leakage of an intentionally placed mirror, non treated at 1070 nm.

With these formulas we can predict the waist evolution in the position where the trap is realized. Furthermore, we can compare the result of our calculation measurements of the waist realized with the “razor” method. This simple method consists of placing a power detector in the laser path, and using a razor placed in a micro metric stage to block gradually the beam. The waist of the laser will be the distance between the positions of the razor where the 16.4% and the 84,6% of the power is detected, a consequence of the Gaussian power distribution of the laser beam.

There exists a more sophisticated method for the determination of the dipole trap dimensions, via the determination of the frequencies of the atomic motion in the trap. Those depend on the traps dimensions as $f_{trap} = (4U_0/mw^2)^{1/2}$, where U_0 is the dipole potential and w the laser’s waist. These frequencies are determined with the use of the parametric excitation technique [Sav97]. In this method, after the dipole trap is loaded, the power of the dipole laser is modified in a harmonic fashion, and in a particular frequency. The loss of atoms in the dipole trap is maximized when the frequency of the dipole power modification matches the frequency of the atomic motion in the dipole trap. In Fig. I.3.9 we see the configuration used for the realization of the parametric excitation measurements. The power of the dipole laser is controlled by the RF power inserted in the AOM. Initially, we insert a constant power RF into the AOM so that the dipole trap is loaded. Then, the RF power is modulated harmonically for approximately half a ms. The number of atoms remaining in the dipole trap is estimated either with the use of the fluorescence or the absorption imaging. The modulation frequency of the RF power is changed and the measurement is repeated for frequencies ranging from some hundreds up to some thousands of Hz. A result of such a measurement is shown in Fig. I.3.10. In this measurement, the dipole laser power was equal to 12 W (6 W in each arm), and the measured frequency corresponds to a waist of 94.9 μm. The presence of a second, less deep resonance is due to the oscillation of the atoms to the vertical direction, and is not used for the measurement of the trap's dimensions.

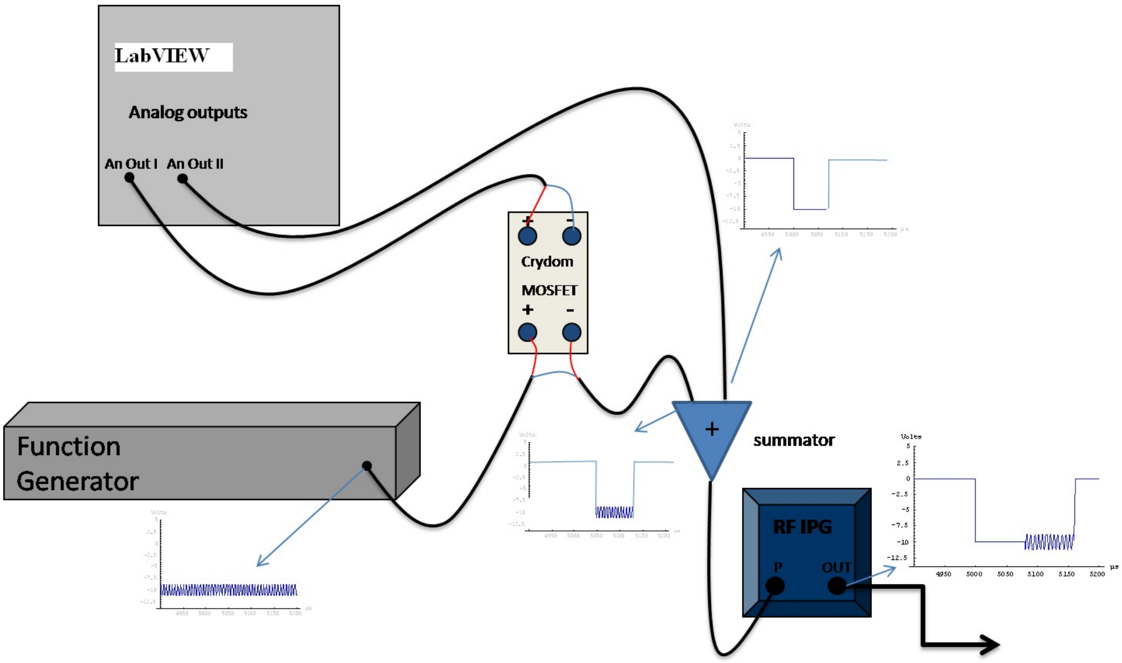

Fig. I.3.9: Configuration used for the parametric excitation measurements. A constant voltage that corresponds to a particular RF output power is combined to a harmonically modulated voltage provided by a function generator and is inserted to the RF driver of the dipole laser's AOM. The voltage that the RF driver ‘ sees' during the measure is shown in the inlet down and left.

The evolution of the waist alone is not sufficient for the calculation of the trap's dimensions, since this is not realized in the minimum waist, but in the intersection of the two beams, and those positions do not necessarily coincide. Actually, if the traps dimensions are to be modified with a system like the one described here, the minimum waist position will definitely be displaced. This is not necessary a disadvantage, and if properly taken into account, increases the range of possible trap dimensions that can be realized with a given translation stage. One point that has to be stressed is that when the trap loading takes place with a trap that has been realized with the laser beams crossed not in their minimum waist, the minimum waist must be positioned far away from the MOT (or whatever the trap that is used for the loading) so that no atoms are loaded to this minimum that could possibly interact with the trap during the evaporation process. In our experiments, usually the minimum laser waist lies out of the cell where the trapping takes place, so it is not possible to load any atoms on it. We also note that modification of a laser beams dimensions without displacing the minimum waist position is possible, but requires a complicated motion in more than one optic element and is not considered. The evolution of the laser waist along the laser's path and versus the piezoelectric stage's displacement (we refer to it as 'zoom position') is shown in Fig. I.3.11.

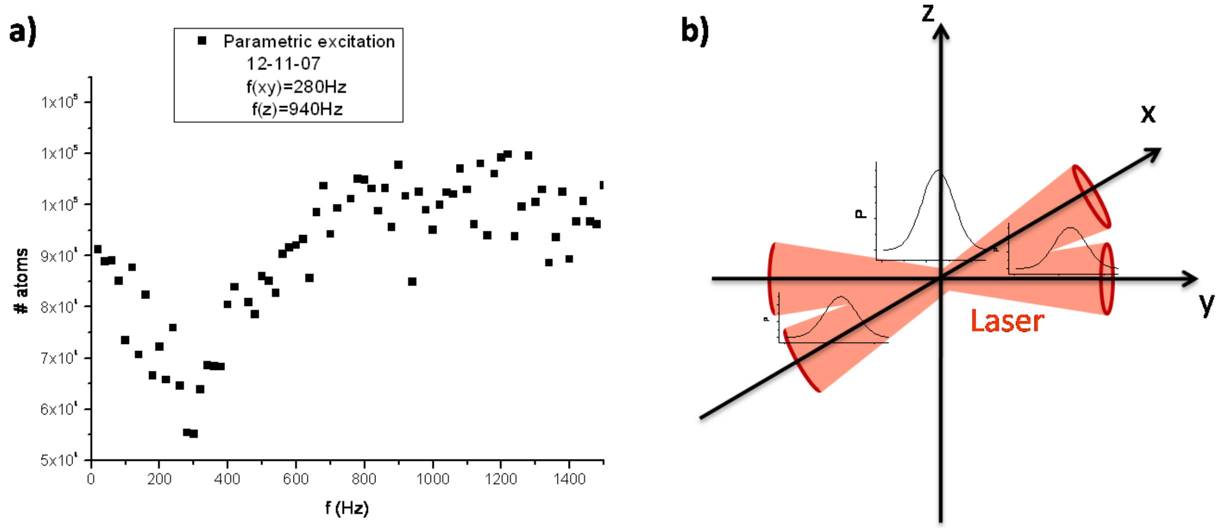

Fig. I.3.10: a) Measurement of the dipole trap's dimension with parametric excitation. In this measurement, the dipole laser power was equal to 12 W (6 W in each arm), and the measured frequency of 280 Hz corresponds to a waist of 94.9 μm. The presence of a second, less profound resonance at 940 Hz is due to the oscillation of the atoms to the vertical direction, and is not used for the measurement of the trap's dimensions. b) Dipole trap geometry. Note that in the x - y plane not both the beams are focused while in the z - x or z – y plane they are, a fact that causes the existence of two different atomic oscillation frequencies, here at 940 and 280 Hz.

An important element of the dipole trap compression is its stability during this process. Small misalignment of the beam out off the axis of the telescope lens motion can result to important displacements of the beam in the trap region. These displacements are actually impossible to be completely eliminated as 'perfect' alignment is impossible. These displacements are more important for larger distances between the zoom and the final position of the trap (~2 m in our case). The fact that the trap is realized relatively close the focus of the final lens (L3) helps, since the lens compensates those displacements to a large extent. The alignment becomes more feasible after placing the moving lens in a x-y-z mounting. What can be verified experimentally is that the possible displacements are significantly smaller than the lasers dimensions and the laser beams remain crossed in most of the zoom's range. This fact is in Fig. I.3.12 where images of the crossed dipole trap are acquired with absorption imaging, a technique which will be explained in the following paragraphs.

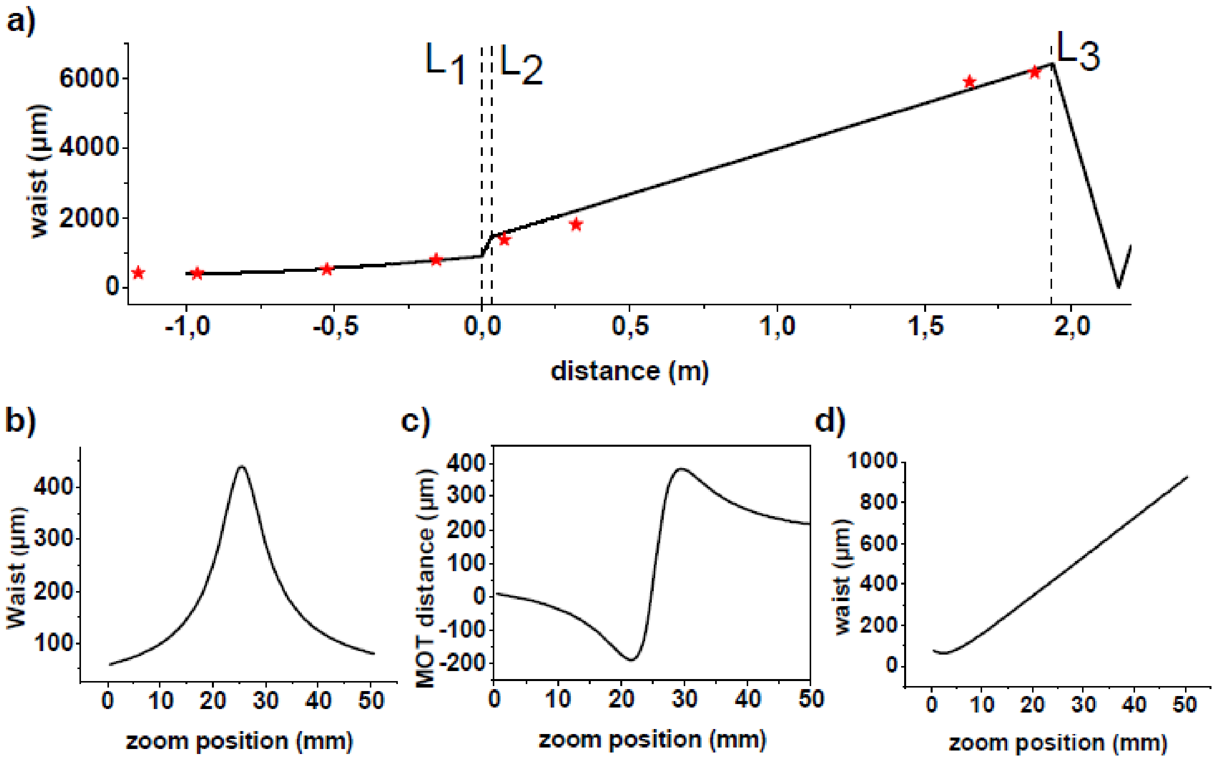

Fig. I.3.11: a) Evaluation of the laser waist along the laser path. Zero coincides with the position of the converging (moving) lens L1, while L2 is the diverging lens position L2 and L3 the position of the final lens (see figure 3.5). The stars correspond to measurements made with the 'razor' technique. b) Minimum waist dimensions versus zoom position c) minimum zoom position with respect to the position of the MOT and d) waist in the crossed beam position.

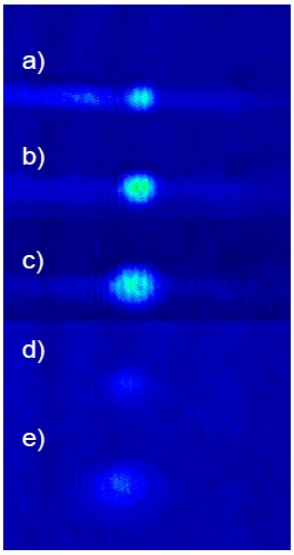

Fig. I.3.12: Absorption imaging pictures for several position of the translation stage at a) 25 mm, b) 30 mm c) 35 mm d) 40 mm and e) 45 mm. The size of the atomic cloud or the image contrast is not proportional to the trap's size since this depends on the number of atoms in the trap. In this point the trap loading is not optimized and it serves only for demonstrating the sufficient laser alignment.

I.3.5. Data acquisition and thermometry

In this experiment all data acquisition is done with the use of two different imaging techniques, the fluorescence and the absorption imaging techniques. The fluorescence imaging technique has the advantage of simplicity; it does not require any additional lasers to probe the atoms as they can be excited by the MOT lasers. Thus, the imaging system consist of a single lens and a CCD camera. Additionally, it has the ability to operate in a CW mode, providing with a feasible way to monitor the MOT. The fluorescence imaging technique though has the disadvantage to fail in the extraction of quantitative information when the atomic sample that is been monitored is optically thick. The absorption imaging technique is more complicated since it requires an additional laser beam of high quality, but delivers more precise measurements while its application is not restricted in the density of the sample. Finally, an additional imaging technique has been explored which is based in diffraction. Out of the techniques discussed here, it is the only one that is non-destructive. The particular interest that our group has in this technique, is that it does not require any repumping, a fact that makes it suitable to probe ultra cold molecules.

I.3.5.a. Fluorescence imaging and Time of Flight temperature determination

It is said that the fluorescence imaging technique is very simple to implement and it requires placing a converging lens between the camera and the MOT in a distance equal to its focal length. For the implementation of this technique we have used a Sony XC-8500CE CCD camera with a pixel resolution of 782 × 582 in an array with dimensions 8 × 8 μm^2. The same camera, operating in a CW mode allows for the continuous monitoring of the MOT which is used in the every day adjustments.

The camera simply collects the fluorescence of the atoms as those are excited by the trapping laser. For sufficient fluorescence imaging an atomic sample is illuminated for some ms (usually 2 ms), and since it is important for the quantitative result of the measurement that all the atoms undertake absorption – emission circles, they are illuminated by the repumper as well. The exact rate of diffused photons per time unit and per atom is given by the expression [Dal99]:

$$R_{Diff}=\frac{1}{N}\frac{\Gamma}{2}\int d^3\vec{r}\sum_{m_f,m'_f} n_{m_f}(\vec{r})\frac{C^2_{m_f,m'_f}\Omega^2_{tot}(\vec{r})/2}{\delta^2\Gamma^2/4+C^2_{m_f,m'_f}\Omega^2_{tot}(\vec{r})/2} \tag{3.7}$$

where N is the number of atoms in the atomic cloud, Γ the spontaneous emission rate of the cooling transition, δ the detuning, $C_{mf,mf'}$ the Clebsch-Gordon coefficient of the considered transition, n_{m_f} the atomic density in the sub-level $|f=4, m_f>$ and $\Omega^2_{tot}/\Gamma^2 = I_{tot}/2\, I_{sat}$ with I_{tot} being the total power of the six beams of the MOT and I_{sat} the saturation intensity. Since the laser power is approximately considered to be independent from r , the resulting formula is:

$$R_{Diff}\approx\frac{\Gamma}{2}\frac{C_1^2\Omega^2_{tot}(\vec{r})/2}{\delta^2+\Gamma^2/4+C_2^2\Omega^2_{tot}(\vec{r})/2} \tag{3.8}$$

where the $C_{1,2}$ are the effective coefficients of Eq. 3.7, which both value ~0.85 for the $\delta\in[-3\Gamma,-2\Gamma]$ and for $I\in[2I_{sat},I_{sat}]$ [Tow95]. The imaging system is collecting the photons that are contained in a solid angle Ω which is defined by the collection lens during a time $\mathbf{T_{exp}}$ which is the exposure time of the atoms in the trapping laser. The number of atoms N will be evaluated by the number of counts in the CCD camera which is given by the formula:

$$N_{counts}=\alpha_{cam}R_{Diff}T_{\exp}\frac{\Omega}{4Pi} \tag{3.9}$$

where a_{cam} is a factor that takes into account the quantum efficiency of the camera as well as other loss sources like the loss in the cell’s walls and the lens. The acquired images are registered and analyzed with the use of the Igor Pro 4.01 software. An example of fluorescence images of the MOT is shown in the Fig. I.3.13.

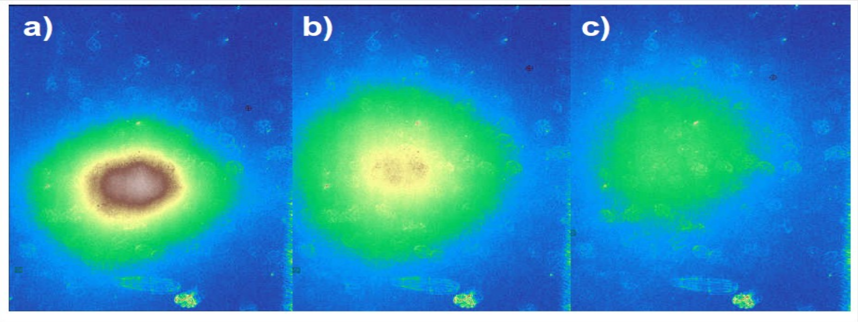

Fig. I.3.13: Fluorescence images of the MOT after a) 5 b) 10 and c) 15 ms of free fall. By taking series of images in different times of free fall we are able to determine the temperature of the atomic sample (Time of flight technique).

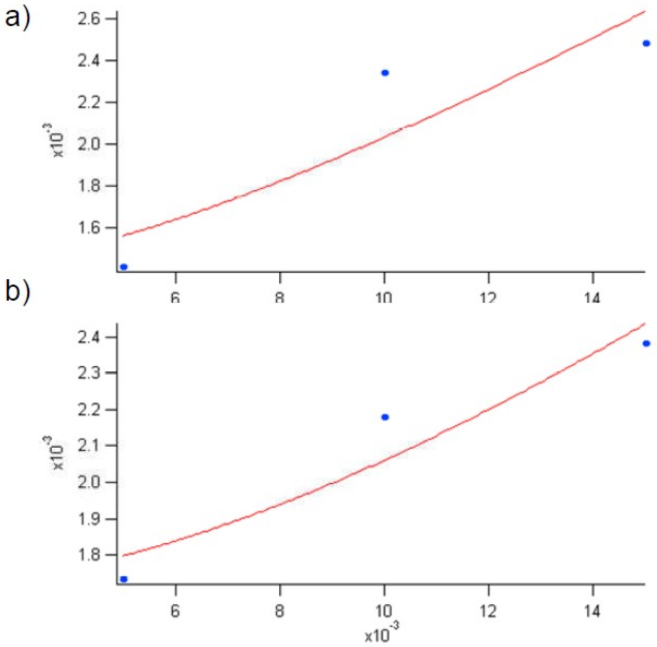

Fig. I.3.14: Evolution of the Gaussian atomic density profile si versus the time of free expansion for the a) axial and for the b) radial directions, along with the fit according to the formula 3.6.This analysis permits to extract the temperature of the atomic cloud, which for this example is 361 ± 180 μK for the axial and 216 ± 69 μK for the radial direction.

By registering images of the atomic cloud after having it fall free for different periods of time we are able to calculate its temperature, by realizing the Time of Flight (TOF) thermometry technique. The TOF technique in general consists of switching of the trap in which the atoms are contained and let the atomic cloud expand as a consequence of its kinetic energy. The supposed Maxwellian distribution of the velocity of the atoms in a harmonic trap has a standard deviation of $\sigma_\upsilon = (k_B T / m)^{1/2}$ which gives to the position standard deviation si a time dependence that equals to

$$\sigma_i(t)=\sqrt{\sigma_i(0)^2+\sigma_\upsilon(t)^2 t^2} \qquad (3.10)$$

Thus, by fitting the size evolution of the atomic cloud in different times of free fall we are able to determine its temperature. As an example, in Fig. I.3.14, we give the fitting that corresponds to the trap shown in figure Fig. I.3.13, from which we are able to determine a temperature ~ 280 μK.

Fluorescence imaging is a simple and flexible technique; nevertheless it has some disadvantages with the relatively weak efficiency and the failure at high densities being the most important. As noted before, the efficiency of the fluorescence detection is limited by the detection solid angle and it is proportional to $\Omega/4\pi \sim 0.02\%$. This means that for a sufficient signal to noise ratio in the pictures we need to have an exposure time of several ms. Since the atomic size continues to expand during the explosion this introduces errors in the temperature determination with the TOF method. Additionally, in samples of high density the probability of re-absorption of an emitted photon is not negligible, but this effect is very difficult to be taken into account in the analysis. These are the two most important reasons for which an additional data acquisition technique, the absorption imaging is employed.

I.3.5.b. Absorption imaging and in-situ temperature determination

The absorption imaging technique is more complicated to implement since it requires an additional diode laser. The laser is provided by a DBR (SDL 5702-H1) laser diode, which is frequency locked to the (4→4)×(4→5) transition and then brought to resonance with the 4→5 after double passing from an AOM. Then the laser passes through an optical fiber and a telescope in order to take a collimated beam with a homogenous power distribution in its center. This beam is inserted to the MOT region and where it is absorbed by the atomic cloud. Then it is imaged by a 150 mm focal lens to the CCD camera after having been magnified by a factor of 5. The images are obtained by an Andor DV437 CCD camera with 512 × 512 square pixels of 13μm. The image acquisition and analysis is done with the Vision 2.0 software, developed by Florian Shreck (available in the electronic address http ://george.ph.utexas.edu/schreck/schreck/) and adapted to the needs and the material of our set-up. A schematic representation of the absorption imaging is shown in the Fig. I.3.15. In contrast to the fluorescence imaging technique, here, the entire signal is contained in the probe beam, thus we expect an improved signal to noise ratio.

The intensity modification of the probe beam, after passing the atomic cloud is given by

$$I = I_0 e^{-\sigma_0 n_a dz} \tag{3.11}$$

where σ_0 is the resonant absorption cross section which equals to

$$\sigma_0 = 3\lambda^2/2\pi \tag{3.12}$$

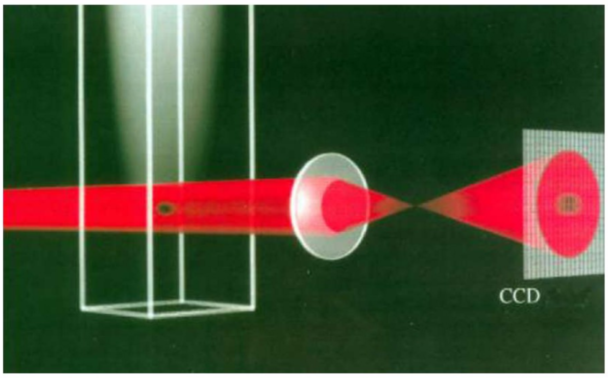

Fig. I.3.15: Schematic representation of absorption imaging technique. The probe beam is imaged on the CCD array by a converging lens, and the atoms are detected by their shadow. Picture taken from [Perr98].

The absorption imaging realized here provides with a spectroscopic tool, since the frequency locked diode laser having a spectral width inferior to the width of the atomic line, equal to $f/2\pi \sim 5.2$ MHz, can be used for the measurement of the $6^2P_{3/2}$ excited level natural width. A measurement of this kind was realized in order to test the limitations of the system. In this experiment, the frequency of the absorption beam was varied in order to sweep the atomic resonance. The result of this measurement is shown in Fig. I.3.16 and it results for the $6^2P_{3/2}$ level natural width a value of 6.9 ± 0.26 MHz[1].

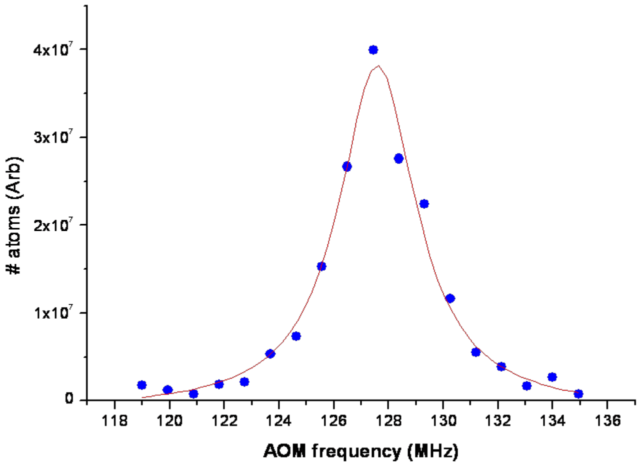

Fig. I.3.16: Measurement of the $6^2P_{3/2}$ level's natural line width. The result of the Lorentzian fit is 3.45 ± 0.26 MHz.

By imaging the probe beam in the CCD camera, after this has passed the atomic cloud in the z direction, we can extract the transverse atomic density in the x-y plane by the total attenuation

$$A(x,y)=e^{-\sigma_0\int n_a(x,y)dz}=e^{-\sigma_0 n_a(x,y)} \tag{3.13}$$

In theory, the attenuation can be obtained by dividing two images of the probe beam, one with the atoms present I_{with}, and one without $I_{without.}$ Nevertheless, here we make use of a third image which is taken without the presence of the probe beam I_{bg}, in order to eliminate the noise coming from the background stray photons. The attenuation factor will be equal to

$$A(x,y)=\frac{I_{with}(x,y)-I_{bg}(x,y)}{I_{without}(x,y)-I_{bg}(x,y)} \tag{3.14}$$

The total number of atoms N will be given by

$$N=\frac{\int\int \ln[-A(x,y)]}{\sigma_0}dxdy=\frac{\sum_{x,y}\ln[-A(x,y)]}{\sigma_0}l^2 \tag{3.15}$$

where l^2 is the active surface of each pixel.

The temperature of the atomic cloud can be estimated with two methods, the in-situ and the time-of-flight measurement. The time of flight measurement is similar to the one that is conducted with the fluorescence imaging technique. The small differences are that the fitting is done automatically by Vision, and not by treating the images with Igor Pro 4.1, and the fitting takes place between two points, one that corresponds to the size of the atomic cloud directly after its release from the dipole trap, and which is saved in the program's memory, and one that corresponds to the size of the atomic cloud of the given picture.

The in-situ thermometry is based in the fact that the size of an atomic cloud in a given trap will depend on the atom number but on the temperature as well, as

---

[1] In the graph, the modulation of the AOM's radio frequency is shown, which is the half of the modulation inserted in the refracted beam's frequency, since the particular AOM operates in 'double passage'. The double passage is necessary for the realization of the 'cat's eye' configuration. Such a configuration minimizes deviations of the direction of the deflection beam, which for this case is important since the beam is later on coupled to an optical fiber.

$$T = \frac{m \omega_i^2 \sigma_i^2}{k_B} \tag{3.16}$$

where ω_i is the atomic motion frequency and σ_i the dimension of the Gaussian atomic density profile. This formula supposes that the sample is thermalised, so that the frequency of the atomic motion and the temperature in the dipole trap is equal in all directions. The automatic analysis done by Vision 2.0, allows for the determination of various parameters like the atomic frequencies, the phase space density and more. Those parameters can be extracted with the use of either the in-situ or the time-of-flight thermometry for the temperature estimation. Practically, the use of the in-situ thermometry can be a source of error, since it is sensitive to the measurement of the atomic number, which is in generally underestimated with the absorption imaging technique. An additional weakness of the in-situ thermometry appears when the dimensions of the dipole trap are very small, close to the imaging resolution, which for our case is close to 4μm.

I.3.5.c. Non destructive imaging based on diffraction[1]

During this study on the Cs BEC experiment, we explored an additional, non destructive imaging technique which was based on diffraction [Lap07]. The particular interest of our team on this technique lies in the fact that this technique requires no absorption of light whatsoever. The two previously explained techniques, required absorption of either the trapping, or the absorption laser light. In both cases, the atoms have to absorb the repumper light as well, in order to be prepared in the F = 3 state. The diffraction imaging technique requires no absorption, which means that it could be suitable for the detection of ultra-cold molecules since there we do not have repumper lasers, and the preparation of the molecules to a particular state is in general non trivial. Additionally, this technique is non destructive, which means that it can be used in order to probe the atomic density without destroying the sample.

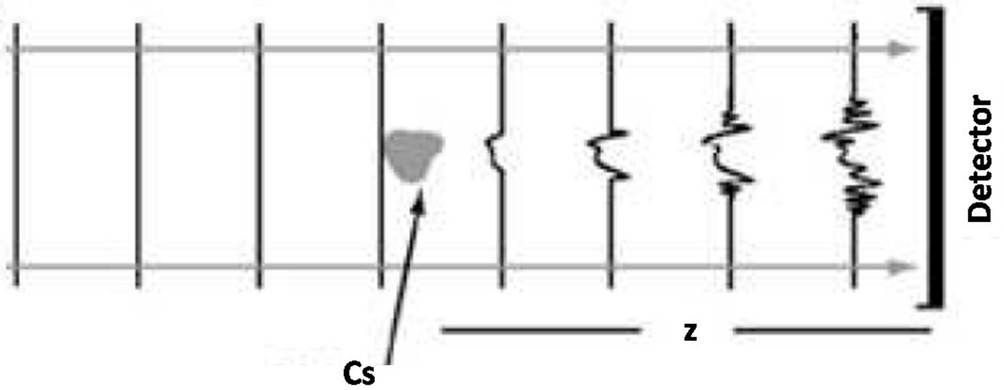

Fig. I.3.17: Principle of the diffraction imaging technique. Vertical lines represent intensity profiles.

The principle of this imaging technique is shown in Fig. I.3.17 and it is described in detail in the references [Turn04, Turn05]. A probe laser beam (the same which is used for absorption imaging), largely detuned from the atomic frequency (~20 MHz to the blue), is passing the atom cloud, and the detected intensity profile is modified due to the difference in the refractive index due to the presence of the atomic cloud. The atomic density *p(x)* profile equals to

---

[1] The study of the non-destructive imaging based of on diffraction was realized in the laboratory by Yannis Lablace, during his stage M2. The purpose of such a technique was to be used for the optical detection of molecules once they are produced in this set up.

$$p(x)=\frac{1}{2k}F^{-1}\left(\frac{h(u,z)}{|h(u,z)|^2+\alpha}F\left(\frac{I_{with}-I_{without}}{I_{without}}\right)\right) \qquad (3.17)$$

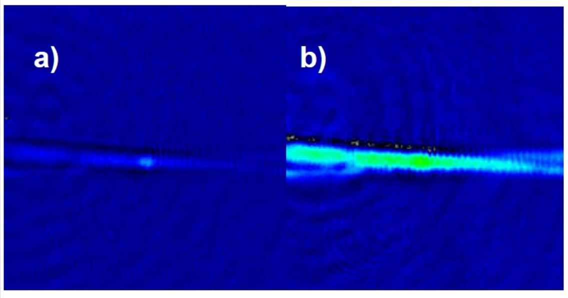

Fig. I.3.18: Image of the dipole trap in the same conditions, acquired a) by diffraction and b) by conventional resonant absorption imaging.

where k is the wavevector associated to the probe beam, h is a the "contrast transfer filter" function, which equals to $\delta*sin(zu^2) - b*cos(zu^2)$, where b and δ are the absorption and phase coefficient corresponding to a refractive index of the form $n = 1+N(r)(\delta+ib)$, $N(r)$ the atomic density and u the frequency conjugate to a direction parallel to the probe laser propagation. Finally, a is a regularization factor, which can be used to calibrate the result of the atomic density with the use of images taken with the conventional absorption imaging technique. In Fig. I.3.18 we see an image required with the use of the diffraction imaging technique, compared to the one acquired with resonant absorption.

I.3.6. Piloting program with LabVIEW

The synchronization of the various elements of the experiment (mechanical shutters, AOMs, magnetic fields and CCD cameras) and the generation of the programming sequences, was initially accomplished with the use of a Real-Time Linux system This operational system, allows for various input/output operations in the computer's PCI gates. The PCI port was coupled to a Measurement Computing DDA-0816 card, equipped with 48 TTL input/output ports and 8 analogue output ports of +10/-10V. The various operations were realized with the Real Time Linux system with time fluctuations of several tens of μs. Additionally, the realization of the experimental sequences with this system was very time consuming, since this had to be done in C. Finally, the system crashed very frequently, forcing the experiment to stop for ~30 min each time.

The Real-Time Linux system was replaced by a system which combined two output cards, which was developed in a similar way as the system which controls the Cr BEC experiment of the Cold Atom group of Laboratoire de Physique des Laser of Universite Paris 13. A Viewpoint DIO64PCI, 64 TTL output card, and a National Instruments PCI6713, 9 analog output card of +10/-10V. These cards are configured to work in a master-slave mode, as far as the timing is concerned, with the digital card playing the role of the master, and thus triggering the analogue card. The information concerning the experimental sequences is inserted in the cards by the computer each time one sequence is successively realized. This means that one or more parameters can be varied, allowing for automated spectroscopic studies and optimization of the experimental sequences.

The cards where commanded via a program developed in Lab-VIEW. The use of this visual programming platform, allowed for the constant development of our piloting system according to the particular experimental need. Since, most of the modern scientific instruments are provided with their LabVIEW drivers by the manufacturing companies, it allowed as to implement easily various components (as the PI translation stage, some web cameras and more) to our experimental set-up. Finally, it was easy to establish communication with the Vision 2.0 program that was placed in a different PC, and though which, most of the data analysis was taking place. The various parameters (laser trap waist, frequency of parametric excitation, time-of-flight etc), usually varied from an experimental sequence to the other, where written to a text file by LabVIEW to the PC that was driving the absorption CCD camera and where Vision 2.0 was running. The Vision 2.0 software was simply programmed to update the various parameters every time before acquiring a new image.

The development of a LabVIEW program, often called VI (acronym for Virtual Instrument) is optimized when the code is broken to various sub-programs (sub-VIs) which have specific tasks and are placed one inside the others. The Lab-VIEW drivers of a particular instrument, provided by the producing company, are often the lowest level VIs found in a LabVIEW program. In our case, the drivers of the two cards provided with an attractive interface where the experimental sequences could be programmed in relative time scales (example: Fact 1 duration of 5 ms, Fact 2 after Fact 1, duration of 5ms). These time sequences were converted to absolute time scales (example: Fact 1 directly after the trigger, duration 5 ms. Fact 2, 5ms after the trigger, duration 5 ms), then converted to machine language and used to update the cards. We developed our LabVIEW program on top of the pre-existing program provided to us by the Cold Atom group of Laboratoire de Physique des Laser of Universite Paris 13. The configuration of the cards in the master-slave mode, the translation to machine language and the conversion of the relative to absolute time scale pre-existed.

I developed several VIs, with which I realized various operations. First, I developed a sub-VI which introduced corrections in the time sequences related to the various component delays. This allowed us to have a simpler and more intuitive programming of the experimental sequences, while these delays where frequently measured and updated in the program. Another sub-VI was responsible for varying several parameters (for example the intensity of the repumper or the magnitude of the magnetic field gradient), in order to optimize an experimental sequence. Another sub-VI was responsible for the commanding and the synchronization of the piezoelectric stage and another for the communication with Vision 2.0. Finally, the unfortunate event of a damage in one of the digital output groups in which the digital output card was organized, was easily confronted by the insertion of a VI that redirected all commands for the digital card to a different output group, without further modifications of the program.

CHAPTER I4: EXPERIMENTAL WORK

I.4. EXPERIMENTAL WORK

In this chapter I present the experimental results of the study of loading a dipole trap with Cs atoms from an magnetic trap reservoir, as well as with the use of different loading methods. The analysis presented in Chapter I2 considered loading the dipole trap from a reservoir of neutral atoms provided by a magnetic trap. Nevertheless, the role or the atomic reservoir can be played by different traps, like a C-MOT or a Dark-SPOT. The experimental study of loading a dipole trap of Cs atoms from a magnetic trap reservoir resulted to be much less efficient than expected. This led to the realization of different types of reservoirs with which the technique could be realized in order to improve the experimental results[1].

The initial approach of loading the dipole trap from a magnetic trap reservoir is presented first. The experimental sequence used is complex and contains most of the elements involved in the experimental set-up. I choose to present it decomposed into its most important elements. Initially the sequence for the preparation of the magnetic trap alone is discussed. Since the ability to load the Cs atoms in the various types of traps depends a lot in our ability to polarize them in particular hyperfine state, the polarization configuration is presented in detail, as well as the experimental tests considered to verify it's performance. Finally, the experimental sequence for the study of loading a Cs dipole trap from a magnetic trap reservoir is presented along with some of the most interesting experimental results.

The second approach to be presented is the use of the Dark-SPOT in the role of the reservoir. Such a configuration was not discussed in the introduction, which considered loading from a magnetic trap. We will briefly explain its operating principle, the configuration used for its realization and the experimental results obtained with its use.

One of the simplest methods used in the laboratory to load a dipole trap was to superimpose it with the MOT during the MOT and the molasses phase. In particular, superimposing the dipole laser to a compressed MOT (C-MOT) was found to be a very efficient loading technique, since, this was the method with which the best loading was actually obtained. This is why we include the C-MOT in the study, even though it does not lie close to the model discussed in Chapter I2, with a reservoir of practically infinite lifetime. The results obtained with the C-MOT were improved if a molasses phase was applied in the end of the loading process. These are the reasons why we perform a study of loading with molasses in combination with the C-MOT. We also study the loading of the dipole trap by molasses alone, a method that goes even further away from the method discussed in Chapter I2, since it does not include a reservoir and the loading process is instantaneous. The operating principle for the preparation of ultra cold atoms with the molasses is presented, as well as the experimental results obtained for the atom cooling and the dipole trap loading.

The experimental set-up was severely damaged in October 2008. Initially, one of the flexible metallic components (bellow) of the vacuum system used to connect the Cs source to the chamber appeared to be leaking. The use of ultra vacuum glue did not solve the problem permanently, and after some days that the leak was absent the vacuum system was destroyed. The vacuum system was restored after a month of hard work but the performance of the set up was not the same.

The last studies performed, started a few weeks before the vacuum collapse and involved the only method that has been successful in providing a Cs BEC for the time being. This approach involves a less dense, but much colder 'reservoir' provided by the Raman Sideband Cooling (RSC) technique. The experimental results obtained with RSC are presented in this paragraph, while an

---

[1] The experimental results are going to be presented themetically, that does not mean that their realization was chronologically such. In reality, most of the times, we were able to support most of the various configurations for loading the dipole trap, but were choosing to emphasize in one or the other depending on the experimental results.

analysis of the most interesting data presented in this chapter will take place in Chapter I5.

I.4.1. Loading the dipole trap from a magnetic trap reservoir

In this paragraph the sequence which allows for the study of loading the dipole trap from a magnetic trap reservoir, as well as the experimental results obtained with this method are presented. The sequence can be explained with more clarity if it is decomposed in its most important elements. These elements coincide with the experimental diagnostics used in the laboratory in order to perform this study in the best possible conditions.

The experimental approach of loading a dipole trap from a magnetic trap reservoir has similarities with the approaches developed for the realization of BEC in the Chromium. In the approach of [Pfau07], the particularities of the atomic species led to the realization of a Continuously-Loaded Ioffe- Prichard (CLIP) trap instead of a MOT. A Ioffe-Prichard trap is a magnetic trap with the special characteristic that the magnetic field does not take the value of zero in the trapping area. This permits the suppression of the Majorana losses which occur in areas where the magnetic field is minimized and limit the lifetime of quadrupole magnetic traps. The Ioffe-Prichard trap consisted of an important improvement in the technology of magnetic traps, since it permitted the application of long evaporation sequences for the production of BEC. In the experiments with Chromium, a magnetic trap of this configuration is continuously loaded by a Zeeman slower, while the cooling method is more complicated as the continuous repumping to the magnetically trapped ground state acts as laser cooling due to the recoil exchange between the atoms and the incoming and the scattered photons. After the CLIP trap is loaded, the atoms undergo RF forced evaporation, and finally are loaded in the dipole trap. The dipole trap is realized in a different geometry than ours, (one horizontal and one less powerful vertical beam), while the loading process is also very different form the one we developed for Cs. The horizontal beam is turned on first, while the atoms are transferred via optical pumping to the ground, high field seeking state, so that they are no longer magnetically but only optically trapped. Finally, the power of the single armed dipole trap is lowered and evaporation is performed, while in the same time, the second, vertical arm, is slowly turned on and BEC is achieved after evaporation in the crossed dipole trap. In a more recent experiment in Villetaneus, BEC is achieved in Chromium atoms after they are loaded in a similar dipole trap in a metastable state, while in the experiment Dark-SPOT and RF ramps are also in use [Beau08].

The first important element of the method is the magnetic trap reservoir. Our experimental sequence must be able to provide a magnetically trapped atomic sample of $\sim 10^7$ atoms in a temperature of some hundreds μK. The experimental sequence used for the preparation of the magnetically trapped atoms is presented, as well as the results of the diagnostics performed on it.

One of the key elements for the successful preparation of the magnetic trap, but as well as for the evaporation process in the dipole trap and more, is the polarization. Not all hyperfine states are low field seekers, and thus magnetically trappable; moreover, polarizing the atoms in the $|F=3,m_F=-3>$ maximizes the loading. On the other hand, this hyperfine state not a good choice for evaporation in the dipole trap. Since the atom collisional properties depend heavily on the hyperfine state they occupy, their polarization must be controlled in order for the collisional losses to be minimized. These losses are minimized if the Cs atoms are polarized in their absolute ground state $|F=3,m_F=3>$. In the second paragraph we will present the experimental sequence that provides polarization control to the Cs atoms, as well as the experimental tests of its success in the various stages of the experiment.

Finally, I present the complete sequence for the study of loading the dipole trap from a magnetic trap reservoir, as well as the experimental results obtained with this method. The general characteristics of the experimental results, and the reasons that led us to the realization of different configurations is only briefly discussed. After presenting all the experimental approaches, an analysis of the most interesting data is attempted in Chapter 5.

I.4.1.a. Preparation of the magnetic trap 'reservoir'

In this paragraph the sequence for the preparation of a 'reservoir' of Cs atoms with the use of magnetic trapping is presented. The atoms are loaded from the Cs vapor in the MOT 1, and guided by the 'pushing-guiding' laser to MOT 2. There, they are pass subsequently form a C-MOT phase and a molasses phase in order for their density to be increased and their temperature to be lowered, they are polarized in the $|F=3,m_F=-3>$ state and loaded in the magnetic trap. These atoms are detected with fluorescence imaging and their temperature is measured with the Time-Of-Flight (TOF) method.

The experimental sequence used for the preparation of the magnetic trap is schematically shown in Fig. I.4.1. Initially, the trapping and re pumping lasers for MOT 1 and 2 are ON, as well as for the pushing laser. The detuning of the MOT 2 trapping laser is ~3Γ (Γ=5.2MHz) slightly to the red with respect to MOT 1,(the MOT 1 is realized a bit more compressed, since it has to be as large as possible). The MOT2 loading process is saturated after five seconds, where the subsequent phase of C-MOT starts. Then, the MOT 1 trapping and repumper as well as the pushing lasers are turned off. These lasers are controlled by acousto-optic modulators which give the ability to modulate their intensity and frequency, which have respond times smaller than microsecond. Nevertheless, the minimum intensity that they transmit cannot be zero, i.e. their 'extinction ratio' is limited. In order to correct this, and to avoid the presence of photon leak in the atomic sample, whenever a laser is turned off, additional to lowering its intensity with the AOM, the laser path is blocked with a small cooper screens. These light metallic leaves are mounted in small motors, and the overall system (called as 'click clack' due to the characteristic sound) has response times of some microseconds (except for the pusher click clack which has response time of ~12 ms, due to the large dimensions of the pusher beam). These time delays were frequently measured and updated in the LabVIEW piloting program where they were taken into account automatically during the experimental sequence.

In the subsequent C-MOT phase the MOT 2 trapping laser frequency is brought to ~5Γ, and the repumper intensity is slightly lowered. In the C-MOT phase the task is to increase the atomic sample's density. Usually, in such a phase the magnetic field gradient is increased with respect to the one used for the MOT. Nevertheless, in this experiment, the magnetic trap loading, as well as the loading of the dipole trap where found to be better when the magnetic field gradient is not increased at this point.

The repumper intensity is further decreased and the MOT 2 trapping frequency is brought to ~8Γ, in the subsequent molasses phase. Then the repumper is blocked and the atoms are left radiated by the trapping laser alone for ~1 ms, in order for them to be optically pumped to the $F = 3$ state. The polarization laser is applied for a period of time that can be as short as 500 μs. In the same time, the magnetic field gradient is turned off, and a small bias magnetic field is applied. The role of this magnetic field is to define a direction with which the polarized atoms are 'aligned' with, and to avoid depolarization due to stray magnetic fields. This bias field is available by the same coils that generate the field necessary to bring the system in the vicinity of a Feshbach resonance during the evaporation process. Its use in the polarization sequence is discussed in the next paragraph along were the polarization is discussed.

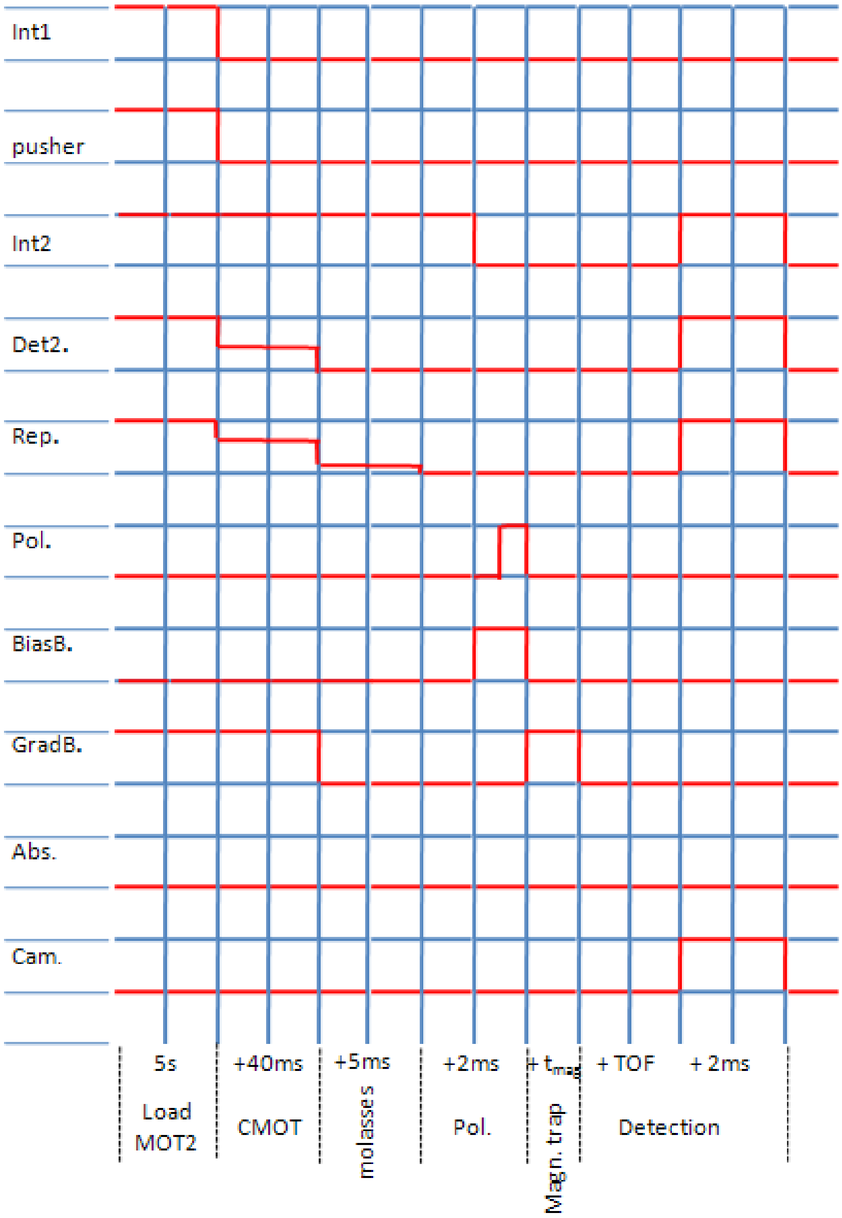

Fig. I.4.1: Experimental sequence used for the preparation of the magnetic trap reservoir, see text for details.

The magnetic field gradient during the MOT and C-MOT phase has been held at the value of ~15 G/cm while it was turned off during the molasses phase. The magnetic field gradient used for the magnetic trap is available by the same coils which provide magnetic field gradients up to some hundreds G/cm. As previously explained, control over the magnetic field gradient is achieved by controlling the current provided in the coils, with the use of a MOSFET switch. which has response times of some microseconds.

After being trapped for a variable time interval, the atoms are detected via fluoresce imaging and their temperature is measured with the TOF method. For the fluorescence imaging to be achieved the atoms are shined with the trapping and the repumper laser light for ~2 ms. The reason that the fluorescence method is preferred is mainly its simplicity. The alternative absorption imaging is more complicated and its realization is more time consuming. Additionally, the VISION software used with this method is configured to analyze automatically images of the dipole trap, and

]

configuring it for different types of traps demands great effort. Finally, absorption imaging is not necessary for this step, since fluorescence imaging exhibits no problems for these densities. An example of the detection of the magnetic trap with the use of fluorescence imaging is shown in the following picture.

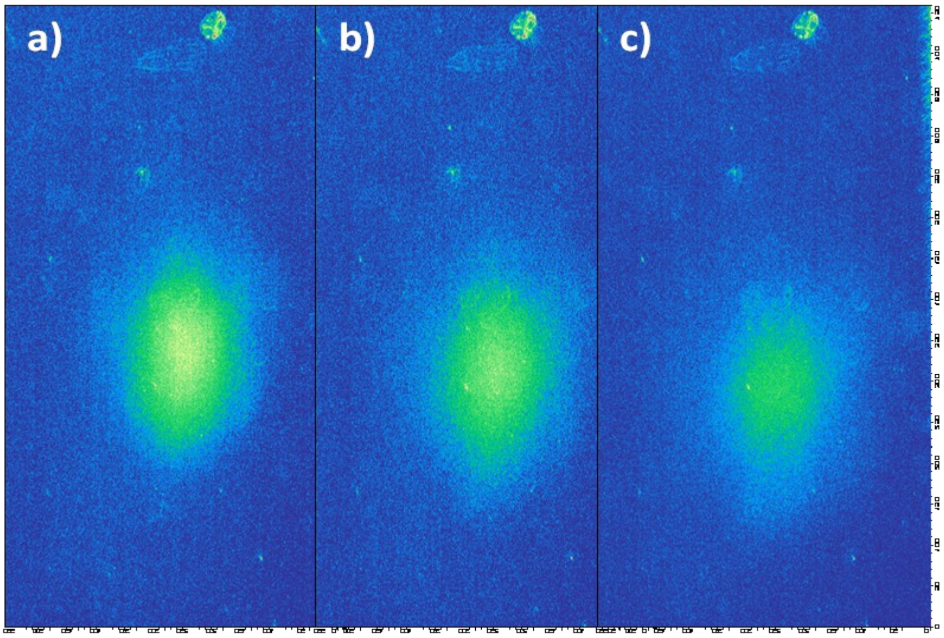

Fig. I.4.2: Images of the magnetically trapped atoms after having performed free ballistic expansion for 5 (a), 10 (b) and 15 ms (c).

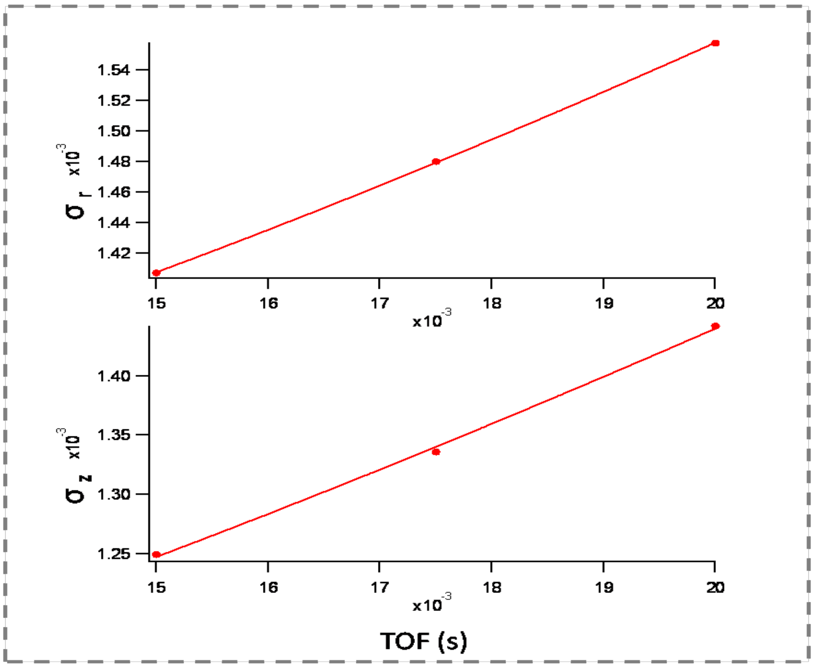

Fig. I.4.3: Fitting the expansion of the atomic cloud dimensions. σ_z and σ_R stand for the size in the point where the density of the atomic cloud reaches the 1/e of its peak value. The fitting is done with Igor, according to equation 3.10. The temperature is found to be 47.3 ± 1.8 μK for the axial and 40.75 ± 3.7 μK for the radial direction.

The atoms are imaged after having performed ballistic expansion under the influence of gravity for 5, 10 and 15 ms. In Fig. I.4.3 we see plots of the dimensions of the expanding cloud in the radial and axial direction versus the TOF. These data points are fitted according to Eq. 3.10 and the radial and axial temperature is determined with the process described in paragraph I3.3.a. Here the atomic cloud has ~10^8 atoms at a temperature of ~45 μK.

I.4.1.b. Polarization

As discussed in paragraph I3.2 where the laser set up is described, the radiation used for the polarization becomes available by taking a part of the repumper's light. This radiation, initially in resonance with the $F = 3 \rightarrow F' = 4$ transition is shifted for ~350 MHz after passing twice an AOM in order to become resonant to the $F = 3 \rightarrow F' = 2$ transition. A part of the radiation is polarized circularly and inserted vertically in the atomic trap region. A smaller part is linearly polarized and inserted in a horizontal direction. The intensity of the circularly polarized beam is ~800 $\mu W/cm^2$ and the one of the linearly polarized beam ~10 times smaller.

Dividing the polarization beam in a strong circular and a weaker linear π component is necessary, since the circularly polarized light alone does not result for 100% atomic polarization. The reason for this becomes clear when we see in Fig. I.4.4 we a diagram of the magnetic sublevels involved in the polarization process. As we see, the excitations induced by the circularly polarized light lead in an increase in the spin projection m_F (σ+ light chosen for this example, where polarization to $|F=3,m_F=3>$ state considered). But for atoms occupying the $|F=3,m_F=2>$ state, such an excitation is impossible due to the lack of an exciting state with spin projection m_F+1. This can lead to population trapping in this state and thus decrease of the polarization efficiency. This problem is confronted with the weak linear component which is able to pump atomic population out of the *'dark'* $|F=3,m_F=2>$ state, and the combination of the two component results to almost 100% population transfer in the desired $|F=3,m_F=3>$ state.

An important element of the polarization process is the small magnetic field bias. It is necessary in order to achieve and maintain polarization, but also it allow us to choose between the $|F=3,m_F=3>$ and the $|F=3,m_F=-3>$ states as the final states of our polarization scheme. Any atom possessing spin if subjected to magnetic field, performs Larmor oscillations around it. In the absence of this magnetic field bias, the polarized atoms will perform these oscillations around any stray magnetic field, resulting to a complete loss of their polarization. The energy shift between

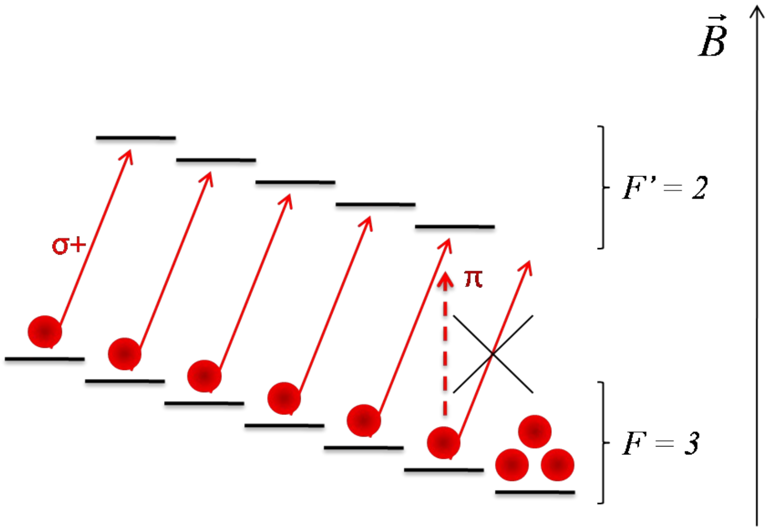

Fig. I.4.4: Diagram of the magnetic sublevels involved in the polarization process. We see that the result of the circularly polarized light alone is accumulation to the $|F=3,m_F=2>$ 'dark' state, while polarization of ~100% in the $|F = 3,\ m_F = 3>$ state is achievable only after the insertion of the weak linearly polarized component.

magnetic sublevels shown in Fig. I.4.4 is caused by this magnetic field. More important, this field defines a direction upon which the whole geometry of the scheme is based. Inverting this field's direction results in the inversion of the target state, since the effect of the σ+ polarized light with the inverse magnetic field is the same as the effect of σ- radiation with the magnetic field direction as the one shown in the scheme.

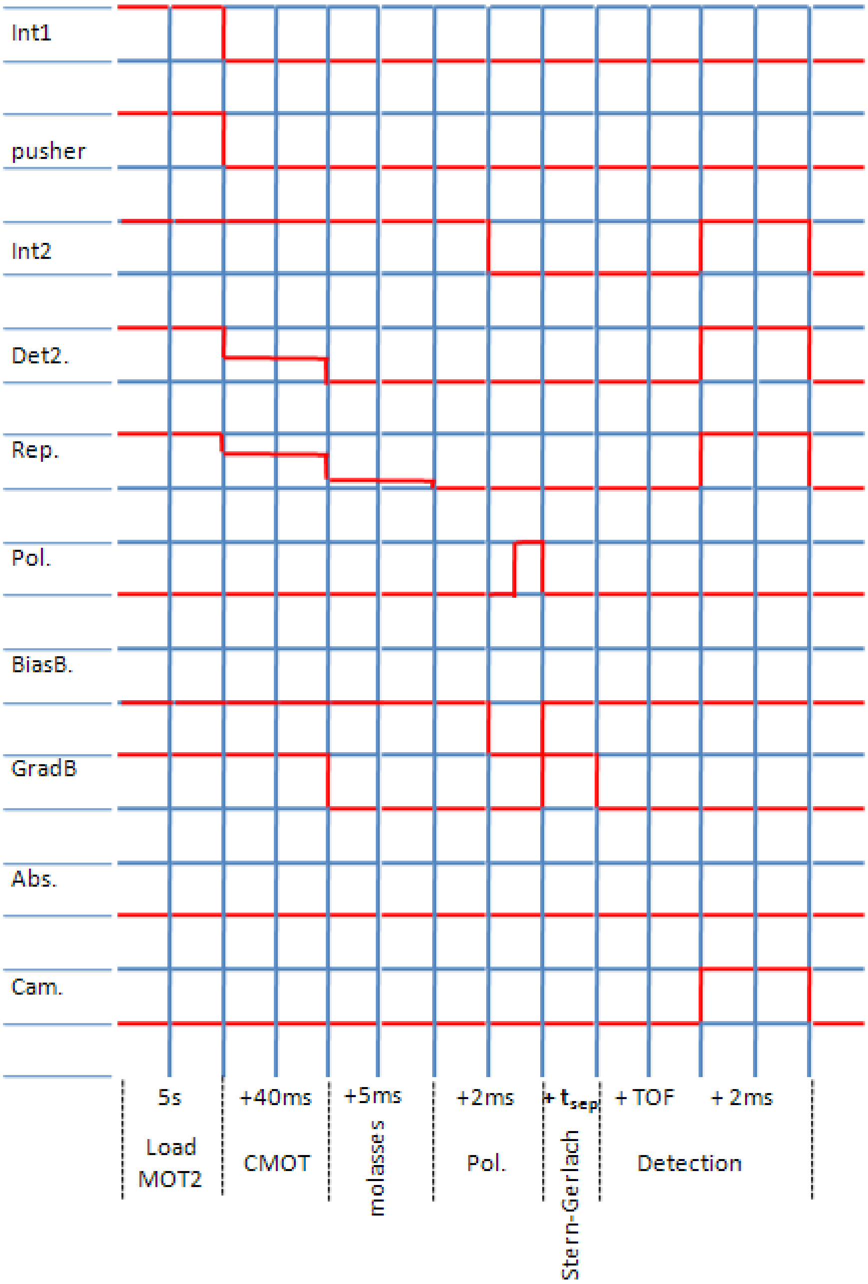

Fig. I.4.5: Experimental sequence used for the polarization of the Cs atoms, and the verification of the polarization performance via Stern-Gerlach separation.

The diagnostic applied in order to verify the performance of the polarization technique is the Stern-Gerlach separation. The separation is realized by letting the atoms fall in the presence of a strong magnetic field gradient. The force created by the interaction of the magnetic field gradient with the atom's magnetic moment depends on the m_F. Thus, the free fall of some atoms (low field seekers) is accelerated, while for others (low field seekers) is decelerated, resulting to spatial separation of the atoms according to their hyperfine state. In Fig. I.4.5 we see the experimental sequence used for the preparation of an ultracold Cs cloud, its polarization to the $|F=3,m_F=3>$ state the realization of the Stern-Gerlach separation and the detection of the atomic cloud via fluorescence imaging. Again the atoms are loaded from MOT 1 to MOT 2, are compressed in a C-MOT phase and cooled by molasses. Finally they are polarized and separated with the Stern-Gerlach magnetic field gradient. The magnetic field gradient is ~120 G/cm and it is provided by a single coil located ~4 cm lower than the atomic sample; in the schematic representation of figure 4.5 it is shown as if it was generated by the MOT fields (which is possible) for simplicity. After magnetically separated the atoms are detected via fluorescence imaging.

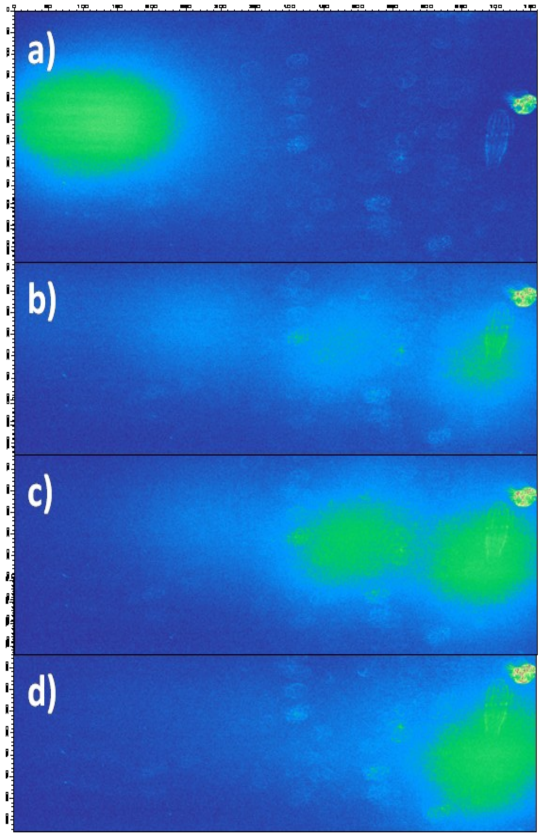

Fig. I.4.6: (a) Cs atoms falling under the influence of gravity. (b) The Stern-Gerlach separation magnetic field gradient is added and we see the appearance of separated atomic clouds corresponding to the $|F=3,m_F=1>$, $|F=3,m_F=2>$ and $|F=3,m_F=3>$ states. (c) The circularly polarized beam is inserted alone and most of the atomic population is found in the $|F=3,m_F=2>$ and $|F=3,m_F=3>$ states.(d) Inserting the linearly polarized component results to the accumulation of the atomic population in the $|F=3,m_F=3>$ state.

In Fig. I.4.6, we see fluorescence imaging detection of the atomic cloud. In part (a) the atoms have fallen freely and magnetic field gradient is not present. In part (b) the magnetic field gradient is turned on. We see that the atoms are separated to atomic clouds that correspond to states having m_F equal to 1,2 and 3 while other states are not visible at these conditions. In part (c) we insert the circularly polarized light alone and we see a a clear difference in the atom's distribution on the magnetic sub-levels since most of them are found in the $|F=3,m_F=3>$ state and some of them in the $|F=3,m_F=2>$ state . Finally, in part (d), the linearly polarized component is also inserted and almost all atoms occupy the $|F=3,m_F=3>$ target state.

In Fig. I.4.6.b, we see that after the insertion of the Stern-Gerlach separation field gradient the atoms are spatially separated in atomic clouds that correspond to different hyperfine states. In those pictures only the states with $m_F = 1,2$ and 3 are shown, while their relative distribution among them depends on the complicated optical pumping scheme involved in the MOT and molasses phase. A different method to verify the efficiency of the polarization scheme and to make sure that no atomic population is lying different states is to see the polarization effect on the magnetically trapped atoms. In Fig. I.4.7 we see three pictures of the magnetic trap realized with the use of the sequence shown in Fig. I.4.1 with the only differences in the polarization. In part (a), the polarization laser is blocked. In part (b) the polarization laser is on and the bias magnetic field is such that the atoms are polarized in the $|F=3,m_F=-3>$ state, so that the total number of atoms in the magnetic trap appears enhanced. In part (c) the direction of this field in making the $|F=3,m_F=3>$ state the target state of the system. We see that the efficiency of the polarization scheme is close to 100% since almost no atoms are detected to be magnetically trapped.

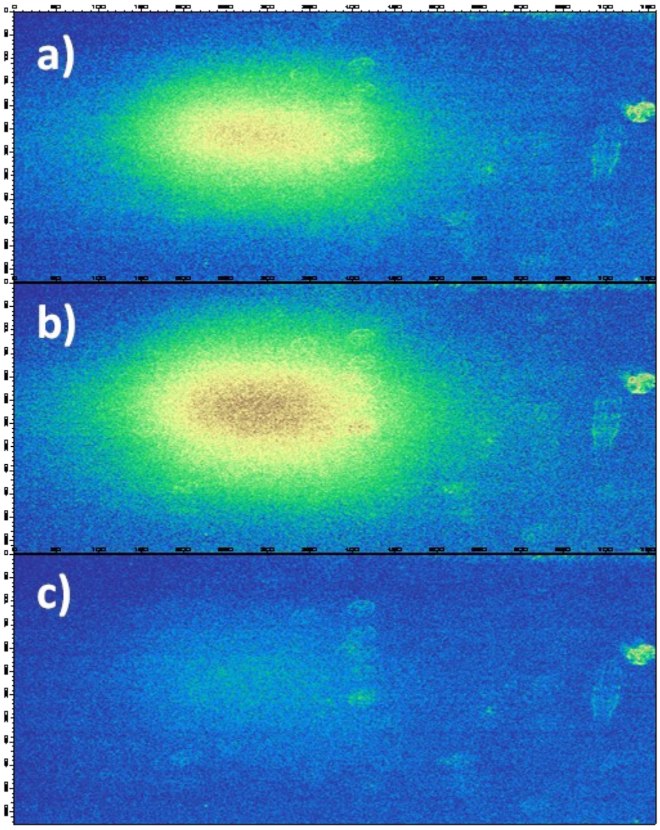

Fig. I.4.7: (a) Fluorescence image of the magnetic trap, (b) after polarization to the $|F=3,m_F=-3>$ and (c) after polarization in the $|F=3,m_F=3>$ state.

I.4.1.c. Loading a crossed dipole trap from a magnetic trap reservoir

The experimental sequence used for the study of the loading of a dipole trap from a magnetic trap reservoir is shown in Fig. I.4.8. It is similar with the sequence shown in Fig. I.4.1, with the difference of adding the dipole trap, applying the polarization twice and performing the data acquisition with the use of absorption imaging. Again the atoms are loaded in MOT 2 for ~5 s and are subjected to compression in the C-MOT phase, cooled in the molasses phase and polarized. Then they are loaded in the magnetic trap and kept for a variable time labeled t_{trap} until the dipole trap is turned on. The duration of the superposition of the dipole trap with the magnetic trap is labeled t_{load} and it is one of the main parameters under study. At the end of the loading process, the magnetic field gradient of the magnetic trap is removed and the atoms are polarized once more in the $|F=3,m_F=3>$ state. This process is necessary in order to minimize the inelastic two body losses and thus increase the lifetime of the dipole trap. Nevertheless, when the loading of the dipole trap is studied and the number of atoms in the dipole trap is detected shortly after the end of the loading process, this second polarization step is not necessary and is omitted. When the lifetime of the atoms in the dipole trap is studied, the dipole trap stays on for time t_{hold} after the end of the loading process and the atoms are detected with the use of absorption imaging.

In this study fluorescence imaging has been replaced by absorption imaging, a fact that has increased the duration of our experimental sequences by 2 s. The reason for this increase is the fact that the data acquisition in absorption imaging makes use of three images, one of the atoms in the dipole trap and the absorption laser together, one with the dipole trap without atoms and one of the background, as explained in I.3.5.b. In the sequence shown in Fig.4.8 we see the absorption camera been triggered four times; this is due to the fact that an initial shot is necessary for the camera's chip to 'flush' the previous images. The use of absorption imaging increases the duration of our sequences and adds one more diode laser in the set-up, nevertheless it is necessary. Apart the technique's increased resolution and, in general, its suitability for the study of dipole traps, our main reason for the choice of absorption imaging is that the use of VISION with combination with the LabVIEW piloting program allowed for the automation of the study. The sequence shown in Fig.4.5 is executed repeatedly and the parameter under study is modified. Each time the data are recorded by VISION along with the value of the parameter under study.

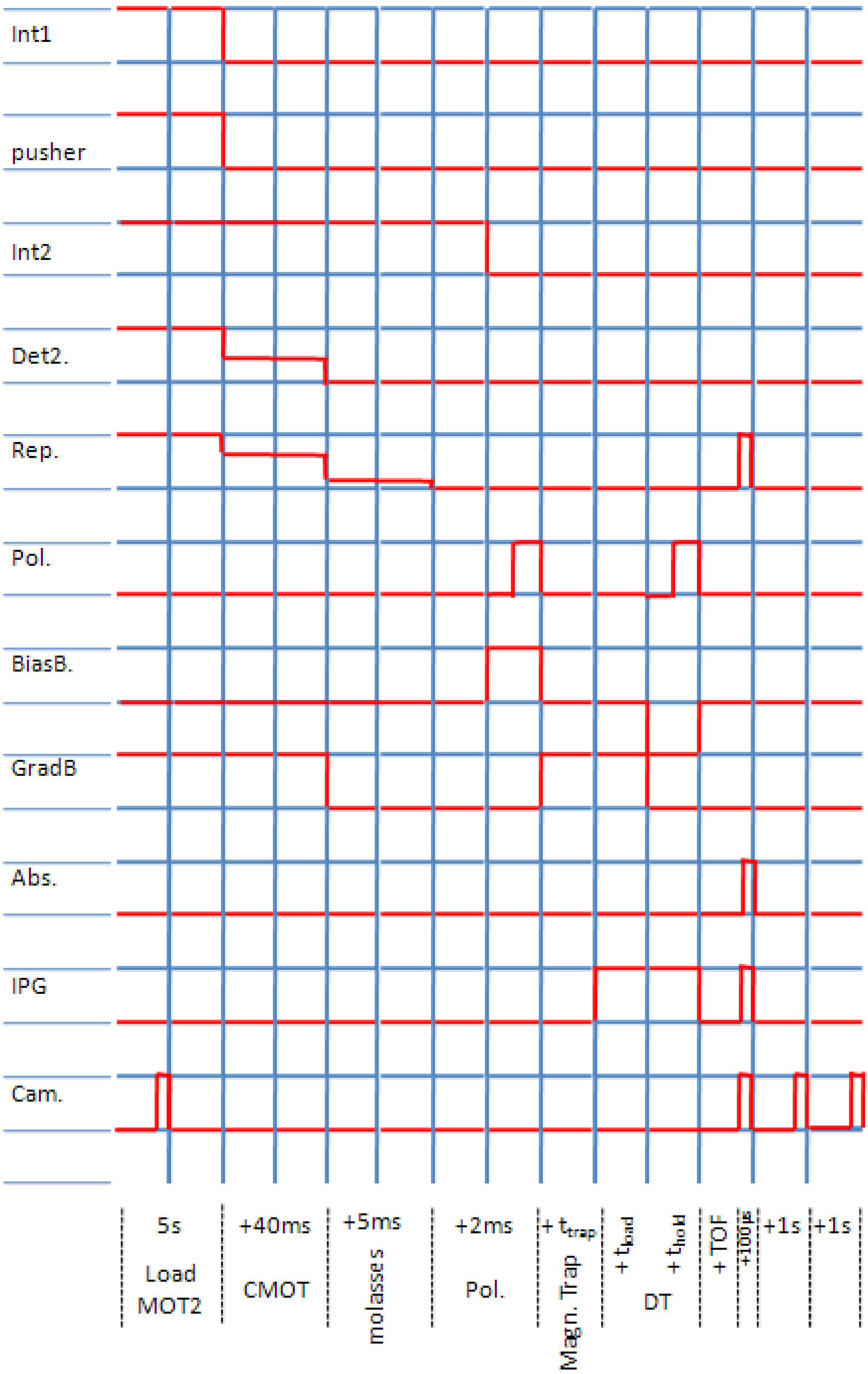

Fig. I.4.8: Experimental sequence used for the study of the loading of a dipole trap from a magnetic trap reservoir, see text for details.

In Fig. I.4.9 we see such a study of the parameter t_{trap} which is the time that the atoms spend in the magnetic trap before the dipole trap is turned on. The time t_{trap} is varied from the initial value of 5 to 300 ms. The dipole trap is loaded for 15 ms and then it is imaged by means of absorption and VISION calculates the atom number and the temperature according to the methods discussed in I.3.3.b. The magnetic field gradient used for the magnetic trap is ~150 G/cm, while the dipole trap's waist is 89 μm (corresponding to the measurement shown in Fig.3.10). The short overlap between the magnetic trap and the dipole trap (5 ms) as well as the small power of the dipole trap (~30W) explain the small atom number. As we see, the number of transferred atoms in the dipole trap and their temperature is unvaried with respect to this parameter.

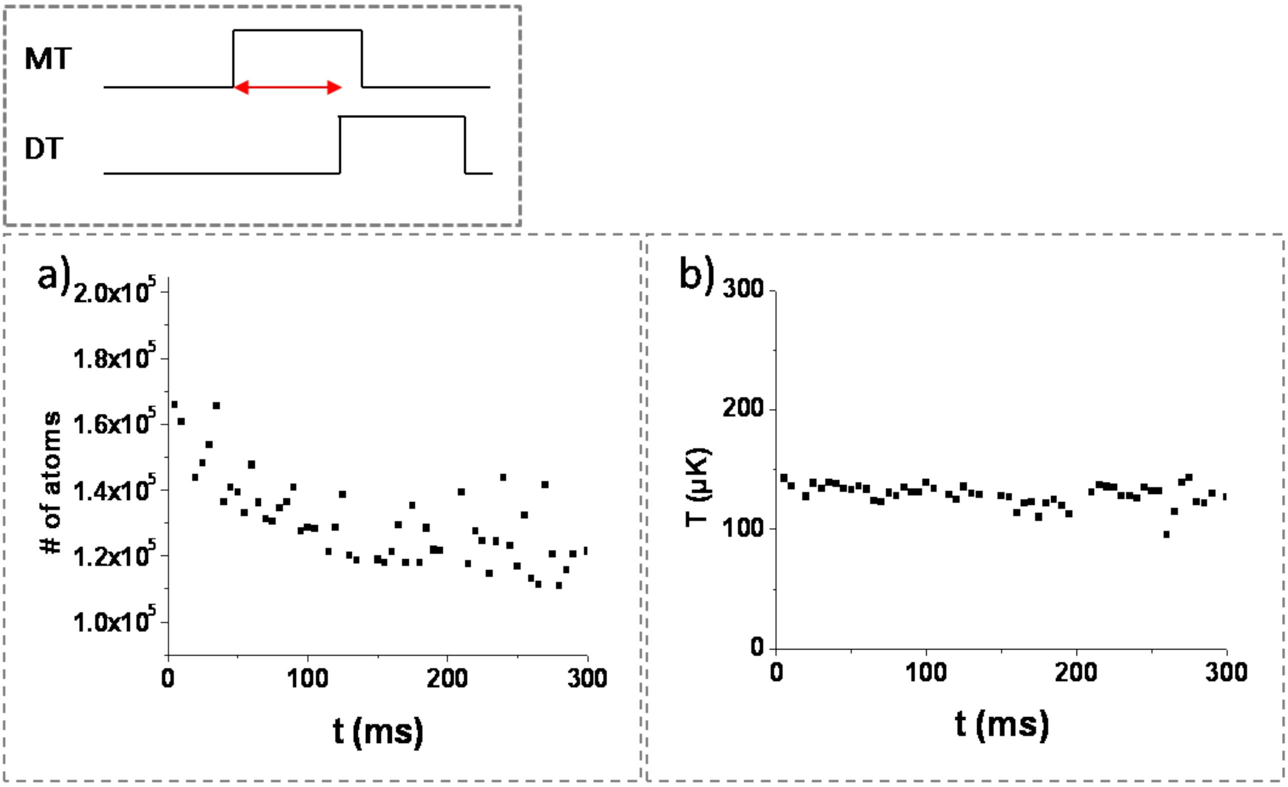

Fig. I.4.9: Evolution of the atoms number (a) and temperature (b) of the dipole trap with respect to $t_{trap.}$ The laser power is ~30W, and the waist ~98 μm.

This measurement showed that t_{trap} is not a critical parameter, thus it can be eliminated and indeed, in the following of this study the starting point of the dipole trap and the magnetic trap coincide. The following parameter to be studied is the time in which the dipole and the magnetic trap coexist, $t_{load.}$ This parameter is perhaps the most important of this study, since, the technique aims to improve loading by increasing the loading time with the use of the reservoir. However, as Fig. I.4.10 shows, even though loading is initially improved as t_{load} is increased, this increase reaches its maximum in less than 10 ms, and gives its place to very violent losses.

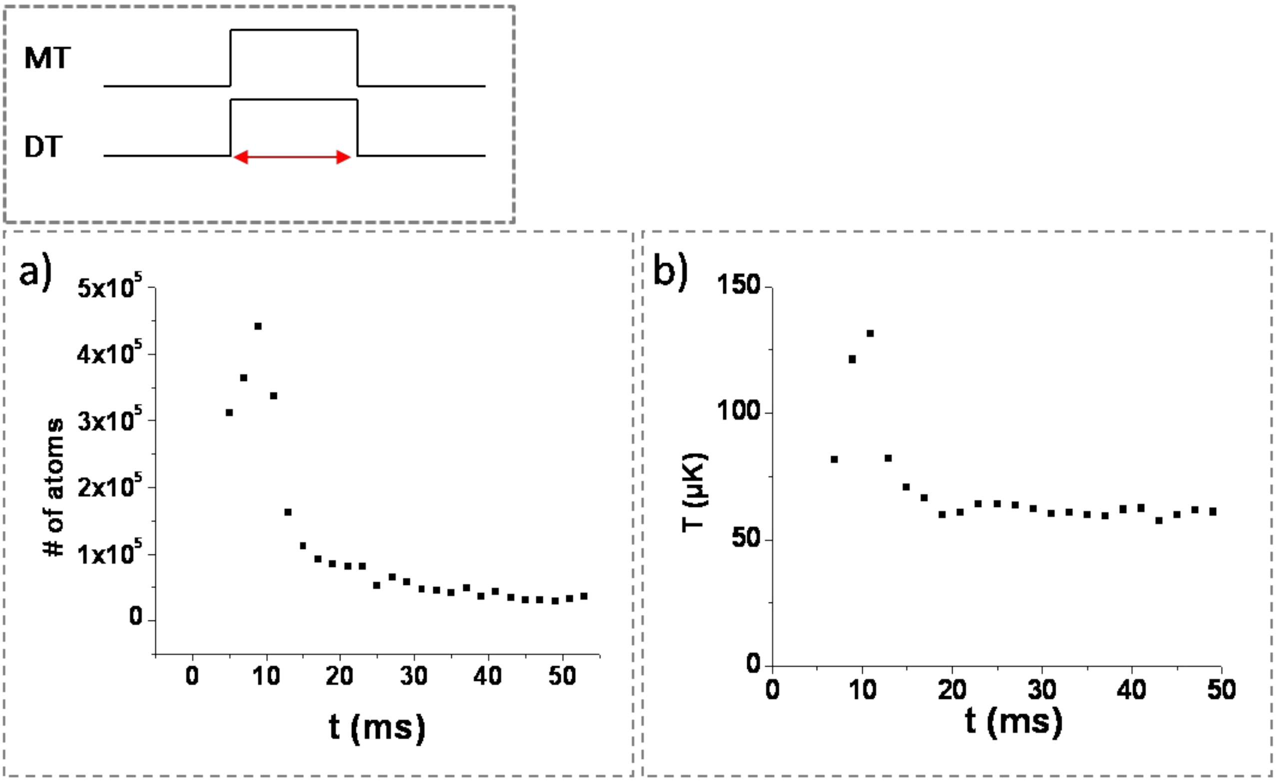

Fig. I.4.10: Evolution of the atoms number (a) and temperature (b) of the dipole trap with respect to t_{load}. Here the laser power is risen to ~60W while the waist is kept at ~98 μm.

The incompatibility of this result with the predictions of [Comp06] is striking, since it predicted that the loading process would last ~10 times more. At the time were the experiment was conducted our efforts were oriented towards the examination of the experimental conditions, in order to identify and to eliminate possible imperfections that could be responsible for the technique's poor performance. Among the various elements that were examined during the period that the experiment was conducted, there was the overlap of the dipole and the magnetic trap. The overlap of the two traps has to be precise and the dipole trap has to be realized as close as possible to the center of the magnetic trap. This is necessary on the one hand in order for the loading to be optimized. When a dipole trap is loaded by a MOT or a molasses, the center of the quadrupole magnetic field gradient of the MOT is not the best position for its realization as demonstrated for the case of ^{87}Rb in [Szcze09] and as we have verified for the case of Cs in the lab as well. For the case of Cs atoms loaded from a magnetic to a dipole trap, overlap in the center of the magnetic trap is necessary. If the dipole trap is realized in the presence of high magnetic field gradient the two body losses between atoms in different magnetic sublevels can be very violent. The way this parameter was controlled was to realize magnetic trap of very small dimensions (~200 μm) with the use of high magnetic field gradients (~250 G/cm). We took advantage of the fact that the two different imaging systems, the fluorescence and the absorption imaging, were realized in different (almost) orthogonal directions, in order to verify the good overlap of the dipole and the 'small' magnetic trap as seen in Fig. I.4.11.

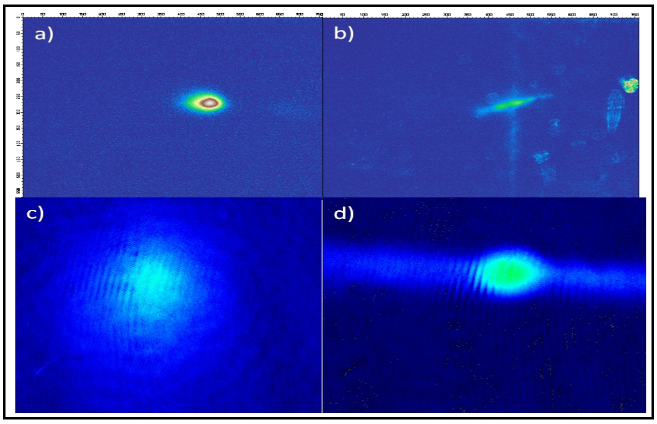

Fig. I.4.11: Magnetic trap of small dimensions (~200μm) imaged with fluorescence imaging in (a) and absorption imaging in (c). Dipole trap fluorescence (b) and absorption (d) images. The two imaging techniques were realized in vertical directions a fact that allows to test the realization of the dipole trap in the center of the magnetic trap.

The study was repeated for various conditions. In Fig. I.4.12 we see the evolution of the atom number in the dipole time versus the loading time for (a) waist ~89 μm but power ~2 times larges (65 W) and (b) for a waist ~130 μm. The final number of atoms is never sufficiently increased. Again the same trend is observed: the number of atoms initially increases with the loading time, until finding its maximum in relatively small times and then it decreases rapidly. For the case of the 89 μm trap this maximum is found at ~50 ms while for the case of the 130 μm trap the maximum is found in ~80 ms. A final parameter to be studied is the value of the magnetic field gradient used to realize the magnetic trap. In Fig. I.4.13 we see the result of such a study for the 89 μm and 60 W dipole trap[1].

---

[1] The number of atoms detected in the dipole trap depends a lot on the time t_{load} . As t_{load} increases, the number of atoms in the dipole trap decreases, initially rapidly (spilling) and more smoothly later, depended on the nature of collisions in the trap. In the studies presented here the traps were detected ~10ms after the end of the loading proccess, except for the measurements shown in Figs.4.11.a and 4.12. where this time was set at 5ms. This is the reason why the final atom number appears ~10 times larger.

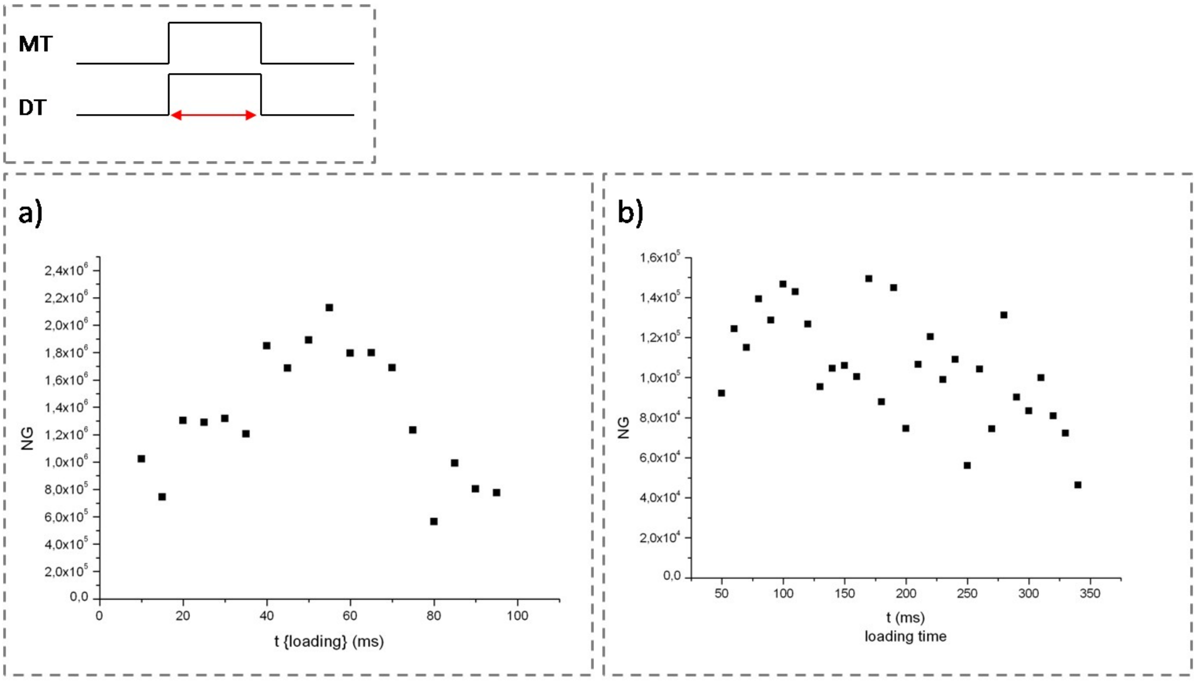

Fig. I.4.12: Evolution of the number of atoms in the dipole trap with respect to t_{load}. In part (a) the trap's dimensions are still~89µm while the power is now ~60W. In part (b) the trap's dimensions is 130µm.

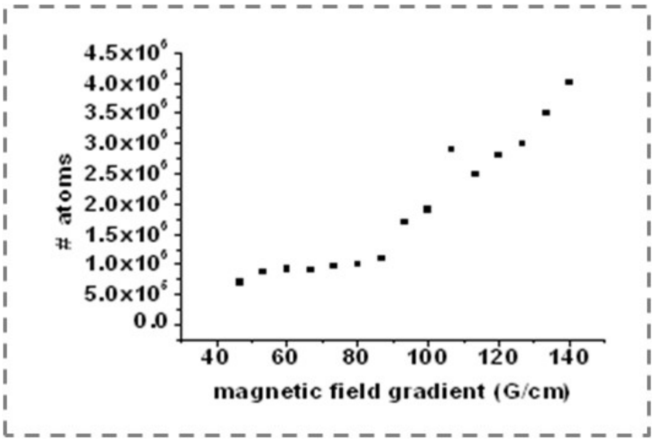

Fig. I.4.13: Modification of the final atom number in the dipole trap with respect to the magnetic field gradient, for a trap of ~89 µm and ~60 W.

I.4.2. Loading the dipole trap from a Dark-SPOT

The idea of loading a dipole trap with cold atoms from a reservoir is not necessary realized with the use of a magnetic trap in the role of the reservoir, even though the analysis presented in [Comp06] and in Chapter 2 adopts the use of such a trap. Since the use of a magnetic trap led to observations inconsistent to the theoretical predictions, a reasonable idea is to substitute it with another kind of trap. This way, the technique's performance does not depend on the characteristics of the magnetic trap and our study of the technique can be more complete. In this paragraph the Dark-SPOT method and the way such a trap was realized in LAC is briefly discussed, and the results of the loading of a dipole trap from such a trap are presented.

I.4.2.a. The Dark-SPOT and its realization in LAC

The Dark-SPOT is an acronym that stands for Dark-SPontaneous force Optical Trap and it is a laser cooling technique that permits the preparation of cold molecule samples in densities increased with respect to a standard MOT . The technique was introduced in 1993 [Kett93] and it has been been proved to be valuable in the search for BEC in the 90's [And95, Dav95]. The reason of its particular importance at the time was the fact that it provides with samples at high densities and high atom numbers at the same time, a characteristic which made it very suitable for combination with evaporation cooling.

The technique takes advantage of the fact that one source of limitation for the preparation of dense samples of cold atoms with laser cooling is caused by the repulsion forces between atoms due to re scattered radiation. These forces are eliminated if the atoms populate hyperfine levels that do not interact with the trapping radiation. Usually this is achieved by blocking part of the repumper's radiation and letting part of the atoms to be optically pumped in the F = 3 state; nevertheless, alternative configurations using depumping lasers have also been reported [Kim01]. Usually, the repumping beam is blocked in it's center and the optical configuration is such that the part of the trap where the repumper radiation does not enter is in the middle of a MOT, so that atoms are continuously provided to the Dark-SPOT region.

The Dark-SPOT proved to be a useful technique for the preparation of an all optical BEC in the case of Sodium [Dumk06]. There, a Dark-SPOT is used to load a dipole trap of nearly 1 μm wavelength. The intensity and the detuning of the trapping laser of the MOT is modified during the loading process which lasts for more than two seconds, while in the end of the loading process a molasses phase is applied. An indirect method for the realization of a Dark-SPOT is demonstrated in [Clem09], where 87Rb atoms are loaded from a Dark-SPOT to a dipole trap in which they are cooled via evaporation to degeneracy. In this experiment, the repumping beam is not partially blocked, neither there is a depumping laser used. The dipole laser radiation at 1565 nm shifts the energy levels involved in the repumping transition with result for the repumping beam to be out of resonance in the area where the dipole laser is applied. A simultaneous decrease of the repumping laser's power of ~30% lead to the creation of a Dark-SPOT in the area where the dipole laser is applied, which is accompanied with the corresponding increase in the density of the trapped Rb atoms.

In our experiment, the repumper laser is mixed early with the MOT 2 trapping laser, and it is inserted in the trap by the six directions parallel to the MOT beams with its power balanced. For the realization of the Dark-SPOT the path of the repumper had to be changed. The repumper was passed by a simple, rectangular mask of 2 mm × 2 mm in order for its central part to be blocked, it was spitted in two beams and it was inserted to the MOT beam by two vertical directions as shown in Fig. I.4.14. A 500 mm converging was placed in an equal distance between the mask and the MOT in order for the contrast between the dark and the bright part of the repumper's radiation to be maximized. It is important for the success of the technique, that the dark parts of the repumper's radiation in the two beams cross eachother. In order to achieve this the following protocol was used. The two repumper beams were placed as close as possible. This is easy to control by using an iris in order to decrease the size of the repumper beam and to use this small beams in order to create small MOTs, barely detectable by the fluorescence camera. Then the mask, placed in a micro-metric translation stage is inserted in the repumping beam as close to the center as possible. If one of the two beams is blocked, and the intensity profile is not very far away from the usual Gaussian, the fluorescence of the MOT has to be minimized when the mask is placed in the center. When both the hollow repumper beams are inserted, the alignment of one of the two is finely twicked by simultaneously monitoring the MOT's fluorescence. The point where the dark holes in the intensity profiles of the hollow beams are crossed is marked by a fluorescence decrease. This decrease quickly recovers when the hollow parts do not overlap, since the intensity of one of the beams is enough to pump the atoms in the F = 3 state.

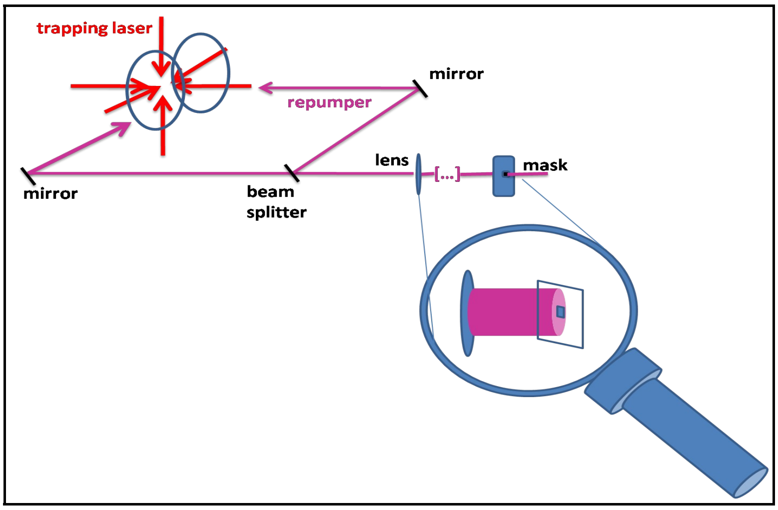

Fig. I.4.14: Optical configuration of the Dark-SPOT. The distance between the mask and the lens equals the distance between the lens and the MOT and is twice the lens focal length.

I.4.2.b. Loading the dipole trap by the Dark-SPOT

The experimental sequence used for the study of the loading of a dipole trap from a Dark-SPOT is very simple. After the geometry of Fig.4.13 is realized, the Dark-SPOT is obtained by having the trapping lasers for the MOT 1 and 2 and the repumper permanently on. In order to study the loading efficiency, the pusher laser is blocked before the dipole trap is overlapped to the Dark-SPOT.

Since the trapping and repumping lasers are present during the loading process, it is necessary to include their parameters in our studies, especially now that the simple time sequence does not offer many parameters for optimization. In Fig. I.4.15 we see the result of the optimization of two parameters, the repumper intensity and the trapping laser detuning. The maximum of the loading coincides with the usual values of the repumper intensity (~5 mW) while the decrease above this value is probably due a decrease of contrast between the bright and the dark part of the repumper beam. Similarly, the maximum loading is obtained for more or less usual values of the MOT operation.

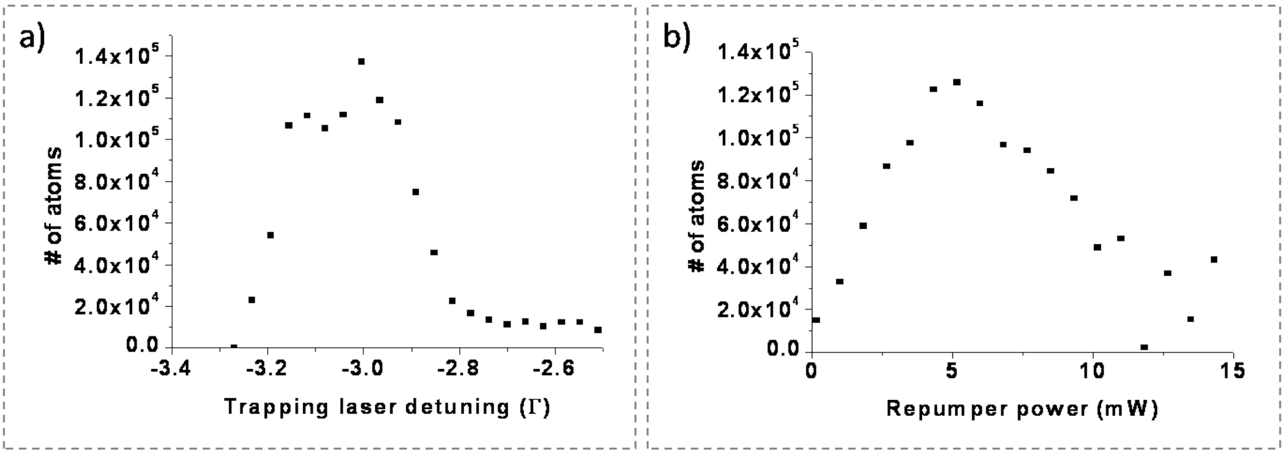

Fig. I.4.15: Evolution of the number of atoms of the dipole trap with respect to (a) the trapping laser detuning and (b) the repumper intensity. The laser power is ~60 W and the waist ~98 µm.

In Fig. I.4.16 (a) we see the result for the evolution of the atom number with respect to the loading time, for a dipole trap of ~100 µm waist and ~60 W total power. The loading time in this simple experimental sequence is again the time in which the dipole trap and the Dark-SPOT coexist. Its beginning coincides with the time in which the dipole trap is turned on and its end is the moment where the trapping and repumping laser's power is set to zero. The behavior observed, showed that large loading times do not improve the loading performance since the final atoms number is constantly decreasing with respect to the loading time. In part (b) we performed the loading sequence again with a much smaller step in order to determine the loading time for which the efficiency is optimized. The curve now reminds a lot the study of the loading of the dipole trap with a reservoir of magnetically trapped atoms. Again, the same trend is observed : a sharp initial decrease that is followed by a fast decay for the atom number in the dipole trap. Finally, in (c) the study is repeated for a larger dipole trap with a waist ~130 µm. The trends do not change and the total number of atoms appears to decrease.

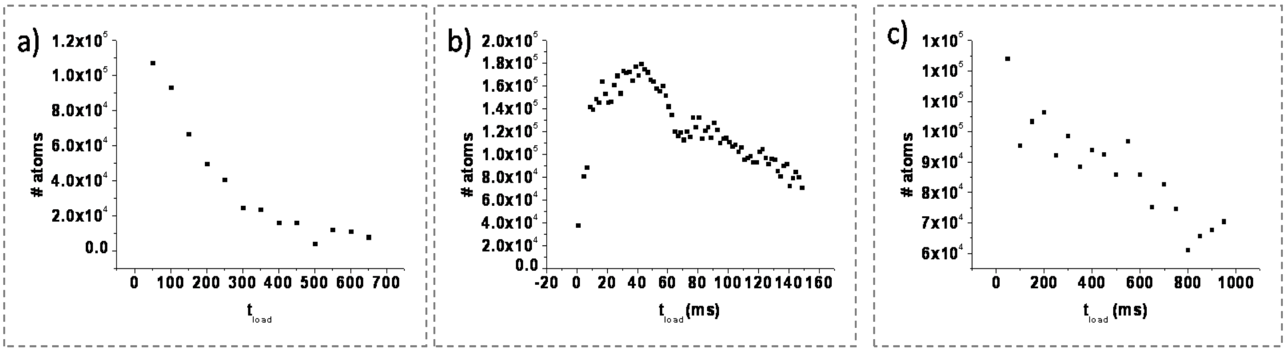

Fig. I.4.16: (a) Evolution of the atom number in the dipole trap with respect to the loading time from the Dark-SPOT. (b) The same study performed with the time step decreased. The laser power is ~60 W and the waist ~98 µm. In (c) the same study is performed with a trap of ~130 µm.

I.4.3. Loading the dipole trap from a C-MOT and molasses

A third type of reservoir of cold atoms from which a dipole trap could be loaded can be provided from a simple MOT or a C-MOT. This type of loading lies further away from the model discussed in [Comp06] and in Chapter I2, since the lifetime of the atomic reservoir cannot be considered infinite compared to the time constant of the loading process. Additionally, the trapping and the repumper lasers are present during the loading process and the atoms are not polarized. Such a loading process is better viewed via a phenomenological analysis, like the one presented in [Kupp00], were a similar approach is used to load a dipole trap of smaller dimensions with ^{85}Rb atoms. In this experiment, the authors manage to load 8 10^6 ^{85}Rb atoms into a 1 mK deep optical dipole trap with a waist of 58 μm. The number of loaded atoms is very high for the particular experiment since it is 40% of the atoms initially trapped in the MOT.

Superimposing the dipole trap to the MOT has always been an easy way to realize a dipole trap in our experiment, and it is the usual way such a trap was realized for all regulating purposes (alining, setting up the detection e.t.c.). Gradually, it was realized that superimposing the dipole trap to the C-MOT and applying a molasses phase in the end of the loading process led to loading efficiencies comparable (if not better) than the ones observed by the processes described in the previous paragraphs. The molasses phase did not change the loading dynamics, but improved the final atom number and decreased the temperature in the dipole trap. Finally, the molasses can be used alone to load atoms in the dipole trap. Such a method is even less related to the analysis presented in Chapter 2, since the loading process is *'instantaneous'* and the atoms are loaded as they fall after they have been further cooled by molasses and are polarized during the polarization phase.

These different loading approaches have been studied and the results of these studies are presented in this paragraph. The results of the study of loading a dipole trap by the various combinations (C-MOT and molasses, molasses alone) are given next. Again, the general trends are commented, but an attempt for a more detailed analysis is left for the final chapter, where the most characteristic data set of all the approaches presented in this chapter are discussed.

I.4.3.a. The C-MOT and molasses phase

As explained in the beginning of this chapter, where the first experimental sequence for the preparation of the magnetic trap is discussed, in our experiment we realize a C-MOT phase without increasing the magnetic field gradient but by increasing the trapping laser's detuning. This is due to the fact that each parameter in our experimental sequence has been optimized with respect to the final atom number in the dipole trap. An increase of the magnetic field gradient leads to an increase of the density in the MOT, while a decrease accompanied with an increase of the trapping laser's detuning can lead to the preparation of MOTs in very low temperatures. When the magnetic field gradient is turned off the atoms are in the molasses phase. This method can lead to the preparation of samples of Cs atoms in several μK, while the exact temperature depends in the trapping laser's detuning, the alignment and the absence of stray magnetic fields.

In our experiment we realized two different molasses cooling schemes, with similar results. One is the $\sigma+\sigma-$ 'bright' molasses scheme obtained simply by turning off the magnetic field gradient of the MOT and by detuning the trapping laser to $\sim 5\Gamma$. An additional scheme was the $\sigma+\sigma-$ gray molasses configuration reported in [Boir96], since this as well scheme allows the use of the same laser beams used for the preparation of the MOT. The necessary $F \rightarrow F\text{-}1$ cooling transition is available by the repumper laser coupling the $F = 3 \rightarrow F' = 2$ transition, while the trapping laser is brought to resonance with the $F = 4 \rightarrow F' = 4$ transition in order to 're-pump' atoms from the $F = 4$ to the $F = 3$ state, as shown in Fig. I.4.17. This is made possible by a home-made electronic system created by the LAC electronic support team, that unlocks instantaneously the frequency locked

DBR lasers and shifts their frequency to a desired value. This system is synchronized by a TTL, which duration defines the time for which the laser's frequencies stay modulated and thus the duration of the gray molasses phase. The fact that the laser used for repumping in the MOT and the conventional molasses phase now realizes the cooling transition makes its aliment and the power balance of its beams more critical than before.

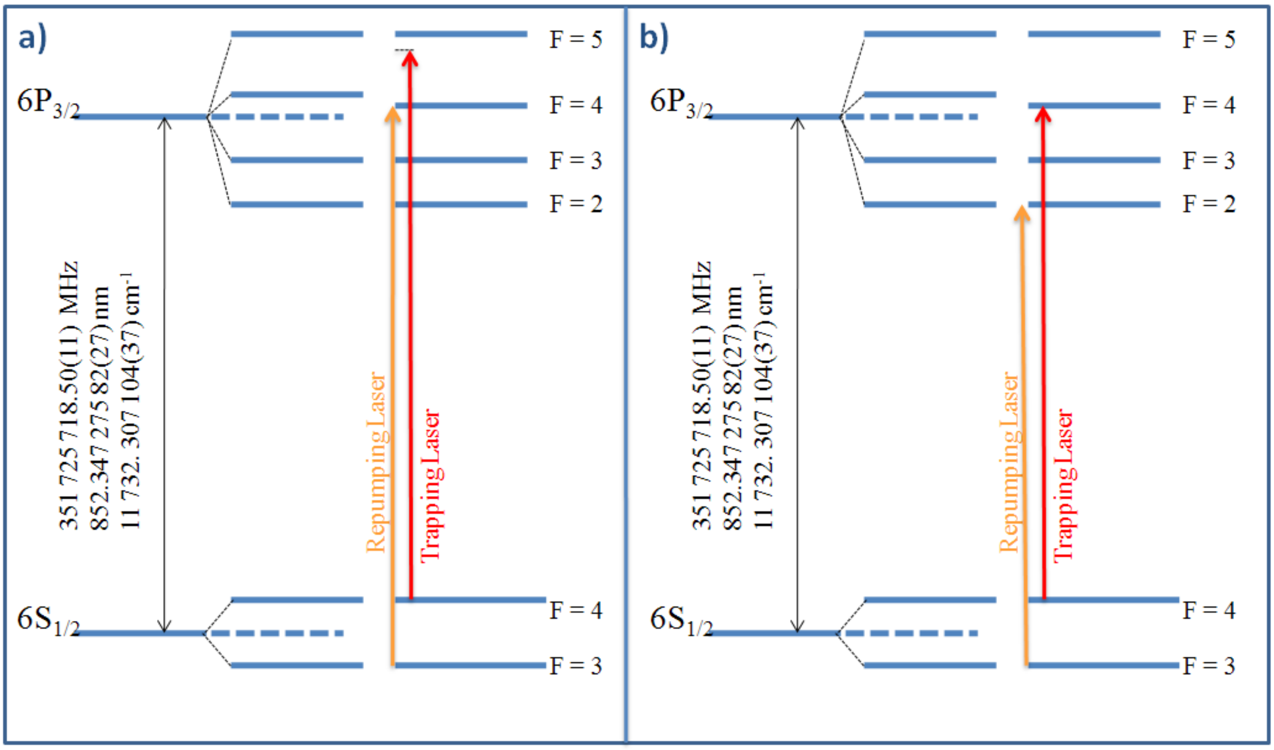

Fig. I.4.17: Tuning of the lasers for the realization of the MOT and the 'bright' molasses (a), and the 'Grey' molasses (b).

Both these molasses cooling schemes, have allowed us to prepare Cs atoms in temperatures of several μK, while the exact temperature depended everyday on a variety of experimental conditions, such as the alignment and the quality of stray magnetic field compensation in the vicinity of our trap. In Fig. I.4.18 we present a TOF study of the temperature of the atoms in the 'bright' molasses phase, which was found to be 5.8 μK. This is a usual value for the temperature of the molasses with which we operated. Temperatures somehow lower could be achieved if the trapping laser's detuning was increased (this was usually kept at ~5Γ but could bet set as high as 10Γ), while the gray molasses permitted the preparation of atoms in ~2μK. However, these low temperatures were achieved at the expense of the atom number and did not correspond to the best loading conditions for the dipole trap, for a variety of traps (dimensions between 80 and 300 μm). The dipole trap loading was optimized for detuning of ~5Γ and temperature close to ~5 μK as the measurement shown in Fig. I.4.18.

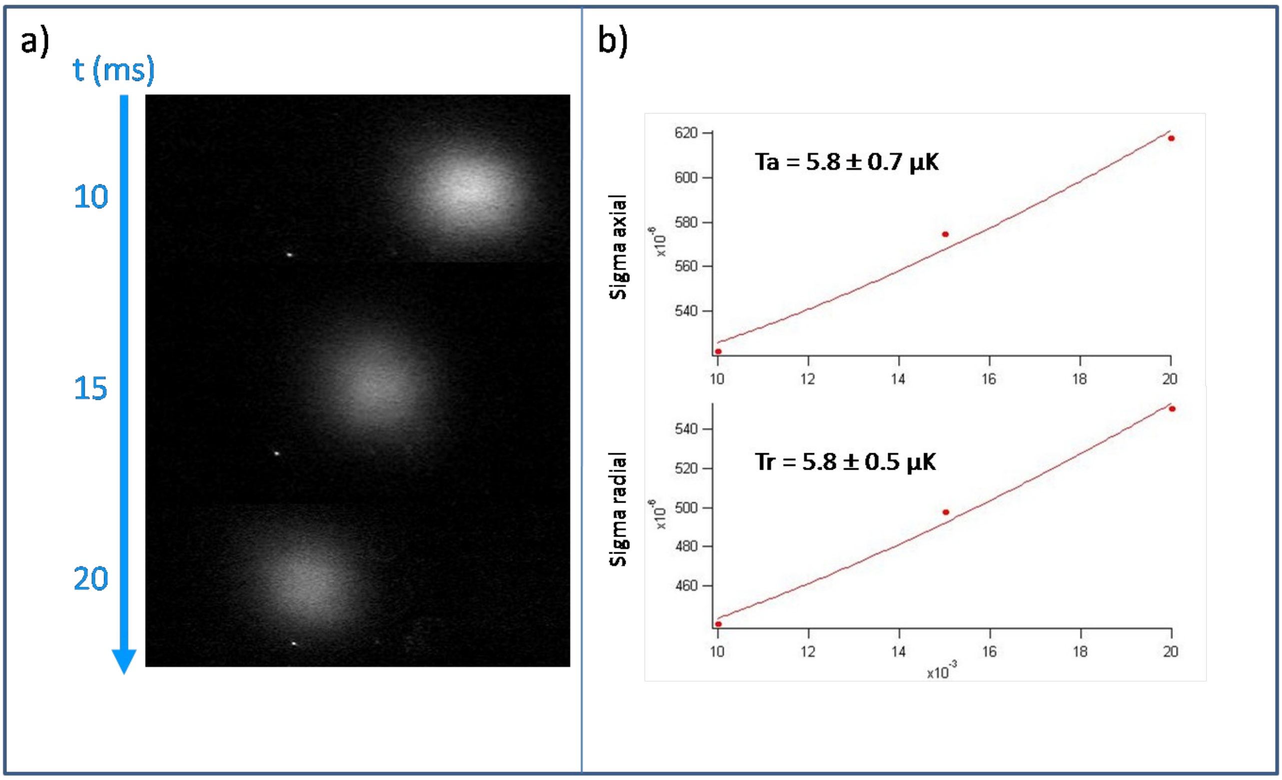

Fig. I.4.18: (a) Fluorescence images of the molasses cooled Cs atoms for three different TOF times 10, 15 and 20 ms. (b) Fitting the atomic cloud's expansion permits the temperature determination in the radial and axial dimensions.

I.4.4. Loading the dipole trap from the C-MOT and molasses

In Fig. I.4.19 we see the experimental sequence used in order to load the dipole trap from the C-MOT. The sequence is initially identical to the previous ones, as the atoms are trapped in MOT 1 and transferred to MOT 2. The dipole trap is turned in the same time with the C-MOT and stays on during the subsequent molasses phase as well. As loading time we consider the parameter t_{load} which corresponds to the time that the C-MOT and the dipole trap coexist. The molasses phase, which comes afterwards and usually has a duration of ~5 ms, reduces the temperature of the atoms trapped in the dipole trap, as well as the fraction of atoms lost in the first milliseconds after the end of the loading process (spilling) but it does not modify the general trends of the evolution of the number of atoms with respect to t_{load}. After the molasses phase the atoms are polarized and detected after the passage of a time t_{hold} equal to 2ms. By observing the number of atoms in the dipole trap for a varying t_{hold} we can can measure the lifetime of the dipole trap and extract information for the collision processes inside it. The polarization is necessary in order to reduce the two body losses and to observe high lifetimes, as well as for the case where evaporation in the dipole trap is attempted. On the contrary, when the loading is studied and the observation of the dipole trap is done ~20ms after the end of the loading process, polarization is not important and is omitted.

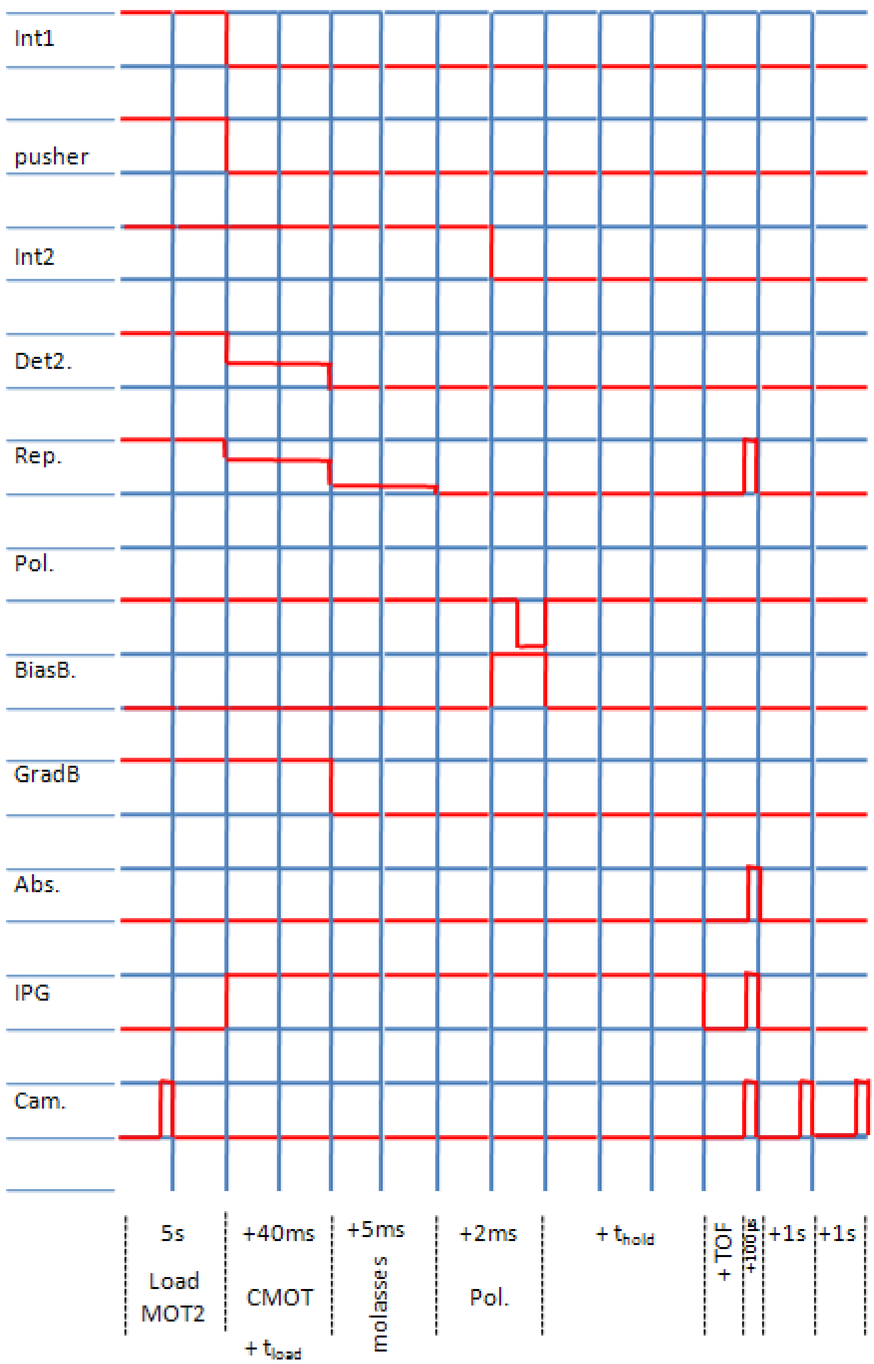

Fig. I.4.19: Experimental sequence used for the loading of a dipole trap by a C-MOT with a subsequent molasses phase.

In Fig. I.4.22 we show a study of the dipole trap loaded by a C-MOT with a subsequent molasses phase, for our usual dipole trap of 89 µm and 60 W, and for a smaller ~50 µm trap in Fig. I.4.21.

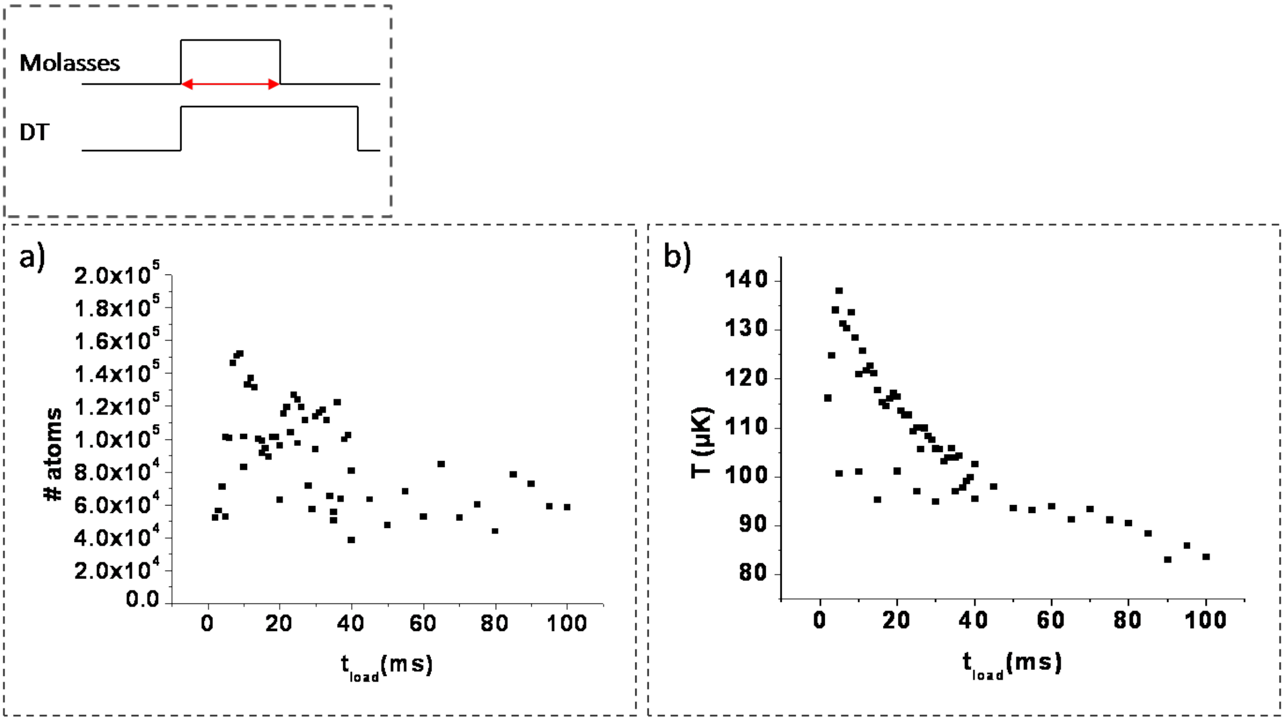

Fig. I.4.20: Loading the dipole trap from C-MOT with a subsequent molasses phase. Evolution of the number of atoms (a) and their temperate (b) in the dipole trap with respect to the t_{load}. The trap has dimensions of ~89μm and power of ~60W.

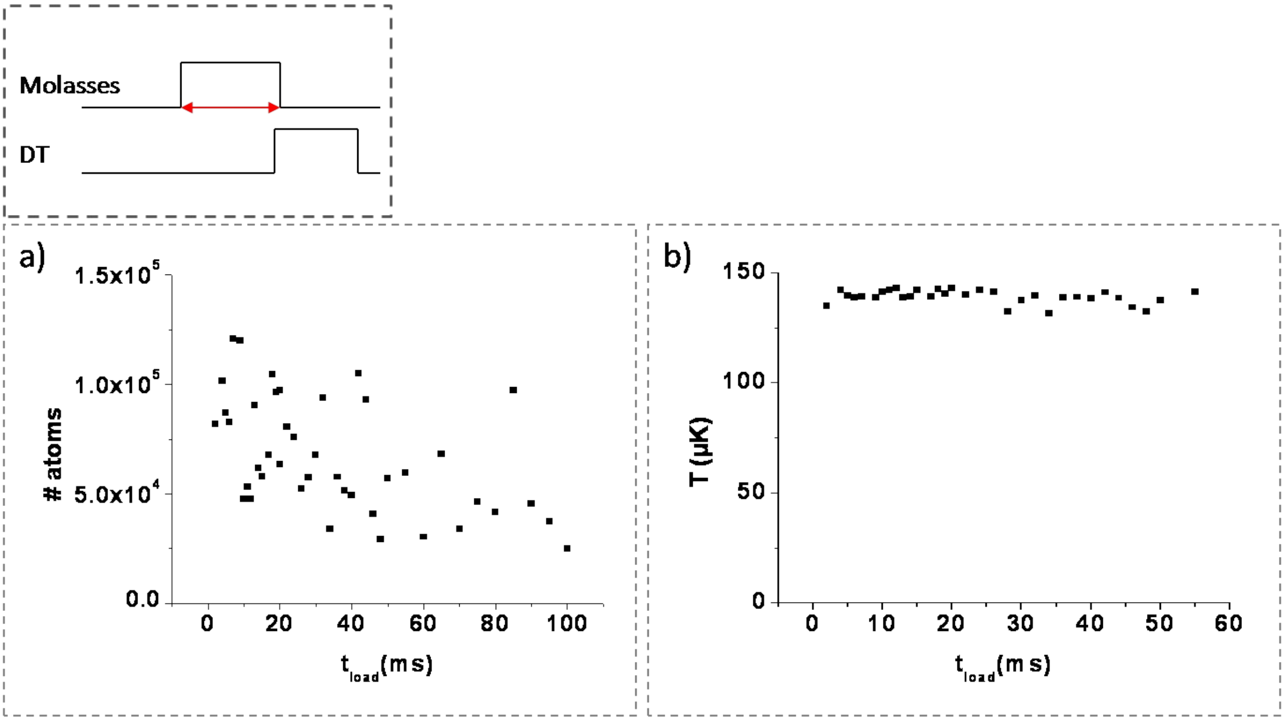

Fig. I.4.23: Loading the dipole trap from a bright molasses. The dipole trap is turned on after the end of the molasses phase. Evolution of the number of atoms (a) and their temperature (b) in the dipole trap with respect to the t_{load}. The trap has dimensions of ~89μm and power of ~60W.

We see that decreasing the dimensions of the dipole trap, does leads to a smaller number of atoms to be transferred in the dipole trap, while their temperature is increased. Larger traps were also realized but the loading was again lower than the ~100 μm dipole trap. The 89 μm trap was loaded by molasses alone in two different ways which are shown in Fig. I.4.20 and Fig. I.4.23. In Fig. I.4.20 the dipole trap is turned on during the molasses phase, and the time t_{load}, which is now the duration of the molasses, is varied. In the second case (Fig. I.4.23), the molasses and the polarization are performed, and the dipole trap is switched on right afterwards, while the duration of the molasses, now noted t_{moll} is varied. The polarization was not omitted in this step, since it's total duration of ~2.5ms (optical pumping to F = 3 and polarization) is comparable to the time it takes for the cold Cs atoms to fall out of the trapping region.

I.4.5. Loading the dipole trap via Raman Sideband Cooling

The Raman Sideband Cooling (RSC) technique allows for the preparation of atomic samples in temperatures of several hundreds of nK, and it has been used in both the two successful approaches for the production of a Cs BEC [Hung08, Web03]. Those approaches aimed in using the very cold atoms produced by the RSC to load 'instantaneously' a very shallow dipole trap in temperatures close to one μK, and apply evaporation cooling for the production of a BEC. Our experiment meant to explore an opposite approach, the one where a deep dipole trap is loaded with not so cold atoms from an atomic reservoir. On the one hand the disagreement of our experimental results with the theoretical predictions, and on the other the impressive results of [Hung08] were a Cs BEC is achieved within 2 seconds by loading a shallow trap by RSC and performing 'runaway' evaporation, led us to an attempt to achieve BEC by such an approach. The beginning of this effort coincides with the first appearance of the vacuum problems that led to severe damages on the experimental set-up. Some of the data presented were obtained after the severe damages of October 08 were some basic characteristics of our system, especially the vacuum, had begin to be questionable. Nevertheless, before the end of the experiment, a RSC had been installed in the experiment, and dipole traps of ~500 μm and of ~3μK had been prepared.

Our effort with RSC was never really completed for a variety of reasons. In a technical level, establishing a proper vacuum system demanded more time and resources than the team disposed at the time. At a scientific level, our studies so far suggested that the idea of loading from a 'reservoir' have to be revisited. At the same time, the work of [Web03] completed the work of [Hung08] in such a way that very little could be added. For example, when the idea of loading a dipole trap from an atomic reservoir was discussed in [Comp06], among the expectations was to achieve BEC after some seconds of evaporation, which would be an improvement compared to some tenths of seconds that were needed in [Web03]. The approach of [Hung08] had already achieved this goal, while it reduced greatly the complexity of the overall experiment in the same time. Finally, the recent developments, that resulted the teams efforts in the area of cold molecule production and manipulation, turned our interest to the study of cold molecules, which is discussed in the second part of this thesis.

In this chapter the RSC technique is briefly explained, the method followed for its preparation in the laboratory is presented and the results of the loading of a dipole trap by it are shown. For the realization of this approach in our set up major modification had to be made. Some of them were presented in paragraph I.3.2.a and consider the configuration of the diode laser in order to provide with the radiation necessary for the realization of the RSC. Another important modification considered the quality of the stray magnetic fields compensation in the trapping volume which is an important parameter for the success of this cooling technique. This is why, after a brief introduction of the RSC operating principle I describe the methods used to compensate stray magnetic fields. Finally, the large dipole trap of ~500 μm size and ~3 μK temperature prepared with the use of RSC is presented.

I.4.5.a. The Raman -Sideband Cooling in LAC

As explained in the introduction chapter, in the RSC technique, light does not interact with free, but with trapped atoms with relatively high 'trapping frequencies' (or small oscillation periods in the trap). The technique succeeds in performing optical transitions between these vibrational states, and transferring the atomic population in the lowest one. The ability to resolve these vibrational states is essential for the realization of the technique, this is why the it requires either enormous resolution or high confinement. For the realization of the technique in neutral atoms, the required confinement can be achieved only by the use of optical lattice traps in one, two or three dimensions. In our experiment we realized RSC in a three dimensional lattice following the work presented in [Treut01].

The laser geometry used for the preparation of the lattice is shown in Fig. I.4.24. The angles a_1 and a_2 shown in the scheme were in the order of 10°. The total power of the RSC beams was ~10 mW and the waist of the RSC beams was ~1 mm. The power of the vertical beam was approximately three times bigger than the one of the beams in the x-y plane. An additional simplification of the technique introduced in [Treut01] is the use of a single σ+ polarized beam propagated with an angle of ~5° with respect to the vertical direction to achieve polarization, substituting the two beam configuration explained in paragraph I.4.1.b. Both those two configurations were used in our realization of the experiment with similar results.

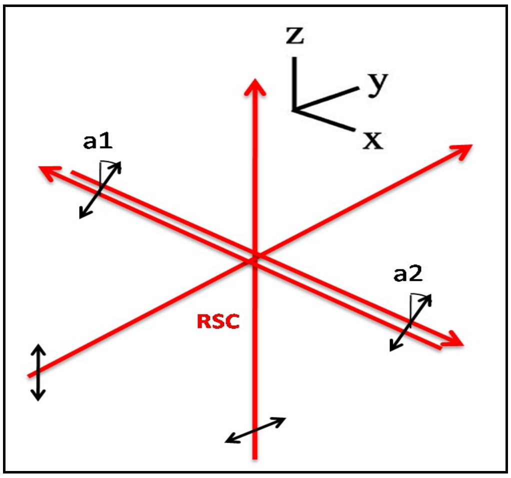

Fig. I.4.24: Configuration of the laser beams used for the Raman Sideband cooling.

I.4.5.b. Stray magnetic field compensation

Perhaps the greatest technical challenge for the preparation of RSC is the magnetic field compensation. The reason is that the magnetic field needed to bring into degeneracy the $|F=3,m_F=3,v\rangle$ and $|F=3,m_F=2,v-1\rangle$ states is, for the case of Cs, equal to 50 mG, so it is clear that stray magnetic field have to be compensated at least below this value. In this paragraph the methods employed for the magnetic field compensation are discussed.

Stray magnetic field compensation is usually done with the use of RF induced transitions between magnetic sublevels. However, since our set-up did not included any RF devices, we were forced to search for alternative methods. The first method initially considered is based on the photo-mechanical, or Hanle effect which is described in [Kais91]. In brief, the Hanle effect is the pushing effect that a resonant beam will have upon an atomic sample due to the radiation pressure. Let us consider an atomic beam or an cloud of cold atoms and a circularly polarized beam that can polarize the atoms by optical pumping via an F → F – 1 transition. When the atoms are polarized, they cannot interact with the light since they are found in a dark state of the system atoms – radiation and the mechanical effect terminates. If the atoms are found in an area with randomly oriented magnetic fields, they will perform Larmor oscillations around these axis, they will loose their polarization and the interaction with the light, as well as the mechanical effect will continue. This is were our magnetic field compensation method is based. A circularly polarized beam, resonant to the F = 3 → F' = 2 polarization transition, shines on a falling cloud of cold Cs atoms as we scan the values of the current in the magnetic field compensation coils. The best compensation is achieved for the values were the displacement of the atomic cloud is minimum. This displacement is easily measured if the fluorescence of the falling atoms is monitored, in a small spatial window that corresponds to the position of the cloud in the absence of the optical pumping beam. The desired value will coincide with the maximum of the acquired graph. In Fig. I.4.25 we show such a data set. It is obvious that such a study has to be performed in more than one directions, since magnetic fields parallel to the polarizing beam propagation cannot be 'sensed' with this method. We examine magnetic fields in the horizontal plane by using the σ+ polarization beam while the vertical direction is examined by polarizing circularly the horizontal beam used usually for polarization (π component).

An additional, more practical approach for the stray magnetic field compensation was also followed. This method used the fact that a small magnetic field is always used in order for the atoms to preserve their polarization, as explained in the paragraph I.4.1.b. This is necessary because if such a field does not exist, atoms will loose their polarization by performing Larmor precession around the axis of the randomly oriented stray magnetic fields. This means, that a field parallel to the quantization axis is always needed, and that this has to be greater than any stay field. If we can polarize and maintain polarization in a sample of Cs atoms, with this 'direction giving' magnetic field smaller or equal to 50 mG, then we are sure that we compensate all stray magnetic fields up to this value. The power supplies of the compensating coils were easily calibrated with the use of a Hall effect sensor while the polarization of the atoms was monitored with the use of the sequence presented in Fig. I.4.5.

With the combination of these two stray field compensation methods we were able to achieve the preparation of an RSC cooled sample, as the one shown in the Fig. I.4.26. The number of trapped atoms was usually $\sim 10^7$ and the temperature was estimated to be somehow smaller than one μK. The experimental sequence used was very simple. The atoms are loaded from MOT 1 to MOT2, they pass a C-MOT and a molasses phase and then the RSC is applied. A difference between this sequence and the experiment described in [Treut01], is that there the authors load the atoms the RSC lattice directly after the C-MOT phase, without any molasses phase in between.

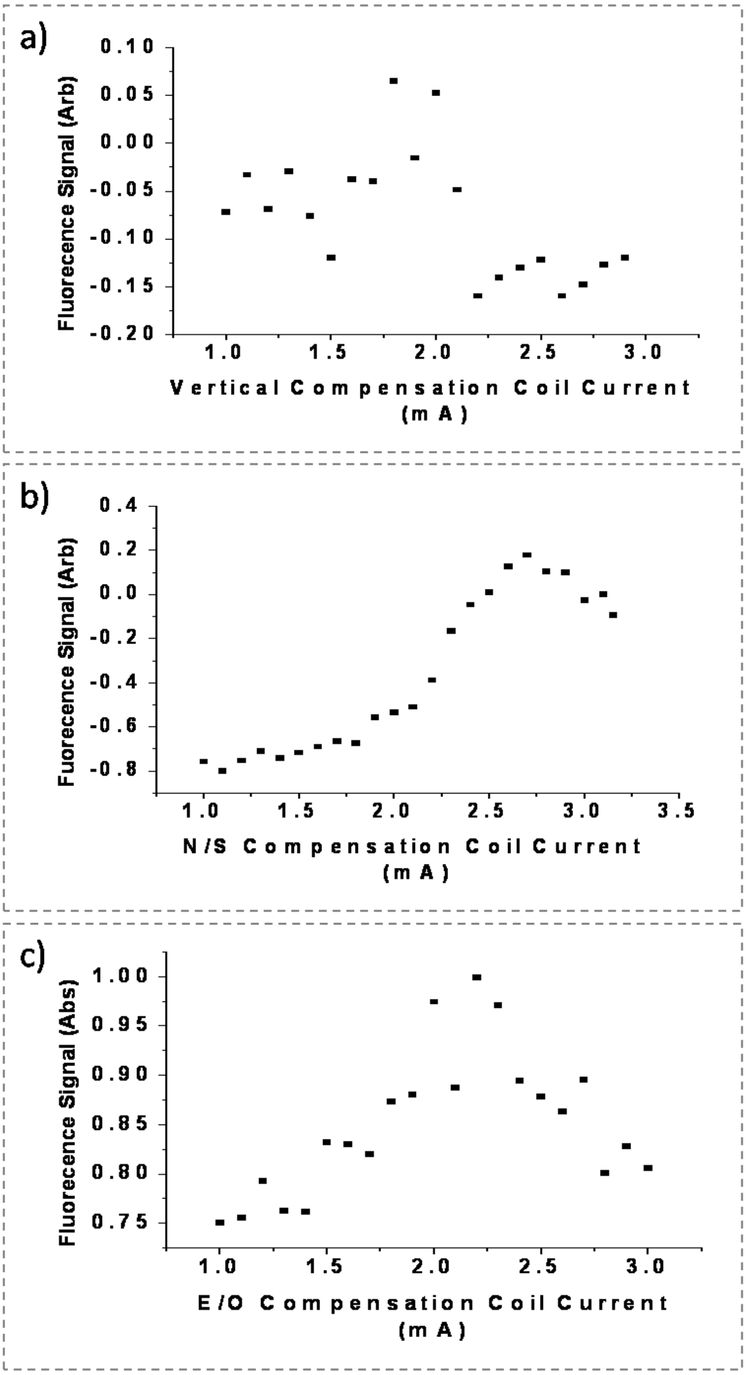

Fig. I.4.25: Compensation of the stray magnetic fields with the use of the Hanle effect, for the vertical (a), the North/South (b) and the East/Ouest (West in French) (c) directions.

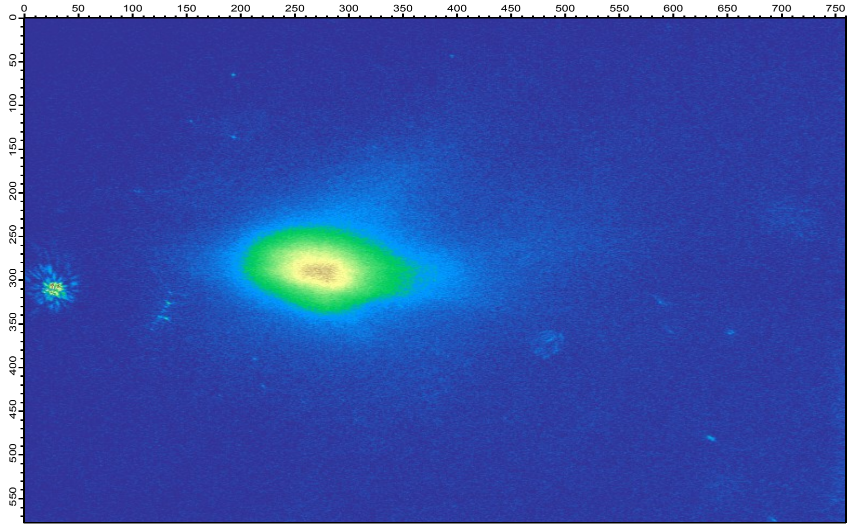

Fig. I.4.26: Fluorescence image of $\sim 2*10^7$ Cs atoms cooled by RSC. Their temperature is estimated with the TOF technique in ~800μK

I.4.5.c. Loading a 600 μm dipole trap

With the RSC we were able to realize completely different dipole traps than the one so far prepared. The approach demanded for shallow traps of big dimensions, where the biggest possible percentage of atoms should be transferred by the RSC. The dimensions of the trap chosen was ~600 μm. In such a loose focalization, the ~60 W of the dipole trap power do not suffice to compensate the gravity and hold the heavy Cs atoms. This is why it is necessary to apply a 'levitating' magnetic field gradient, similarly to [Web03b]. This magnetic field gradient results to a force on the Cs atoms which depends on the hyperfine state they are in. Thus, levitation is achieved for different values of the magnetic field gradient for each hyperfine state. If the value of the magnetic field gradient is chosen to be the one that compensates gravity for the $|F=3,m_F=3>$ state, then levitation plays an additional polarization-filtering role and contributes to the purity of the atomic sample distribution.

In Fig. I.4.27 we see an absorption imaging picture of such a magnetically levitated dipole trap. The atoms are cooled by means of RSC in a temperature ~0.8 μK and one second after the end of the loading process $\sim 2\ 10^5$ of them are found in the dipole trap in a temperature of ~3 μK. The number of atoms might seem similar to the numbers achieved by the 'reservoir' methods presented in the previous paragraphs. The very big difference here is that this is the number of atoms trapped in the dipole trap one second after the end of the loading process, when all spilling effects are over. If the number is observed some ms after the end of the loading process, as it is done for the case of the tight dipole traps discussed previously, the atoms number is more than an order of magnitude higher. Similarly, observation of the dipole traps prepared with the use of the molasses or any other technique discussed in previous paragraphs, one second after the end of the loading process was practically impossible, as the usual lifetimes observed was close to 400 ms. This qualitative difference between this shallow dipole trap and all the previously reported trap is shown in Fig. I.4.28. As we see the lifetime of the RSC prepared, 600 μm trap, shown in part (a) is close to 2.5 s. The lifetime measurement shown in part (b) corresponds to a C-MOT loaded trap of ~89μm trap[1].

---

[1] Such measurements of the lifetime are useful for the determination of the collisional losses of the dipole trap, which are essential for the subsequent evaporation process. Despite the fact that such a study was made for all the different types of dipole traps prepared, I choose to show only one of them in the main body text, for two reasons . First, if after the loading process, the atoms can be efficiently polarized in the ground state, the lifetime is not depended on the loading process, but just to the final temperature and atoms number achieved by it. Second, our efforts to realize

Even though the dipole trap realized with the use of RSC appears to have an improved lifetime with respect to the previously prepared dipole traps, it is still not possible to perform evaporating cooling on it. Even if the lifetime seems barely sufficient (the authors of [Bal09] achieved BEC in less than 2 s), the atom number is too low and the oscillation frequencies are slower than the ones necessary for evaporation. The atoms number is an order of magnitude lower than the ones reported in [Web03, Hung08] in similar timescales and all our efforts did not lead to any improved result.

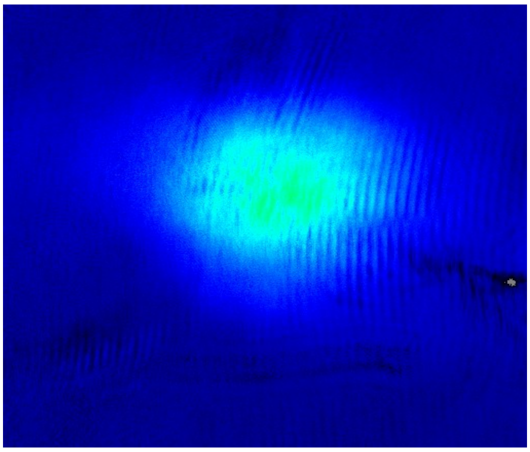

Fig. I.4.27: 2 10^5 Cs atoms trapped in a dipole trap of ~600μm. The atoms are cooled by means of RSC and have a temperature ~0.8μK before and ~3μK after the loading.

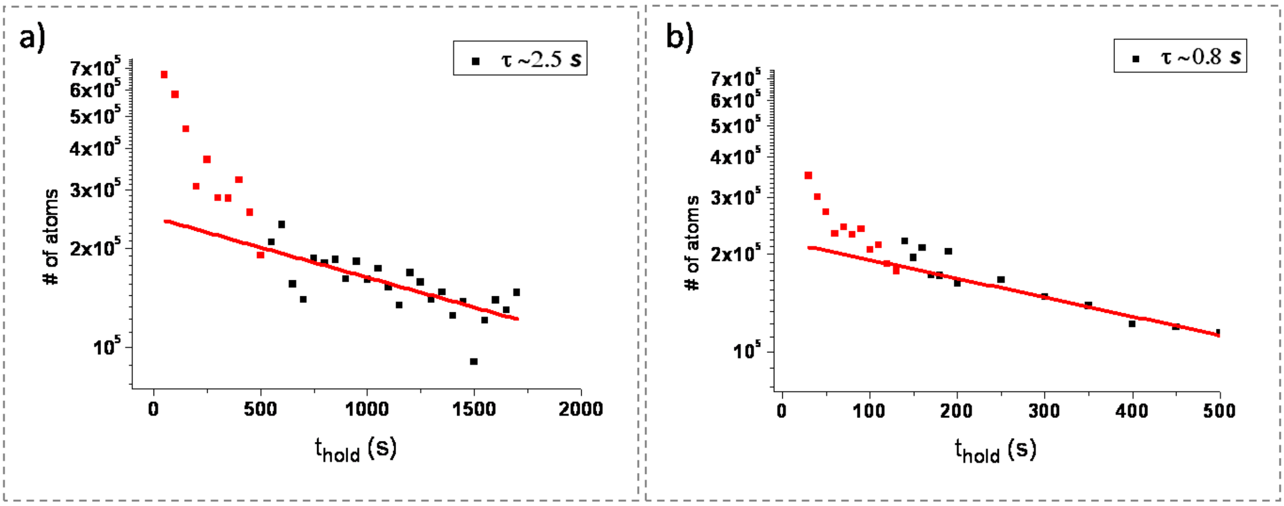

Fig. I.4.28: Study of the lifetime of the Cs atoms (a) in the levitated dipole trap of 600 μm loaded by RSC and (b) in a 89 μm dipole trap loaded by C-MOT and molasses combination The red points in both graphs correspond to measurements of the atoms number in very early times where spilling is mostly responsible for the its decrease, and are not taken into consideration for the estimation of the lifetime.

---

evaporating cooling, which were many, did not lead to any notable result. Feeling that the problematic performance of the experiment begins in the loading process, I chose to focus on it and not to refer to the not interesting and haze evaporation cooling results. However, all the experimental and theoretical study related to the evaporation and the lifetime of the dipole traps is presented in the Annex.

I.4.6. Summary

In this chapter the process of loading a dipole with Cs atoms was studied with various methods. The initial idea involved the use of an atomic 'reservoir', from which the crossed dipole trap could be loaded for larger time intervals than from conventional loading techniques. The first candidate for the realization of the reservoir was a magnetic trap of Cs atoms. However, since the experimental results did not agree with the theoretical simulations, which predicted very efficient loading, the study was expanded to include two additional reservoir types, the C-MOT and the Dark-SPOT. The results of these types of loading were compared to the loading obtained by a more conventional cooling technique, which involved loading from molasses.

Since none of the above mentioned techniques resulted to the preparation of an atomic sample, sufficiently large and cold in order to be interesting for the subsequent evaporation experiments, the RSC method was finally employed. Even though this technique has been an important element of the so far successful Cs BEC experiments, its implementation in our experiment was proved not enough for the achievement of BEC. As explained in the current paragraph, this was due to the fact that the RSC technique was realized in a period that our experimental set-up suffered from important, vacuum related problems, and the technique's implementation was most probably incomplete.

However, with the use of RSC, we were able to load dipole traps of large dimensions, that exhibited lifetimes that were larger than ever before. Unfortunately, we were not able to complete this last approach, which was based in RSC and dipole traps of large dimensions, since the experimental set-up collapsed due to vacuum breakdown in October 2008. Leaving discussion of the experimental results to be discussed in the following chapter, I list the most important characteristics of the dipole traps loaded with each of the methods discussed in the current chapter, in the following table.

Loading Method	N_{max}	T_{Nmax}	t_{max}	t_{hold}
Magnetic trap	$2.2\ 10^5$	~140 μK	60 ms	~400 ms
Dark-SPOT	$2\ 10^5$	~140 μK	40 ms	~400 ms
C-MOT	$3\ 10^5$	~140 μK	10 ms	~400 ms
molasses	$1\ 10^5$	~130 μK	instantaneous	~400 ms
RSC	$7\ 10^5$	~3 μK	instantaneous	~2.5 s

TABLE 4.1 Table resuming the most important characteristics of the dipole traps loaded with each of the methods discussed in the current chapter. These are N_{max} (maximum number of atoms loaded in the dipole trap), T_{Nmax} (temperature of the maximally loaded dipole trap), t_{max} (maximum loaded time) and t_{hold} (lifetime of the dipole trap)

CHAPTER I5: DISCUSSION ON THE EXPERIMENTAL RESULTS

I.5. DISCUSSION ON THE EXPERIMENTAL RESULTS

The preparation of a Cs BEC in LAC involved a study of the loading of a dipole trap by an atomic reservoir, which was initially considered to be provided by a magnetic trap. This is the subject of the proposal paper [Comp06] and of the thesis of G.Stern [Stern08], with whom I collaborated for more than a year during my thesis. Since the strategy of the loading from a magnetic trap did not result to the preparation of a dipole trap with the necessary characteristics for the successful realization of evaporation, different approaches for the loading process were considered. Theses approaches involved substitution of the magnetic trap by a Dark-SPOT or a C-MOT and instantaneous loading by bright and gray molasses and they were discussed in the previous chapter.

A big part of our experimental activity had to do with the evaporation process. We have realized numerous efforts to perform evaporating cooling, by various methods that involved magnetic expulsion, real-time modification of the dipole trap's dimensions and more. Our goal at the time was the observation of a phase space density increase as a preliminary evaporation result. The results of these studies were very haze and no important increase in the phase space density was observed. These evaporation studies were chosen not to be discussed in the main text and the results of the most characteristic of them are presented in the Annex, along with results on the real time compression of the dipole trap. A reason for the failure of the evaporation cooling in our experiment is the very small lifetime of the dipole traps we managed to prepare, which leads for the majority of the trapped atoms to be lost in smaller timescales (~100 ms) than the ones in which an efficient evaporation process can be realized (usually several seconds)

Initially, I intended to devote a large part of the analysis of the experimental results in the study of the lifetime of the dipole traps prepared. Indeed, the lifetime of every trap prepared in the lab was measured, while I have made several attempts to fit the most characteristic ones with theory discussed in [Web03b]. However, I soon abandoned this idea for two reasons. The data analysis discussed in [Web03b] was performed in atomic samples of much smaller temperature, were the collisional process are less complicated, and the derivation of collisional parameters is possible. Such an analysis is perhaps not suitable for our traps, often at 100 - 1000 times higher temperatures than the ones discussed in [Web03b].

The second reason is that the lifetime of the dipole trap is not the first point of disagreement between the experimental results and the predictions of [Comp06]. In the loading process we not only see much lower efficiency than the one expected, but also very different temporal behavior than what we would expect considering the basic assumptions of [Comp06].

Finally, the time scales in which we observed our trap were too small for safe conclusions to be extracted by their analysis. It could be that the behavior of our atoms in the time scale that it is examined to be much more determined by the 'spilling' process in the dipole trap, than by the collision properties as they are considered in the analysis presented in [Comp06]. Indeed, the parameter η of our dipole traps, which is the ratio of the potential depth over the temperature of the atoms was almost always smaller than four. This value is a technical limit, below which, the equations that describe evaporation, which were developed in [Comp06] and discussed in Chapter 2 are not valid, and more complicated analysis has to be performed [deCar04].

For these reasons, the lifetime studies are generally not shown in the main body text, with the only exception of Fig.4.28, where such two lifetime studies are compared. The one corresponds to a ~600 μm prepared with the use of RSC and the other to a ~100 μm dipole trap prepared with the use of a combination of C-MOT and molasses. Demonstration of more lifetime studies is not necessary, since the lifetime shown in 4.28 (b) is characterizes more or less all traps of similar dimensions prepared with the methods discussed in all paragraphs before 1.4.4. Indeed, if after the end of the loading process the atoms are polarized in the absolute ground state |F=3,m_F=3>, the loading process cannot be considered to be related with the lifetime of the dipole trap, but only the number of atoms and the temperatures achieved by it.

The attention during the presentation and the analysis of the experimental results is mostly on the loading process. Even though the equations developed for the evaporation process in [Comp06] cannot be applied, the equations for the loading process are still valid, while many of the basic magnitudes calculated there can be very useful for the understanding of our results. On the other hand, the basic trends of the temporal evolution of all our loading process, except the RSC, cannot be explained in the contest of [Comp06] and Chapter 2. In this analysis, the reservoir ensures a constant flow of atoms in the trapping region and does not explain the atom number decrease after some tens of ms observed in the experimental realization of all these approaches. In our bibliographic search, similar trends have been found in the results presented in [Kupp00]. Even though this experiment is performed in ^{85}Rb atoms, the approach is very close to the one described in paragraph I.4.3. Additionally, the phenomenological theory developed in this paper to describe the loading process is very general, and it could be able to describe all the techniques discussed in the paragraphs I.4.1 to I.4.3.

I.5.1. Phenomenological approach for the description of the loading process

In reference [Kupp00], an experiment of loading a dipole trap with Rb atoms trapped in a MOT is reported. The authors report the transfer of 8*10^6 ^{87}Rb atoms into a 1 mK deep optical dipole trap by overlapping it with a C-MOT, in a very similar way to the approach described in paragraph I.4.c. The authors present the evolution of number of atoms transferred in the dipole trap with respect to the loading duration, and a decreasing trent is observed, similar to the decreasing trent observed in our studies, only that the time scale of the decrease is in the case of [Kupp00] several seconds.

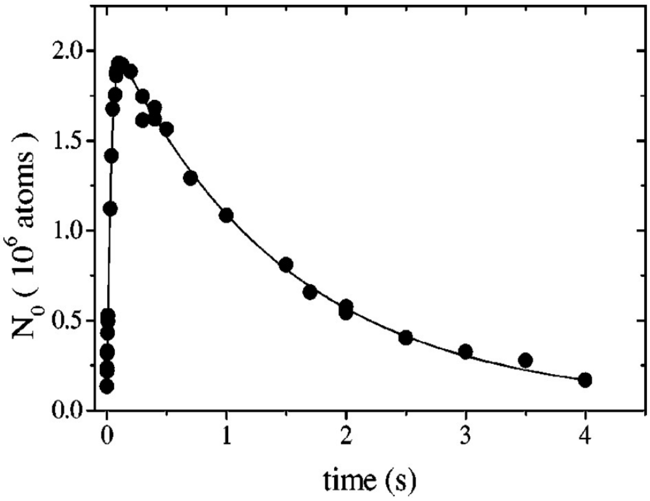

Fig. I.5.1.1: Evolution of the number of Rb atoms loaded in the crossed dipole trap versus time, in the experiment reported in [Kupp00].

Furthermore, the authors develop equations that describe the evolution of the number of atoms transferred in the dipole trap with respect to the loading duration. Their approach is very different to the one developed in [Comp06] and discussed in Chapter 2. Instead of estimating all relevant parameters and developing differential equations that can describe the evolution of the system, the authors of [Kupp00] develop a simple phenomenological formula with a few free parameters with which they fit their experimental results. This equation succeeds in describing a decrease in the atoms number that is observed in these results, and which is similar to the decrease observed in the results of our studies. The simplicity of the formula makes more attractive an attempt to describe our experimental results with a similar approach.

The phenomenological approach of [Kupp00] is consisted in the development of the rate equation 5.1 and its use to fit the experimental result for the temporal evolution of the dipole trap loading. In this analysis, the different loss mechanisms are grouped according to their dependence on the atom number participating in the process. One group of losses are the losses that do not depend on the atoms number (density), such as the background gas collisions, losses due to absorption of stray photons etc. In the case where such an analysis is considered for the description of loading a dipole trap from a magnetic trap 'reservoir', the Majorana losses could be added in this group. A second group is the two body losses and finally the weaker three body losses. In equation 5.1, these losses are labeled as γ_L for the density independent losses and as β_L for the density depended losses, while the three body losses are negliged. The remaining term is the rate with which the dipole trap is loaded from the atomic reservoir which has a finite lifetime equal to $1/\gamma$.

$$\frac{\partial N}{\partial t} = R_0 e^{-\gamma t} - \gamma_L N - \beta_L N^2 \tag{5.1}$$

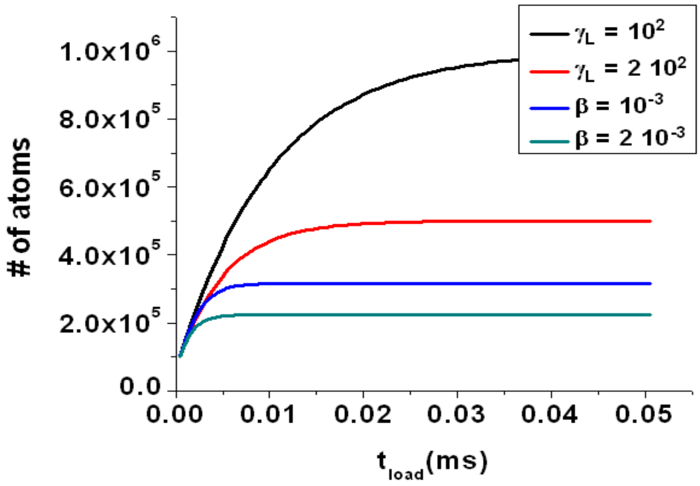

Fig. I.5.1.2: Number of atoms transferred from the magnetic to the dipole trap as predicted by Eq.5.1 for an initial loading rate of $R_0 = 10^8$ atoms/s, and infinite magnetic trap lifetime ($\gamma_L = 0$ atoms/s). For each curve all losses are set to zero except for the one indicated. This picture aims to display the fact that collisional losses cannot justify a decrease in the atom number during the loading process.

The advantage of this description with respect to the one presented in Chapter I2, apart from its simplicity, is that it considers a finite lifetime for the reservoir, a fact that allows it to treat the decrease of the final atoms number with respect to the loading time. This possibility does not exist for the analysis of Chapter I2, since the constant flow of atoms from the reservoir to the trapping region does not allow to the number of atoms to decrease. The loading process terminates when a thermodynamic equilibrium is achieved between the trap and the reservoir. This situation can also be described by Eq.5.1 if the lifetime of the reservoir γ is considered to be infinite. In Fig. I.5.1.2 this situation is displayed for various values of the remaining loss parameters. We see that no matter how great the various losses are, they can only reduce the final number of atoms transferred, but cannot justify a decrease of the final atom number during the loading[1].

---

[1] This is true since the dipole trap thermalization time ($\sim 3t_{coll} \sim 5$ ms, where t_{coll} the elastic colision time) is very small with respect to the times in which the observations are taking place.

I.5.2. Fitting the experimental data

Since Eq.5.1 can treat a decrease of the number of transferred atoms during the loading process, we can try to fit our experimental results with it. The interest in such a fit is to see weather the time dependance of this decrease can indeed be correlated to the lifetime of the atomic reservoir in our experiments. Apart for the reservoir lifetime γ, the remaining parameters R_0, γ_L and β_L are irrelevant to the atom number decrease and can be seen as free parameters for the time being. In Fig. I.5.2.1 we see the fit of 5.1 in three different studies. A 89μm waist and 60W power crossed dipole trap is loaded a) by a magnetic trap, b) by a Dark-SPOT and c) by a C-MOT (data corresponding to figures 4.10a, 4.16.b and 4.19a). The values used for the parameters R_0, γ, γ_L and β of Eq.5.1 in each case are shown in Table 5.1.

The parameter R_0 represents the rate in which atoms are loaded in the dipole trap by the reservoir in this description and γ_L the density independent losses, while no density depended losses were considered. This fact does not change much in this analysis, since the losses are there only to balance the loading rate into a final atom number that corresponds to the maximum value experimentally obtained. The losses, as well as the loading rate R_0, are irrelevant to the atom number decrease during the loading, which is described only by γ and which this analysis aims to determine. The inverse of γ corresponds to the lifetime of the atomic reservoir which could explain such a temporal evolution. We see that for the case of loading a dipole trap from a magnetic trap reservoir, the required lifetime is 3 ms, which is ~4 order of magnitudes less than the values experimentally measured (in the order of 20 s). This result shows that the finite lifetime of the atomic reservoir cannot explain the temporal evolution of the atom number versus the loading time of the magnetic trap. For the case of the Dark-SPOT shown in Fig.5.2.b the required lifetime is 150 ms. The lifetime of the Dark-SPOT has not been measured, but the lifetime of an ordinary MOT is ~15 s, and it is not expected to be very different, thus the 150 ms required by Eq.5.1 is still considered a very small value. Finally, for the case of loading from a C-MOT shown in Fig.5.2.c, the required lifetime is 2.5 s, a value that is less than ten times smaller than the lifetime of an ordinary MOT, and can be seen as more realistic.

Unfortunately, the lifetime of the C-MOT was never measured in the experiment, so the prediction of Fig.5.2.c cannot be verified. However, the value of 2.5 s does not lye far from the value observed for a regular MOT, while the lifetime of a compressed MOT, is expected to be reduced due to temperature increase. The relative success of Eq.5.1 in this case was expected, since the loading method involving the C-MOT is very close to the experiment reported in [Kupp00] and the fitting process yields only a rescaling of γ by a factor of 10. On the other hand, the values extracted for the parameter γ in the case where the dipole trap was loaded by a magnetic trap or a Dark-SPOT, suggest that a different explanation, other than the finite reservoir lifetime has to be proposed.

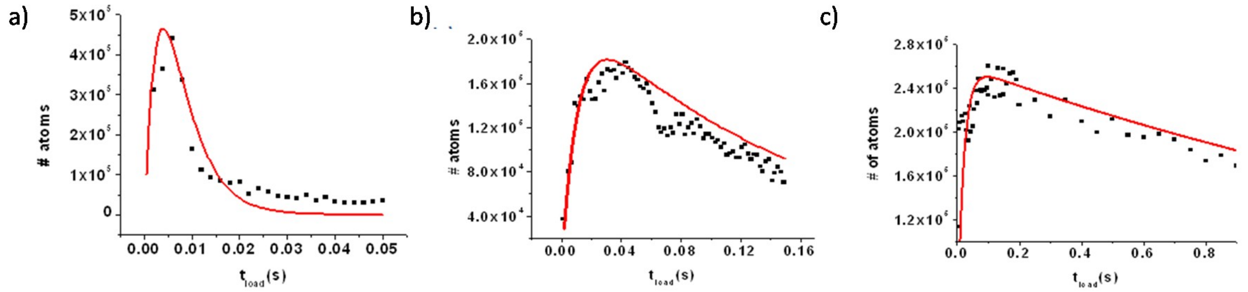

Fig. I.5.2.1: Fitting with 5.1 the evolution of the atom number loaded in the dipole trap by a) a magnetic trap, b) a Dark-SPOT and c) a C-MOT.

	R_0 (atoms/s)	γ (s^{-1})	γ_L (s^{-1})
a) Magnetic Trap	3.0 10^8	333,33	200
b) Dark – SPOT	2.2 10^7	6,66	100
c) C-MOT	1.3 10^7	0,4	50

TABLE 5.1. Values of the various parameters of Eq.5.1 used for the fits shown in Fig. I.5.2.1

The analysis presented in Chapter I2 and [Comp06] can be useful in the search of an explanation after inserting some modifications. As suggested in Fig.5.1, no type of losses can justify the atom number decrease during the loading, which can only be explained by a modification in the 'reservoir'. The modification of the number of atoms in the reservoir considered so far does not yield reasonable results for the case of a magnetic trap or a Dark-SPOT in the role of the reservoir, but the atoms number is not the only thing that can be modified. An additional parameter that could be modified during the loading process is the reservoir temperature. Indeed, this parameter is considered to be fixed in the analysis of Chapter I2, since there the reservoir is considered to have an infinite size and number of atoms with respect to the dipole trap. The temperature of the atoms in the reservoir is an important parameter in which the total number of atoms transferred from the reservoir to the dipole trap is strongly depended. In Fig. I.5.2.2 we see this dependance for the initial reservoir temperature ranging from 20 to 300 μK. The number of atoms transferred in the dipole trap is calculated by numerically integrating Eq.2.13 and taking into account the losses by substructing Eq.2.22 for a waist of 89 μm and a power of 60 W.

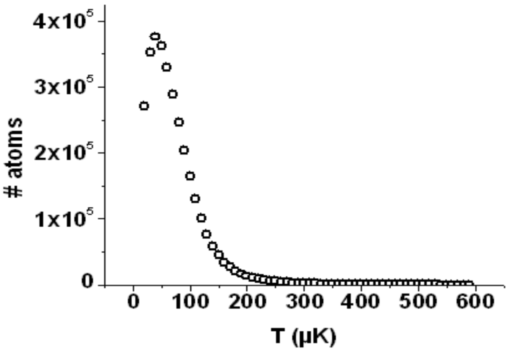

Fig. I.5.2.2: Evolution of the number of atoms loaded in the dipole trap versus the reservoir temperature, as predicted in by the analysis of the paragraph I.2.b (Eqs.2.13 and 2.22)

By following the same logic as the one used in Fig. I.5.2.1, we can try to fit our experimental data with this loading efficiency evolution. The idea is to see what kind of increase in the reservoir temperature can justify the atoms loss during the loading observed in each case. In fitting attempts shown in Fig. I.5.2.3, the dependence on the efficiency on the reservoir temperature, as shown in Fig. I.5.2.2 is plotted on top of the experimental data shown in Fig. I.4.2. The temperature scale is the only parameter used in the fit, and it is adjusted so that the number of atoms predicted for optimum reservoir temperature to coincide to the number of atoms detected for maximum t_{load}.

We see that this simple operation provides with good fitting in cases (a) and (b) where the loading is done via a magnetic trap and a Dark-SPOT respectively, while this is not the case for (c) where the dipole trap is loaded by a C-MOT. In the case of the magnetic trap loading shown in Fig.

I.5.2.3(a), a temperature increase in the reservoir that could justify the atom number evolution is ~300 μK in ~40 ms, ie 7,5 mK/s. The required temperature increase for the case of a Dark-SPOT reservoir, shown in Fig. I.5.2.3(b) is in the order of 100 μK, during the period of 120 ms ie 0,83 mK/s. Finally, for the case of loading from a C-MOT, shown in Fig. I.5.2.3(c), the required temperature increase is ~40μK during a period of 800 ms ie 0,05 mK/s..

We see that the required reservoir heating is much higher in the case of the loading from a magnetic trap. If the hypothesis is made, that the loading decrease is due to heating inserted in the reservoir, and if this heating source is assumed to be more or less the same for all loading cases, it is reasonable to expect that it would affect the magnetic trap more than the Dark-SPOT or the C-MOT. The magnetic trap is not only small compared to the other traps, with the exception of the Dark-SPOT, but is also a conservative trap, and no cooling mechanism is there to balance the heating effect. While in both the Dark-SPOT and C-MOT cases such a mechanism is present. In the case of the Dark-SPOT, the atoms collide frequently with atoms in the border of the area where both the trapping and the repumping lasers are applied (bright MOT area), or even cross to that area, with a result for them to be in a thermal equilibrium with the laser cooled atoms. Finally, in the case of the C-MOT, all lasers are always present, and the laser cooling is maintained, perhaps slightly modified due to the dipole laser induced Stark shifts in the energy of the Cs levels.

If the temperature increase in the reservoir is a hypothesis that can explain the temporal evolution of the atom number during the loading process, the source of this heating has to be identified. Unfortunately, an experimental study of such the possibility of heating the atoms in the reservoir during the loading process has not been made. A possible heating source is the trapping laser. The Cs atoms scatter photons of the dipole laser at 1070 nm, in a rate which is given by [Web03b].

$$\Gamma_{sc}=\frac{3\pi c^2}{2\omega_{eff}^3}\left(\frac{\Gamma}{\omega_{eff}-\omega}+\frac{\Gamma}{\omega_{eff}+\omega}\right)I \qquad (5.2)$$

For the case of the IPG laser at 1070nm, both the D1 and D2 lines have to be taken into consideration. In this reference, the system is modeled as a two-level atom with an effective transition defined by the weighted average of both D lines. Thus

$$\omega_{eff}=\frac{\omega_1}{3}+\frac{2\omega_2}{3} \qquad (5.2)$$

while

$$\Gamma_{eff}=\frac{\Gamma_1}{3}+\frac{2\Gamma_2}{3} \qquad (5.3)$$

while the values are available from [Steck02].

In the center of a dipole trap realized by a 60 W crossed in a waist of 89 μm the photon scattering rate is 0,11 s^{-1}. Each scattering event is associated to heating due to the photon recoil of ~200 nK, which means that photon scattering can insert in the system 1,78 μK in one second. The heating associated with photon scattering form the dipole trap can be even bigger, if we consider that photons are scattered by the atoms not only in the crossed region but in all the length of the dipole laser beams that lies in the ~0.5 mm magnetic trap. But, in any case, the heating associated to absorption of the dipole laser radiation seems to be too small to justify the reservoir temperature increase that could justify the loading performance in each case.

Additionally, the loss mechanisms described in Chapter I2, such as the background collisions, the inelastic two and three body losses, are associated with some kind of heating. In the case of inelastic two body collisions, one of the two colliding atoms has its spin changed, and inserts into the system heating equal to the energetic difference between the initial and the final spin state. In the case of three body recombination, two out of the three colliding atoms form a molecule, and the heating inserted to the system equals the energetic difference between the two atoms bound and unbound state. These heating mechanisms are described in Chapter I2, in order for the temperature of the transferred atoms in the dipole trap to be calculated.

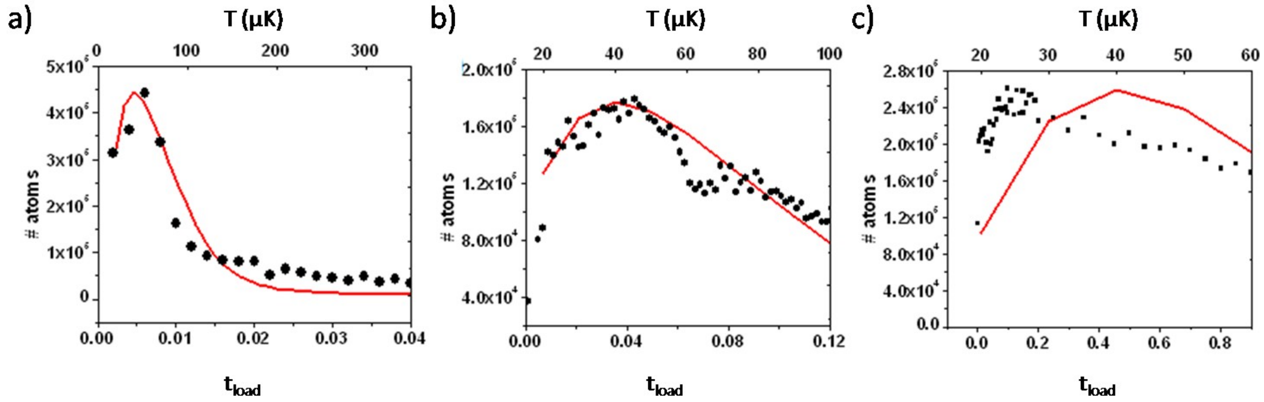

Fig. I.5.2.3: Fitting on the evolution of the atom number versus the loading time with the loading efficiency dependence curve on the reservoir temperature, as this is predicted in Eqs.2.13 and 2.22 and shown in Fig. I.5.2.2.

I.5.3. Conclusion

The aim of the analysis presented in this chapter was to present the efforts to understand the evolution of the atom number during the loading process. This is done with the use of a phenomenological theory that assumes modifications of the reservoir characteristics. After showing that the temporal evolution of the atom number during the loading process cannot be explained by losses such as those described in Chapter I2, we consider the analysis presented in [Kupp00], which was initially developed in order to fit the loading of ^{87}Rb atoms from a C-MOT to a dipole trap. This simple analysis, successfully treats the similarly observed decrease of the atom number during the loading, since it takes into consideration the finite lifetime of the reservoir.

This analysis is used in order to fit our similar data, in 3 different cases of loading from a magnetic trap, a Dark-SPOT and a C-MOT. If we consider, that it is the reservoir finite lifetime that causes the atom number decrease observed during the loading, the required lifetime of the magnetic trap is found to be ~3ms, while is is 150 ms for the case of the Dark-SPOT and 2.5 s for the case of the C-MOT. The fact that the required lifetimes are much smaller than the ones expected for the case of the magnetic trap and the Dark-SPOT, means that such a consideration is not reasonable for these cases. However, the relatively small discrepancy between the required and the expected lifetime of the C-MOT, makes this explanation possible for this case of loading.

Since the idea that modification in the reservoir is necessary in order to explain the observed atom number decrease during the loading, I continue by considering modification of the reservoir temperature. The number of atoms loaded in the dipole trap, results from the equilibrium of the loading rate and the various losses. Since the loading rate is strongly depended from the reservoir temperature, we see that such a variation could perhaps explain the remaining cases of loading form a magnetic trap and a Dark-SPOT. The hypothesis of heating in the atomic reservoir during the loading, manages to fit these loading cases fairly well, and the required heating is fairly reasonable. It is true, that my calculations on the heating due to the absorption of photons from the dipole trap shows that this mechanism alone, cannot explain the required heating. However, the accidental absorption of photons (coming either from the dipole trap, either from the trapping lasers of the MOT), leads to secondary effects, as depolarization, which can contribute to the reduction of the loading efficiency. Finally, parametric heating[1] can always be considered as the source of heating in

---

[1] Meaning the heating due to vibrations on the optical table, which was a very old, marble table, in our experiments.

the reservoir. The fact that the required heating in is in the case of the magnetic trap reservoir much larger than in the case of the Dark-SPOT, is easily explained; the magnetic trap is a conservative trap, so if it is heated by any reason it stays hot. On the other hand, the temperature of the Dark-SPOT (and all other non conservative traps), is the result of an equilibrium between the (laser) cooling and the heating mechanisms.

However, this modification on the reservoir characteristic during the loading process is only indicated through our studies, and not proved. However, despite the fact that some of the numbers resulting from the fitting procedure presented in Chapter I5, are not reasonable, the idea of a modification of the reservoir during the loading process, is the only one that can explain the loading dynamics. Perhaps the modification has not been successfully identified. An important limiting factor for this search, is the fact that this idea was considered long after the experiment was stopped, thus, no experimental studies could support my considerations.

I.6. CONCLUSION & PERSPECTIVES

In this part of my thesis, I described the experiments that took place between November 2006 and October 2008, and concerned the loading of a dipole trap of Cs atoms by various methods. The main motivation for this line of experiments, was the expectation to provide with ultra-cold Cs atomic samples (and eventually condensates), via a method that would be simpler and faster with comparison to the only successful method reported at that time [Web03b]. The group's special interest on Cs ultra-cold samples and condensates originated from the group's research activity in cold molecules, and in particular in cold Cs dimers. The long term goal for the Cs atomic experiment, was to allow the study of formation and manipulation of cold molecules in these ultra-cold conditions. Such an experiment would permit the study of several methods, explored by members of the group in a different set up, like photoassociation for the production of cold molecules [Fio98], like trapping and accumulating cold molecules in conservative traps [Zahz06, Vanh02] and like cooling their internal degrees of freedom [Vit08c].

The main approach followed in the atomic Cs experiments, in which I participated in the period 2006-2008, was based in a proposal reported in [Comp06], and involved loading of the dipole trap from an atomic reservoir provided initially by a magnetic trap. The experimental realization of this proposal was already the subject of [Stern08]. I continued this line of studies, by trying various types of traps in the role of the atomic reservoir (C-MOT, Dark-SPOT), as well as an additional loading strategy which was similar to the ones followed by [Web03b, Hung08], and which was based in Raman-Sideband cooling.

The results of our studies are discussed in Chapter I4 and summarized in Table 4.1. The number of atoms, obtained in all the different loading approaches, is almost the same (in the order of 10^5 atoms), while their temperature is always close to 150 μK. The results for the Raman-Sideband cooling were somehow improved, with the number of atoms being ~7 10^5 and a much lower temperature of ~3 μK. However, this loading strategy, as well as the strategy involving instantaneous molasses loading, are very far from the analysis considered in Chapter I2 and in [Comp06]; so these results serve only to compare the reservoir loading to other loading methods which do not involve an atomic reservoir, in the same set up. The temperature of the trapped atoms seems to be mostly due to the heating during the transfer to the dipole trap, since whenever the trap is localized in ~100 μm the temperature is ~150 μK and it drops to ~3 μK for the case of the much shallower ~700 μm trap loaded with RSC. The application of evaporating cooling on these traps did not result to a significant phase density increase. The reason for this, is that the general characteristics of the dipole traps obtained in our studies (mostly the obtained density, but also the small lifetime of the traps), were such that they could not be considered as a good starting point for evaporation; this is why I chose to focalize on the loading techniques in the body-text of my thesis.

In brief, we considered evaporation in order to improve the characteristics of our dipole traps (decrease temperature/increase density), and to approach the required conditions of the very efficient evaporation process predicted in [Comp06]. Since the density of the atoms in the dipole trap were always smaller than the ones required for evaporation, we attempted to 'compress' our dipole trap with the use of the mechanical 'zoom' described in I.3.4. Despite the partial success of compression, it did not led to a successful evaporation, since it was not accompanied by evaporating cooling which could compensate the heating caused by compression. All our studies on dipole trap lifetime evaporation and compression are discussed in the Annexes I1 and I2. Additionally, in Annex I3, I present a set of experimental studies of the quality of the dipole laser potential and of interferences. Again, the concussion is that the low densities obtained in our set up could not be explained by none of these two experimental parameters.

The results of our experimental realization of the reservoir loading, show striking differences between the theoretical prediction [Comp06] and the experiment. These differences are not only in the final output of the method, i.e. the number of atoms transferred by the reservoir to the dipole trap and their temperature, but also in the dynamics of the loading process. In particular, the models developed in [Comp06], predict a loading process of several hundreds of ms, while in the experiment it was found to be ~10 times smaller, which had as a consequence the poor loading of the dipole trap. In a sense, we could say that our experimental realization of the technique failed in providing the conditions considered in [Comp06]. One possible explanation, the reservoir is considered to have an infinite lifetime with respect to the duration of the loading process, and none of its basic characteristics, as the density and the temperature, are considered to change during the loading process.

In a more general point of view, where in our studies we include the results of all other relevant experiments [Perr98,Boir98,Hung08,Web03b], it seems that the combination Raman-Sideband Cooling and shallow dipole traps, consists of an approach which is difficult to be 'beaten', especially after the improvements reported in [Hung08]. The Raman-Sideband Cooling manages to provide with a sufficiently high number of atoms (~10^7). Similar number of atoms loaded from a magnetic trap reservoir, is only reported in [Stern08], in the case of loading a single-arm dipole trap. Loading a single-arm dipole trap from an atomic trap reservoir, could perhaps provide with an attractive alternative to the combination of Raman-Sideband Cooling and shallow dipole traps, as it has lead to notable results in the case of Cr [Pfau07, Beau08]. However, even if such an approach was widely discussed among the group, it was not studied tested during my involvement to the dipole trap experiments.

Recent developments in the area of cold molecules, which resulted the form the efforts of members of the Cold Molecule group, have shifted the interest of our team towards this area. The demonstration of a novel method that permitted the cooling of the vibration in Cs dimers [Vit08], had opened the way towards many fruitful applications. The initial, long term goal of my thesis, was the preparation of ultra-cold Cs dimers in an optical dipole trap via photoassociation, as demonstrated by its initial title : “Preparation of cold Cs molecules, in their ground state, without vibration or rotation, in a classical or quantum gas”. These developments in the area of cold molecules opened new perspectives, thus, we have decided to devote the rest of my time in the studies of cold molecules, which will be discussed in the second part of this thesis.

Part II - Abstract

Preparation and manipulation of cold Cs dimers.

In November 2006, when I was enrolled in the activities of the experimental group of Cold Molecules, in Laboratoire Aimé Cotton, the main two areas of interest were, on the one hand the production and manipulation of cold molecules, and on the other, the preparation of a cold and dense dipole trap of Cs atoms. My initial enrollment was in the preparation of the cold and dense Cs atom dipole trap, via various loading methods, and the corresponding study is presented in the first part of this thesis. Through this experiment, the group aimed to study in the future, the creation and the manipulation of ultra-cold Cs dimers in a dipole trap[1]. Up to now, the group has already demonstrated the dipole trapping of cold Cs dimers created by photoassociation [Zahz06], as well as trapping of molecules in magnetic traps [Vanh02].

In October 2008, this experiment was temporally stopped. The reasons were technical and are related to a failure of the vacuum system which appeared in October 08 and evolved to major malfunctions especially in the upper ion pump. Proper restoration of the vacuum system demanded for the replacement of this pump, and most probably of a large part of the Ultra High Vacuum (UHV) system. A complete restoration of the experiment demanded more effort and resources than what the team was decided to invest at this period. The reasons for this hesitation were also partially explained in the Chapter I4. The experiment was proposed at 2006 [Comp06] at a time where Cs BEC was achieved by a single group in Innsbruck [Web03b]. The preparation of the Cs BEC was the result of a many year effort that increased considerably our current knowledge for the behavior of Cs atoms in ultra-cold temperatures. However, the Cs BEC was achieved with the use of a complicated set – up, and after an evaporation process of more ~20 s. The analysis presented in [Comp06] was predicting large improvements towards the simplification of the Cs BEC production. These simplifications were related to the use of a less complicated set-up, where Raman-Sideband Cooling and multiple dipole traps were not necessary, and to the achievement of BEC with shorter evaporation processes close to one second. Additionally, at the time were some of these experimental results were produced, a high discussion on the possibility of observation of Efimov trimer state in ultra-cold Cs contributed to our motivation [Krae06]. However, the experimental results reported in [Hung08] achieved most of the goals our technique was aiming. The authors were able to achieve BEC in ~2 s, with the use of one single dipole trap in the crossed configuration. They have loaded a large and shallow dipole trap by RSC, while they have developed a new evaporation technique, the runaway evaporation, which permitted them the preparation of BEC in such sort evaporation sequences.

As mentioned in the first part of my thesis, the developments in the area of cold molecules achieved by members of our group in the spring of 2008 shifted the group's interest towards this area. These developments concerned the achievement of vibrational cooling of cold Cs dimers via optical pumping with the use of shaped femtosecond pulses [Vit08]. The Cs dimers where produced by photoassociation in a Cs MOT, directly in their ground electronic state $X^1\Sigma_g^+$. The vibrational cooling technique allowed to transfer the molecular population in the ground vibrational state, in

---

[1] Although I have already worked experimentally towards a dipole trap for Cs dimers with the use of a CO_2 laser, we soon realized that experiments for the trapping of cold Cs dimers with excited vibration and rotation, would have very small differences to the ones reported in [Zahz06]. Thus, trapping experiments are going to return within the group's priorities after a rotational cooling in Cs dimers is achieved.

several rotational levels. The first demonstration of this novel cooling technique, as well as the full line of experiments that lead to the preparation and the observation of the Cs dimers in their ground electronic state has, been the subject of [Vit08c].

My enrollment in the cold molecule experiment involved the study of the possible extensions and generalizations of this recently developed technique. The operating principle of the vibrational cooling technique which is optical pumping, suggested useful extensions. In this context, many different studies were considered. These were population transfer to any preselected vibrational level, vibrational cooling with the use of an incoherent light source, vibrational cooling of heteronuclear molecules as well as cooling of the molecular rotation. Moreover, while those experiments were performed, our studies were extended to meet other interesting questions, like cooling of Cs molecules in their ground triplet state, or preparation of Cs trimers, that were keep coming out during this period.

In the initial chapter I give a small introduction divided in two main parts. In the first part, I try to present the area of cold molecules as simply as possible and to point out the complexity which arises when the conceptual step from atoms to molecules is considered in the context of low temperature physics. In the second part, I give some elements of molecular physics which can be useful for the ongoing discussion.

In the second chapter, I initially discuss the main directions, towards which modern research in cold molecules is oriented. When molecules are discussed in the context of low temperature physics, one can consider either to create cold molecules from already cooled atoms, either to cool directly the molecules (their internal or their external degrees of freedom). In this chapter, I will initially try to point out this distinction and to present the most important techniques in the area of cold molecules. This is done with a special interest to the technique used and explored by our group, the '*photoassociation*'. Finally, I describe the recent developments achieved by various groups around the world, concerning the preparation of molecules in their absolute ground state, as several breakthroughs have been accomplished very recently in the area of cold molecules.

In the third chapter, I describe the vibrational cooling technique reported in [Vit08], as well as the experiments that led to this achievement. Initially, I try to describe the main idea behind our group's approach for the production of Cs molecules with neither vibration nor rotation, via the use of optical pumping with broadband light. Then I describe the experimental set-up that made these studies possible. Finally I describe our team's efforts towards the formation of cold Cs dimers in their ground vibrational state, which resulted the development of the vibrational cooling technique mentioned above based in [Vit08, Vit08c, Vit09].

After these introducing chapters, the particular studies that I realized in the production and manipulation of cold molecules are going to be discussed. Initially, in Chapter II4, I report the extension of the vibrational cooling technique in order to realize molecular population transfer in a given vibrational state. Then, in Chapter II5, the implementation of a similar vibrational cooling technique, with the use of a diode instead of a femtosecond laser is discussed, as the technique appears to be greatly simplified technically and to be more attractive economically. These two generalizations were proposed and realized in the beginning of my involvement in the Cs_2 experiment, while they have supplied for the material for the two related articles [Sof09, Sof09b]. These two chapters make use of the material of the corresponding articles in a large extent. However, this is done in a more detailed way, so that the continuity of the text is ensured, while a part of [Sof09] which concerns rotation is moved to the appropriate chapter (Chapter II7).

In a separate chapter, Chapter II6, I discuss the generalization of the vibrational cooling technique, in order to be realized in other molecular transitions or other molecular systems. Initially, I discuss the cooling of molecules in their $a^3\Sigma_u^+$ triplet state, as this was theoretically proposed and studied in the laboratory. Then, I discuss generalization towards other molecular systems, with a special interest to heteronuclear molecules and NaCs. Finally, in Chapter II7, our activity towards the study of the expansion of the vibrational cooling technique to include the rotation, is presented. A step towards this goal is the experimental detection of the cold Cs dimer rotational distribution. This is attempted by the realization of depletion spectroscopy technique, with the use of a spectrally narrow diode laser. All the theoretical studies of the possibility of rotational cooling via optical pumping, in which I participated, as well as the preliminary results of the depletion spectroscopy, are discussed though this chapter.

CHAPTER II1: INTRODUCTION

II. PREPARATION AND MANIPULATION OF COLD MOLECULES

II.1. INTRODUCTION

In this introductory chapter I try to present briefly the area of cold molecules and to give a fast description of the theoretical tool-work used in this thesis.

Initially I outline some basic differences between molecules and atoms and the reasons why cold molecules are a distinct part of the international cold atoms community. When instead of atoms, molecules are considered in the context of low temperature physics, major complications rise. These complications are due to the existence of additional degrees of freedom, which are related to the ability of molecules to vibrate and to rotate, and which do not exist in the simpler, point-like atoms. In addition to the electronic states considered in atoms, in molecules one has to consider states that correspond to the various ways in which the molecule can rotate and vibrate. As a result, the interaction of molecules with light becomes more complicated, as transitions between all these vibrational and rotational states have to be considered.

In the next part of this chapter I present some elements of molecular physics, which are useful in the ongoing discussion. I try to briefly present the way that molecules are considered theoretically, the two most useful and most related to this work spectroscopic notations and to summarize the theory available for the interaction of molecules with light.

II.1.1. The cold molecules as a separate field of scientific research

Laser cooling and cold atoms in general are without doubt one of the most expanded fields of research in atomic physics over the last thirty years, marked by two Nobel prizes, one in 1997 concerning laser cooling and one in 2001 concerning Bose-Einstein condensation. Molecules have been left out of this exciting game for several years. The main reason for this was the fact that they cannot be cooled by means of laser cooling, which was without doubt the breakthrough that allowed many exciting developments in cold atoms.

As explained in the introduction of the first part of this thesis, laser cooling relies on the large number of absorption – emission cycles that the atoms undergo under the influence of the cooling laser field. In the case of molecules, the existence of the additional degrees of freedom, which correspond to rotation and vibration, increases the density of states making the preparation of a closed transition almost impossible. The fact that laser cooling cannot be applied to molecules makes their preparation in low and ultra-low temperatures particularly difficult.

However, the special characteristics of molecules create great interest in the scientific community if they are combined to ultra-cold technology existing in atoms. There are many interesting applications of cold molecules, ranging from quantum computation to the measurement of fundamental constants, that have been described in various theoretical proposals, in which the experimentally difficult field of cold molecules finds motivation [Huts06, Doy04, Krem05, Jon06, Dul06].

II.1.2. Atoms and molecules in the context of laser cooling

In the previous paragraph, it has been noted that the additional degrees of freedom corresponding to vibration and rotation, modify dramatically the behavior of molecules with respect to the one of atoms. As far as interaction with light is concerned, the existence of these additional degrees of freedom results to dramatically more complicated optical spectra, a fact which makes optical manipulation of molecules very different to what it is when atoms are concerned.

Let us simplify the discussion by considering diatomic molecules. When molecules are concerned, the energy of the electronically active electron in the molecular potential does not only depend on the electronic excitation number but also in the separation between the atomic nuclei that participate in the molecule, so that one should consider molecular potential curves (PECs) rather than electronic levels. In each PEC, which results from the combination of the electronic excitation number of the participating atoms in the infinite separation limit, is separated to an (infinite) number of states corresponding to the possible rotation and vibration that the molecule can have. Ab-initio calculation of the molecular potentials and their ro-vibrational structure can be very complicated even in the simplest case of diatomic homonuclear systems. The insertion of those additional degrees of freedom, rotation and vibration increases dramatically the complexity of the system. In a sense, the description of the optical properties and the optical manipulation is much more different between atoms and homonuclear diatomic molecules than it is between homonuclear diatomic and more complicated heteronuclear, polyatomic molecules.

As far as laser cooling is concerned, the complicated molecular structure inserts great difficulties since it is very difficult to find optically closed transitions in order to implement it. Laser cooling, as explained in the introduction of Part I of this thesis, owes its success to a series of absorption-emission circles, through which momentum is carried away in all possible directions reducing the temperature of the atomic sample. In order for laser cooling to have any appreciable effects in the macroscopic temperature of the sample, a large number of absorption-emission circles is required. That means that after excitation the atoms have to return to the initial state, via a single or many steps of spontaneous emission relatively fast. The ideal situation of an optically closed transition, where the only possibility for spontaneous emission form the excited state is back to the initial state, can almost never be found even in atoms. In most cases, the addition of a second laser that re-pumps the atomic population back to the initial state is necessary for the successful realization of laser cooling.

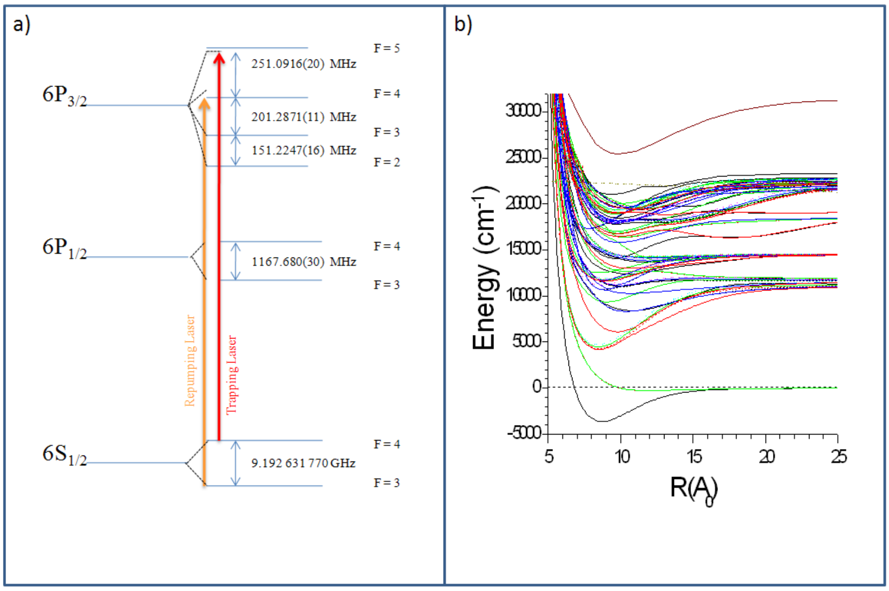

Fig. II.1.2.1: (a) Schematic representation of the electronic levels and lasers used for laser cooling in atomic Cs (b) PECs of the Cs dimer (the vibrational and rotational states are not shown, but an infinite number of them corresponds to each of these PECs). The aim of the picture is to stress the complication rise, when we consider the conceptual transition from atoms to diatomic molecules.

In molecules, the structural complication is so high that the insertion of one or more repumping lasers would have very little to add in the search for a closed transition. In Fig. II.1.2.1 we see a comparison between the electronic levels of the Cs atom that are used for laser cooling, along with the corresponding laser beam frequencies and the electronic structure of the Cs dimer in similar energies. If we add in this picture the (theoretically infinite) vibrational and rotational states, the complication that rises, when laser cooling of even such a simple homonuclear dimer is considered, is made evident.

There exist a variety of methods for the preparation of molecules in low and ultra low temperatures, which are under development. I will briefly present the most important ones in the following chapter, after discussing some of the basic elements of molecular physics which are useful for understanding the rest of the thesis. Moreover, there are several theoretical proposals on laser cooling of molecules [Bart93,Tann99,Bart01,Schi00,Voge02]. We will return to the subject much later in this thesis, where we discuss how developments reported in this thesis can contribute in the interesting subject of laser cooling of molecules.

II.1.3. Some elements of of molecular physics

In this paragraph I will try to briefly report some of the basic elements of the molecular physics that are useful for the following of this thesis and for the study of cold molecules in general. The physics of cold molecules, by context, concerns mostly simple molecules made from few atoms and in the case of our studies the molecules are homo-atomic diatoms. Thus, I will mostly attempt to describe the conceptual passage from the description of atomic to the description of molecular systems and their interaction with light, rather than attempting to describe more complicated, multi-atomic molecular systems.

II.1.3.a. The cases of Hund.

The increase in the degrees of freedom in molecules with respect to atoms naturally leads to an increase of quantum numbers that are necessary in order to describe a molecular system in the context of quantum mechanics. In molecules with small number of participating atoms, these quantum numbers can be known precisely. However, in order for the some basic calculations to be more attractive, they are considered in the context of perturbation theory. Depending on which terms are treated fully in the molecular Hamiltonian and which terms are treated as perturbations, some of quantum numbers are considered as 'good' quantum numbers and others not.

The Hamiltonian, which we use to describe the molecular system (also referred to as 'molecular' Hamiltonian), can be decomposed in various terms, which correspond to the various interactions in the molecular system. By comparing the energy, with which each of the terms of the molecular Hamiltonian is associated, we can have an idea of the importance of each interaction. The various cases that emerge this comparison are the widely known Hund's cases. In each of these cases, the quantum numbers that correspond to the Hamiltonian's most important terms are considered as 'good' quantum numbers of the system, while the remaining terms of the Hamiltonian are treated as perturbations. These various cases, in which one of the Hamiltonian's terms prevails over another, yielding different good quantum numbers, determine the choice of symmetries that can be considered in order for the Schrödinger equation to be simplified and finally determines the notation that is used and which emerges by these symmetries.

For the determination of the molecular symmetries we consider three principal components for the molecular energy: the electronic component (E^{el}), the energy of the spin-orbit coupling (E^{SO}) and the rotational energy (E^{rot}). An additional term that is useful for the definition of the Hund's cases is the term $\boldsymbol{L} \cdot \boldsymbol{A}$, which describes the coupling of the electronic angular momentum $\boldsymbol{L}$ with the molecular axis (parallel to $\boldsymbol{A}$) [Huts06]. The vibrational component of the molecular energy is neglected, not because of its magnitude, which is important, but simply because the molecular vibration does not intervene in the definition of these molecular symmetries. It is the relative magnitude of these terms that determines the molecule's description organized in the Hund's cases.

In TABLE I, I give a list of the Hund's cases according to this picture of the relative 'weight' of each of the Hamiltonian's terms [Leo98]. An additional description of the Hund's cases considers the different ways in which the several angular momentum vectors can be coupled in a molecule. I adopt elements of this description, which can be found in [Dem98], namely the term $\boldsymbol{L} \cdot \boldsymbol{A}$, in order to simplify the presentation of TABLE I. There, the various Hund's cases are presented in column (a), while in column (b) we give the conditions of validity for each one of them. These conditions are consisted of the comparison between the most important terms of the molecular Hamiltonian. The 'effective' Hamiltonian, with which the molecular system is studied in each case is shown in column (c), while the terms in the brackets are the terms that are considered as the principal perturbations.

Hund's case	**Validity**	**H^0**
(a)	$(\Delta E^{SO}) >> (\Delta E^{rot})$	$H^{el} + [H^{SO}]$
(b)	$(\Delta E^{rot}) >> (\Delta E^{SO})$	$H^{el} + [H^{rot}]$
(c)	$(\Delta E^{SO}) >> \boldsymbol{L} \cdot \boldsymbol{A}$	$H^{el} + H^{SO}$
(d)	$(\Delta E^{rot}) >> \boldsymbol{L} \cdot \boldsymbol{A}$ and $(\Delta E^{SO}) << (\Delta E^{rot})$	$H^{rot} + [H^{el}]$
(e)	Extremely rare case	$H^{rot} + H^{SO}$
(f)	Extremely rare case	

TABLE 1: (a) The various cases of Hund. (b) The conditions of validity for each of the Hund's cases. (c) The term H^0 which is the dominant term of the molecular Hamiltonian. The terms in brackets are the principle perturbations.

II.1.3.b. Cases (a) and (c) and corresponding notation.

When heavy diatomic molecules such as Cs_2 are discussed, the important cases are the cases (a) and (c) (rather than the (b) case used more frequently). Hund's case (a) is when $(\Delta E^{el}) >> (\Delta E^{SO}) >> (\Delta E^{rot})$. For short internuclear distances, the spin orbit coupling energy is considered to be small, and so the total spin of the electrons S is considered to be a good quantum number. The systems Hamiltonian can be written as

$$H^{(a)} = \sum_i \frac{p_i^2}{2 m_e} + V^{NN}(R) + V^{eN}(R, \vec{r}_i) + V^{ee}(\vec{r}_i) + [H^{SO}] \qquad (1.1)$$

where the spin-orbit term H^{SO} is considered as perturbation and is placed in brackets. The rest of the terms are the $p_i/2m_e$ term which expresses the kinetic energy of the electrons, and the terms $V^{NN,eN,ee}$ which express the potentials between the nuclei (NN), the nuclei and the electrons (eN) and the electrons themselves (ee). Note that the Hamiltonian is written in the context of the Born-Oppenheimer approximation, and neglects the kinetic energy of the nuclei. The Born-Oppenheimer approximation is considering the nuclei motionless compared to the electrons, and is based in the fact that the nuclear mass is much larger than the electronic mass.

The following notation is used to represent the molecular states in this case:

$$^{2S+1}|\Lambda|_{g\,|\,u}^{+\,|\,-} \qquad (1.2)$$

where

- Λ is the orbital angular momentum projection of the electrons in the internuclear axis. It is noted as $\Sigma, \Pi, \Delta, \Phi$ for the values $|\Lambda| = 0,1,2,3...$

- S total spin of the electrons
- g|u symmetry of inversion of the nuclei with respect to the center of mass: g (gerade [German]) even states and u (ungerade) odd states. This symmetry is valid only for the case of the homonuclear molecules.
- +|- Symmetry of reflexion of the orbital coordinates of the electrons with respect to a plane that contains the internuclear axis. This symmetry is useful for the Σ state where Λ= 0.

Hund's case (c) is when (ΔE^{SO}) ≥ (ΔE^{el}) >> (ΔE^{rot}). For large inter atomic distances or for the case of heavy molecules like the Cs dimer, the spin orbit coupling cannot be treated as perturbation. There, the spin orbit coupling energy is in the same order of magnitude with the electronic energy, thus we have to consider these terms together. The interaction Hamiltonian is written as in Eq.1.1, only that the spin orbit term is not treated as a perturbation; one can also describe the system with the use of a case (c) Hamiltonian consisted of the summation of the spin-orbit term and the term describing the electronic component

$$H^{(c)}=\sum_i \frac{p_i^2}{2m_e}+V^{NN}(R)+V^{eN}(R,\vec{r}_i)+V^{ee}(\vec{r}_i)+H^{SO} \tag{1.3}$$

The good quantum number is here the total angular momentum J, which consists of total electronic orbital angular momentum L + total electronic spin S and angular momentum due to molecular rotation O. The notation used is

$$|\Omega|_{g|u}^{+|-} \tag{1.4}$$

again with the same symmetries +|- (which intervenes only in cases where Ω is 0), and g|u.

II.1.3.c. Interactions with light

The interaction of molecules with light is governed, just like in the case of atoms, from an integral which expresses the recovering of the related wavefunctions, with the electric field of the light. The transition probability from and initial molecular state *i*, associated to the wavefunction Ψ_i to a final state *f*, associated to the wavefunction Ψ_f is

$$\sigma_{i\to f}\propto|\langle\Psi_f|\vec{\epsilon}\vec{D}|\Psi_i\rangle|^2 \tag{1.5}$$

where $\vec{\epsilon}$ is the polarization vector of the corresponding electric field and $\vec{D}$ is the corresponding dipole operator. In the next part of this chapter we shall consider homonuclear diatomic molecules. By making use of the so-called adiabatic approximation, we can divide the molecular wavefunction into three parts, concerning the electronic part of the wavefunction, the vibrational and the rotational part, and treat them separately.

$$\Psi(\vec{r}_i,\theta,\phi,\vec{R})\sim\Psi^{rot}(\theta)\Psi^{\upsilon}(R)\Psi^{el}(\vec{r}_i\vec{R}) \tag{1.6}$$

where with θ and φ we symbolize the angular parts of the internuclear vector $\vec{R}$ in the laboratory framework, $\vec{r}_i$ the position of each electron. With these considerations, the expression on the transition probability becomes:

$$|\langle\Psi_f|\vec{\epsilon}\vec{D}|\Psi_i\rangle|\sim$$
$$\int_{\theta,\phi}\Psi_f^{rot*}(\theta)\Psi_i^{rot}(\theta)\sin(\theta)d\theta d\phi\int_0^\infty\Psi_f^{\upsilon_f*}(R)\Psi_i^{\upsilon_i}(R)\int_{\vec{r}_i}\Psi_f^{el*}(\vec{r}_i,R)\vec{D}(\vec{r}_i)\Psi_i^{el}(\vec{r}_i,R)d\vec{r}_i dR \tag{1.7}$$

The total probability of the transition is proportional to this integral. The part in which the electric dipole is included is often refereed to as the transition's dipole moment which is written as

$$\langle\vec{D}\rangle(R)=\int_{\vec{r}_i}\Psi_f^{el*}(\vec{r}_i,R)\vec{D}(\vec{r}_i)\Psi_i^{el}(\vec{r}_i,R)d\vec{r}_i \tag{1.8}$$

Normally, this part cannot be separated from the integral of 1.8. however, the simplification is done in the context of the so-called centroid approximation, which states that

$$|\langle \Psi_f | \vec{\epsilon}\vec{D} | \Psi_i \rangle| \sim AngularPart \times [\int_0^\infty \Psi_f^{\upsilon_f *}(R)\Psi_i^{\upsilon_i}(R)\partial R] \times \langle \vec{D} \rangle(\bar{R}) \qquad (1.9)$$

with $$\bar{R} = \frac{\int \Psi_f^* R \, \Psi_i}{\int \Psi_f^* \Psi_i} \qquad (1.10)$$

The square of the radial term represents the well known Franck-Condon factors. The Franck-Condon factors are useful, especially for the current study since they control the relative transition probabilities between different vibrational levels of the same electronic states. The Franck-Condon coefficient between an initial υ_i and a final vibrational state υ_f is

$$FC(\upsilon_i, \upsilon_f) = |\int_0^\infty \Psi_f^{\upsilon_f *}(R)\Psi_i^{\upsilon_i}(R)\partial R|^2 \qquad (1.11)$$

Finally, the rotational part of the overlapping integral as expressed, in Eq. 1.8 consist the well known Hönl-London coefficients, which control the relative probability for the transition between different rotational levels. Moreover, if all the possible polarizations are averaged, the result of the rotational part of the integral (1.8) can be expressed in a much more compact way, with the use of the 3j coefficients [Comp99].

$$S_{\Lambda',J',\Lambda'',J''} = \langle \Lambda', J' | \Lambda'', J'' \rangle = (2J'+1)(2J''+1)\begin{pmatrix} J' & 1 & J'' \\ -\Lambda' & \Delta\Lambda & \Lambda'' \end{pmatrix}^2 \qquad (1.12)$$

where Λ is the projection of electronic angular momentum upon the internuclear axis, J the total molecular angular momentum without the nuclear spin, (') marks the final and (") the initial state, so that $\Delta\Lambda = \Lambda' - \Lambda''$.

From the above expression, it turns out that the molecular angular momentum can be modified as ΔJ = 0,±1 during a transition, while transitions between states with J = 0 are forbidden. This fact gives the well known P,Q and R branches which corresponds to transitions with ΔJ = J' - J" = -1, 0 and 1 respectively.

II.1.4. Conclusion

In this introducing chapter, I initially tried to define the framework in which the area of cold molecules is placed and to point out the particular difficulties which arise, when molecules are considered in low temperature physics. Secondarily, I tried to give a comprehensive introduction to those elements of molecular physics theory which are useful for the ongoing discussion.

As we saw in the first part of this chapter, the complexity of molecular systems in comparison to atoms is highly increased due to the additional degrees of freedom associated to vibration and rotation. Thus, the search of a 'closed' transition, with which a laser cooling scheme can be implemented, becomes extremely difficult. In the case of atomic alkaline systems, the relatively low complexity of the atomic structure, makes laser cooling possible with the use of a repumper laser.

The figure presented in Fig. II.1.2.1(a), concerning the structure of atomic Cs is characteristic for most alkali atoms, nevertheless it is not unique; more complicated schemes can exist, while a closed transition is not always easy to be found, or to be 'prepared', with the use of one or more repumping lasers. On the other hand, laser cooling and trapping without repumper has been reported, for the case of Erbium atoms [McCleO6]. In this experiment, the lack of repumper is not justified by a simple electronic structure, on the contrary, the electronic structure used in [McCleO6] is much more complicated than the one corresponding to Cs, shown in Fig. II.1.2.1(a). The success of laser cooling without repumper is in this case due to convenient values of the relaxation constants of the states involved in the cooling transition. Finally, even though the atom is excited to a highly excited state and relaxes to more than one states, the system finds its way to the initial state at timescales that are short enough for laser cooling to operate. Such an argumentation indicates that laser cooling in molecules is not impossible despite the complexity of the electronic structure of diatomic molecules. However, direct laser cooling of molecules has not so far been reported, and the difficulty of the subject is generally acknowledged.

CHAPTER II2: TECHNIQUES FOR THE STUDY OF COLD MOLECULES

II.2. TECHNIQUES FOR THE STUDY OF COLD MOLECULES

In this chapter I will try to describe some of the most important techniques in the area of cold molecules, in order to set the framework in which the current study took place, and to point out the position of the group of cold molecules in Laboratoire Aimé Cotton in the corresponding international scientific community.

In the first paragraph, I try to group the various techniques according to their objectives and the involved instrumentation. Cold molecules can be either prepared by cooling directly molecular samples or by creating molecules by associating cold atoms, with several techniques implementing each possibility. I try to distinguish between techniques that aim either to cool (or decelerate) the molecular translation in space, and techniques that aim in to cool the molecule's internal degrees of freedom.

In the second part, I initially discuss some of the basic techniques for the preparation and the study of cold molecules. I will briefly present the most important ones starting from the techniques for directly cooling (and/or decelerating[1]) molecules, such as the Stark decelerators, the cryogenic techniques and the techniques involving collisions. After having discussed some of the most important existing techniques, I devote a paragraph for the description of one of the most interesting proposals for the direct laser cooling of molecules. This is due to the fact that the operating principle of this proposal is closely related to the vibrational cooling technique described in this part of my thesis. Moreover, such a discussion can be related to the ongoing chapters of this thesis, since several results reported here can lead to possible breakthroughs in this area.

Next, I discuss the techniques that involve association of cold and ultra-cold atoms for the preparation of cold molecules, namely the magneto-association or Feshbach resonance technique, and most important for the case of this thesis, the technique which is studied in Laboratoire Aimé Cotton, the photoassociation.

The last years, many exciting developments have been reported by various groups worldwide concerning cold molecules, and in particularly the preparation of cold molecules without vibration and/or rotation. The developments are rapid and the scenery in the field is changing fast, so that many experiments show that control of the internal degrees of freedom of molecules is now possible with more than one method. In the final part of this chapter, I will briefly present some of the most important ones, such as the first reported preparation of cold potassium dimers in their ground electronic and vibrational state [Niko00], the first production of heteronuclear molecules in their ground vibrational level [Sage05], the preparation of Cs dimers in their ground electronic vibrational and rotational level by magneto-association and subsequent population transfer by STIRAP [Danzl08] and the preparation of LiCs molecules in their ground electronic and vibrational state with rotation zero or one, by photoassociation [Del08].

II.2.1. General description of the various methods for the study of cold molecules.

The various methods employed for the study of cold molecules can be grouped by more than one way. One could consider grouping them in terms of objective, meaning on weather they aim in the cooling of the internal or the external degrees of freedom. Additional grouping can be considered in terms of 'approach', meaning on whether the technique involved is aiming to cool

---

[1] In the area of cold molecules, several techniques aim to the cooling of molecules, while others to the deceleration of a molecular beam. Both these approaches are considered to belong in the cold molecule area (as shown by the interest of the biggest groups and conferences). Naturally, confusion between cooling and deceleration can be easily produced; however I will try my best to avoid it in the corresponding chapters.

preexisting molecules or to create cold molecules using already cooled atoms, the 'associative' techniques. Obviously, the associative techniques provide with a molecular sample which is already transnationally cold to the extend that it was for the pre-existing atoms. In the most usual cases, additional cooling techniques have to be considered to cool the internal degrees of freedom. In Fig. II.2.1.1, I give a schematic diagram of the grouping I do for the various cooling techniques discussed in this chapter.

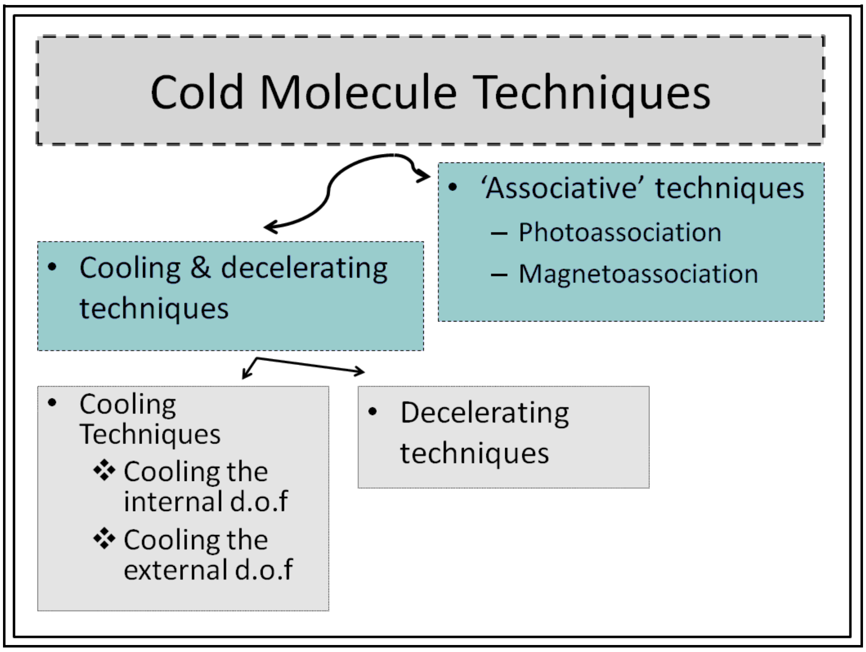

Fig. II.2.1.1: Grouping of the various techniques (or theoretical proposals) for the study of cold atoms as considered in the rest of this chapter, see text for details.

As mentioned before, the so-called association techniques do not deal with translational cooling of the molecules, since this is already done in the atoms that are used to create them. The two techniques belonging to this category, the photoassociation and the magneto-association or Feshbach resonance, are as their names suggest, aiming to create cold molecules by associating two cold atoms to form a molecule. The main difference between these two techniques, apart from the means employed to achieve association by each one (light or magnetic fields), is in the different states in which these molecules are produced. In particularly, the photoassociation usually produces molecules in a variety of vibrational and molecular states[1]. Since the objective of the area is the production of molecules internally and externally cold, an additional technique for the cooling of the internal degrees of freedom is usually required. The Feshbach resonance technique on the other hand, produces molecules in a single rovibrational state. The only 'disadvantage' in this case, is that this rovibrational level is an excited one, which can decay to various other states, and the system is not stable. Here, a molecular population transfer technique can be employed in order to transfer the molecular population in a state with neither vibration nor rotation and stabilize the system.

In the other big group of experimental techniques, the ones that deal with already formed molecules can be divided in two main groups: the ones that aim to the cooling, and the ones that aim to the deceleration of a molecular sample. The importance of this final branch is due to the

---

[1] Except of course from various, particular photoassociation schemes which manage to provide with molecules in few or a single rovibrational state. Some of the most important among these photoassociation schemes are discussed in the second part of this chapter.

major breakthrough consisted in the Stark deceleration technique reported in [Bert99] and described in the following paragraph, as well as to the resulting generalizations which involve magnetic instead of electric fields. In this type of experiments, a supersonically expanded molecular beam, in which vibration and rotation are (fairly) cooled by expansion, is decelerated with means of fast varying fields which interact with the molecule's permanent (electric or magnetic) moment. Apparently, deceleration considers the external degrees of freedom (translation).

From the remaining techniques (or theoretical proposals), other aim in to cool the internal and others the external degrees of freedom. In the first category we find a theoretical proposal involving Optimal Control Theory [Kim01], as well as the technique which is the subject of this thesis[1]. On the second category we find a variety of methods involving 'collisional' cooling, cooling due to the rotating frame of reference, and finally, the technique of sympathetic cooling.

II.2.2. Methods for molecular cooling

II.2.2.a. Sympathetic or 'buffer gas' cooling

Molecular cooling has been demonstrated via various experimental techniques. Some approaches involved cryogenic techniques and molecules have been loaded with this method into conservative traps were evaporating cooling can follow [Wein98]. In Fig. II.2.2.1 adapted from [Wein98], we see an schematic representation of a set up that permits this kind of cooling. In this method, the cooling in CaH_2 molecules is achieved by collisions and thermalisation with cryogenically prepared cold helium atoms and the temperature of the molecular sample can reach as low as ~450μK. The CaH_2 molecules are produced by laser ablation of a solid CaH_2 sample. The ablated molecules are colliding with the cold helium atoms and are magnetically confined in the center of the chamber by the confining magnetic potential produced by the superconducting coils, where they are detected.

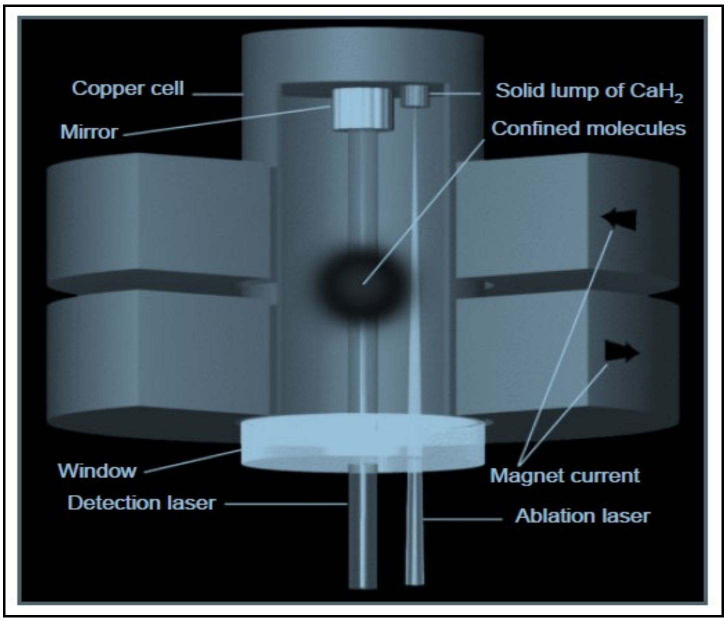

Fig. II.2.2.1: Experimental set up for the cryogenic cooling of CaH, taken from [Wein98].

---

[1] An additional proposed method considers enchantment of the spontaneous emission towards a particular ro-vibrational level with the use of external cavities. However, this and more proposals involving the use of cavities are not considered here, especially due to economy.

II.2.2.b. Stark and Zeeman deceleration

Except for directly cooling molecules, there exist several techniques for the deceleration of molecules. One of the first demonstrated techniques for the deceleration of molecules in a molecular beam is the Stark deceleration technique, which manages to decelerate polar heteronuclear molecules, via the Stark interaction [Bert99]. In these experiments, electric fields are employed in order to interact with these molecule's permanent electric moment and the objective is to decelerate a supersonic beam of molecules either in their ground or in an excited 'Rydberg' level [Bert99, Pro03], while in other variations of the technique, the magnetic moment can provide the interaction with which molecules can be decelerated [Vanh07, Nar08]. Other techniques use electric fields combined to differential pumping, in order to select the slowest velocity groups in expanded molecular clouds [Rang03]. These methods have in common the electrostatic nature of the interaction, except for the case of the Zeeman decelerators, where the magnetic interactions substitute the electric ones.

InFig. II.2.2.2 we see the operating principle for the two most characteristic 'electrostatic methods', the Stark deceleration and the velocity selection. In part (a) we see the example of the Ammonia molecule as it is moving in the decelerating electrostatic potential. A low-field seeking molecule approaching the first pair of dipoles in the Stark decelerator will slow down a little as it experiences an increasing field. When it reaches a position close to the top of the energy hill (at (2), on the left) the fields are switched off in order to prevent it from running down the hill the other side (and hence accelerating). The voltages of the first and second pairs of electrodes are then swapped over so that the hill moves along suddenly, as shown in gray. The molecule thus instantaneously finds itself at the bottom of another hill and continues climbing, slowing down a little more. By repeating this sequence 100 times over with a carefully timed field it is possible to slow a subset of the molecules down to any arbitrary velocity. In part (b), we see the operating principle of the velocity selection technique. This technique uses the electrostatic field, shown up and to the left, to 'guide' the lowest velocity group of the expanded molecular cloud towards the detection chamber, or the conservative trap.

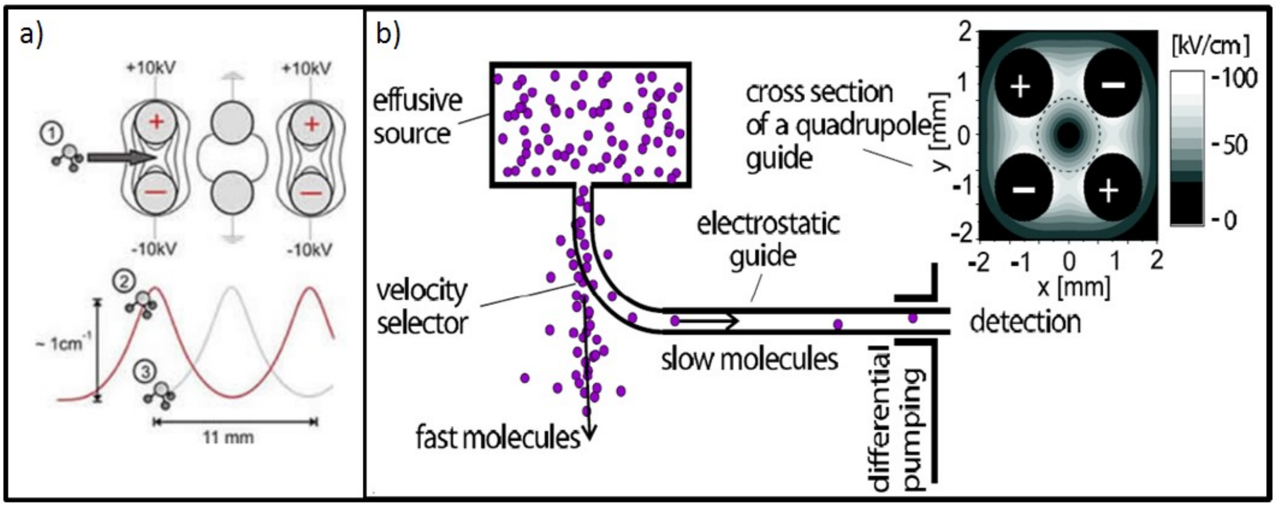

Fig. II.2.2.2: (a) operating principle of the Stark deceleration technique in the Ammonia molecule [Bert99]. (b) The velocity selection technique uses the electrostatic field shown up and to the left to 'guide' the lowest velocity group of the expanded molecular cloud towards the detection chamber, or the conservative trap [Rang03].

II.2.2.c. 'Mechanical' cooling

The techniques proposed or implemented for the cooling of molecules can be very diverse. I will try to group two interesting techniques in a family of 'mechanical' techniques, while there might exist more techniques that could be grouped in this 'family'. In these techniques the cooling mechanism does not come by electrostatic interactions or by cryogenic cooled atoms, but has more to do with simple classical dynamics of the moving molecules. In the technique reported in [Gup99] and shown in Fig. II.2.2.3 (a), the flow velocity of gas emerging from a supersonic nozzle mounted on a high-speed rotor can be largely canceled by the rotor velocity, therefore producing an intense beam of molecules traveling in vacuum with translational speeds slowed to a few tens of m/sec. These features are demonstrated by model calculations and experimental results for beams of Xe, O_2 and CH_3F seeded in Xe. In part (b) we see the operating principle of a technique that manages to produce NO molecules in low temperatures by collisions between two jets, an atomic and a molecular one in particular angles [Eli03]. The technique, relies on a kinematic collapse of the velocity distributions of the molecular beams for the scattering events in particular angles, which produce NO molecules in sub-Kelvin temperatures.

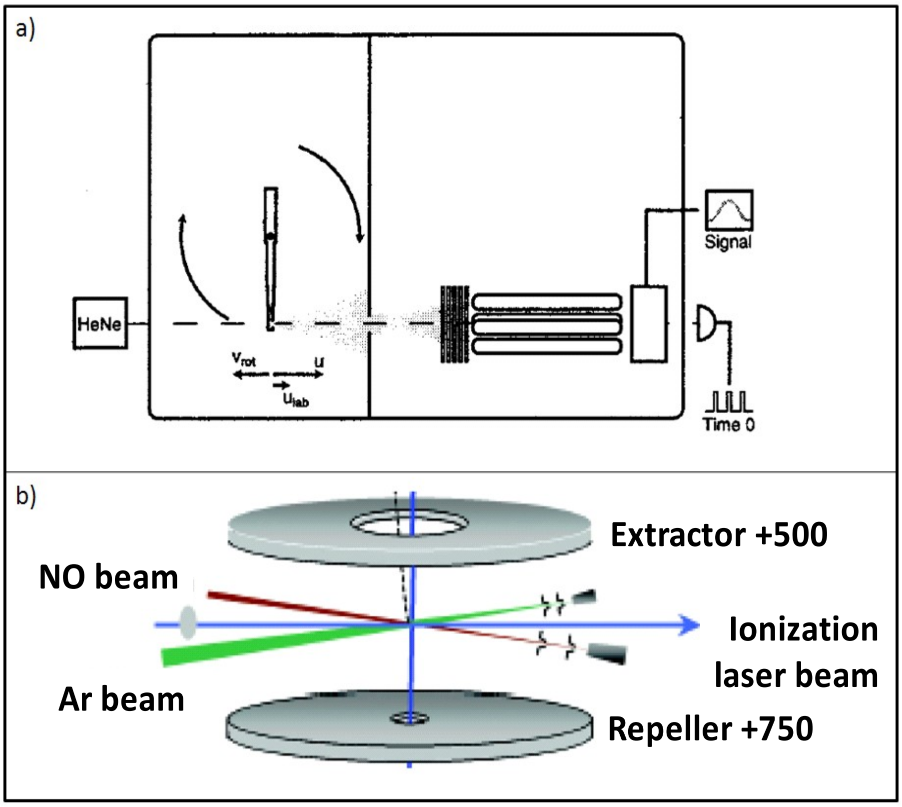

Fig. II.2.2.3: Operating principle of the 'mechanical' techniques: (a) a supersonic nozzle mounted on a high-speed rotor. The flow velocity of the emerging gas can be largely canceled by the rotor velocity, thereby producing an intense beam of molecules traveling in vacuum with translational speeds slowed to a few tens of m/sec [Gup99]. (b) Operating principle of the technique reported in [Nar08], which manages to prepare NO molecules in low temperatures by collisions between two jets, an atomic and a molecular one, in particular angles [Nar08].

II.2.2.d. Theoretical proposal for the molecular cooling via dynamically trapped states

Finally, there exist a variety of theoretical proposals for the achievement of laser cooling. Some of these proposals involve femtosecond lasers, shaped or not [Tann99], others the use of frequency combs [Pe'Er07, Saph07], while others the use of coherent population transfer via STIRAP [Ooi03]. Another group of proposals are the ones that involve high quality cavities, which can be used to favor spontaneous emission to a particular level, and thus create a closed transition with which the molecules can be laser cooled [Mor07]. In [Vul00] we see an alternative approach, where cooling is achieved inside a cavity, since preferential scattering due to the molecule-cavity interaction can lead to cooling. However, to our knowledge, no direct laser cooling of molecules is demonstrated for the time being.

However, one theoretical proposal is chosen to be described here, due to the close relation to the vibrational cooling technique reported in [Vit08] and discussed throughout this part of my thesis. This is the “vibrationally selective coherent population transfer” technique described in [Tann99, Bart00]. It is addressing the issue of vibrational cooling in molecules as a problem of population transfer to the ground vibrational state. Having as background, coherent population transfer between atomic states with STIRAP [Berg98], and S-STIRAP (extension of the previous) the authors propose a technique for the laser cooling of the internal degrees of freedom (vibration) in molecules. The preparation of an internal, dynamical dark state, in corespondent to the dark states in the atom field 'dressed' states picture considered in STIRAP, can be achieved via Optimal Control Theory. The condition for the creation of the dark state, and thus population trapping is achieved by the instantaneous phase-locking of the laser to the transition dipole moment of the 'target' state v = 0. Thus, molecules that are transferred to the desired state by spontaneous emission, are 'dynamically' trapped and finally accumulated in it. The pulse that can create such a dynamical trapping is calculated with the use of Optimal Control Theory. In Fig. II.2.3.3, the basic elements of the proposed experiment are schematically displayed.

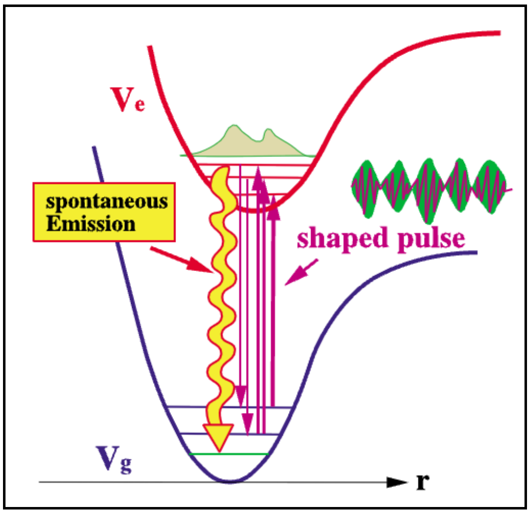

Fig. II.2.2.4: The “vibrationally selective coherent population transfer” technique; A pulse optimized with means of OCT excites a group of molecular transitions. The pulse is such that the molecule's ground state is a 'dark' state of the system and all molecular population is transferred there by spontaneous emission. Figure adapted from [Kim01].

In summary, this proposal aims in the molecular population transfer to the ground (or a nearby) ro-vibrational level via spontaneous emission. This is accomplished by exciting the system in such a way, that the state in which we need to transfer the molecular population is a 'dark state' of the system, which means that it does not interact with the driving pulse. This is accomplished with the use of sophisticated pulse as described earlier. However, if we leave aside the mechanism with which the 'dark state' is obtained, we find great similarities between this proposal and the vibrational cooling method described in this part of my thesis. These similarities will become evident in the beginning of the following chapter, where the operating principle of the vibrational cooling technique is going to be discussed.

II.2.3. Methods for the preparation of cold molecules by association

Magneto-association

An alternative approach for the production of cold molecules is to create them from ultra cold atoms by the use of an associative technique. In the introduction of the first part of this thesis, the magneto-association technique or Feshbach resonance was discussed. We show how the variation of a bias magnetic field in the area of the Feshbach resonance can lead to the association of ultra cold atoms in long range molecules. In particular for the case of Cs, the magnetic resonances have been used not only for the creation of ultracold molecules, but also for the modification of the Cs collision properties towards condensation as discussed in [Web03b]. Apart from that, the Feshbach resonances find extensive applications in the area of cold and ultracold atoms, since they are related the study of BEC-BCS crossover, superfluidity and more [Kett07, Sal07]. The Innsbruck group, reported extensively in the first part of this thesis [Web03], is a pioneering group in the study of cold molecule formation via magneto-association, since directly after the preparation of a Cs BEC, a molecular BEC prepared via magneto-association was reported. In Fig. II.2.3.1, we see the first observation of ultra-cold Cs_2 molecules created by this method [Herb03]. The different magneto-dipole moment is used to separate the cold molecules by the atomic BEC. The molecules are either left to fall or they are levitated with respect to the Cs BEC.

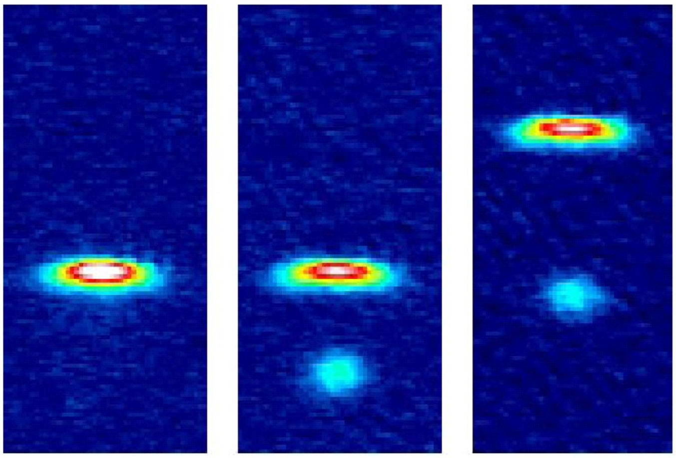

Fig. II.2.3.1: Cold molecule formation by magneto-association. Figure adapted by [Herb03]. On the left we see a pure atomic Cs condensate. On the center, we see molecules created by magneto-association falling from the condensate, while in (c) they are levitated by means of external magnetic fields.

Photo-association

1. General description

Photoassociation is also a technique that permits the creation of cold molecules from an sample of cold atoms, usually performed in a MOT. Photoassociation is the process in which two atoms are colliding in the presence of a laser field. This laser can bring the atoms into resonance with a long range, but bound molecular state. Because the free-state thermal energy spread is negligibly small, this process leads to a well resolved free-bound absorption spectrum. This "photoassociation spectroscopy" is proving to be a powerful tool for the analysis of atomic interactions at long range. Performing photoassociation in a MOT leads to loss in the number atoms magneto-optically trapped. The atoms which undergo photoassociation form loosely bound molecules, which are in their largest percentage dissociated to give hot free atom pairs. In any case, the photo-associated atoms exit the MOT, either because the MOT cannot support molecules, or because the atoms, that result from the dissociation of the molecules formed by photoassociation, are hot and escape the trapping. Thus, observing the losses in the MOT as a function of the photoassociation frequency, provides perhaps the easiest method for the realization of photoassociation spectroscopy. Another methods consist of detecting the molecules which are formed by photoassociation, usually by laser induced ionization. In Fig. II.2.3.2, we see photoassociation spectra acquired by both these methods. The red curves represent photoassociation spectra obtained by the 'trap-loss' method, while the black curves represent spectra of the ground singlet and triplet Cs_2 states, acquired by pulsed laser 2 photon Resonance-Enhanced Multi-Photon Ionization (REMPI) [Comp99, Drag 00].

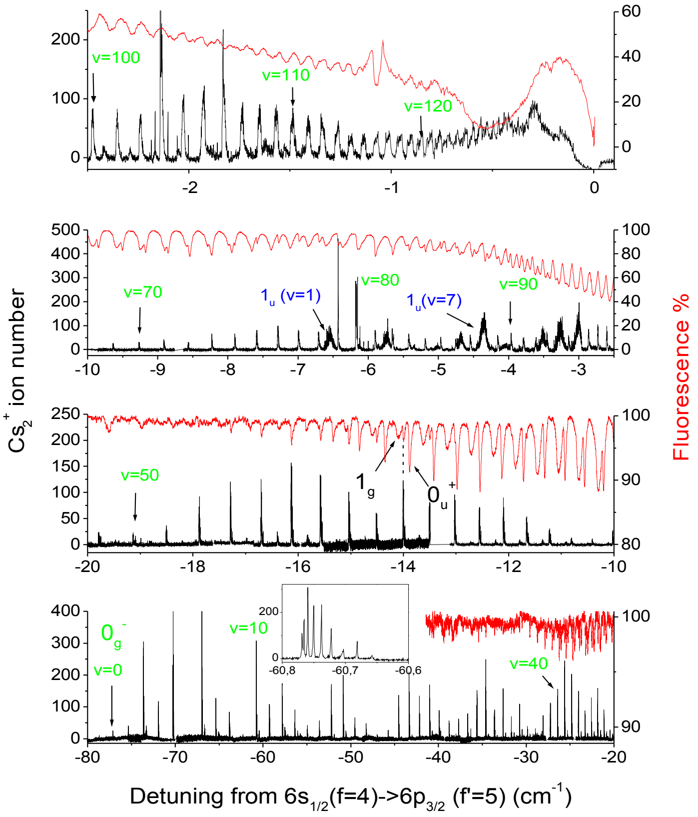

Fig. II.2.3.2: Photoassociation spectra acquired by two methods. The red curves represent photoassociation spectra obtained by the 'trap-loss' method, while the black curves represent spectra acquired by pulsed laser REMPI.

2. Stabilization of the produced molecules

The principle of photoassociation of cold atoms has been proposed in 1987 [Tho87] and was originally demonstrated six years later with sodium [Lett93] and rubidium atoms [Mill93], while potassium and lithium followed some years after [McAl95, Wang96]. Photoassociation was also performed in Cs and stabilization of the produced molecules has been demonstrated in [Fio98]. In our group, cold Cs molecules produced by photoassociation have been loaded to a magnetic [Vanh02] and a dipole trap [Zahz06], while their vibrational cooling was recently demonstrated with the use of shaped femtosecond pulses [Vit08].

Photoassociation can be represented as a light-assisted collision as in Eq. 1.13. Two colliding atoms absorb a photon resonant with an excited molecular level. This molecule is relaxing typically in some tens of nanoseconds.

$$Cs + Cs + h\nu_L \rightarrow Cs_2^* \qquad (1.13)$$

Whether the relaxation is towards a bound molecular state, or towards two unbound hot atoms depends on the inter-nuclear distance in which the wavefunction of the excited molecule is centered. This is depended on the molecular potential via which photoassociation is realized. For the case of homonuclear atoms, the typical molecular potentials ('single well') leads to the production of molecules which are localized in large internuclear distances, and which relax principally to two unbound and hot atoms. In Fig. II.2.4.a.2, we see a schematic representation of photoassociation via a typical homonuclear molecular potential. Initially, the two free atoms collide with a photon resonant with an excited molecular level, with only their initial thermal energy k_BT. This photoassociation scheme created an excited molecule localized in large internuclear distances, a fact which principally results to the relaxation of the excited molecule to a pair of hot atoms, while relaxation towards a bound molecular state is strongly suppressed.

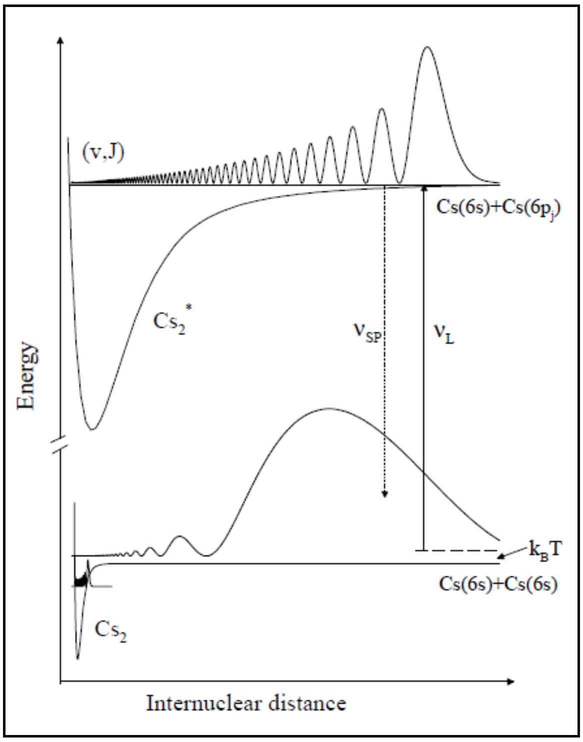

Fig. II.2.3.3: Schematic representation of photoassociation via a typical homonuclear molecular potential, which principally results to the relaxation of the excited molecule to a pair of hot atoms [Niko00].

However, relaxation towards a bound molecular state can be enhanced, if the potential via which the photoassociation is taking place is particular. In Fig. II.2.3.4 adapted by [Dion01], we see the two potential cases. In the upper part of the picture, photoassociation is taking place via a non particular molecular potential and relaxation towards unbound atoms is favorable. In the middle part, the photoassociation is taking place via a particular potential, which has an additional local minimum at an intermediate internuclear distance. The existence of this additional potential minimum leads to enhanced relaxation in short interatomic distances. In the lower part, coupling to an additional molecular potential perturbates the molecular wavefunction and leads to the stabilization of the produced molecules.

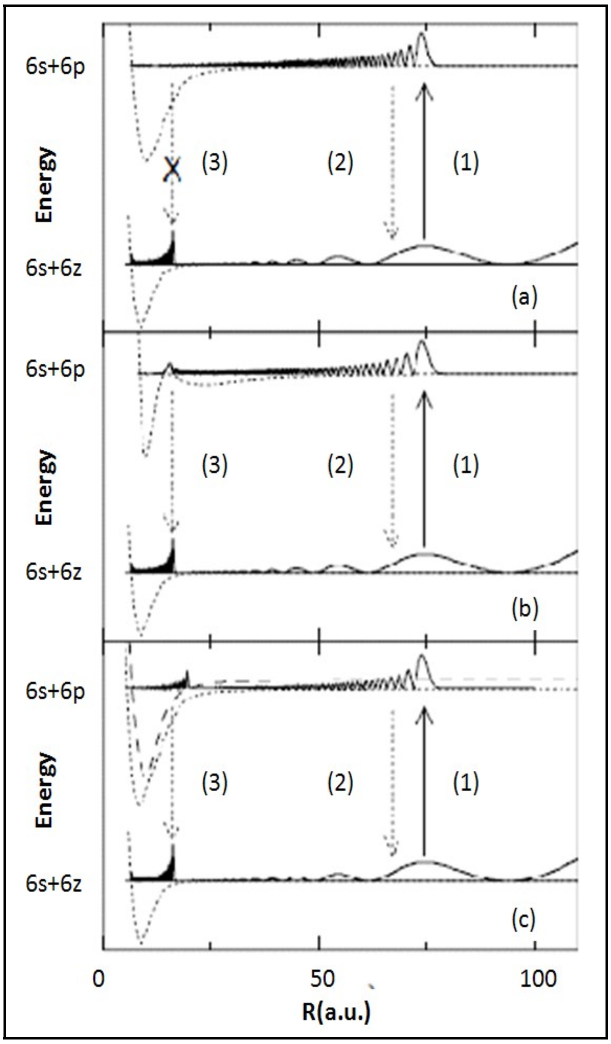

Fig. II.2.3.4: Figure adapted by [Niko00] showing (a) the photoassociation of molecules via a non particular molecular potential, (b) via a particular potential and (c) stabilization of the produced molecules in short internuclear distances, via coupling to another molecular potential.

In the case of heteronuclear molecules, photoassociation can be different, since the excited (as well as the fundamental) potentials lead to the creation of molecular states in shorter internuclear distances. This has as an effect the reduction of the photoassociation efficiency, but on the other hand, leads to enhanced relaxation rates towards the ground molecular states. This characteristic of photoassociation in heteronuclear molecules is widely used for the preparation of molecule without vibration or rotation, in some of the techniques discussed in the next paragraph.

II.2.4. Recent developments in the area of cold molecules

The last years many exciting developments have been reported by various groups worldwide concerning cold molecules, and in particularly the preparation of cold molecules without vibration and/or rotation. The developments are rapid and the scenery in the field is changing fast, so that many experiments show that control of the internal degrees of freedom of molecules is now possible with more than one method and molecular samples. In this paragraph, I will briefly present some of the most important developments, trying to describe the evolution of the field historically up to the time of my involvement into it. The various experiments discussed, are chosen in order to outline the diversity observed within the various approaches for the preparation of cold molecular samples; perhaps many interesting experiments escaped my attention, however the paragraph does not intend to give a detailed review of the field.

II.2.4.a. Photo-association

In Fig. II.2.4.a.1, we see the operating principles of three, very important photoassociation experiments. In part (a) the photoassociation scheme reported in [Nik00] allowed for the preparation of K_2 molecules in deep vibrational levels of their ground electronic states. In summary, the first photon at ~769 nm performs photoassociation via the $\upsilon = 89$ vibrational level of the $1\ ^1\Pi_g$ electronic state of the K_2 molecule. The formation of these molecules is verified by ionization detection via a continuous laser not shown in the picture. The second photon at ~853 nm transfers the excited molecules to the the $5\ ^1\Pi_u$ state. The successful population transfer is verified since these molecules are also detected by a cw laser not shown in the picture. Finally, spontaneous emission transfers the molecular population to the fundamental electronic state $X^1\Sigma_g^+$, distributed in two major bands, one in states with $\upsilon = 25\text{-}42$ and one with $\upsilon < 10$.

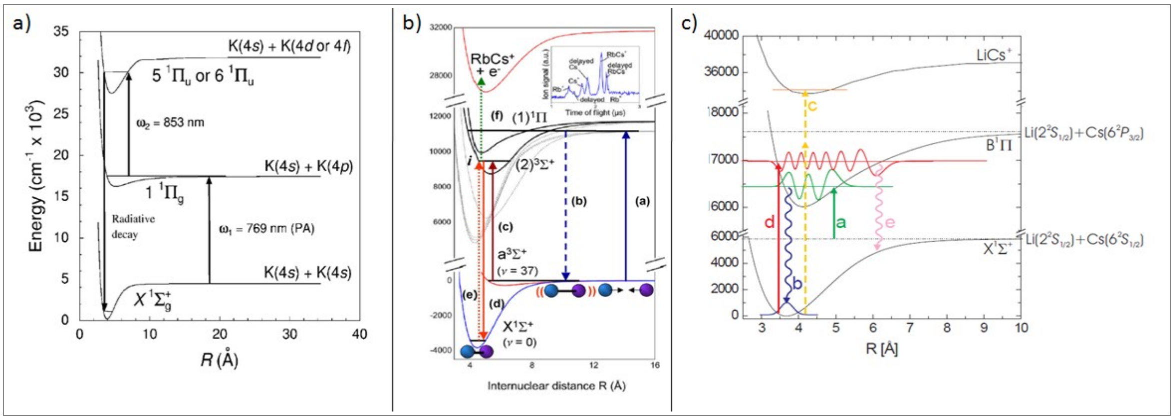

Fig. II.2.4.a.1: Photoassociation techniques that result to the creation of molecules in the ground electronic state, without vibration and/or rotation. (a) Two photon photoassociation scheme that results to the preparation of K_2 molecules molecules in deep vibrational levels of their ground electronic states [Pro03]. (b) Photoassociation of RbCs molecules and Raman transfer to the fundamental electronic state [Sag05]. (c) Direct photoassociation of LiCs molecules in short internuclear distances [Del08].

In part (b) we see the configuration reported in [Sag05] which involves photoassociation of RbCs molecules at the $^1\Pi$ state, from which they relax to the $\upsilon = 37$ vibrational level of the $\alpha^3\Sigma^+$ electronic state. Then it follows the Raman transfer, in which a first photon excites molecular population to the $^3\Sigma^+$ and a second to the $X^1\Sigma^+$ electronic state, either in the $\upsilon = 0$ or in the $\upsilon = 1$ vibrational level. This transfer is possible due to the coupling of the intermediate $^3\Sigma^+$ state to the $B^1\Pi$ state, caused by spin-orbit interaction. This coupling permits the transition between a molecular state with a singlet to a triplet symmetry.

In part (c), we see the photoassociation scheme used for the production of LiCs molecules reported in [Del08]. There, photoassociation is performed with one photon, directly to the fundamental electronic state, resulting to molecules in the υ = 0 vibrational level with very few rotational energy (J = 0 or 1). The experiment is conducted to a mixed LiCs MOT, while the repumper of the Cs trap is shaped in order to create a Dark-SPOT. Initially, photoassociation creates molecules in the υ = 4, J = 1 or 2 rovibrational levels of the $B^1\Pi$ electronic state (a). Spontaneous emission creates the molecules in the υ = 0 vibrational level of the fundamental electronic state. These molecules are detected via a two photon REMPI ionization scheme, one photon at 575 and another at 600 nm (c) A cw laser excites the created molecules towards the υ = 14 vibrational level of the $B^1\Pi$ electronic state, creating a depletion in the two photon ionization signal and permitting the detection of the rotational distribution.

A similar photoassociation experiment has led to the creation of cold NaCs molecules [Haim04, Haim06]. In Fig. II.2.4.b.1 we see the photoassociation and detection configuration. Again the photoassociation process is taking place in very small interatomic distances (< 4 Angström) while the trapping lasers provide the photoassociation radiation since Na or a Cs trapping photons can photo-associate the two atoms into an excited-state NaCs molecule. The excited state molecules are distributed over a range of rotational and vibrational states near the dissociation limit. A fraction of these excited molecules decays to a range of rovibrational states within the electronic ground state manifold with a distribution governed by the bound-bound Franck-Condon factors.

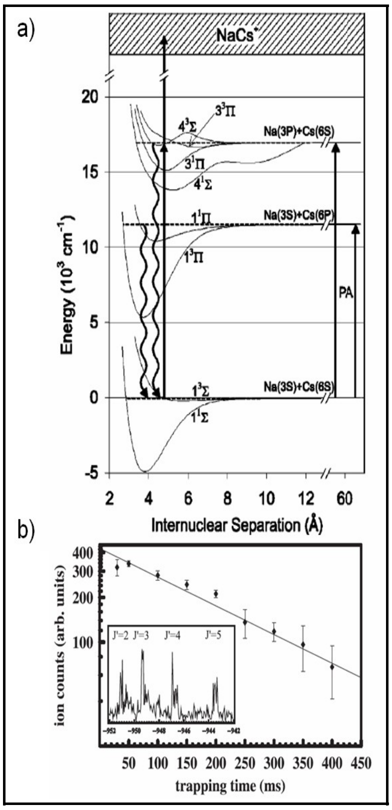

Fig. II.2.4.a.2: (a) Principle of the photoassociation experiment for the production of NaCs cold molecules via photoassociation in a mixed Ka and Cs MOT. (b) Lifetime of the NaCs molecules in an electrostatic 'TWIST' trap. Picture taken by [Klei07b]

Those polar NaCs molecules are trapped by means of electrostatic forces via a novel trapping configuration reported and reviewed in references [Klei07, Klei07b]. The novel trapping configuration consist of a dc-electric field trap created by the use of thin (~75 μm wide) tungsten wires, where the name TWIST (Thin Wire electroStatic Trap) comes form. The wires are forming four 8 mm diameter rings which are separated with each other by 3, 2 and 3 mm. By charging the inner rings with +1 kV and by grounding the outer ones, a trap of ~6 mK depth can be obtained for the $J = 1$, $M_J = 0$ ($\upsilon = 0, 30$) NaCs molecules. The rings overlap with the MOT and the cold molecules which are continuously formed by PA are loaded in a CW fashion in the trap. In part (b) of Fig. II.2.4.b.1 we see a measure of the lifetime of the trapped cold NaCs molecules. The inlet shows detection of these trapped molecules after 100 ms of trapping, proving that simultaneous tapping of various rotational states was achieved.

II.2.4.b. Magneto-association

A method for the creation of molecules without vibration or rotation, without the use of photoassociation is reported in [Danz08]. In this method, molecules are created in an ultracold Cs sample by magneto-association, in a single rovibrational level. The experiment starts with a Cs ultra-cold atomic sample, from which molecules are created via magneto-association in the last vibrational level of the fundamental state. There, the molecular population is coherently transferred to the $\upsilon = 73$ vibrational level of the $X^1\Sigma_g^+$ electronic state., via the Stimulated Raman Adiabatic Passage (STIRAP) technique. A subsequent STIRAP step, permits the preparation of a very cold and dense molecular sample in the fundamental state, without vibration or rotation. However, the realization of this experiments is complicated, due to the difficulty in the phase stabilization of the very different wavelength lasers, at 1126 and at 1006 nm. For this purpose the lasers are stabilized by locking to a frequency comb.

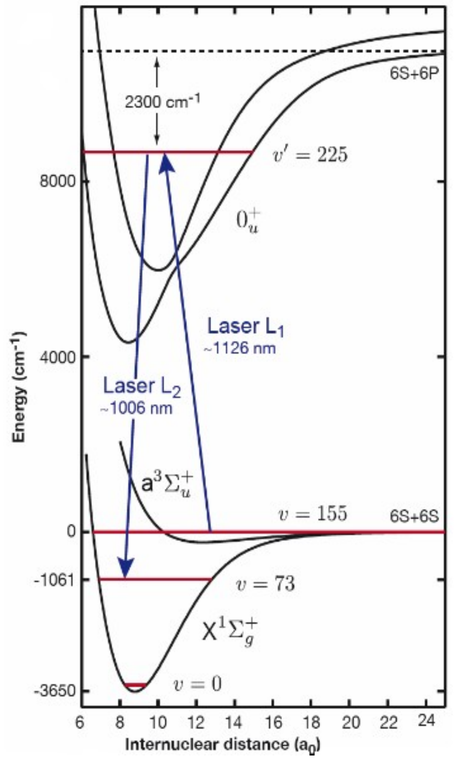

Fig. II.2.4.b.1: Operating principle of the experiment reported in [Danz08]. The molecules created by magneto-association are transferred towards the absolute ground state by two subsequent STIRAP steps (only one shown here).

II.2.5. Conclusion

In this chapter I intended to give a short but comprehensive review of some of the most important techniques for the study of cold molecules. I begin with a short introductory paragraph, in which I try to point out the difference between cooling of the internal and the external degrees of freedom, as well as to justify the grouping I followed in the next paragraphs. I continue by describing these techniques according to this grouping, starting from the conceptually simpler cryogenic method, to the deceleration techniques, the 'mechanical' techniques as well as the two 'associative' techniques, the photoassociation and the magneto-association. In those, I add the description of a theoretical proposal which is closely related to the vibrational cooling technique discussed in this part of my thesis. Finally, I review the most important developments towards the preparation of molecules with neither vibration nor rotation, in order to describe the point in which research in cold molecules was at the beginning of my studies.

CHAPTER II3: VIBRATIONAL COOLING WITH BROADBAND LIGHT

II.3. VIBRATIONAL COOLING WITH BROADBAND LIGHT

In the first part of this chapter, I intent to give a fast but yet comprehensive review of the vibrational cooling technique reported in [Vit08] as well as of the hole line of experiments that lead to this achievement, and which are described in detail in [Vit09b, Vit08c]. In the second part I describe the experimental set-up used in this line of experiments as well as in this part of my thesis.

In the beginning of the first part, I try to outline the operating principle of the vibrational cooling technique, in a small, introductory paragraph. We see that the technique is based on a simple operating principle, and thus enjoys in the same time simplicity and generality. The use of broadband radiation allows for the simultaneous excitation of several vibrational states. Later on, the molecular population is redistributed via spontaneous emission in several other vibrational states. The existence of a 'dark' state in the molecule-pulse system, leads to the accumulation of the molecular population in this state after the repetition of several excitation-relaxation cycles, similarly to optical pumping in atoms.

In the following paragraph, I describe the line of experiments that lead to the preparation of deeply bound Cs dimers and to the demonstration of the vibrational cooling technique. This was made possible only after an innovating spectroscopic study, that managed to determine photoassociation channels that could provide with Cs_2 molecules in their ground electronic state. The molecules produced by photoassociation where distributed in low vibrational levels, (v_X = 1-10), a fact that simplified demonstration of vibrational cooling. During this spectroscopic study, a large range of frequencies was studied with the use of broadband dye laser pulses, and several photoassociation lines were observed in order to identify those that could provide with sufficiently deeply bound Cs dimers. I will briefly outline this experimental activity, while a detailed discussion can be found in [Vit09b]. In the following paragraph, I describe the experimental demonstration of the vibrational cooling technique originally demonstrated in [Vit08].

In the second part of this chapter, I present the experimental set-up that is used in the Cold Molecule experiment. The basic set-up stays more or less common in the studies reported in the following of the thesis; the elements added for particular studies are going to be refereed to in the corresponding chapters. In the first paragraph, I list the characteristics of the Magneto-Optical trap, which is very similar to the ones described in the first part of this thesis, and I describe the photoassociation laser. In the second part, I describe the ionization laser and the data acquisition process. Finally, in the third part I describe the femtosecond laser used for the optical pumping, as well as the simple shaping technique originally used in our laboratory.

II.3.1. Vibrational Cooling technique

II.3.1.a. Operating principle

As discussed in the previous chapter, the operating principle of the vibrational cooling technique is closely related to the theoretical proposal concerning molecular cooling via dynamically trapped states [Bart01]. This is due to the fact that both methods rely on accumulation of the molecular population to a particular state through spontaneous emission. This is made possible by forcing this particular state to be a 'dark' state of the system, and thus not to interact with the light and participate in the repeated absorption – spontaneous emission cycles. The simultaneous excitation of several vibrational levels is achieved with the use of broadband femtosecond radiation.

In the case of the vibrational cooling technique described here, the ground vibrational level is a 'dark' state of the system due to the particular shaping of the femtosecond pulse. In such a pulse, all frequency components that can excite the ground vibrational level towards any excited state have been removed. Thus, this level does not interact with the light, and all population that ends up there by spontaneous emission is no longer re-excited. In Fig. II.3.1.a.1, we see a schematic representation of such a situation. The optical pumping scheme is considered between the X $^1\Sigma_g^+$ and the B $^1\Pi_u$ state and the shaping of the pulse is such that no transition from the vibrational ground state can be supported. Thus this state is considered to be 'dark', and does not participate in the absorption – emission cycles. Finally, after repetition of several steps, all molecular population is accumulated in the ground vibrational level. Note that, apart from the mechanism with via which the ground state is excluded by the absorption – emission cycles, the principle coincides with the one of the proposal for molecular cooling via dynamically trapped states [Bart01].

This simplified picture suggests that the technique is applicable in all cases, and that a population transfer efficiency of 100% should be expected at all times. This is, of course, not true and this oversimplified picture needs to be improved in order to become more realistic. In this example we supposed that all the vibrational levels involved are connected via the optical transition with a satisfactory rate. Nevertheless, there are situations were the possibility to perform a transition from a given vibrational level to another specific vibrational level is very small. As we recall from the first chapter of this part of this thesis, the relative strength between transitions of different vibrational number depends on the spatial overlap of the vibrational wavefunctions, or simply in the Franck-Condon factors. It is not always easy to find a situation where the Franck-Condon factors are suitable for vibrational cooling, while the reduced efficiency in realistic implementations of it, is most often due to the relative magnitude of these Franck-Condon factors.

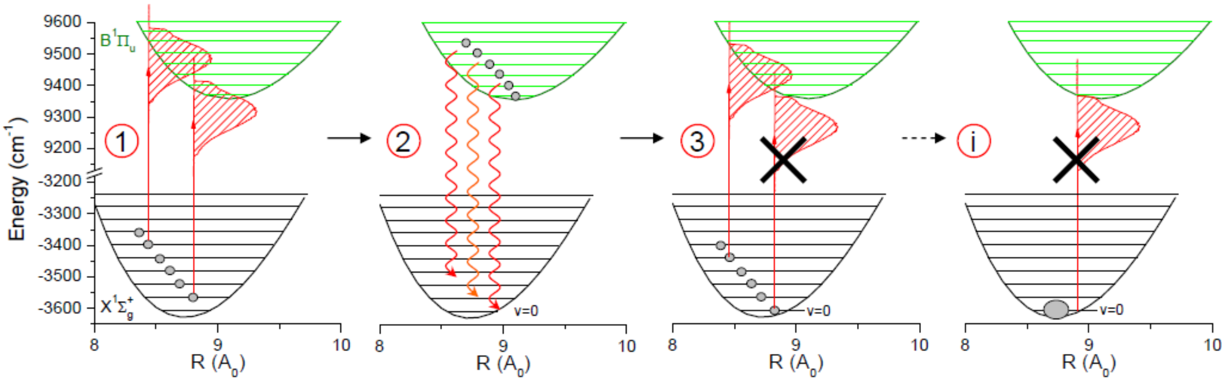

Fig. II.3.1.a.1: Accumulation to the ground state due to spontaneous emission. (1) All molecular population is simultaneously excited with the use of shaped femtosecond pulses. (2) Spontaneous emission redistributes molecular population among the various vibrational levels. (3) The pulse shaping is such that the pulse do not support excitation of the ground vibrational state. Thus this state is a 'dark' state of the system. (i) After a long a sufficient number of steps all molecular population is accumulated to the ground vibrational level. Figure adapted from [Vit08c].

For the study of the vibrational cooling technique, it is often very useful to plot the Franck-Condon factors in a pictorial way, where their relative value is indicated with the corresponding color in a gray scale. An example of such a plot is shown in Fig. II.3.1.a.2.. We see in (b) that for the choice of potentials shown in (a) the Franck-Condon factors form a parabolic shape. This leads to the terminology 'Franck-Condon' parabola. We will return in the study of various Franck-Condon parabola, in Chapter II 6.

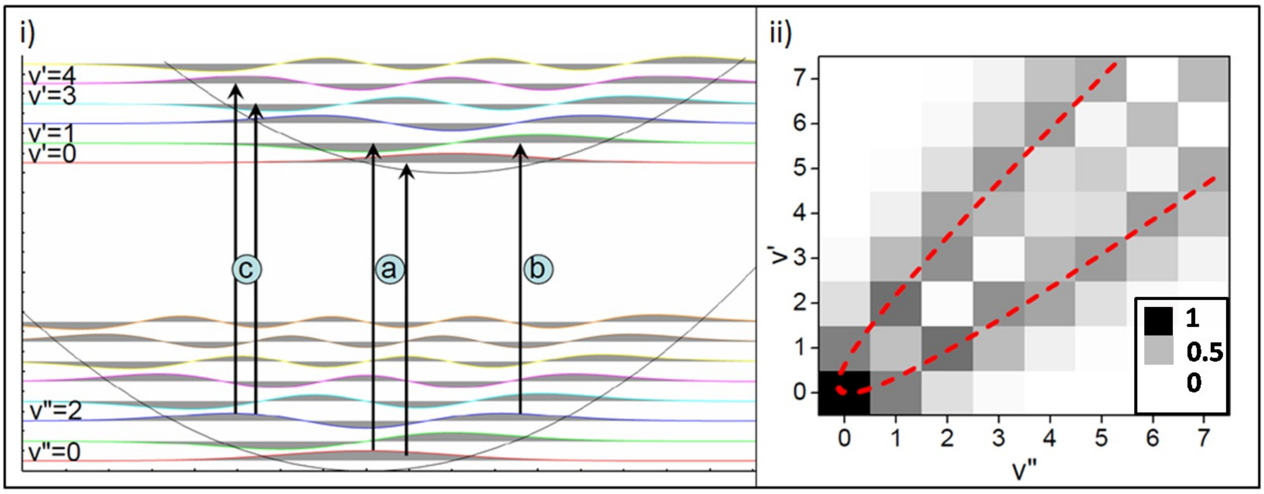

Fig. II.3.1.a.2: (i) Transitions between two identical but shifted molecular potential with the most favorable transitions noted: (a) transition v"=0→v'=0,1 (b) transition v"=2→v'=1 (c) transition v"=2→v'=3,4 (i) Plot of the values of the Franck-Condon coefficients in gray scale arranged in table for all transitions between v=0 to 7. Figure adapted by [Vit08c].

II.3.1.b. Broadband detection of deeply bound Cs dimers

In this part of the introduction I will summarize the experiments that led to the preparation of the Cs dimers in the $X^1\Sigma_g^+$ singlet state and the development of the vibrational cooling technique. The preparation of molecules in the $X^1\Sigma_g^+$ singlet ground electronic state was verified by a spectroscopic study with the use of broadband laser radiation which is described in detail in [Vit09b, Vit08c] and it has been summarized in [Vit09].

In this spectroscopic study, the idea of simultaneous excitation of several vibrational levels by broadband radiation was also employed. Thus, for this spectroscopic study, an additional, Continuum dye laser ND6000 was used. This laser was modified in order for the radiation to be spectral broadened to permit the rapid study of many photoassociation lines by simultaneously exciting many vibrational levels. However, after the creation of molecules in the $X^1\Sigma_g^+$ singlet state was identified, the molecules detection is done by the simple ionization scheme at ~16000 cm^{-1} (described in the following paragraph). This spectraly broadened dye laser was no longer used in the cold molecule experiment and is now in use by another group.

In order to observe deeply-bound molecules in the $X^1\Sigma_g^+$ singlet state (hereafter noted simply as X state), they are excited with the broadband radiation, through vibrational levels v_B of the spectroscopically known $B^1\Pi_u$ excited state [Diem89] (refereed to as the B state). A two-photon transition is induced by radiation at a wavelength of 770 nm, while a third photon can ionize the molecules if the power is sufficient. Otherwise, an additional single photon transition induced by the pump laser (532 nm wavelength) as illustrated in Fig. II.3.1.b.1 can realize the ionization step. In all cases, the intermediate level enhances the ionization signal; the general technique is known as Resonance-Enhanced Multi-Photon Ionization (REMPI). The ionization probability due to the second photon at 532 nm is independent of the specific v_B level, so that it is proportional to the population of this level induced by the first photon at 770 nm.

The narrow-band ionization scheme allows the ionization of a single v_X level at a given frequency. In contrast, the broadband scheme involves a laser pulse width of the order of the vibrational spacing of both the X and B states (up to 40 cm^{-1}), so that many vibrational v_X levels can be ionized in a single shot. With the broadband detection laser (13000 cm^{-1}) and scanning the photoassociation laser frequency over a few wavenumbers below the 6s + $6p_{3/2}$ dissociation limit, several intense photoassociation lines are found, labeled with crosses in Fig. II.3.1.b.2, revealing a large number of ultracold molecules formed in low ($v_X < 70$) vibrational levels of the X state. The single frequency, narrow-band REMPI detection scheme at 720 nm, optimized to detect triplet $a^3\Sigma_u^+$ molecules, was blind to these singlet molecules.

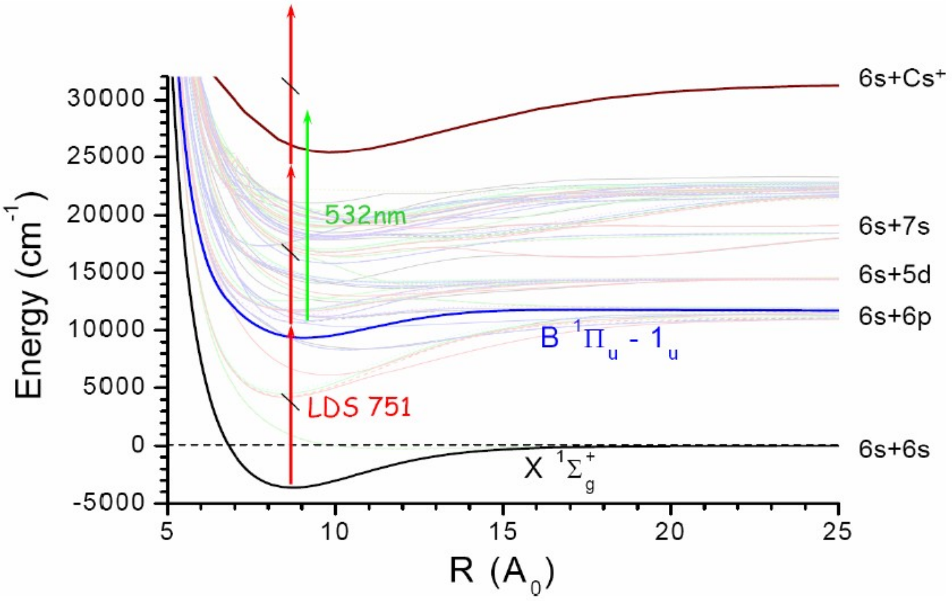

Fig. II.3.1.b.1: Detection of molecules in the $X^1\Sigma_g^+$ singlet state via the $B^1\Pi_u$ state. Two different ionization schemes can be considered: three photon, single frequency detection with narrow-band radiation at 751nm and 1+1 ionization with large-band radiation at 751 and narrow-band radiation at 523 nm.

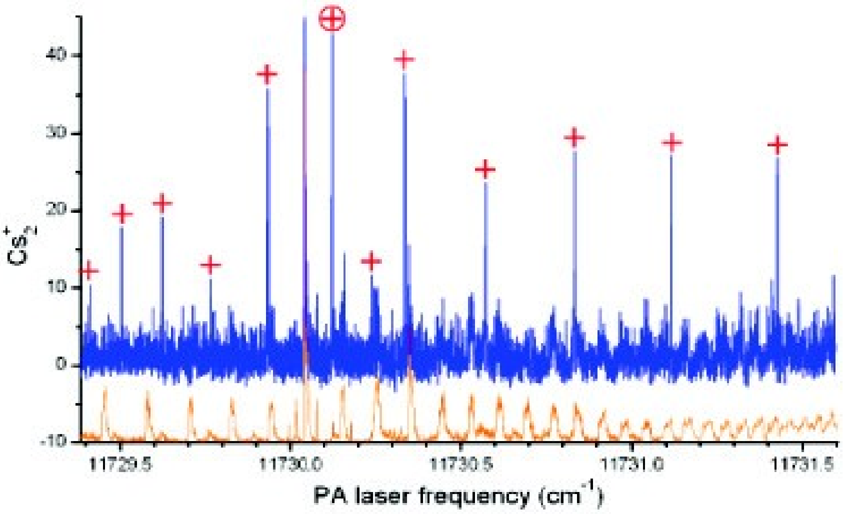

Fig. II.3.1.b.2: Upper trace: Cs_2^+ ion spectrum recorded after scanning the frequency of the PA laser below the 6s + $6p_{3/2}$ dissociation limit, and using the broadband REMPI detection laser with energy around 13000 cm^{-1}. The crosses label the previously unobserved PA lines. Lower trace: Cs_2^+ ion spectrum obtained using the conventional narrow-band REMPI detection, displayed with an offset of 10 ions for clarity. Figure adapted from [Vit09b].

To determine precisely the internal state of these formed molecules, a more conventional REMPI spectrum was acquired using the narrow-band detection described previously with the

(DCM) dye laser (wavelength 627 nm). The PA laser energy was fixed on the most intense line of Fig. II.3.1.b.2 (at 11730.1245 cm1), about 2 cm^{-1} below the 6s + $6p_{3/2}$ asymptote. Then ionization laser frequency was scanned to record the ionization spectrum of the ground state molecules excited through the intermediate $C^1\Pi_u$ state. Since the X–C transitions where known [Wei85, Diem89] the lines, shown in Fig. II.3.1.b.3, were assigned to transitions from ground state vibrational levels. Taking into account the efficiency of the detection the ion signal corresponds to a cumulative formation rate for the v_X <10 molecules close to 10^6 per second.

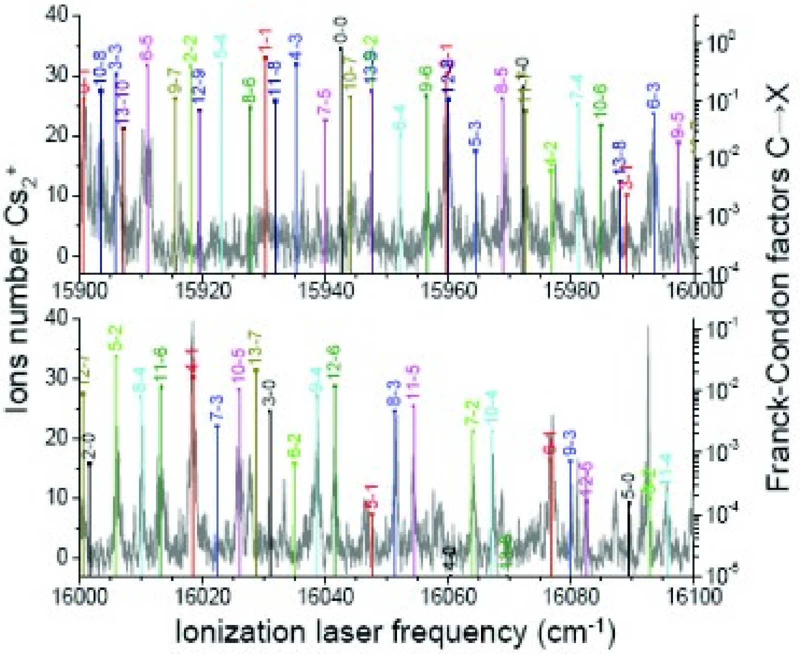

Fig. II.3.1.b.3: Cs^2_+ion count (left vertical axis) resulting from a narrow-band REMPI detection (frequency 627 nm). The PA laser energy is fixed at 11730.1245 cm^{-1} corresponding to the position of the most intense line marked with a circled cross in Fig. II.3.1.b.2. Transition labels v_C–v_X are extracted from computed Franck–Condon factors (right vertical axis) between vibrational levels of the spectroscopically known C and X states. Figure adapted from [Vit09b].

II.3.1.c. Cooling the molecular vibration with the use of shaped broadband lasers

The next challenge was to prepare these molecules in a well-defined vibrational level. This was accomplished by the realization of a novel optical pumping scheme which operating principle is displayed in Fig. II.3.1.a.1. The effect of the broadband radiation is such, that all vibrational levels of the X state can be simultaneously excited towards the B state, with the exception of the fundamental $v_X = 0$ vibrational state. The frequency components of the femtosecond pulse that lied above ~13030 cm^{-1} (energy of the $v_X \rightarrow v_B$ transition) have been removed. Thus the $v_X = 0$ vibrational state cannot be excited and is a dark state of the system. Since all other vibrational levels are repeatedly pumped to the B state and relax to various vibrational levels of the X state, it is expected that a large part of the molecular population will end up been accumulated to the $v_X = 0$ vibrational state, since once relaxed in this state, it is not excited anymore.

Ending up in the $v_X = 0$ vibrational ground state is not the only possibility. It is possible that a series of excitation-relaxation circles transfers the molecules to high vibrational levels that lie outside of the femtosecond spectral range. In this case, the molecules are trapped in those high lying vibrational states and the process leads to heating instead to vibrational cooling of the molecules.

Weather the molecular population will end up to higher or lower lying vibrational levels depends on the relative value of the Franck-Condon coefficients, as long as the dipole transition moment can be considered constant. The Franck-Condon coefficients for the Cs_2 X-B optical pumping transition considered in the initial experiment, were calculated by O.Dulieu and N.Bouloufa, members of the theoretical group of 'Cold Molecules'. This information, gives the possibility to simulate the evolution of the system under the influence of the femtosecond pulse. The result of this simulation is shown in Fig. II.3.1.c.1 along with a plot of the Franck-Condon coefficients in gray scale. The femtosecond laser spectra shown in the inlet up and to the right does not excite the transitions corresponding to the hatched area. The example of the excitation of the v_X=5 state is shown with the red arrow. The most possible final state after the broadband excitation (corresponding to larger Franck-Condon factor) is to the v_B = 1 state an for the relaxation step, the most possible state is the fundamental v_X = 0. Relaxation to a higher lying vibrational level is possible, but the corresponding probability is smaller.

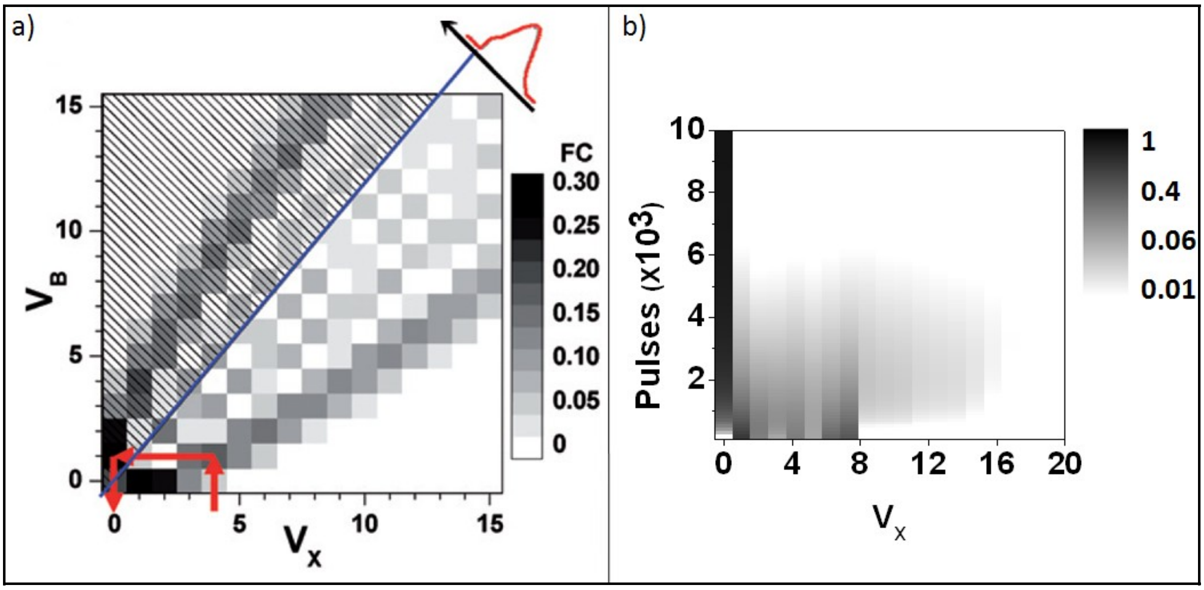

Fig. II.3.1.c.1: Simulation of the optical pumping process (b) with the use of the the Franck-Condon coefficients shown in (a). The red arrows indicate the most probable evolution of the molecular population initially lying in a given vibrational level, for example the v_X = 4. The relative probability of excitation or relaxation to a particular vibrational level is given by the Frank-Condon factors shown in gray scale. Figure adapted from [Vit08c].

The result is shown in the part (b) where the evolution of the system is plotted as a function of the number of pulses. The evolution of the molecular population is calculated as follows. The original population is extracted by the analysis of the spectrum in Fig. II.3.1.b.3, and can be used as an initial situation for this study. However, it is not necessary since to know the precise distribution of the molecular population initially, since the large number of excitation-relaxation circles redistributes molecular population in such a way, that the final distribution does not depend on the initial one, as long as all the initially populated states lye within the range of the femtosecond laser. This is the case here since Cs_2 molecules are populating levels with vx = 1-10. The number corresponding to the initial population of one vibrational level is multiplied to the laser power and the Franck-Condon coefficient which corresponds to transitions towards all exited states. The process is repeated for all initial states and this way the population distribution in the exited state is obtained. Then, the population after relaxation is calculated with the same way, only that here the laser power does not get inserted to the calculation. As we see, a large part of the total molecular population which corresponds to ~69% is pumped to the the ground vibrational level.

The experimental demonstration of vibrational cooling consists in the comparison of REMPI spectra of molecules that have been radiated with the femtosecond laser and of molecules that have not. This is shown in Fig. II.3.1.c.2 while the scan is now focused to an area from ~15900 to 16050 cm^{-1} to detect transitions from the v_X=0 state. We see that the femtosecond laser modifies dramatically the molecular population distribution as displayed by the two REMPI spectra. The resonance lines corresponding to the transition $v_X = 0 \rightarrow v_B = 0–3$, mostly absent in the initial spectrum, are now very strong. Their broadening corresponds to the saturation of the resonance in the REMPI process. The intensity of the lines indicates a very efficient transfer of the molecules in the lowest vibrational level, meaning a vibrational laser-cooling of the molecules. Taking into account the efficiency of the detection (<10%), the detected ion signal corresponds to about one thousand molecules in the $v_X = 0$ level, corresponding to a flux of $v_X = 0$ molecules of a few 10^5 per second. Fig. II.3.1.c.3 shows the time evolution of the population in the different vibrational levels. We see that for a power of ~100 mW the transfer of population in the $v_X = 0$ level is almost saturated after the application of 10000 pulses, which requires one hundred microseconds.

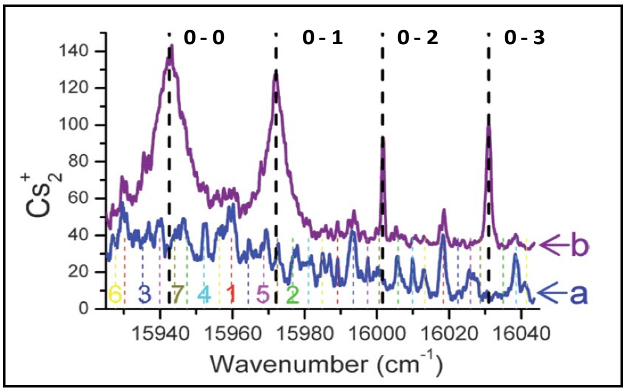

Fig. II.3.1.c.2: Original data set for the demonstration of vibrational cooling. The presence of the shaped femtosecond radiation results to the observation of strong lines corresponding to transitions from the ground vibrational level (b-purple line) which were absent in the spectrum acquired without its presence (a-blue line). The colored numbered lines indicate the position of transitions corresponding to excitation from different initial vibrational levels. Figure adapted from [Vit08c].

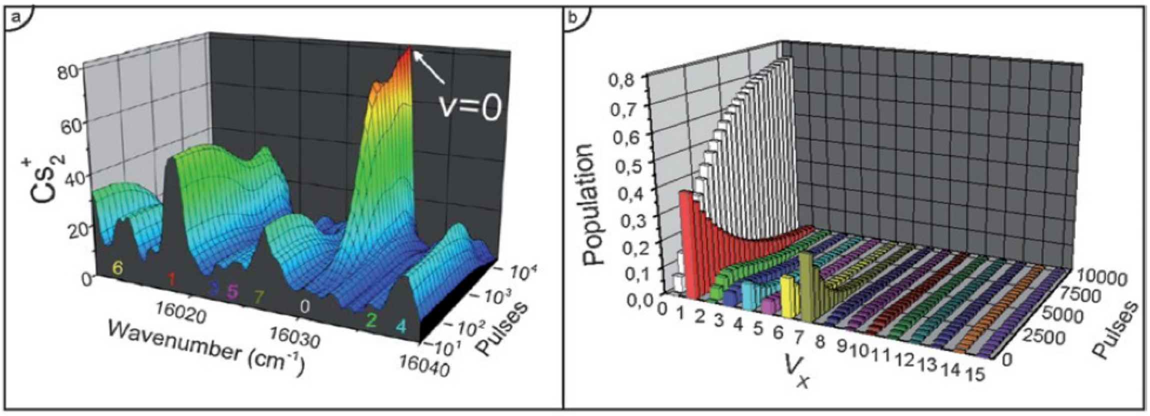

Fig. II.3.1.c.3: Temporal evolution of the population transfer. (a) Compilation of experimental spectrum for different durations of the femtosecond laser (number of pulses). (b) Simulation of the vibrational laser cooling. Figure adapted from [Vit08c].

II.3.2. Experimental set-up

In this paragraph, I describe the experimental set-up, with an emphasis in the laser set-up, since the MOT is very close to the ones described in the first part of this thesis. However, I give its general characteristic alongside with the description of the photoassociation process, before advancing to the description of shaped femtosecond laser and the ionization detection used in the experiment.

II.3.2.a. Photoassociation in the MOT

The magneto-optical trap is provided by six, circularly polarized trapping beams provided by a diode laser (SDL 5422 H1), injected by a DBR diode laser (DBR SDL 5702 H1) frequency locked in the D2 Cs line (see Introduction Part I of this thesis), and have total power of ~40 mW in ~5 mm diameter beams. The repumper radiation is provided by an DBR diode laser (DBR SDL 5712 H1) and is inserted in the MOT region be being overlapped with two trapping beams. The magnetic field gradient is provided by a set of coils in the anti-Helmholtz configuration which are fed by a current of 10 Amp and deliver a magnetic field gradient ~15 Gauss/cm. The stray magnetic fields are compensated with the use of six, low current coils in a similar manner as the MOTs described in the first part of this thesis. This MOT is continuously loaded by Cs vapor in ambient temperature (as the MOT 1 in the first part of this thesis) and traps $\sim 10^7$ atoms in densities of maximum $\sim 10^{11}$ at/cm^3, in temperatures in the order of 150 μK.

Photoassociation is performed in the MOT with the radiation available by a cw Titanium:Sapphire laser (Coherent Ti :Sa, Ring 899) pumped by an Ar^+ laser (Power ~12W). The Titanium:Sapphire radiation is passed through an AOM and reaches the MOT region with an intensity of up to 300 W/cm^2. It has a spectral bandwidth smaller than a MHz while it can be tuned in a range between 700 to 1100 nm. The photoassociation radiation is occasionally provided by a DFB (Toptica) 100 mW diode as well.

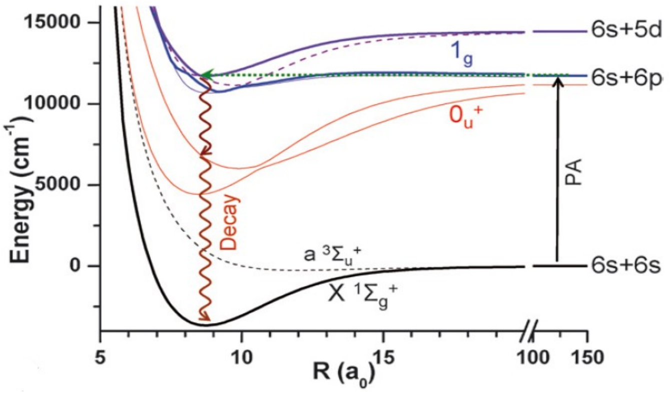

Fig. II.3.2.a.1: Electronic molecular states of the cesium dimer, converging towards the dissociation limits 6s + 6s, 6s + 6p, and 6s + 5d. Photoassociation of cold atoms and formation of cold molecules.

The electronically excited molecules created by photoassociation have a short lifetime of a few tens of nanoseconds due to spontaneous emission. Most often they decay back to a pair of ‘‘hot’’ atoms (i.e. with a large relative kinetic energy). In the cases were photoassociation leads to the formation of stable molecules, as described in the previous chapter, these are available for studies for ~10 ms before they fall out of the detection region. In Fig. II.3.2.a.1 we see the fixed photoassociation scheme that was used for the vibrational cooling experiments. The Titanium:Sapphire laser is red-detuned by roughly 2 cm^{-1} with respect to the $6s \rightarrow 6p_{3/2}$ atomic transition, resonant with an excited molecular level. The PA laser excites the atom pair into a bound level of the lowest ($6s + 6p_{3/2}$)

long-range potential curve which is coupled at short distances to the lowest (6s + $6d_{5/2}$) potential curve, through several avoided crossings induced by spin–orbit interaction (situation similar to that of Fig. I.1.12). The ground-state molecules, $X^1\Sigma_g^+$, are formed in a cascading spontaneous emission via the 0_u^+ potentials yielding to the production of nearly 10^6 molecules per second. This is the photoassociation scheme used for most of the experiments reported in this part of my thesis. However, when different photoassociation schemes are used they will be analyzed in the corresponding chapter.

II.3.2.b. Shaped femtosecond laser for optical pumping

The broadband radiation used for the optical pumping and the vibrational cooling of Cs dimers was made available by a Tsunami laser of Spectra Physics. This laser is pumped by a 10 W, 532 nm CW “Millenia” laser, and is able to deliver 80 fs pulses in a repetition rate of 80 MHz and with a total power of up to 2 W. The laser wavelength can be tuned in a range from 700 to 1000 nm. The laser is combined to a home made 'pulse picker' which offers the possibility to control the number of pulses applied in the cold molecules. The pulse picker is consisted by an AOM controlled by a 2 W RF radio-frequency generator which delivers 50-90 MHz radio-frequency and which can be turned off rapidly (faster than 5 ns). The radio-frequency generator, developed by Alain Richard of the electronic support team, is triggered by a TTL generator which is synchronized with the femtosecond laser with the use of a fast photodiode (Thorlabs DET 10A). The pulse picking system was useful for the characterization of the vibrational cooling technique, but is not necessary for its realization, since control of the number of applied pulses does not have to be very strict and it can be controlled by a synchronized shutter or simply an AOM.

The shaping on the femtosecond radiation is realized with the use of a 4-f line which is schematically represented in Fig. II.3.2.b.1 [Mon05]. The femtosecond radiation with central wavelength λ_0 and bandwidth $\Delta\lambda_L$ is guided to a 1800 Grooves/mm Spectrogon optical grating. There, the different frequency components are dispersed in an angle equal to

$$\Delta\theta_d = \frac{\Delta\lambda_L}{d\cos(\theta_d)} \tag{3.1}$$

where d is the grating step in meters, and θ_d the reflection angle of the central wavelength λ_0, with respect to a direction vertical to the grating's surface. The laser is then passed through a 500 mm cylindrical lens which collimates the radiation to a fixed spacial width, which is simply

$$\Delta L = f\tan(\Delta\theta_d) \tag{3.2}$$

The cylindrical lens width is three times larger than this spacial width, so that we can say that less than 0.2% of laser power escapes from the borders of the lens.

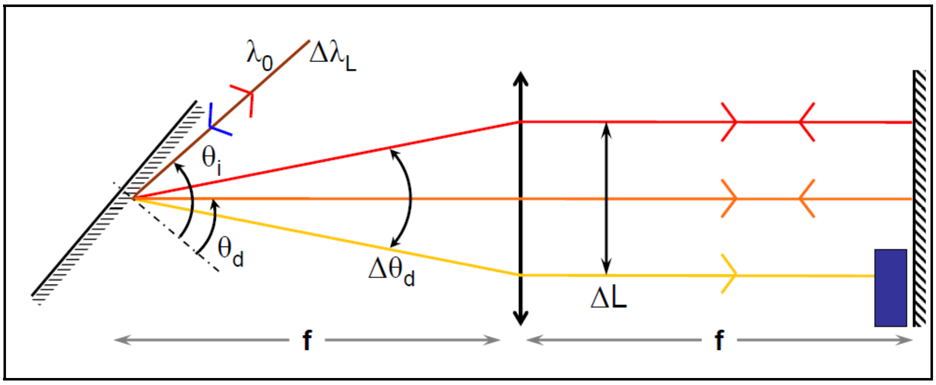

Fig. II.3.2.b.1: Schematic representation of the 4-f line used for the shaping of the femtosecond pulses.

The distance of the cylindrical lens to the grating is equal to its focal length *f*. In an equal distance after the cylindrical lens we have the Fourier plane of the system in which the spectral components of the femtosecond radiation are spatially separated in Gaussian spots of size

$$\Delta X = \frac{2\ln(2)\lambda_0 f \cos(\theta_i)}{\pi \Delta x \cos(\theta_d)} \tag{3.3}$$

where θ_i the reflection angle of the frequency component *i* and Δx the FWHM of the intensity profile of the incoming beam [Dan89]. In the Fourier plane we place a mirror, which reflects the femtosecond radiation in the same horizontal but slightly different vertical direction, so that its frequency components are spatially recombined but the beam exits the 4-f line due to the vertical displacements. In the Fourier plane the frequency components are separated and they can be selected with the maximum accuracy (resolution). There we place a dark screen (black paper) in a micro-metric translation stage and we cut a part of the beam, while the resulting spectrum is monitored in real time by an Avantes AvaSpec-128 Fiber Optic spectrometer.

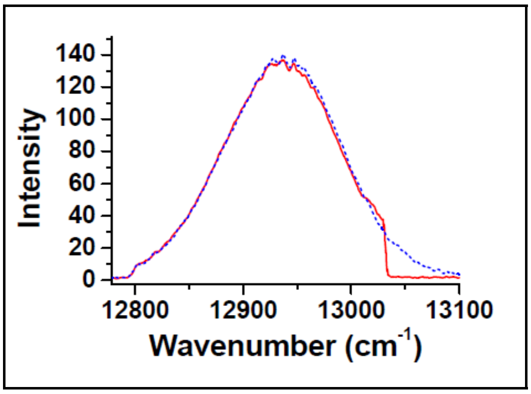

Fig. II.3.2.b.2: Result of the femtosecond radiation shaping with the use of the 4-f line. In blue, we see the initial, unshaped radiation and in red the shaped radiation in the exit of the 4-f line.

The result is shown in Fig. II.3.2.b.2, where the inserted and the resulting femtosecond pulses are compared. By moving the micro-metric translation stage and simultaneously observing the femtosecond laser spectra obtained in the exit of the 4-f, we remove frequencies above ~13030 cm^{-1}, while the central wavelength is ~12950 cm-^{1}. The method provides with the possibility to remove spectral components of the laser radiation with an accuracy of less than 0.8 cm^{-1}, which, as we will see in following chapters, is more than enough for the realization of the experiment.

II.3.2.c. Dye lasers and ionization detection

The detection of the molecules formed by photoassociation is done by ionization via various REMPI schemes. In order to calculate the efficiency of the ionization process, we have to take into consideration the spacial overlap of the photoassociation laser with the atoms, the molecule's free fall (they are not trapped) and the overlap with the ionization laser. As we find in [Comp99], for a position of the ionization laser displaced by the MOT by *d* and *h* (horizontally and vertically), for a time *t* we have for the number of produced ions N_{ions}

$$N_{ions}(t) = \eta R_{mol} N_{at}^{PA} \int_0^t \frac{\omega_{ion}^2/4}{\sigma_r^2 + \sigma_\upsilon^2 (t-t')^2} e^{\frac{d^2 + [h^2 - \frac{1}{2} g(t-t')^2]^2}{2[\sigma_r^2 + \sigma_\upsilon^2 (t-t')^2]}} dt' \tag{3.4}$$

with

$$\sigma_r = \sqrt{\frac{1}{2}\frac{(\sigma_r^{at})^2\omega_{PA}^2}{2(\sigma_r^{at})^2+\omega_{PA}^2}+\frac{\omega_{ion}^2}{4}} \tag{3.5}$$

where ω_{PA} and ω_{ion} are the waists of the photoassociation and the ionization lasers respectively and with velocity distribution of the molecular cloud

$$\sigma_\upsilon = \sqrt{k_B T_{mol} / m_{Cs_2}} \tag{3.6}$$

The terms R_{mol} and N_{at}^{PA} correspond to the molecule formation rate and to the number of atoms in the zone which overlaps with the photoassociation laser. The factor η corresponds at the efficiency of the Multi-Channel Plate (MCP) ions detector multiplied with the efficiency of the ionization process

$$\eta = \eta_{MCP}\,\eta_{ion} \tag{3.7}$$

where η_{ion} is the efficiency of the ionization process. Our experimental parameters are: σ = 300 μm, ω_{PA} ~ 170 μm and ω_{ion} ~ 300 μm the size of the photoassociation and ionization lasers, while the time for which detection of molecules is possible is between 1 and 16 ms, with the optimal timing to be in t ~ 10 ms. With the detection laser crossing the MOT approximately at a distance of 200 μm from its center the integral 1.16 gives 0.15, which means that only 15% of the molecules are in the detection zone. If we consider that 30% of the formed ion reach the MCP detector we take η_{MCP} ~0.27 and for the total detection efficiency something more than 4%. That means that when 100 ions are detected, the total number of molecules formed in the MOT is around 2500.

The MCP detector is mounted and power supplied as shown in Fig. II.3.2.c.1. Our MCP detector is consisted of two parallel MCR arrays which are power supplied with a total voltage of -1700 V in the front side of the MCP, with -810 V in the middle and with -81 V in the back. The circuit is placed in a Cooper box in order to minimize the external noises, while the connecting cable length is minimized in order to increase the signal to noise ratio.

The signal is amplified by an RF amplifier and is inserted to one of the eight channels of an 1GHz LeCroy Waverunner 104xi digital oscilloscope. The digital oscilloscope is also connected to an Ansgstrom WS8 optical fiber lambdameter. The lambda meter detects the wavelength of either the photoassociation or the ionization laser. The digital oscilloscope is equipped with LabVIEW, and a software permits the simultaneous registration of the ion signal and the corresponding wavelength. By scanning the photoassociation or the ionization laser we can acquire photoassociation or ionization spectra of up to one million points (measurements).

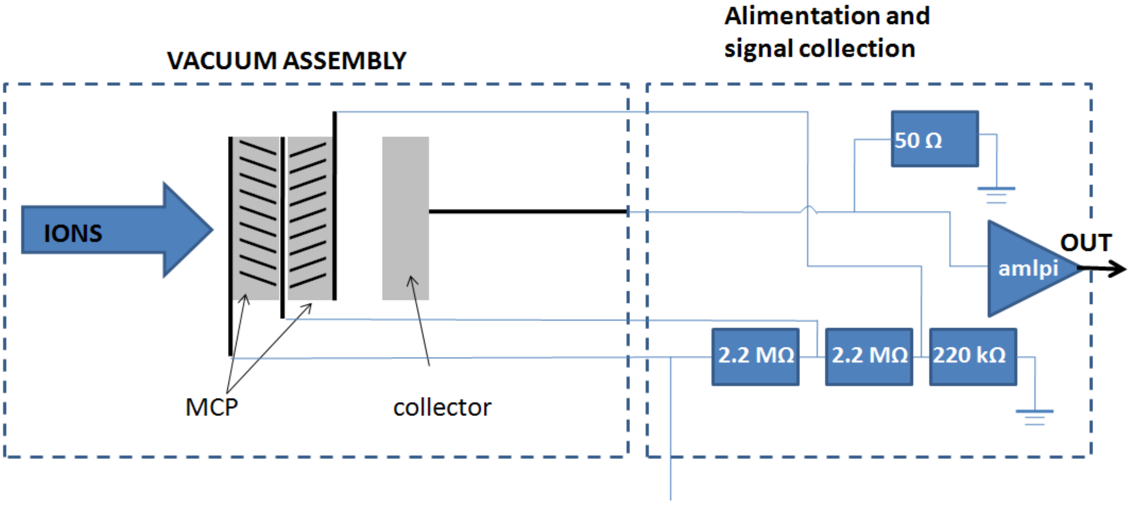

Fig. II.3.2.c.1: Set up of the MCP ion detector. On the left, the under-vacuum assembly which is consisted of the two MCP stages and the collector. On the right, the power supply diagram. After collected by the collector, the signal is amplified before being read in the output.

The laser used for the molecule ionization is a Nd:Yag pumped, home made dye laser which delivers pulses of ~10 ns with a spectral width of ~3 GHz. The wavelength can be tuned in a large range of values, depending on the choice of the laser dye used. The usual detection frequencies are ~16000 cm^{-1}, which corresponds to the DCM dye (wavelength range 14500 – 16450 cm^{-1}). In this wavelength range we have the possibility to detect both the $X^1\Sigma_g^+$ singlet and the $a^3\Sigma_u^+$ triplet state molecules, as shown in Fig. II.3.2.c.2.

For the case of the $X^1\Sigma_g^+$ singlet state, detection is done via the $C^1\Pi_u$ state which is shown with the blue line in part (a). This is a standard ionization scheme reported in [Raa82]. The states shown with the dotted green and red lines perturb the $C^1\Pi_u$ state, with result for the states with vibration v > 12 to be pre-dissociated and not to be detected by this ionization scheme. As far as the $a^3\Sigma_u^+$ triplet state, which is shown in part (b), detection can take place by both the 0_g and 1_g states. By this detection scheme, three major photoassociation lines are observed in a detuning of -2.1, -6.1 and -6.4 cm^{-1} from the $6s+6p_{3/2}$ dissociation limit. Due to the high number of molecules produced by these photoassociation lines, they are called 'giant lines' [Vata99]. The possibility to detect both the $X^1\Sigma_g^+$ singlet and the $a^3\Sigma_u^+$ triplet states with the same dye is very useful. The giant rates give an easy way to produce a large molecular signal, with the position of the photoassociation and the detection lasers can be experimentally optimized. Then the detection can switch to the $X^1\Sigma_g^+$ singlet state, which is much more difficult to detect since the signal is smaller.

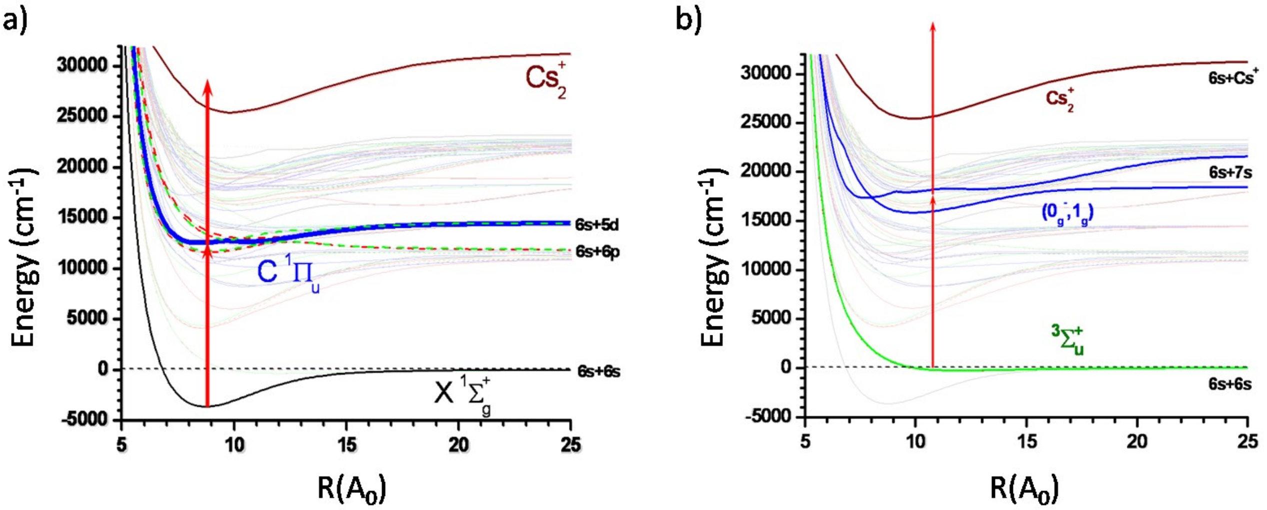

Fig. II.3.2.c.2: Usual ionization scheme for the detection of the Cs dimers in the $X^1\Sigma_g^+$ singlet (a) and the $a^3\Sigma_u^+$ triplet states (b) in ~16000 cm^{-1} and ~14000 cm^{-1} respectively.

Finally, in Fig. II.3.2.c.3 we show the modification that permitted the generation of broadband laser radiation by a different dye laser (Continuum dye laser). Originally, the laser cavity contains a series of four anamorphic prisms and a 2400 lines/mm optical grating as shown in part (a). The grating permits the selection of a part of the laser's bandwidth and the laser radiation generated this way has a spectral bandwidth of 0.2 cm^{-1}. After the modification, which consisted of removing the prisms and the grating and substituting them by a single prism (and a mirror), the laser bandwidth is increased to ~25cm^{-1}.

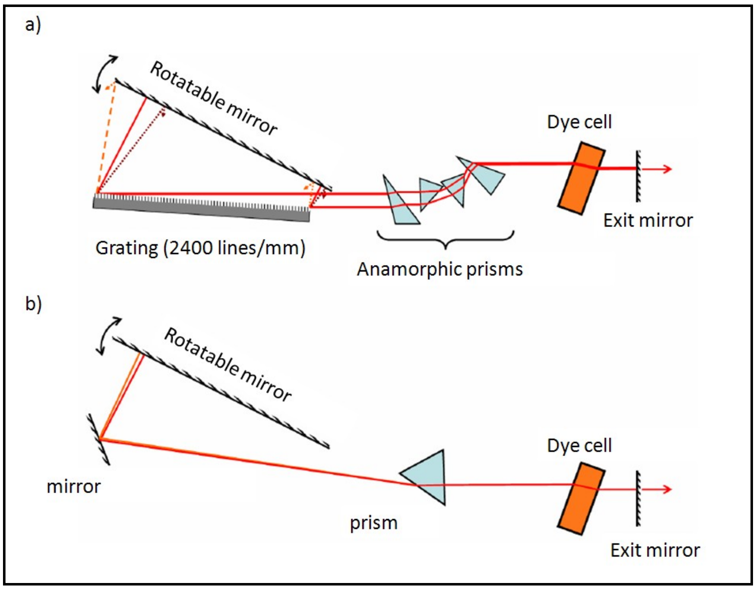

Fig. II.3.2.c.3: Modification in the Continuum dye laser cavity for broadband detection of molecules. In (a) optical cavity before and in (b) after the modification.

II.3.3. Conclusion

In this chapter I tried, on the one hand, to describe the vibrational cooling technique and the line of experiments that lead to its demonstration, and on the other, to present the experimental set up usually used in the Cold Molecule laboratory, with economy and clarity. After a small introduction and a summary of the most important cold molecule technique in the previous chapters, I describe the technique, in the study of which, this part of my thesis is reporting. This is done with an emphasis on the operating principle in which the technique is based, so that the various extensions and generalizations can be more easily discussed. Then, I describe the spectroscopic studies that lead to the preparation of tightly bound Cs dimers and the demonstration of the vibrational cooling technique in Laboratoire Aimé Cotton. Finally, I describe the basic components of the experimental set up used in the initial experiment and in the following of this study.

CHAPTER II4: MOLECULAR POPULATION TRANSFER TO A GIVEN VIBRATIONAL STATE

II.4. MOLECULAR POPULATION TRANSFER TO A GIVEN VIBRATIONAL STATE

In this chapter I present the first generalization of the previously described vibrational cooling technique. Here, we consider as the level in which the molecular population has to be accumulated (so called 'target' level, or 'target' state), not only the ground vibrational level but an arbitrary one. In the first, introductory paragraph, I explain how such a generalization is possible, and why does it lead to the demand for a more complicated pulse shaping than the one described in the previous chapter. Then I present the device which enabled this shaping, the Spatial Light Modulator. In the following paragraph, I describe the experiment of the demonstration of molecular population transfer to a given, pre-selected vibrational state, and in the following, an additional, optimized method for molecular population transfer. Finally, I discuss the potential of the application of the optimized molecular population method to laser cooling of molecules and I conclude.

II.4.1. Introduction

In the previous chapter, we discussed how the vibrational cooling technique manages to transfer almost all molecular population to the ground vibrational level. This is done with the use of a simple shaping, which removed all frequencies that could excite this population from this state by the femtosecond pulse. In the same time, the broad-band laser radiation excites simultaneously all other vibrational levels leading to accumulation of the molecular population in the $v_X = 0$ state, which now is a dark state of the system. This means that, if we choose to remove from the femtosecond pulse the frequencies which correspond to the excitation of a different vibrational level of the X electronically ground state, the optical pumping can result to accumulation of the molecular population in this vibrational level. In other words, we can choose the 'target' state of our molecular population transfer method, by removing all frequency components that excite it from the femtosecond pulse.

However, for the population transfer to be successful, all other vibrational levels of the X electronic state have to be addressed. Since our target is to transfer molecular population in a single pre-selected vibrational level, only this level can be a dark state of the system. If the laser shaping results to the removal of all the resonant frequencies of another vibrational level, molecular population will be trapped in this additional dark state and will not be transferred in the desired level. In Fig. II.4.1.1, we see that the frequencies that correspond to the excitation of a level different than the $v_X = 0$, are not placed in the edge of the femtosecond spectrum as was the case for the $v_X = 0$. In the particular example, I show the positions of the frequency components that can excite the $v_X = 0$ and 1 level. It is clear that, it is not possible to remove uniquely the frequencies of any other vibrational level with the simple shaping described in the previous chapter.

Thus, the realization of the experiment was made with the use of a more advanced shaping technique which involves the use of a Spatial Light Modulator (SLM). The experiment reported in [Sof09] was made into collaboration with of the group FEMPTO of Laboratoire Collisions Agrégats Réactivité - UMR5589 and in particular with Béatrice Chatel and Sébastien Weber. The group is specialized in femtosecond pulse shaping and they have transferred their SLM to LAC in order for the experiment to be realized.

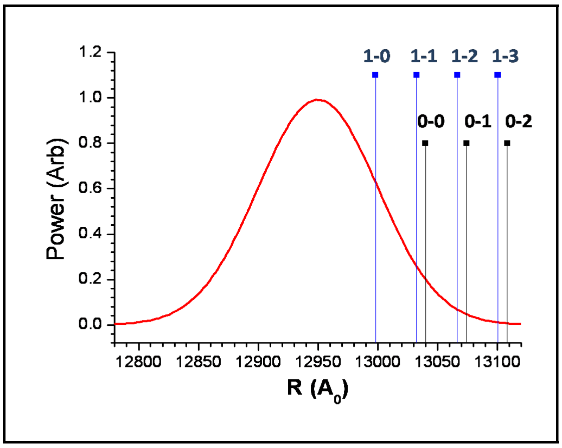

Fig. II.4.1.1: The energy components that excite transitions from the $v_X = 0$ and 1 levels, plotted along with the pulse used in the vibrational cooling technique.

II.4.2. The Spacial Light Modulator

The femtosecond pulse shaping was achieved with the use of high resolution pulse shaper [Mon04] which consists of a dual Liquid Crystal Spatial Light Modulator (LC-SLM) placed in the Fourier plane a zero dispersion line. The operating principle of the pulse shaper is shown in Fig. II.4.2.1. The incoming laser field E_I is polarized along the x axis, z being the propagation axis. The Liquid-Crystals are rod-like molecules that have a variable birefringence. They tend to align themselves with an applied electric field. In this set-up, the Liquid-Crystal molecules are aligned along axis at 45 degrees (for the first SLM) and −45 degrees (for the second SLM) in the x-y plane.

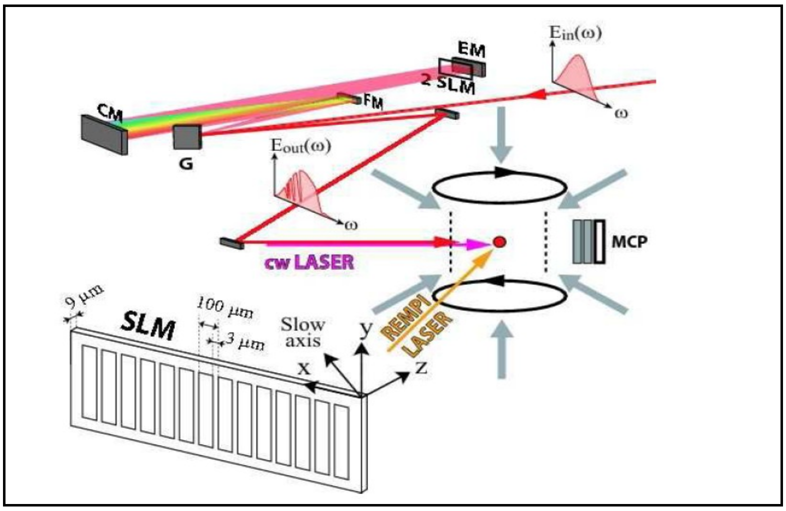

Fig. II.4.2.1: Experimental setup for the pulse shaper and the cold molecule production and detection. Upper part: folded zero dispersion line . The beam is dispersed by the grating G and then each spectral component is spatially separated and focalized by the cylindrical mirror CM in the Fourier plane. FM is a plane mirror. Both Spatial Light Modulator (SLM, detailed in the lower-left side of the figure) are placed at the Fourier plane. An end mirror EM is placed just after the SLM and the beam goes twice through the folded line. The shaped light is then send to the cold molecular cloud which is created by photoassociation in the MOT.

In the present experiment, amplitude-only modulation is used. The Liquid-Crystal (SLMS640/12) produced by Jenoptik company, possesses 640 pixels and has been described in ref [Sto01] (stripes of 97 μm×10mm separated by gaps of 3 μm). The birefringence of each pixel is controlled by a voltage with a dynamic range of 12 bits. The regions of Liquid-Crystal between the patterned electrodes cannot be controlled and are referred to as gaps. In these gap regions the Liquid-Crystals behave in a first approximation as though there were zero applied voltage so that the filter for the gap regions is assumed to be constant across the array. This limits the off-on ratio (degree of extinction) of theoretically 20 dB (99% intensity extinction). However, probably due to imperfect experimental polarization, one has measured, using an OCEAN Optics HR 4000 spectrometer, only an off-on ratio of 3% of the light intensity in the worse case. In the simulation of the experiment this 3% conservative value is the reference.

The incoming beam is first dispersed by a gold-coated grating with 2000 lines/mm and then focused in the horizontal plane by a cylindrical mirror with a focal length of 600mm in the Fourier plane. The two Liquid-Crystal- SLMs (64 mm width) are placed in the Fourier plane just behind the end mirror. This set-up provides with an average resolution of 0.06 nm/pixel corresponding to a spectral width of 38 nm. This spectral width is large enough to transmit the spectral pedestal width of our laser source (Full Width at Half Maximum (FWHM) of 10 nm). The beam FWHM in the Fourier plane (57 μm, corresponding to an input beam diameter of 2.3mm) is roughly set to the width of a pixel, and therefore maximizes the resolution of the pulse shaper. The overall transmission in intensity of all the device is currently of 60%, mainly limited by the grating’s efficiency. This is enough in the present experiment since one uses an average laser power of only few milliwatts focused on the molecular cloud with a waist of nearly 500 μm. A similar laser power of 3 mW, corresponding to an intensity of 700 mW/cm^2, is used in the simulations.

II.4.3. Simulation of the vibrational cooling method

The experiments performed to study molecular population transfer into a given vibrational state, which are described in this chapter, where prepared with the use of simulations of the optical pumping process. These simulations helped to conclude to those particular pulses and shapings which optimize population transfer to the desired vibrational level. Those simulations were already used in the earlier stages of the experiment, where population transfer to the state with zero vibration was studied, and they are based to calculations that provided with most of the Potential Energy Curves (PECs) of the Cs molecule, performed by Olivier Dulieu and Nadia Balufa. The evolution of the molecular population, among the various vibrational states of the electronic potentials participating the optical pumping process, is calculated with the use of rate equations for the system molecule-shaped pulse for any shaping of the pulse. The use of rate equations is justified by the small pulse intensities used in the involved experiments, which implies small, if any, contribution of coherence effects in the population final distribution.

Fig. II.4.3.1 shows the optical pumping process, as this is considered in our simulations. It is divided in two steps, the spontaneous emission from excited electronic potential A to the ground electronic potential X, and the femtosecond pulse excitation (absorption) from X to A. The small pulse duration (<100 fs) leads us to neglect the spontaneous emission during the absorption step, as its contribution to the final molecular population distribution is very small. Stimulated emission is also neglected due to the small femtosecond laser intensity. The equations that describe the redistribution of the molecular population among the various vibrational levels are equations 4.1 – 4.4 listed below. A description of the derivation of these equations is given in the Annex, for reasons of continuity.

Emission step:

$$p_{v_X} - p_{v_X}(0) = \frac{1}{\sum_{v_X} \Gamma_{v_{A'} \to v_X}} \sum_{v_A} \Gamma_{v_A \to v_X} p_{v_A}(0) \tag{4.1}$$

$$p_{v_A} = 0 \tag{4.2}$$

Absorption step:

$$p_{v_A} = \sum_{v_X} \Gamma_{v_X \to v_A} p_{v_X}(0) \tag{4.3}$$

$$p_{v_X} = p_{v_X}(0)\left(1 - \sum_{v_A} \Gamma_{v_X \to v_A}\right) \tag{4.4}$$

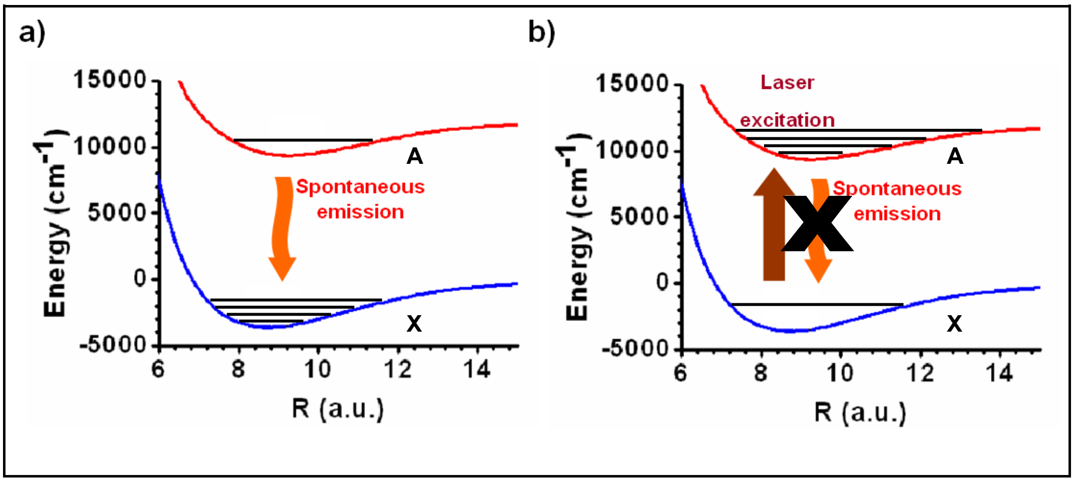

Fig. II.4.3.1: The two physical process with which the rate equations used in the simulations of the vibrational cooling are associated. With X we symbolize the ground and with A the excited state. (a) The conceptually simpler spontaneous emission step, in which molecules relax from a vibrational state of the A potential to all the vibrational states supported by X. (b) The absorption step, in which a state of the X potential is excited towards several vibrational states of the A potential. Both excitation and relaxation occur; however, in our simulations this spontaneous emission step is omitted, see text for details.

With p_{vA}, p_{vX}, we symbolize the population of the vibrational levels v_A and v_X of the excited and the ground electronic potentials respectively. With $\Gamma_{vA \to vX}$ we symbolize the rates with which molecular population is transferred from one vibrational level v_A of the excited electronic potential A to all the vibrational potentials v_X that are supported by X, via the spontaneous emission step. Similarly, with $\Gamma_{vX \to vA}$ we symbolize the molecular population transfer from one vibrational level v_X to all the vibrational levels of v_A that lie inside the excitation spectrum of the femtosecond laser. These rates are proportional to

$$\Gamma_{v_A \to v_X} \propto FC[v_X][v_A](D[v_X][v_A])^2 \omega^3_{A \to X} \tag{4.5}$$

$$\Gamma_{v_A \to v_X} \propto FC[v_X][v_A] D[v_X][v_A]^2 \omega^3_{A \to X} I_{laser}[v_X][v_A] \tag{4.6}$$

where with $FC[v_X][v_A]$ and with $D[v_X][v_A]$ we symbolize the Franck-Condon coefficient and the dipole moment of the associated vibrational transition, while with $\omega_{A \to X}$ the transition frequency.

II.4.4. Molecular population transfer via the creation of dark states

As already explained, accumulation in a given vibrational level comes from the fact that all the frequencies that could excite molecules decaying in this level during the optical pumping process are removed, making it a dark state of the system. The femtosecond laser spectrum needed to realize such dark state is first theoretically calculated, and then implemented using the pulse shaper. In order to predict the best possible laser spectrum, we have modeled the optical pumping with the method described in the previous paragraph. Initially, in each simulation, the molecules are found in the levels $v_X = 1$ to 7, with a distribution measured experimentally in [Vit08c] and corresponding to the spectrum shown in Fig. II.3.1.b.3.

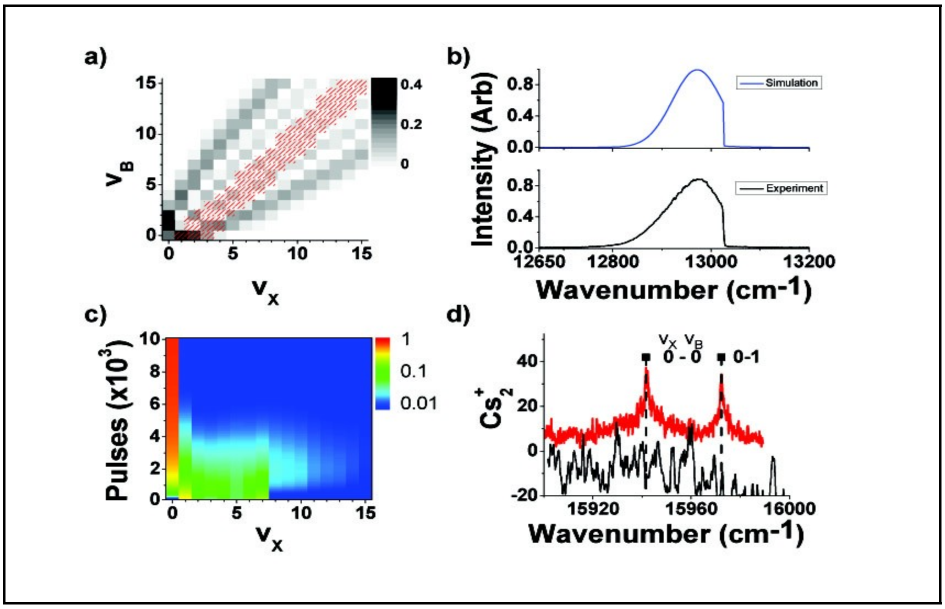

Fig. II.4.4.1: Simulation and experimental results for the transfer in the vibrational ground state. (a) FC coefficients (grey scale) for transition between the X ground state and the B excited state. The hatched (red) area represents the transitions that are excited by the pulse shaped laser intensity, only transitions with laser intensity more than 10% of maximum intensity are shown. (b) The shaped pulse used for the simulation (upper part) and in the experimental one (lower part). (c) Results of the simulation of the vibrational cooling where the (log scale) color level indicates molecular population. The accumulated population in each v_X level is plotted as a function of the number of femtosecond pulses. The femtosecond laser pulses occur every 12.5 ns. After 10^4 pulses the population in the $v_X = 0$ level is 70%. (d) REMPI molecular ion spectrum. With the shaped femtosecond pulses (in red). This is the signature of $v_X = 0$ molecules because only transition from $v_X = 0$ to $v_C = 0$ and $v_C = 1$ are present in the spectrum. The spectrum (in black, with an offset of -20 for clarity) without femtosecond pulses, indicating the presence of molecules in several low vibrational levels, is reported for reference.

Initially, our goal is simply to repeat molecular population transfer to $v_X = 0$ state, in order to study the effect of the non zero extinction ratio of the SLM in the technique's efficiency. Our theoretical prediction finds that the non zero extinction ratio hardly affects the population transfer efficiency. The theoretical (assuming a Gaussian shape and a 3% extinction ratio) as well as the experimentally realized spectrum are presented in Fig. II.4.4.1 b. In order to understand the basics of the optical pumping process we represent (in hatched red) in Fig. II.4.4.1 a, the transitions that can be excited by the pulse shaped laser and (in grey) the Frank-Condon (FC) factors for the transitions between the v_X and the v_B vibrational states. The (grey) Frank-Condon parabola is useful to study the spontaneous decay of an excited molecule whereas the hatched red part is useful to study the laser excitation. As example, let's follow the optical pumping of a molecule initially in the $v_X = 4$ level: its most probable optical pumping walk is first to be excited into $v_B = 1$ (stronger FC factor in the hatched area) then to decay in $v_X = 0$ (stronger FC factor) where no more excitation is possible (no hatched transition). More generally, the result is given by the complete simulation and is shown in Fig. II.4.4.1 c. After the application of 10^4 pulses, 70% of the initial population, spread among several vibrational levels, have been transferred into the $v_X = 0$ level. The remaining 30% of the population is transferred to high vibrational levels that are not affected by the femtosecond laser, because the possible transitions lie out of the range of frequencies available in the laser pulse we use.

The idea of removing the frequencies that correspond to (all) possible excitations of a particular vibrational level, in order to form a dark state, can be applied not only to the $v_X = 0$ level. Fig. II.4.4.2 shows the case where the target vibration state is $v_X = 1$ where we have shaped the pulse by removing any transition frequencies between $v_X = 1$ and B state. The required spectrum and its realization by the pulse shaper are shown on Fig. II.4.4.2 b. Several tests have been performed in order to study the effect of the number of pixels (between 1 and 5) used to make the ”holes”. No substantial difference has been shown on the REMPI signal. In all the experiment two neighboring pixels are usually set to zero. This emphasizes that although our pulse shaper has a high resolution, the molecular transitions are narrow enough to be killed by only one “dark pixel”. The 0.06 nm limited resolution of the pulse shaper does not cause any problem as long as this does not lead to a second ”dark” state in the system, a condition which is easily fulfilled due to the relatively large spectral separation (~ 40 cm^{-1}, corresponding to 2.3 nm at 13000 cm^{-1}) of the lower vibrational levels. In Fig. II.4.4.2 b, the experimental spectrum is recorded by a spectrometer (Ocean optics HR 4000) with a resolution twice less than the pulse shaper's one. The simulation, shown in Fig. II.4.4.2 c, predicts a total transfer of 53% to the $v_X = 1$ level, value which could be increased up to 67% if a perfect off-on ratio is simulated (3% experimentally). Finally, Fig. II.4.4.2 d shows the detected ion spectrum, where frequencies corresponding to $v_X = 1 \rightarrow v_C = 0, 1, 2, 3$ transitions, appear with a strong signal.

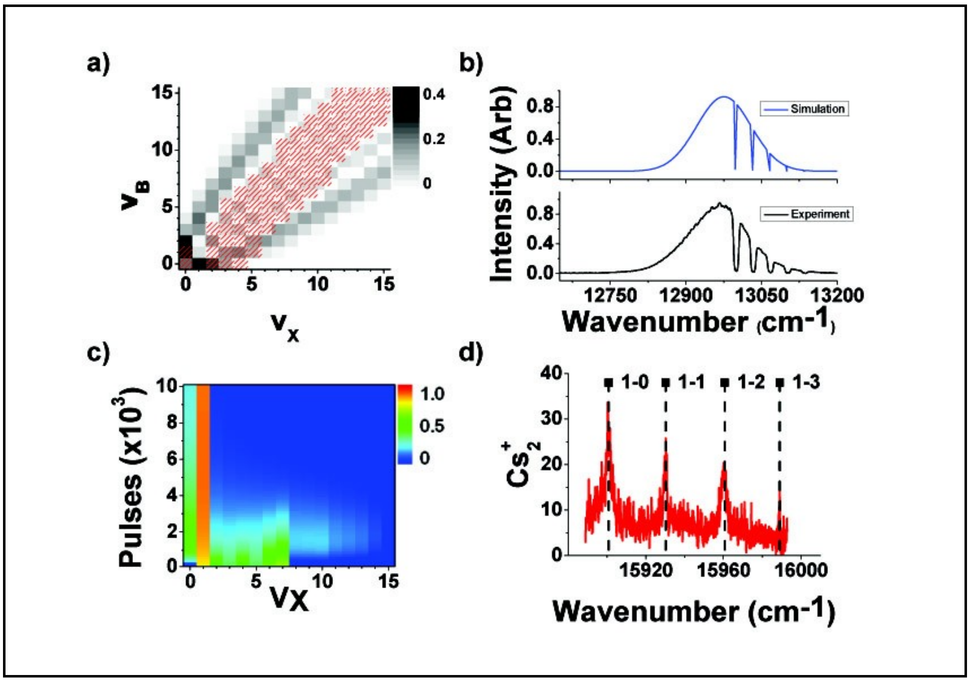

Fig. II.4.4.2: Simulation and experimental results for the transfer in the $v_X = 1$ level. a) FC coefficients (grey) for transition between the X ground state and the B excited state. The hatched (red) area represent transition allowed (i.e. having an intensity higher than 10% of the maximum) by the shaped laser pulse: transitions from $v_X = 1$ level, which is now the ”target” state are completely removed. b) The shaped pulse used for the simulation (upper part) and in the experiment (lower part). c) Results of the simulation of the vibrational cooling. The population of the $v_X = 1$ level after 10^4 pulses is 53%. d) Experimental detection spectrum of molecule (mainly in $v_X = 1$) via two photon REMPI.

The generality of the method is demonstrated in Fig. II.4.4.3, where the case for the v_X= 0,1, 2 and 7 target states are presented. For each chosen target v_X, the ionization spectrum contains mainly lines in positions corresponding to transitions from the selected target state to several excited vibrational levels. In principle, any vibrational level can be chosen as the target state. The obvious limitation lies upon the available laser bandwidth and upon the initial molecular distribution. The laser has to be strong enough in the vicinity of transitions between the initial states and the target one. For the femtosecond laser used here (bandwidth 55 cm−1), $v_X = 7$ is an extreme choice, a fact that is indicated by a lower signal to noise ratio and the existence of v_X = 0, 1 contributions to the signal.

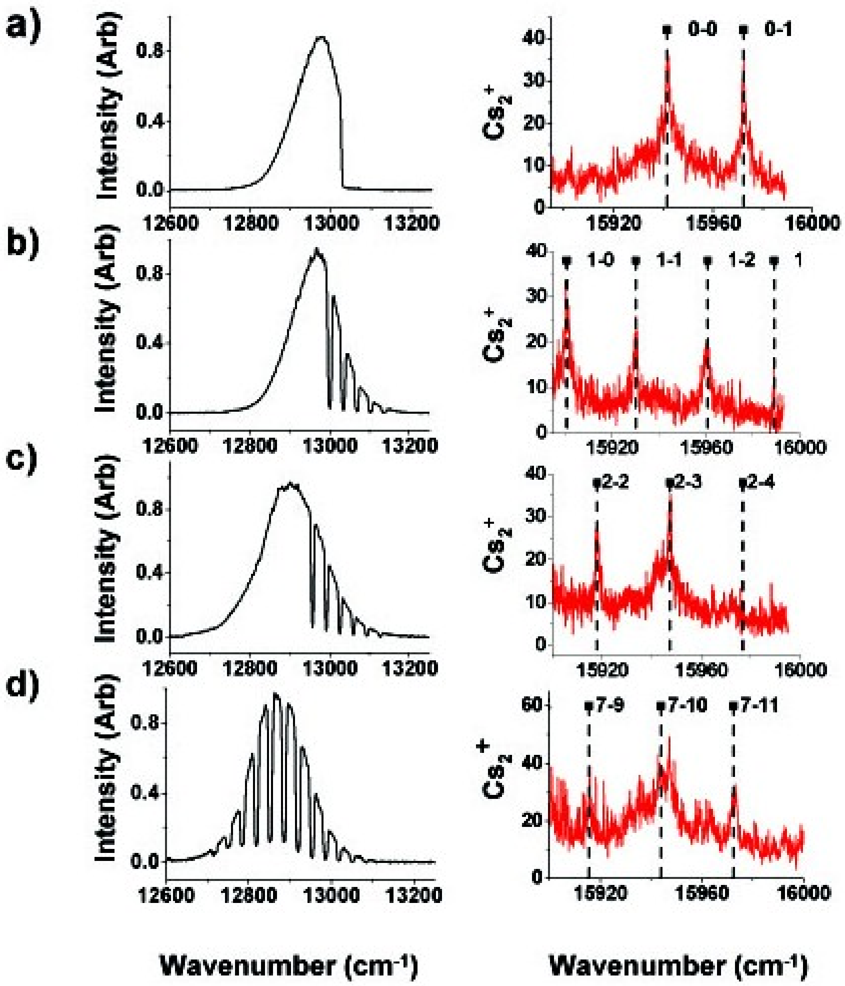

Fig. II.4.4.3: Left part the experimental pulse spectra used to populate the $v_X = 0$ (a), $v_X = 1$ (b), $v_X = 2$ (c) and $v_X = 7$ (d) levels. Right part: the corresponding experimental ionization spectra. Notice that in spectrum (c) a small signal corresponding to molecules in the $v_X = 0$ remains, and that in spectrum (d) molecules in the $v_X = 1$ level also remain.

II.4.5. Improved optical pumping via optimized pulses

As already mentioned, the creation of 'holes' into the femtosecond spectrum which correspond to transitions from the 'target' vibrational state, is not the unique approach in order to achieve molecular population transfer. Moreover, the pulse shaping can be optimized in order for the molecular population transfer to be improved. The importance of such an improved optical pumping method will be discussed in the next paragraph, where the perspectives for laser cooling of molecules based on the current work, are going to be discussed.

It has been demonstrated that population can be transferred to a desired vibrational level when the frequencies that connect it to any of the excited states used in the optical pumping scheme are removed from the femtosecond pulse. However, the efficiency of such optical pumping process depends on the Frank-Condon factor (i.e. of the relative position of the electronically excited potential with respect to the ground-state one), on the bandwidth of the femtosecond pulse used and on the extinction ratio of the pulse shaper. In this paragraph a more complex pulse shaping will be discussed, which could lead to a more efficient vibrational cooling, in terms of number of molecules finally transferred to the desired state, than the one just described.

As a particular example we will study the case of a ”comb” of selected laser frequencies, chosen in such a way to induce only the transition required to produce efficient optical pumping from the initially populated levels to the target level. Several approaches exist for the choice of such an optimized spectrum but of course, the target state has to remain a dark state and all frequencies resonant to it must be removed. A possible criterion for the choice of the allowed excited states is that their Franck-Condon coefficients with the target vibrational level should be as high as possible. However, in our case, due to the limited laser bandwidth, it is more important to limit the transfer of population to high vibrational levels that are no more affected by the femtosecond laser. Therefore, one has chosen to favor excitation in levels that correspond to the ”lower branch” of the FC parabola. With such a choice, once a v_X molecule is excited in this ”lower branch”, it will decay either in the same v_X level or in the ”upper branch” of the FC parabola i.e. in lower vibrational levels than its initial value.

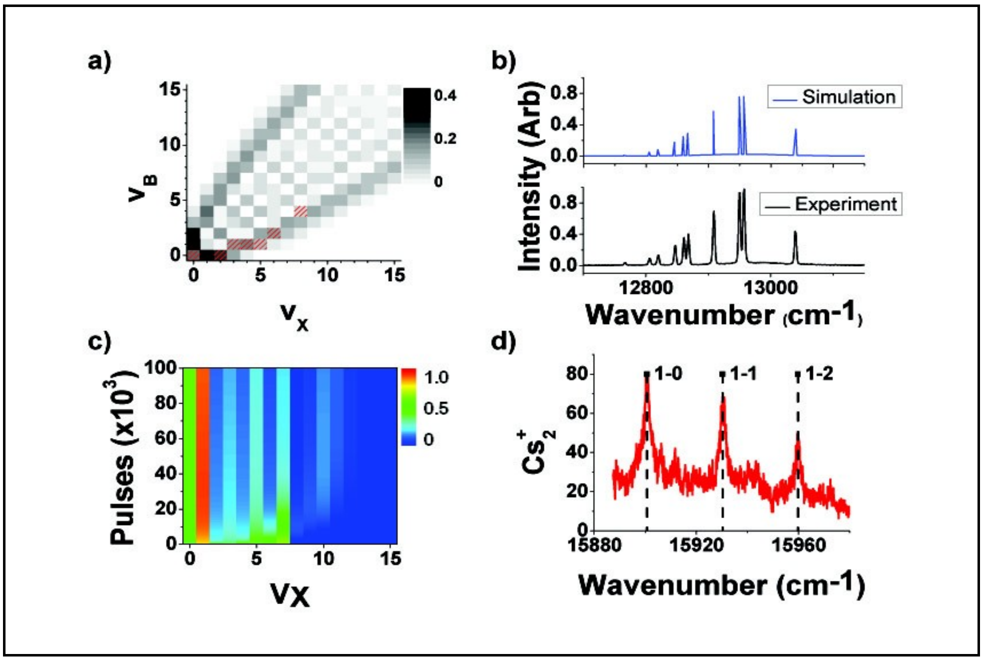

Fig. II.4.5.1: Population transfer in the vX = 1 level with an improved shaping. a) FC coefficients (grey) for transition between the X ground state and the B excited state. The hatched (red) area represents transitions allowed by the shaped laser pulse: i.e. between v_X non-equal to 1 to v_B levels that decay in levels $v'_X \leq v_X$. b) The shaped pulse used for the simulation (upper part) and in the experiment (lower part). c) Results of the simulation of the vibrational cooling. The population of the $v_X = 1$ level after 10^5 pulses is 57% value which could be increased up to 98% if a perfect off-on ratio is simulated. d) Experimental detection of (mainly $v_X = 1$) molecules via two photon REMPI.

An example is given in Fig. II.4.5.1 where the target state is again the $v_X = 1$ level. Using the SLM all laser frequencies are removed from the pulse spectrum, except those that excite the various vibrational levels $v_X \neq 1$ to levels v_B that decay in levels $v'_X \leq v_X$. The simulation of the required pulse (shown in Fig. II.4.5.1 upper part) predicts a transfer for the ”comb” pulse of 57%, which is better than the 53% of the corresponding ”hole” pulse used in Fig. II.4.4.2c. On the experimental side, the larger signal in Fig. II.4.5.1d with respect to the corresponding Fig. II.4.4.2d seems to indicate that the population transfer is indeed, in the ”comb” pulse case, more efficient than using the ”hole” pulse case.

By controlling the number of femtosecond laser pulses with an acousto-optic modulator, we analyzed the time dependence of the optical pumping scheme in Fig. II.4.5.2. The temporal evolution of the vibrational cooling has been recorded as a function of the number of femtosecond pulses with the use of the pulses shown in Fig. II.4.4.2 and Fig. II.4.5.1, compared to the result of the simulation. If it is difficult in the current experiment to make precise statement concerning the efficiency of the process, it is clear that, as expected, the optimized ”comb” pulse is slower than the ”hole” one.” This is not a general feature but is simply due in our case to the limited laser bandwidth which limit the ability to excite the ”lower branch” of the FC parabola especially for high vibrational levels.

Due to the limited laser bandwidth and the imperfect extinction ratio of our SLM, the transfer efficiency seems to be limited to roughly 60%. The simulation clearly indicate that both effects are important. Indeed, it is calculated that, a three times broader laser, shaped in a similar manner than the previous one (excitation on the lower part of the Condon parabola), would lead to a transfer efficiency toward $v_X = 1$ of 67%.

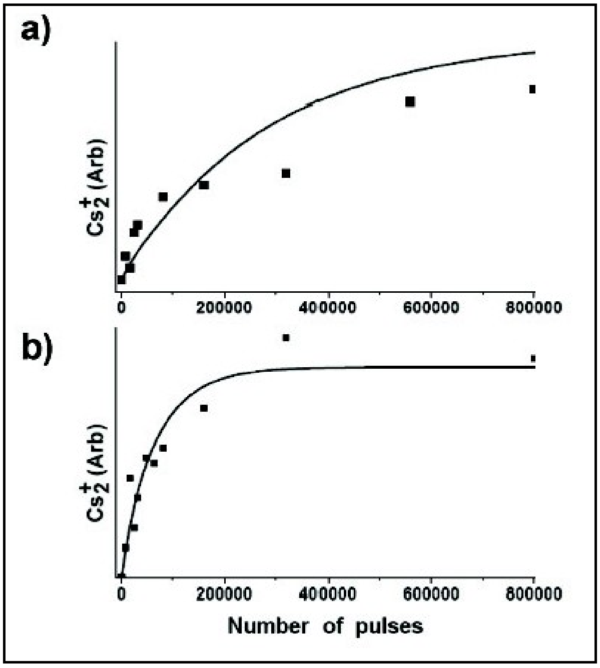

Fig. II.4.5.2: Temporal evolution of the population of the $v_X = 1$ level. a) with the pulse plotted in Fig. II.4.5.1b and b) with the pulse plotted in Fig. II.4.4.2 b . The lines correspond to the simulation and the dots to experimental measurements, i.e. to the Cs^+_2 ion signal recorded with the REMPI ionization.

II.4.6. Perspectives for direct laser cooling of molecules

In the paragraph II.1.2. , the differences between atoms and molecules as far as laser cooling is concerned were discussed. It was explained that direct laser cooling of molecules is not possible due to the lack of closed transitions in which optical pumping can be realized. However, we see that the technique of vibrational cooling with the use of femtosecond pulses has in its core a broadband optical pumping scheme on molecules. Thus, the perspectives that the current developments open on direct laser cooling of molecules are worthy to be studied.

However, the population transfer efficiencies achieved are far from being capable to support optical pumping useful for laser cooling. The efficiency of the method is reduced due to experimental weaknesses that can be overcomed. In particular these weaknesses are related to the femtosecond bandwidth, and the SLM non zero extinction ratio. The efficiency of the molecular population transfer can be improved if the femtosecond laser bandwidth is increased, since then, it would be more difficult for molecular population to be trapped in high lying vibrational levels, out of the region pumped by the femtosecond laser. A perfect extinction ratio improves also the population transfer efficiency. In Fig. II.4.6.1 we see the theoretical study of population transfer towards the $v_X = 0$ state with the use of an optimized femtosecond pulse. The pulse width is 3 times larger than the ones used in the previous studies, and a perfect extinction ratio is considered. The result for the population transfer efficiency is 99.4%.

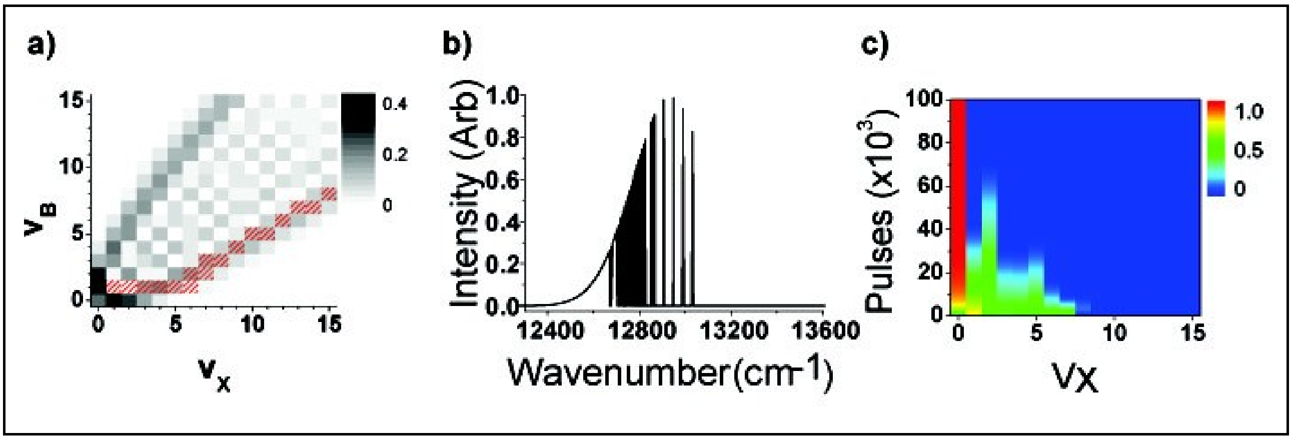

Fig. II.4.6.1: Simulation for the vibrational cooling, similar to Figure 5, but with the use of a broader shaped pulse (but with the same total intensity) and with a perfect off-on extinction ratio. a) FC coefficients (grey) for transition between the X ground state and the B excited state. The hatched (red) area represent absorption allowed transitions. b) The shaped pulse used for the simulation. The bandwidth is now three times larger than the one of the previous pulses (165 cm^{-1}) c) Results of the simulation of the vibrational cooling. The population of the $v_X = 0$ level after 105 pulses is 99.4%

The efficiency predicted in this study can be sufficient for the realization of a broadband molecular repumper laser for the achievement of laser cooling of molecules [Bah96, DiRo04]. The experimental requirements in order to achieve such a performance were not available to our laboratory, they are however well within the current technological capabilities. The increased bandwidth can be made by the use of super-continuum sources, while the shaping imperfections can be improved with better (no gap) SLM or with mechanical shutters, with the later possibility being discussed in another paragraph of this thesis.

II.4.7. Conclusion

In this chapter I have described the first, perhaps most obvious generalization of the vibrational cooling technique. The vibrational cooling is achieved with the use of an optical pumping scheme which simultaneously pumps all vibrational levels of the X ground electronic state except the target v_X state. This is achieved via a particular shaping in the femtosecond pulse via which all frequencies resonant to transitions from the v_X vibrational level are removed. We see that selecting to remove from the femtosecond pulses a set of frequencies which corresponds to excitation of a particular vibrational level leads to accumulation of molecular population in this vibrational state. Thus, molecular population transfer to a specific, pre-selected vibrational state, can be realized by removing all the frequencies that can excite the dark state from the femtosecond pulse.

The required shaping cannot be realized with the simple scheme described in the previous chapter. Instead, an advanced shaping technique based in the use of a LC-SLM is employed thanks to the collaboration with the members of the FEMPTO group of Laboratoire Collisions Agrégats Réactivité – UMR5589. Molecular population transfer has been demonstrated via two different methods: a simple one that consists of simply removing the frequencies resonant to transitions from the target state from the femtosecond pulse, and an other which involves a more complex, optimized shaping. The increased efficiency of the molecular population transfer technique, when realized with optimized shaping, is encouraging. If particular experimental weaknesses, which are solvable with technological means available today, could be surpassed, the molecular population transfer efficiency is predicted to exceed 99%, a number that starts to be attractive for the implementation of direct laser cooling of molecules.

CHAPTER II5: NON-COHERENT SELECTIVE POPULATION TRANSFER IN Cs_2 MOLECULES

II.5. NON-COHERENT SELECTIVE POPULATION TRANSFER IN Cs_2 MOLECULES

In this chapter I will describe a second generalization of the technique which is consisted in the use of a non-coherent broadband source for the vibrational cooling. This study is aiming to demonstrate that the use of a femtosecond laser is not necessary for the realization of the vibrational cooling technique, if a sufficiently broadband source can used instead. This opens the way to the use of a variety of simpler, and less expensive sources such as diode sources and collimated LEDs.

In this chapter I will describe the experimental study for the vibrational cooling in Cs dimers with the use of a simple, non coherent broadband diode source [Sof09b]. Initially I will describe the first part of this study which involves vibrational cooling to the ground vibrational state. In this case, the shaping is performed with the use of a simple system of interference filters. Next, I describe the demonstration of selective molecular population transfer towards the $v_X = 1$ vibrational level with the use of the same broadband diode. In this case the shaping is performed with the use of the 4-f line and a simple mechanical mask, and the problem of the non zero extinction ratio of the SLM based shaping is, at least for this simple shaping case, resolved. Finally, I discuss in the conclusions, how this simple experiment, proves the validity of the operating principle of the vibrational cooling technique presented in Chapter III.

II.5.1. Vibrational cooling with the use of a non coherent broadband source

In the experiments described in the previous chapters, the population transfer is achieved by performing amplitude shaping on a femtosecond pulse. These results show that the vibrational cooling technique can find interesting applications and become a popular method in the field of cold molecules, as far as some limitations can be confronted, namely the high complexity and cost of the set up and the limited extinction ratio of the SLM. Other broadband light sources than femtosecond ones could be considered for the realization of optical pumping as long as they are compatible with the main requirements of the technique, i.e. the large bandwidth, sufficient power and the possibility to perform frequency shaping. In various simulations that we have performed in order to explain the technique and to explore its possible extensions and limitations, the intensity of the broadband light used for the optical pumping is very small and coherence effects seem not contribute in the population transfer. This means that a wide range of non coherent, broadband sources, like Light Emitting Diodes or lamps, could be used in order to perform the optical pumping. However, the source light has to be collimated, in order to realize the necessary shaping to it.

II.5.2. Population transfer to $v_X = 0$

In this paragraph I discuss molecular population transfer towards the $v_X = 0$ state. This is done with the use of an incoherent broadband source provided by a broadband diode laser (BDL) operating near threshold used to perform optical pumping. The shaping of the spectral components of the radiation is achieved with the use of a much simpler and less expensive optical apparatus than before. Nevertheless, our current simplified setup conserves all necessary characteristics (power and bandwidth) and it eliminates the limitation to the transfer efficiency caused by the non perfect extinction ratio of the SLM involved in the previous experiments. The simplicity and flexibility of this setup allows further development towards new applications.

In the current experiment, the broadband radiation is provided by a Laser 2000 LD1227 HPD 1110 broadband diode laser operating in the 780 nm range and focused to a waist of 800 μm on the MOT position. This represents a substantial simplification of the required laser apparatus. The BDL bandwidth is 2 nm for the laser part of the spectrum, but it increases to 10 nm when considering also the luminescent part of the spectrum. This light couples again the ground X and the excited B potentials for the optical pumping. The method does not require any temporal control of the BDL radiation that operates in cw mode. In the case shown in Fig. II.5.2.1a, where the goal is to transfer the molecular population into the $v_X = 0$ level, we need to remove only the blue part of the spectrum, so that transitions from $v_X = 0$ level to any vibrational level of the B state are not longer excited. In this way the molecular population is accumulated in the $v_X = 0$ level that now becomes a dark state of the system. This requires the removal of frequancies larger than 13030 cm^{-1}. The stiffness of the shaping is not important as long as all vibrational levels of the X state, other than the $v_X = 0$ are excited by the laser light. The desired shaping was obtained with the use of three Semrock RazorEdge 785 long-pass filters placed on top of each other in order to achieve an extinction ratio of more than 99%. The filters were mounted at an angle with respect to the incident diode radiation to allow fine tuning of the cut-off frequency to the desired value.

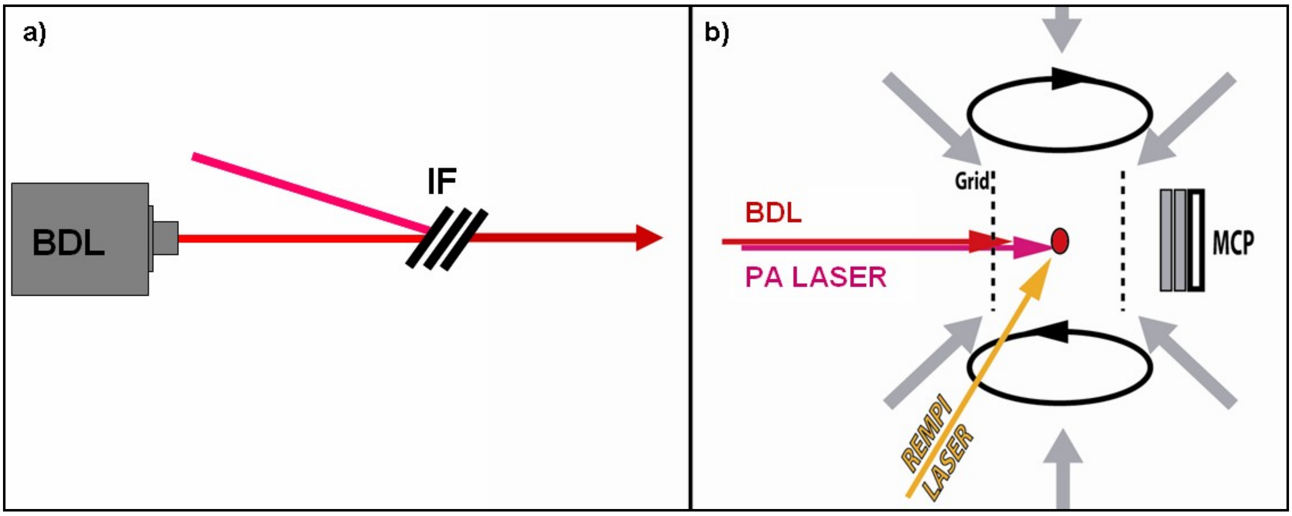

Fig. II.5.2.1: (a) Shaping of the BDL radiation with three interference filters (IF) placed on top of each-other. The filters are placed at an angle of 30° in order to finely adjust the cut-off frequency to the desired value, resulting in a less sharp 'cut' than for 0° (b) The BDL radiation is superimposed with the photoassociation (PA) radiation and inserted into the MOT.

In Fig. II.5.2.2.a, we see all potential curves and laser frequencies that are related to this experiment. In part (b) we see the diode spectra, before and after shaping, monitored by an Ando AQ6317B optical spectrum analyzer, while in (c) we see which vibrational transitions are within the area where the diode power is higher than the 0.001 of its maximum value. In part (d) we see the usual demonstration of vibrational cooling by the comparison of the ionization spectra with and without the cooling radiation. We see that the various peaks that appear in the spectrum acquired without any cooling radiation, which correspond to transitions from states 0,1,4 and 8 give their position to two broadened peaks that correspond to transitions originating from $v_X = 0$, a fact that proves vibrational cooling.

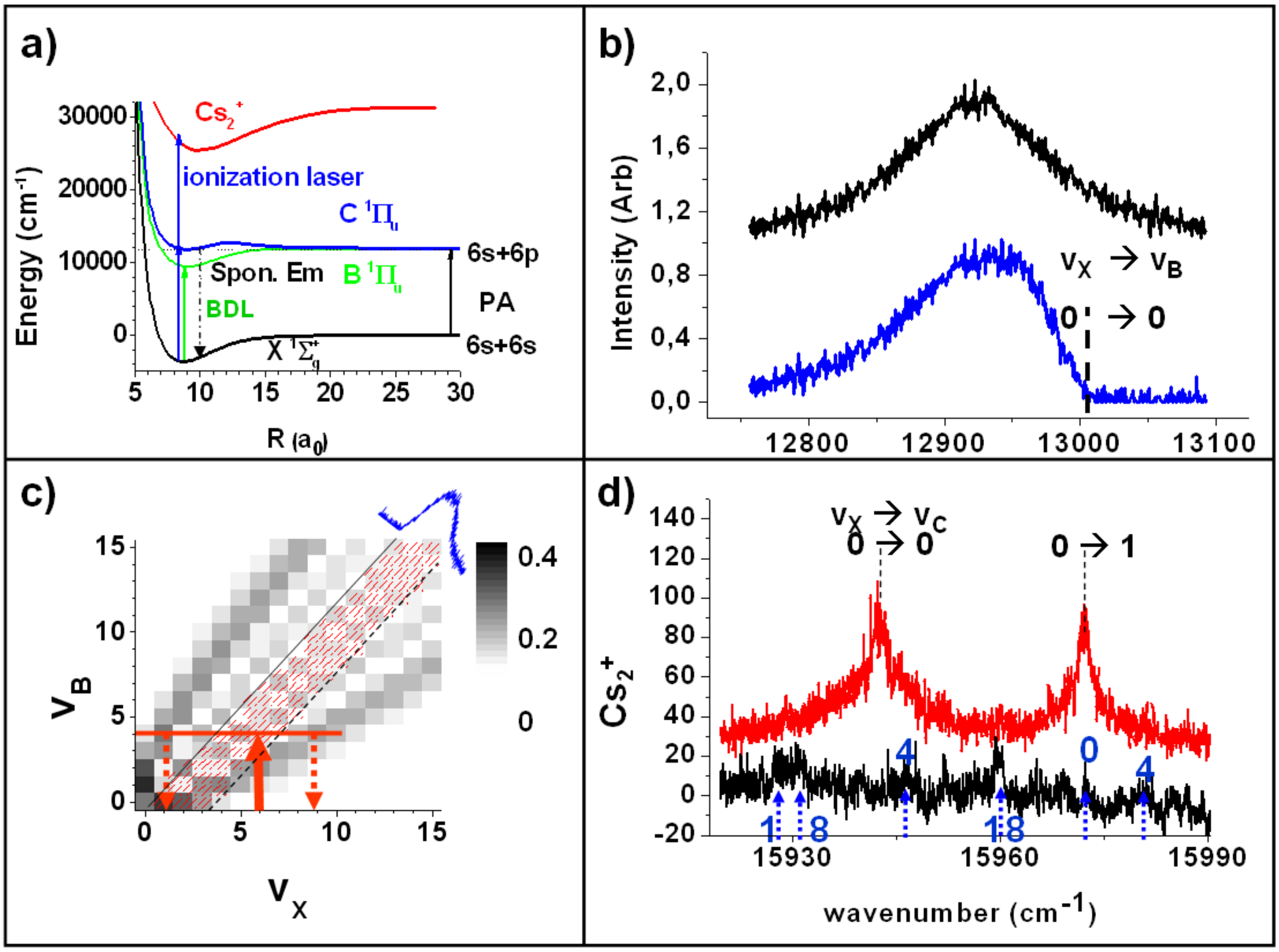

Fig. II.5.2.2: (a) The potential energy curves and the lasers related to the experiment. (b) Spectrum of the diode laser before (upper black line) and after passing through the interference filters (lower blue line), with a mark on the $v_X = 0 \rightarrow v_B = 0$ transition frequency above which all the BDL frequencies are suppressed. (b) Plot of the Franck-Condon parabola where the transitions that are within the are where the shaped diode power is higher than 0.001 times its maximum. (c) The REMPI spectrum of the $X^1\Sigma_g^+ \rightarrow C^1\Pi_u$ transitions with (upper trace, offset of 10 ions for clarity) and (lower trace) without optical pumping.

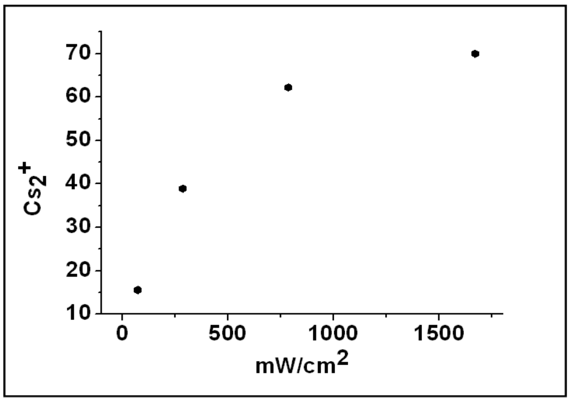

Fig. II.5.2.3: Experimental measurement of the evolution of the finally transferred molecular population with respect to the BDL power.

The BDL was at all times operated below lasing threshold, with a bias current of 308 mA, producing an output power of 26.5 mW. We note that operating the diode above threshold does not modify the results, as long as the broadband part of the radiation is still present. After the shaping, the remaining collimated beam power was 17.1 mW. The intensity used in this experiment was 1.2 W/cm^2. Population transfer efficiency saturates for higher intensity values, while it dropped to half this value at an intensity of 0.3 W/cm^2, as seen in Fig. II.5.2.3. Taking into account the efficiency of the REMPI detection, the total number of molecules in the $v_X = 0$ level is estimated to be of the order of 10^3. As it is very hard to experimentally measure the population transfer efficiency, we estimated it through simulations to be ~80%.

II.5.3. Population transfer to $v_X = 1$

In this paragraph the above described technique based in the use of a broadband diode is extended in order to achieve population transfer to $v_X = 1$ vibrational level. A different, but still very simple setup allows us to adapt the technique in order to achieve this goal. Again, the general idea for the shaping, is to remove all frequency components that can excite molecules from the target level while being able to excite all other vibrational levels.

Interference filters cannot be used since the transitions from the $v_X = 0$ level, which have now to be addressed, are at an higher frequency than the transitions from the $v_X = 1$ level that we need to block. In preceding experiments, the necessary shaping was achieved with the use of a LC-SLM, which allowed a great versatility but at the price of high cost, experimental complexity and non perfect (97%) extinction ratio for the removed frequency components. This last point was limiting considerably the population transfer efficiency. In the present experiment we can recover the selective molecular transfer to the $v_X = 1$ level by removing the undesired frequency components with a mechanical mask placed in the Fourier plane of a 4-f dispersion line, as shown in Fig. II.5.3.1. This not only greatly simplifies the apparatus, but also increases the extinction ratio to 100%.

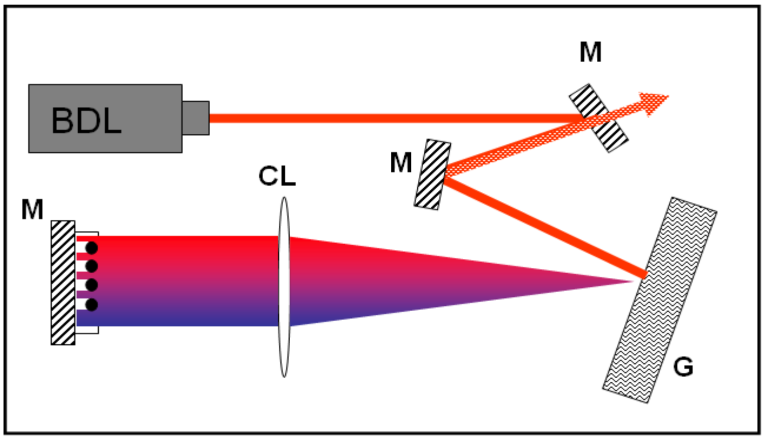

Fig. II.5.3.1: The BDL shaping realized with the folded 4-f line setup, consisted of three mirrors (M) a grating (G) a cylindrical lens (CL) and a mask.

The BDL radiation is diffracted by a 1800 lines/mm optical grating. A cylindrical lens is placed at a distance equal to the effective focal length of the grating (500 mm in this case), is used to collimate the radiation and to focus each of its frequency components in the Fourier plane, where a mirror is placed. In the returned beam all frequency components are recombined again by the grating while a slight misalignment in the vertical direction allows the radiation to exit the system by ’missing’ one of the guiding mirrors. In the Fourier plane we remove some particular frequency components by blocking them with a dark mask. In this case it is composed by four 1.5 mm diameter needles but other types of (photo)masks could also work[1]. The optical throughput of this second setup is much lower than in the filters case because of the limited reflectivity of the grating in the first diffraction order. Thus, in order to have enough laser power after the shaping system, we operate the BDL with 30% higher bias current (660 mA), i.e. above the lasing threshold, in order to have nearly 0.5 mW of shaped laser power on the molecules.

The BDL spectrum is shown in Fig. II.5.3.2a, before and after the shaping. The gaps in the spectrum are 4 cm^{-1} wide and correspond to transitions originating from the $v_X = 1$ level that lie within the excitation spectra of the femtosecond pulse. The efficiency of the technique is not sensitive to the removal of more frequencies than the necessary, as long as no dark states of the system are created other than the target one. The resulting REMPI spectra, with and without BDL radiation, are shown in Fig. II.5.3.2.b. Once more we see a clear effect of the optical pumping, since the spectral features corresponding to the $v_X = 1$ to the $v_C = 0$,1 and 2 transitions emerge in the presence of the shaped diode radiation.

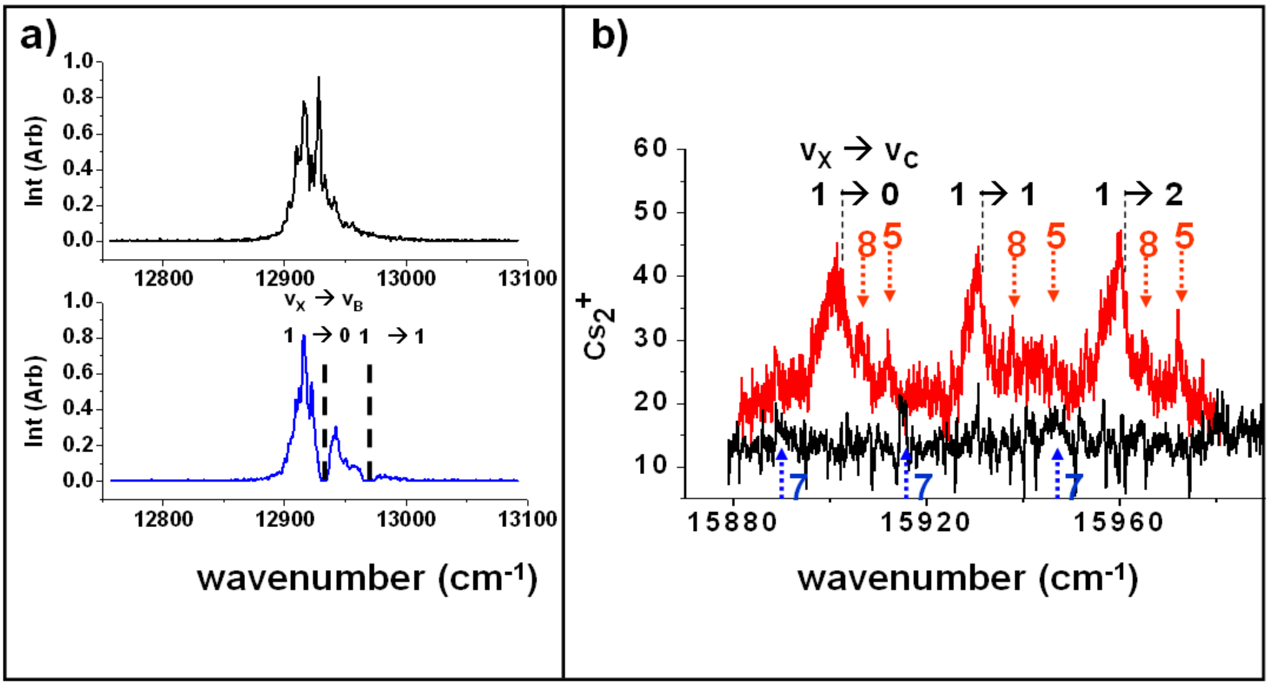

Fig. II.5.3.2: (a) Spectrum of the diode source with a bias current of 660 mA before (upper black line) and after passing the 4-f line (lower blue line). At this bias current the diode is just above the lasing threshold, as the dominant frequency at 12930 cm−1 becomes more apparent. The frequencies of the $v_X = 1 \rightarrow v_B = 0$, 1 transitions are removed. (b) The REMPI spectrum of the $X^1\Sigma_g^+ \rightarrow C^1\Pi_u$ transitions with (upper trace, offset of 5 ions for clarity) and (lower trace) without optical pumping.

However, in the spectra on the upper part of Fig. II.5.3.2.b, we see peaks that do not correspond to transitions originating from the $v_X = 1$ vibrational level. The presence of these lines indicate that not all the molecular population has been transferred to the desired $v_X = 1$ vibrational state and part of it remains in states $v_X = 5$ and 8. This insufficient pumping is a result of the limited power of our shaped radiation. As previously explained, the 4-f line used for the shaping of the broadband diode results to a not very intense beam in the output. Additionally, it is possible that the large diameter of the needles used for the realization of the 'mask' partially blocks frequencies that excite the $v_X = 8$ vibrational level, which are very close to the frequencies that correspond to

---

[1] In future studies, a photo-mask will consist of a 'chip', on which the 'needles' will be mechanically printed.

excitation of the $v_X = 1$ target state. However, these technical imperfections can be easily resolved in an experiment that aims in complete population transfer in a particular vibrational level. The experiment discussed here, is a 'proof-of-principle' experiment, and these imperfections do not create big problems as well as they the mechanisms that create them are fairly understood.

II.5.4. Conclusion

In conclusion, we have demonstrated selective vibrational population transfer in cesium dimers with the use of a collimated broadband diode laser. The simplicity of this experimental setup can make this technique very attractive, since the cost is significantly reduced with respect to the cost of previous experiments which involved a femtosecond laser and a spatial light modulator. An important application that can be foreseen for such a method is in the use of a shaped BDL as a repumper light in a scheme for a direct laser cooling of molecules. The relatively low cost and the simplicity of such a set up allows for the use of more than one diode laser sources if needed, for instance each of them addressing transitions between different vibrational or even electronic states.

Additionally, the use of a mechanical mask eliminates the problem of the non perfect extinction ratio that existed in the SLM setup. Since the precision required in order to realize an optimized pulse like the one discussed in II.4.5. , cannot be achieved with needles as the ones used in the experiment discussed here, we consider the use of a micro-mechanical photo-mask. Such a mask has been constructed in a collaboration with Selba S.A , and is shown, along with some preliminary femtosecond pulse spectra in Fig. II.5.4.1.

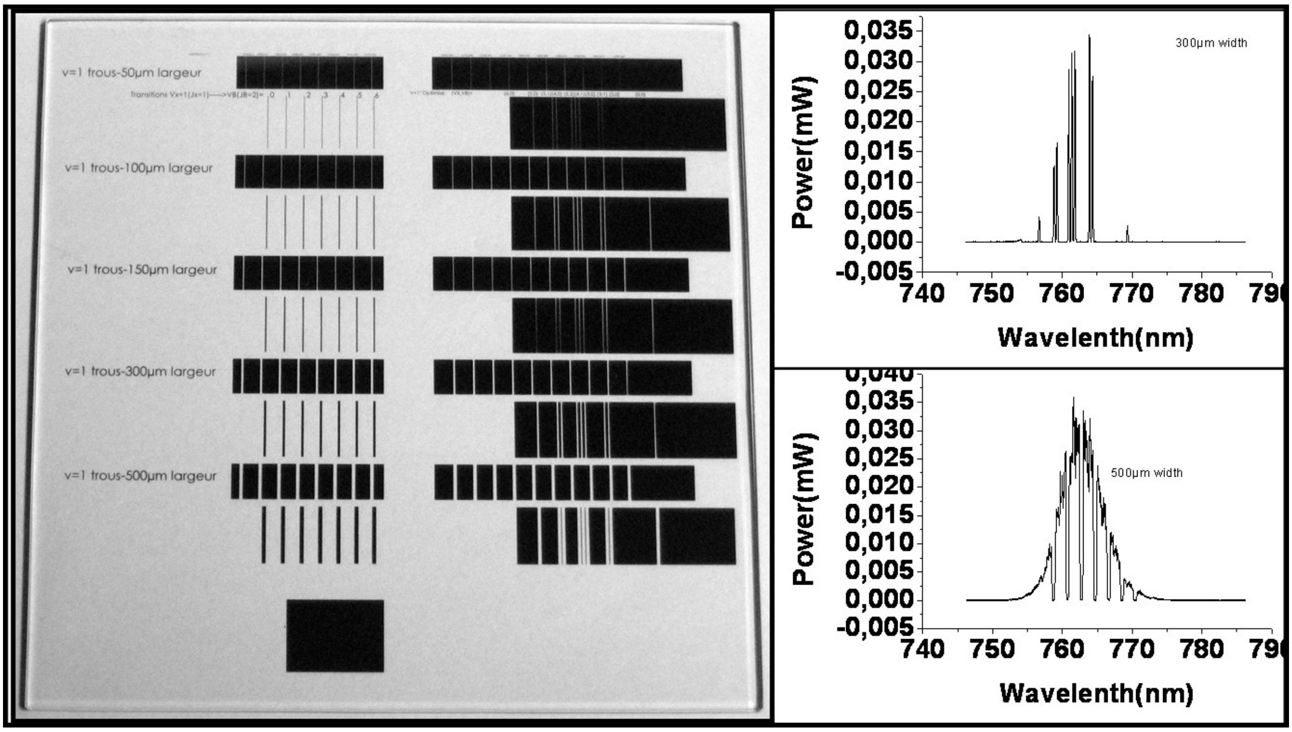

Fig. II.5.4.1: On the left we see some photo-masks constructed with the *photo-lithography* method by Selba S.A. On the left, we see two spectra of the femtosecond light transmitted trough the photo-masks. The upper spectra corresponds to an optimized pulse.

One of the reasons that justify a study of molecular population transfer with the use of an incoherent light source, is related to the clarification of the operating principle of the vibrational cooling method. In the months that followed the techniques demonstration, a dialog concerning the clarification of the vibrational cooling mechanism was developed. In the simulations presented up to now, the operating principle involved one photon interactions described in the perturbative regime. This was so far justified by the low femtosecond intensity and by the coherence between the simulations and the experimental data. However, it was discussed that perhaps high field interactions with accumulation of coherence in the excited levels could contribute to the coherence effect. A fact that justified such a discussion was that the repetition rate of the femtosecond laser used in the previous experiments is very close to the lifetime of the excited levels (~12 ns) in the molecular optical pumping scheme. The realization of molecular population transfer with the use of a non coherent, diode based source can be conclusive in this discussion, since it excludes all explanations involving coherent effects and supports the simple explanation adapted in the previous chapters.

Concluding, I can say that the realization of the vibrational cooling technique with the use of the broadband diode considerably simplifies the experimental set -up, while it makes its realization more attractive financially. This way, one can consider the realization of complex repumping schemes towards the realization of direct laser cooling of molecules, without having to consider the increased complexity and the high cost that is included by the use of a femtosecond laser.

CHAPTER II6 : GENERALIZATION OF VIBRATIONAL COOLING

II.6. GENERALIZATION OF VIBRATIONAL COOLING

In the previous chapters, we show that optical pumping with shaped femtosecond pulses lead to the achievement of vibrational cooling in Cs dimers. In the chapters IV and V, two different expansions of the technique were demonstrated: the one considering selective molecular population transfer to a pre-selected vibrational level and the other considering population transfer with the use of an incoherent broadband source.

However, the subject of generalization of the vibrational cooling technique is far from exhausted. In this chapter I attempt to discuss the extension of the vibrational cooling technique to include different molecular systems. Up to now, the technique has been demonstrated for the case of ultracold Cs dimers, and more specifically, in the transition between the ground and the $B^1\Pi_u$ electronic potential (or B state). It is evident, that not all the choices of excited state for the optical pumping can lead to successful vibrational cooling, no matter how detailed the shaping can be. In this chapter, I try to study the conditions under which an optical pumping scheme can lead to efficient vibrational cooling, and to determine which choices of molecular electronic potentials can be promising for optical pumping. The study consists of choosing a set of two molecular electronic potentials, describing their general geometrical characteristics and then generating the Franck-Condon parabola, with the use of which a simulation of the molecular pumping process is performed.

This chapter is organized as follows: In the introduction, I discuss how the general geometrical characteristics of the potentials used in the optical pumping can affect the form of the Franck-Condon parabola and consequently the result of the optical pumping. The first part of this paragraph is based in [Stand99]. In this publication, the Franck-Condon parabola which correspond to couples of analytical harmonic potentials are constructed. The simple analytical potentials are used in order to simplify the study of the geometric characteristics of the potentials upon the parabola. In the following part of the paragraph, I discuss which forms of Franck-Condon parabola are suitable for vibrational cooling.

In the second paragraph, I study the possibility of vibrational cooling of Cs dimers in the $^3\Sigma_u$ 'triplet' state. This is due to the fact that such a study initially seemed attractive by the group and was studied experimentally. However, the experimental study showed that such a process could not be achieved, at least in the particular optical pumping scheme. One could say, that the study of cooling in the $^3\Sigma_u$ 'triplet' state gives the opportunity to study a 'bad' choice of potentials for vibrational cooling, and to outline the factors that should not be neglected in such a study.

Finally, I attempt to study the perspectives of the use of the vibrational cooling technique in different molecular species and in particular in three heteronuclear alkali dimers the NaCs, the NaRb and the NaK. The choice of the heteronuclear molecules is mostly related to the availability of molecular potentials and transition dipole moments calculated by members of the theoretical group of Cold Molecules in the laboratory [Aym07].

II.6.1. Key parameters for optical pumping of molecules

In this paragraph, I try to identify the molecular characteristics that are crucial for the realization of optical pumping, and thus, of vibrational cooling in molecules. Initially, I discuss the general form of the Franck-Condon parabolas as a function of the geometrical characteristics of the molecular potentials involved in the transition, with the use of a simple analytical 'toy' model. In the following, I discuss which forms of Franck-Condon parabolas make optical pumping feasible. With this, I intent to explain the intuitive argumentation followed in the following paragraphs.

II.6.1.a. 'Toy model' for molecular potentials

In order to understand how the geometrical characteristics of the electronic potentials affect the optical pumping I begin this study with the toy model discussed in [Stand99]. Here, the molecular potentials that are associated with the electronic transition, are substituted by analytical, harmonic oscillator potentials. From the two harmonic potentials involved, the excited potential is identical to the ground potential, except the fact that it lies in higher energy and it is shifted. The analytic form of the potentials is

$$V_g(x)=\frac{1}{2}k_g x^2=\frac{1}{2}m\omega_g^2 x^2 \tag{6.1}$$

$$V_e(x)=d+\frac{1}{2}k_e(x-b)^2=d+\frac{1}{2}m\omega_e^2(x-b)^2 \tag{6.2}$$

where with *k* we symbolize the force constant of each of the oscillators, and with $\omega_{g,e}$ the oscillation frequencies. With *b* we symbolize the displacement, with *m* the mass and with the letters *g* and *e* the ground and excited state respectively. The eigenenergies of the harmonic oscillator states are

$$E_g=(\frac{1}{2}+v_g)\hbar\omega_g,\, E_e=(\frac{1}{2}+v_e)\hbar\omega_e \tag{6.3}$$

where with $v_{g,e}$ we symbolize the vibration number of the ground and the excited state respectively. In Fig. II.6.1.a.1 we see the Franck-Condon parabolas that can be generated with the use of these analytic potentials as the upper and the lower states of a molecular transition. Initially, we see what are the characteristics of the Franck-Condon parabola generated with $b = 0$. In the following, the excited molecular potential has his equilibrium distance (b) shifted, so the separation between the two minima is gradually increased. Finally, the excited potential is replaced to a 'wider' (less confining) potential, now centered on top of the fundamental one. The red dotted lines represent the iso-energetic lines, that is the lines that correspond to excitation by a single frequency. As we see, these iso-energetic lines have a tilt of 45° for all cases where the force $k_{g,e}$ constants of the upper and the lower potentials are equal. In the cases where $k_e < k_g$, this tilt grows. This is easily seen, since now that the upper potential is less confined it leads to smaller separation between the vibrational states it supports. Thus, a frequency that would excite, let's say, states with equal vibration is the case of equally confined potentials, now will excite transitions were $v_e > v_g$.

As we see in part (a), the Franck-Condon parabola corresponding to two identical potentials is a line, indicating that the probability of transition between states with equal vibrational number is maximum, and is almost zero elsewhere. As the excited potential is shifted towards the right, the Franck-Condon factors form a parabola with increased radius (parts (b) and (c)). If instead of modulating the separation, the force constant of the oscillators is modified, the initial line 'breaks' to a parabola with inverse curvature, as shown in parts (f) and (g), for decreased values of k_e.

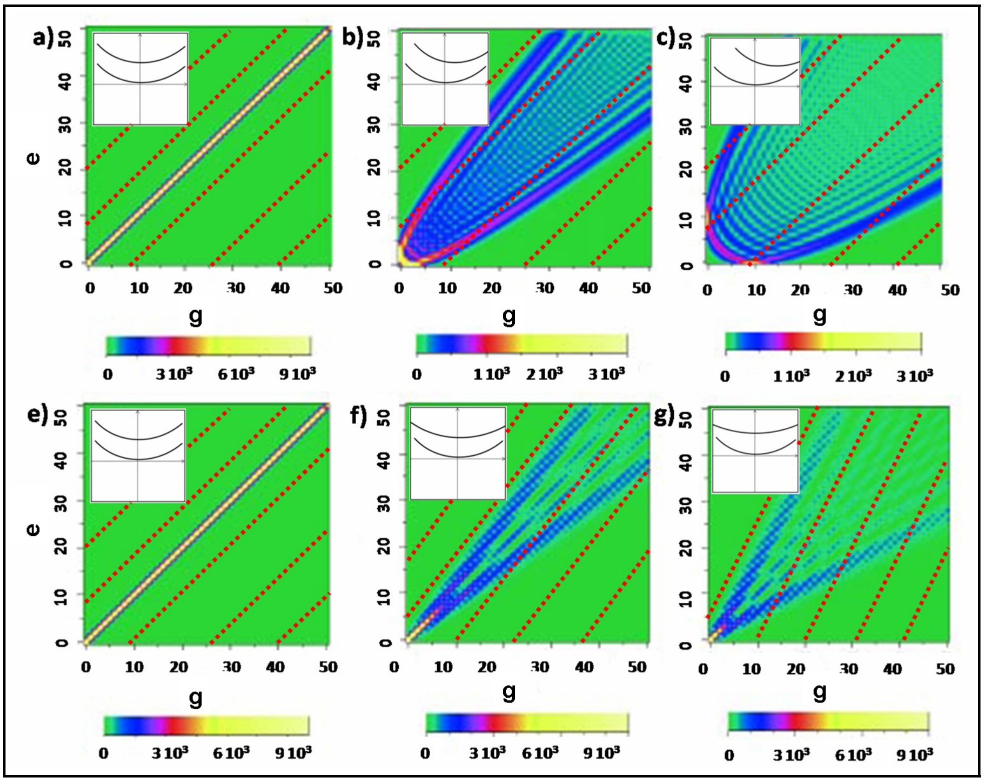

Fig. II.6.1.a.1: Franck-Condon parabola corresponding to the various combinations of analytical molecular potentials. The values shown in the false color scales below are multiplied by a factor of 10^4 and otherwise correspond to probability. The red dotted lines correspond to excitations by a single frequency (iso-energetic lines). In the first line, we see the effect of the variation of separation b, as shown schematically in the inlets. The force constant k is equal to 1560 N m^{-1} for both potentials. In (a) the displacement b is 0 Angström, in (b) it is 0.1 Angström and in (c) 0.2 Angström. In the second line, the force constant of the excited state k_e is varied while the displacement is kept equal to 0. In (a) k_e = 1560 N m^{-1} (and equal to k_g) , in (b) it is equal to 780 N m^{-1}, while in (c) it is equal to 390 N m^{-1}. Graphs are adapted from [Stand99]

II.6.1.b. Optical pumping in molecules

Let us consider the use of each of the potential couples considered in our various studies for the realization of optical pumping and vibrational cooling. The cases (a) and (e) are trivial. No vibrational cooling can be accomplished with such a scheme, nor any modification of the vibrational distribution. The reason is that the wavefunctions which correspond to vibrational levels of equal vibration number v, overlap so well, that all excitation and emission steps are performed between states with equal v. As a small displacement, like the one considered in (b) is introduced, the situation is improved. Now, there exist Franck-Condon coefficients that correspond to states of different v and which have a non zero value, a fact that permits population transfer between the vibrational states. If this displacement increases considerably, as in (c), the Franck-Condon coefficients which correspond to transitions between low vibrational levels start to have very low values. This situation is undesirable, because it reduces population transfer between low lying vibrational states and insert difficulties in vibrational cooling. Finally, the effect of the variation of the force constant of the excited state k_e, is studied. Once the two potentials are not identical, we see the appearance of non zero Franck-Condon factors for the transitions between states with different v. The transition between the states v = 0 remains maximum, no matter how much k_e has been modified and no 'hole' appears in the positions corresponding to transitions between low lying vibrational levels. This is expected, since for no displacements between the potential minima, we do not expect important decrease in the overlap of the fundamental wavefunctions.

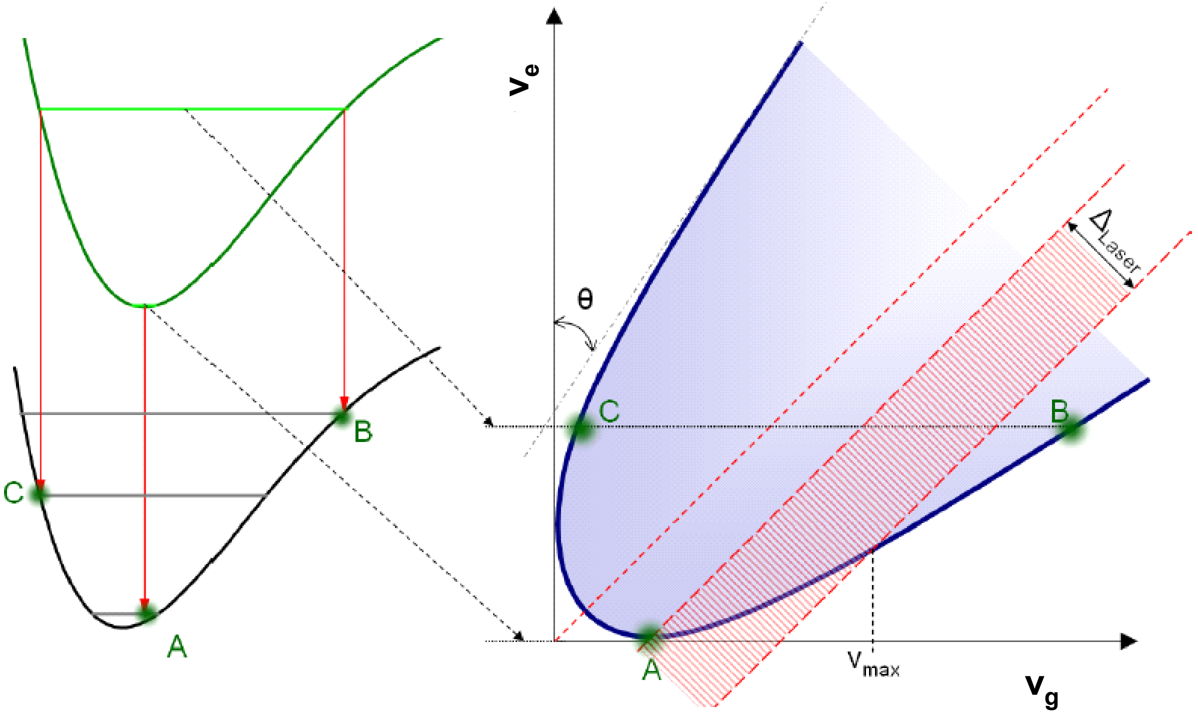

Fig. II.6.1.a.2: Schematic representation of the geometric characteristics of the molecular potentials and how they affect the form of the generated Franck-Condon parabola. Figure adapted from [Vit08c].

In Fig. II.6.1.a.2, we see a schematic representation of how the basic geometrical characteristics of the potentials involved in the transition affect the form of the corresponding Franck-Condon parabola. With the help of this figure, we can outline the criteria that define the applicability of optical pumping and thus of vibrational cooling, in a given electronic transition. In the following, I list those criteria, without dealing with experimental issues, like for example the availability of light sources for the excitation of the transition or the power requirements.

- the first criterion is that the electronic transition should be as 'closed' as possible, with the sense that spontaneous emission should return molecular population in the initial electronic potential, in its biggest possible percentage, after excitation. Molecular population can be lost during the optical pumping process for a variety of reasons, such as ionization, pre-dissociation or coupling to other electronic potentials; some of these processes are going to be examined in the following paragraph.
- The internuclear position of the minimum (equilibrium point) of the excited potential has to be as close as possible to the minimum of the ground potential. If the objective of the optical pumping is to transfer the molecular population in the lowest vibrational state possible, then all frequencies which lie lower than this point (point A in Fig. II.6.1.a.2) should be cut, since if they participate to the process, they lead to an increase of vibration. In the case of Cs_2, as examined in Chapter III, IV and V, this point coincides with the transition $v_X = 1 \rightarrow v_B = 0$, thus it was relatively easy to transfer molecular population to these two vibrational levels.
- The angle θ gives an idea of the rapidity of the vibrational cooling. The biggest this angle is, the 'faster' the cooling is (less transitions are required for a certain decrease in vibration). This could be easily seen by 'bending' the parabola's arms up to the point where they touch the axis. In this case we can see that all transitions towards v = 0 are

favored (v_X for the upper and v_A for the lower arm).

In the light of the study of these Franck-Condon parabola presented, we can consider realistic choices for molecular electronic potentials and analyze the morphology of the resulting parabola. I consider the Franck-Condon parabola associated with the $X^1\Sigma_g^+ \rightarrow B^1\Pi_u$ vibrational cooling scheme, which is the only vibrational cooling scheme demonstrated experimentally. I also consider the $X^1\Sigma_g^+ \rightarrow C^1\Pi_u$ vibrational cooling scheme, which, even if it has not been experimentally demonstrated, it is a suitable scheme for vibrational cooling (to be discussed in the following chapter). Those potential are shown in Fig. II.6.1.a.3, along with their corresponding Franck-Condon parabola. We are in position to identify the parameters that ensure the successful implementation of vibrational cooling via these states, since we see that the involved molecular potentials are more or less of the same confinement, while their minimum point are located in the same or in close internuclear distances. This ensures the sufficient magnitude of the Franck-Condon parameters for the transitions between states of small vibrational number, and permits molecular population transfer to any of these low lying states.

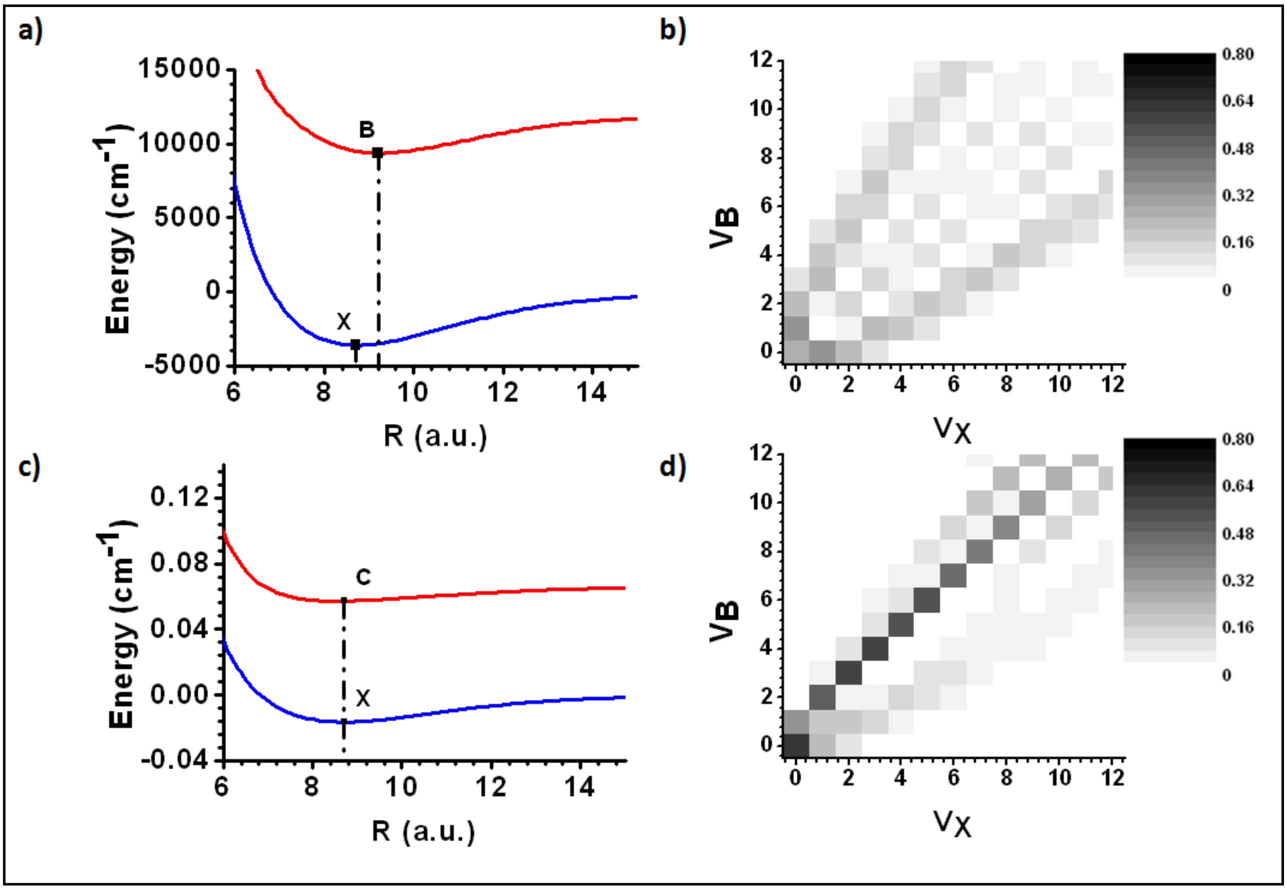

Fig. II.6.1.a.3: (a) Molecular potentials corresponding to the $X^1\Sigma_g^+$ to $B^1\Pi_u$ transition in Cs_2 and corresponding Franck-Condon Parabola (b). (c) Molecular potentials corresponding to the $X^1\Sigma_g^+$ to $C^1\Pi_u$ transition in Cs_2 and corresponding Franck-Condon Parabola (d). The dashed lines note the equilibrium positions of the corresponding potentials.

II.6.2. Study for the cooling of molecules in the $a^3\Sigma_u^+$ triplet state.

In this paragraph I examine a first example of generalization of the vibrational cooling technique to include molecules in their $^3\Sigma_u^+$ state. Initially, this paragraph was intended to describe generalization towards heteronuclear diatomic molecules alone. However, the experiments performed for the vibrational cooling of the $^3\Sigma_u^+$ triplet state molecules can be discussed in the context of this chapter. Moreover, the general conclusions of this paragraph, which seem to explain the experimental results of the $^3\Sigma_u^+$ triplet experiment, could be useful for the discussion of generalization to heteronuclear molecules.

II.6.2.a. Motivation

In this paragraph I will present the results of the experiment which aimed to cool molecules lying in the $^3\Sigma_u^+$ state. The motivation for cooling Cs dimers in the triplet state, is not constrained in demonstrating just another efficient vibrational cooling scheme. This motivation is evident to those who have a small experience with Cs photoassociation experiments, since photoassociation can provide with triplet molecules in much larger number than singlet molecules. Since the lifetime of the Cs triplet state is expected to be in the order of some seconds, they are considered stable enough for a variety of studies, while the number of problems that are easier to solve in the laboratory with the use of the huge triplet signal, is more than appealing.

Optical pumping of molecules that lye in the $a^3\Sigma_u^+$ triplet state was initially considered via the $(2)^3\Pi$ state, due to the fact that the separation between the equilibrium distances between these state and the ground state is minimized. However, since the $(2)^3\Sigma_g^+$ state can be coupled to the 'ground' $a^3\Sigma_u^+$ state in similar laser frequencies, we are obliged to take $(2)^3\Sigma_g^+$ as well into consideration

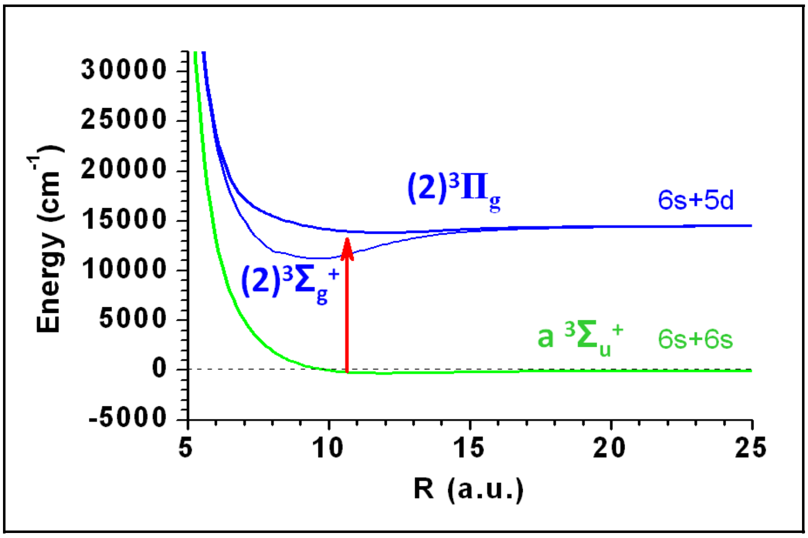

Fig. II.6.2.a.1: Possible excitation schemes for the $^3\Sigma^+$ Cs_2 state, at ~720 nm, via the $(2)^3\Sigma_g$ and the $(2)^3\Pi$ state.

In Fig. II.6.2.a.2.a we show the chosen $a^3\Sigma_u^+$ and $(2)^3\Sigma_g^+$ potentials along with the position of the first three vibrational states. The wavefunctions that correspond to those vibrational states are found in (b); the wavefunctions corresponding to the first five vibrational states of the $^3\Sigma^+$ potential are shown in the lower, and the ones corresponding to the $(2)^3\Sigma_g^+$ potential are shown in the higher part. The resulting Franck-Condon parabola, shown in (c), indicates the fact that the chosen transition is non-suitable for vibrational cooling[1].

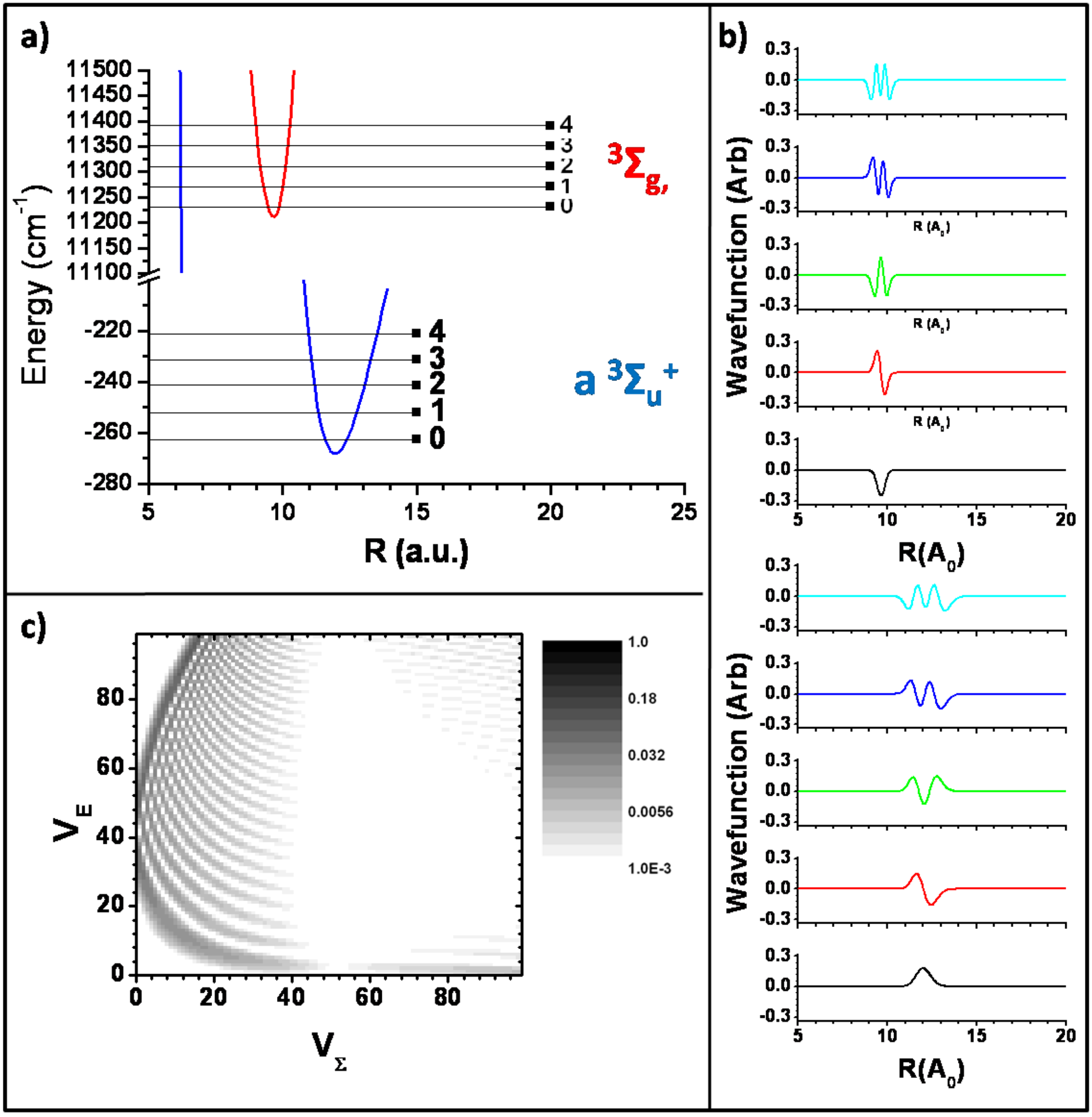

Fig. II.6.2.a.2: (a) trapping potentials and positions of the first five bound states for the a$^3\Sigma_u^+$ and (2)$^3\Sigma_g^+$ states. (b) Wave-functions of the first five vibrational states, with the one corresponding to the a$^3\Sigma_u^+$ state lower, and the ones corresponding to the (3)$^3\Sigma_g^+$ state higher. (c) Franck-Condon parabola corresponding to the specific transition.

The Franck-Condon parabola resulting from the next choice of states is much more promising as seen in Fig. II.6.2.a.3. The two potentials are now much better matched in shape and internuclear separation as shown in (a), while the wavefunctions corresponding to the vibrational states are centered in the same position as shown in part (b). The Franck-Condon parabola is shown in the part (c) of the figure.

---

[1] In this chapter the notation v_X for the vibration of the ground potential is changed to v_Σ since now, the excited potential is not the B. Similarly, the notation adopted for the vibration in the excited potential is v_E both for excitation in the $^3\Sigma_g$ and in the $^3\Pi_g$ state.

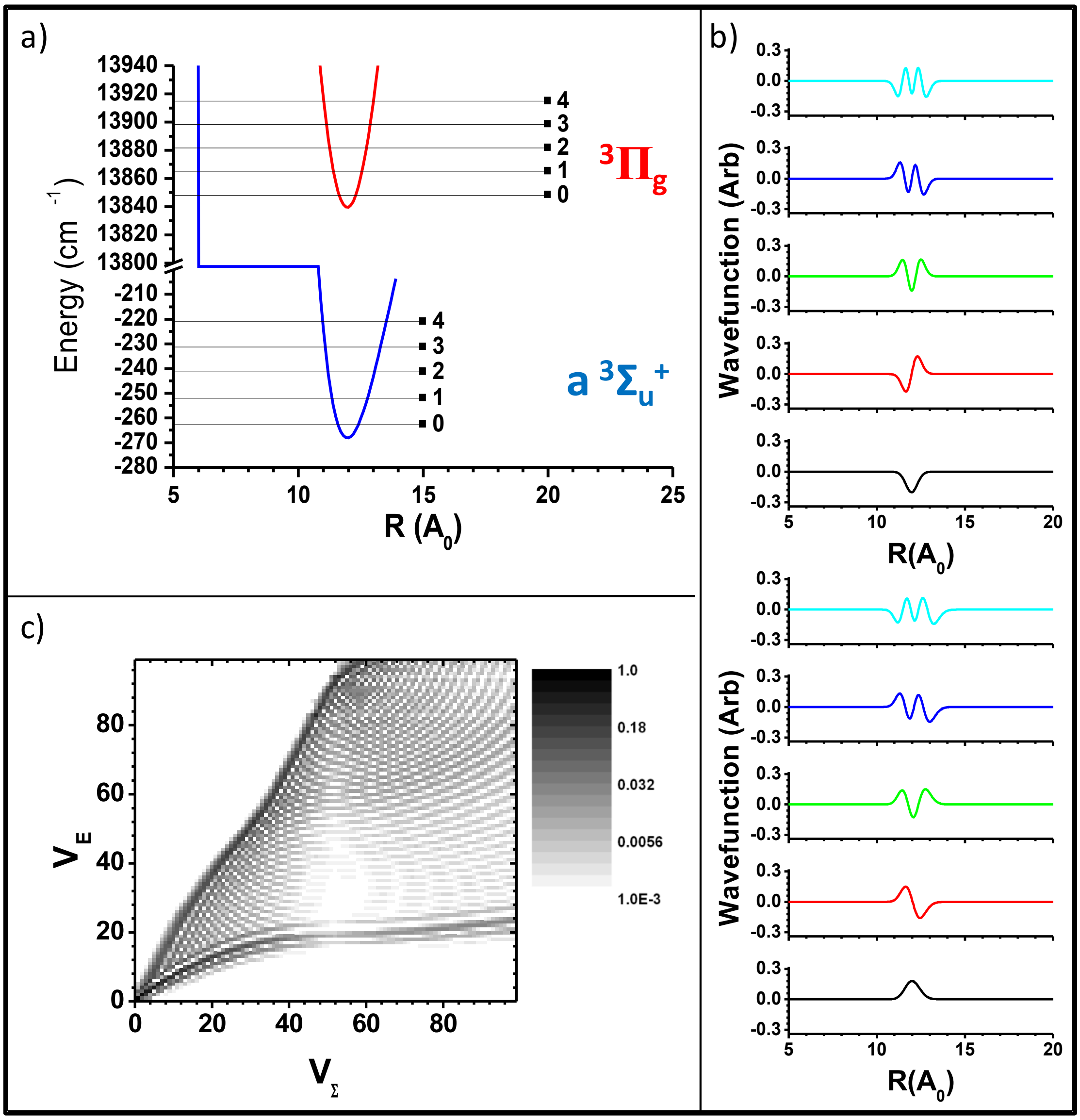

Fig. II.6.2.a.3: (a) trapping potentials and positions of the first five bound states for the a$^3\Sigma_u^+$ and (2)$^3\Pi_g$ states. (b) Wave-functions of the first five vibrational states, with the one corresponding to the a$^3\Sigma_u^+$ state lower, and the ones corresponding to the (2)$^3\Pi_g$ state higher. (c) Franck-Condon parabola corresponding to the specific transition.

In Fig. II.6.2.a.4, we see again in (a) the Franck-Condon parabola corresponding to the (a)$^3\Sigma_u^+$ - (2)$^3\Pi_g$ state transition. The blue squares correspond to those transitions excited by the shaped femtosecond pulse shown in (b). The blue squares indicate those transitions for which the laser field has power larger than 0.001 of its maximum power. With the red arrows in part (a) we indicate the most probable paths for the excited molecules. As we see, the Franck-Condon parabola is such, that the most probable evolution of the state with $v_\Sigma = 3$ used in this example, is to lose a vibration quanta in each step, resulting to the accumulation in the $v_\Sigma = 0$ state shown in (c).

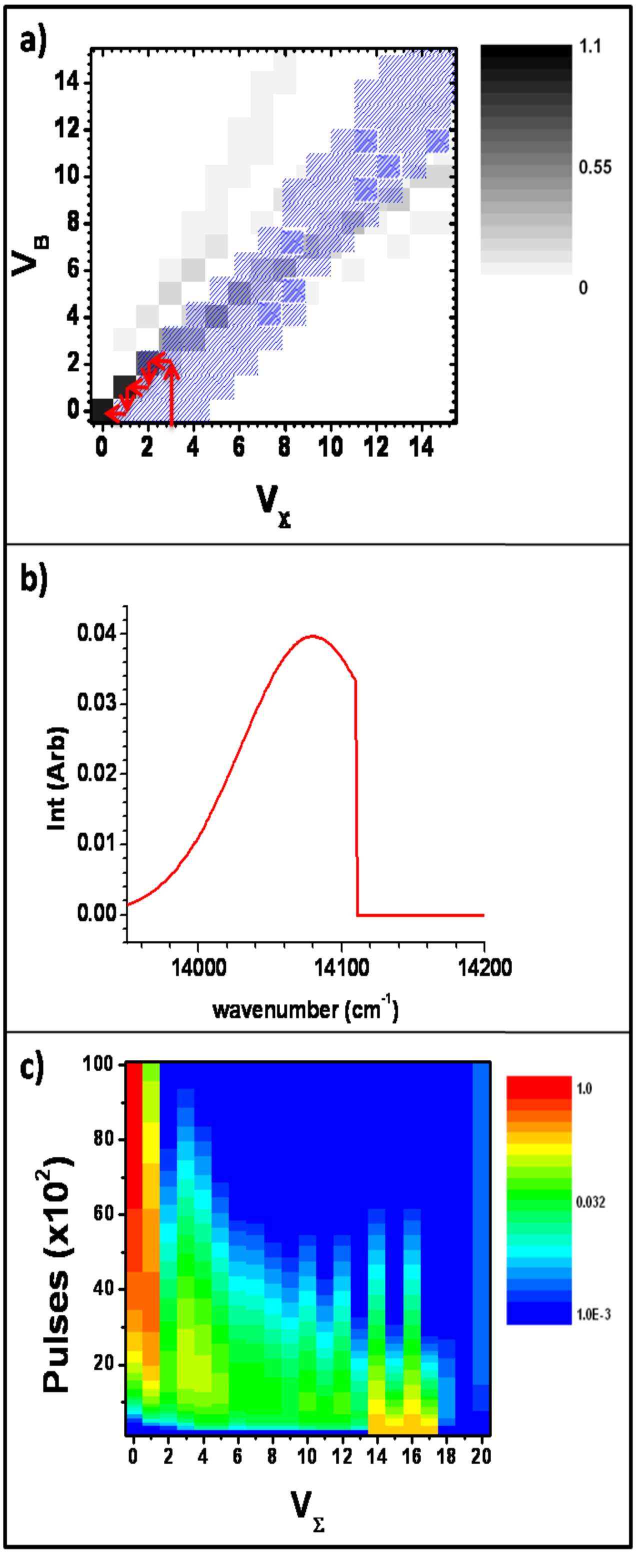

Fig. II.6.2.a.4: (a) Franck-Condon parabola corresponding to the $a^3\Sigma_u^+$ to the $(2)^3\Pi_g$ state transitions, in gray scale, while in blue are marked the transitions excited by the shaped pulse shown in (b). In (c) we see a simulation of vibrational cooling in these conditions which leads to the accumulation of ~91% of the molecules in the ground vibrational state.

II.6.2.b. Experimental study

Theoretical considerations like this, motivated us to study experimentally the possibility of vibrationally cooling the $a^3\Sigma_u^+$ molecules, using the $(2)^3\Pi_g$ state as the excited state of the optical pumping scheme. As always, the study of vibrational cooling is done via comparison of the vibrationally resolved REMPI spectra obtained in the presence and in the absence of the cooling radiation. In Fig. II.6.2.b.1, we see a set of experimental results, corresponding to this study. The study is done in two different detection frequencies. In the first range, between ~15900 and ~15950 cm^{-1}, triplet molecules can be detected via a REMPI ionization, with the position of the spectroscopic lines having been assigned to vibrational levels in [Diem91], while for the assignment of the vibrational levels in the ~14000 cm^{-1} detection, the reference [Kim93] is used.

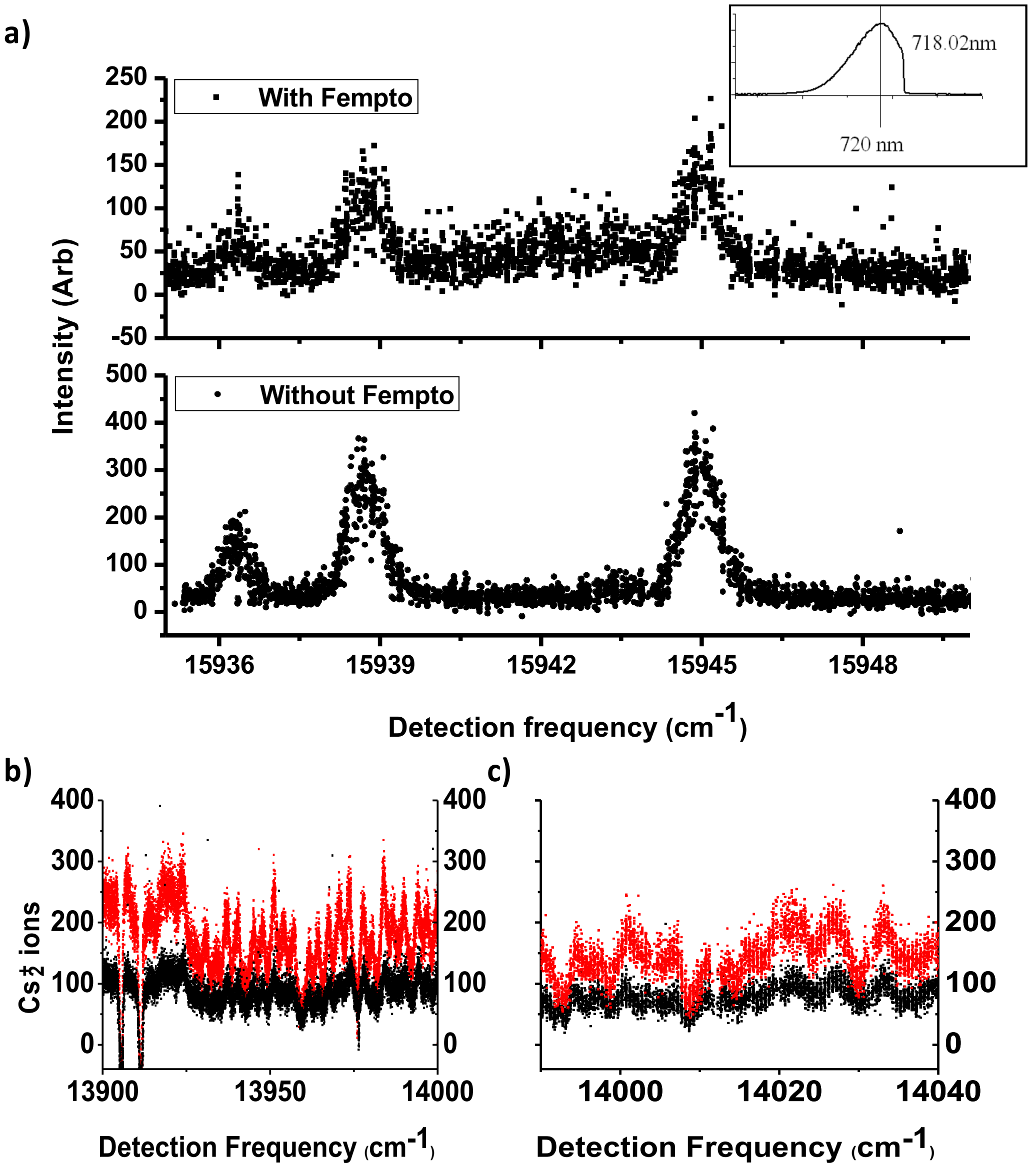

Fig. II.6.2.b.1: Results of the experimental study for the cooling in the triplet state. (a) Ionization spectrum of the $a^3\Sigma_u^+$ molecules in the area of 15950 cm^{-1}, where the assignment of the vibrational levels is done according to [Diem91]. (b) Similar spectra in the area of 14000 cm-1, where the assignment is done according to [Kim93].

Nevertheless, the exact position of each spectroscopic line in Fig. II.6.2.b.1 is of small significance. What is of importance here, is that in all these spectra, no structural difference between spectra acquired in the presence and in the absence of the femtosecond radiation is observed, but only the spectra acquired in the presence of the cooling field have somehow reduced signal. This means that the molecular population that was initially excited, did not return to the triplet state to be redistributed among different vibrational levels. In perhaps the most promising data set presented in part (a), very few, if any, molecular population is detected in a spectroscopic position different than the initial one.

II.6.2.c. Interpretation of the results

In this paragraph, I describe my efforts to explain the inconsistency between the theoretical predictions and the experimental results concerning vibrational cooling of the $a^3\Sigma_u^+$ molecules. Our first attempt to demonstrate vibrational cooling using a transition different from the $X^1\Sigma_g^+$ - $B^1\Pi_u$ used so far, was not successful. However, this gives us the opportunity to study all the parameters that could result to a failure of the optical pumping process, which could be of great value towards the generalization of the vibrational cooling technique to include other molecules. Among the possible reasons we consider the transition dipole moment, ionization, parasitic coupling (here to the $(2)^3\Sigma_g^+$ potential), hyperfine structure and losses due to spontaneous emission.

Dipole moment

One of the first considerations was to improve our theoretical description by including the dipole moment in the production of the related Franck-Condon parabola. Information on the transition dipole moment was not available to us initially, but the calculation was carried out by Nadia Baloufa and the resulting, slightly alternated Franck-Condon-dipole parabola[1] is shown in Fig. II.6.2.c.1 (a). The simulation of vibrational cooling with a simple shaping similar to the one shown in Fig. II.6.2.a.4 (b) is shown in part (b), and it shows that the alternations introduced to the Franck-Condon parabola due to consideration of the transition dipole moment, do not explain the experimental results presented in Fig. II.6.2.b.1.

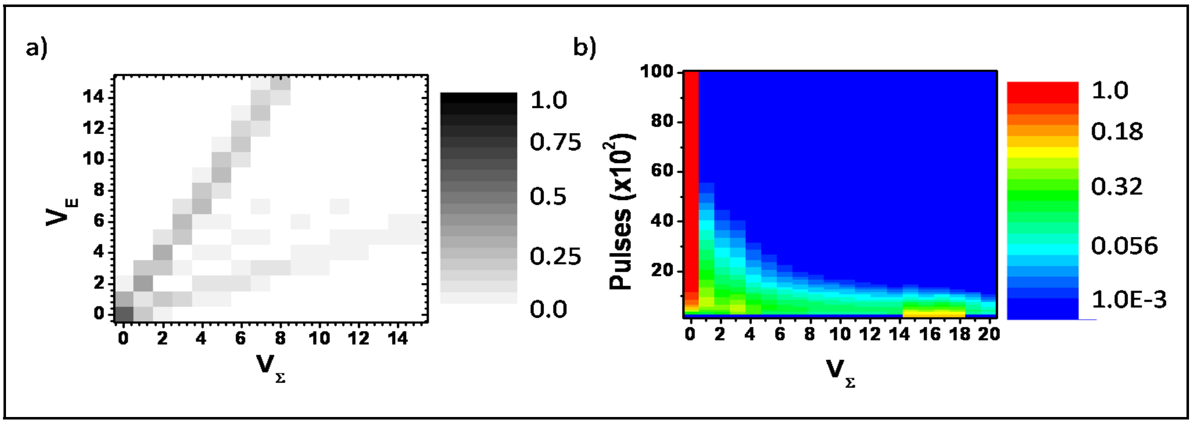

Fig. II.6.2.c.1: (a) FC-dipole parabola for the $a^3\Sigma_u^+$ to the $(2)^3\Pi_g$ state transition, in the calculation of which the transition dipole moment is included. (b) Simulation of vibrational cooling with a pulse similar to the one described in Fig. II.6.2.a.4(b).

---

[1] The use of the term Franck-Condon is not valid here. This is due to the fact that the coefficients from which the plot now is consisted, do not only include the overlap of the vibrational wavefunctions but the transition dipole moment as well. As a result, the coefficients do not sum to unity and thus cannot be seen as probabilities. The value of the dipole moment is never a very large number; usually it ranges somewhere higher than 1 and lower than 5. In general, these FC-like parabolas are still suitable for the analysis of the evolution of the system, so I introduce the name FC-dipole parabola in order to illustrate the similar use of the two, physically different plots.

Ionization

The reason for the failure of vibrational cooling might be searched in more general characteristics of our optical pumping scheme. A first important difference between this optical pumping scheme, and the one involving the $X^1\Sigma_g^+$ to $B^1\Pi_u$ transition in the singlet state, is that the femtosecond laser now can ionize the excited molecules, with absorption of an additional photon as displayed in Fig. II.6.2.c.2 (a). This means that an additional loss channel, the one of the ionization, has to be considered. An estimation of the probability of ionization by the femtosecond laser can be done with similar arguments that lead to Eq.II3.4 (calculation of the dye laser ionization probability). For conditions similar to the ones of our experiment, such an estimation would result to negligible losses due to ionization (<<0.1%). A more detailed calculation can be found in [Dion02]. We simulate the optical pumping process in the presence of ionization, by introducing losses equal to the 0.1, 0.5 and 0.8 of the excited molecules in each circle, with the results shown in Fig. II.6.2.c.2 (b). We clearly see that, ionization losses are not leading to considerable differences in the simulation's results, unless if the ionization probability is risen to an exaggerated value (80%). This, in combination to our estimations on the ionization probability, leads to the conclusion that ionization cannot explain our experimental results.

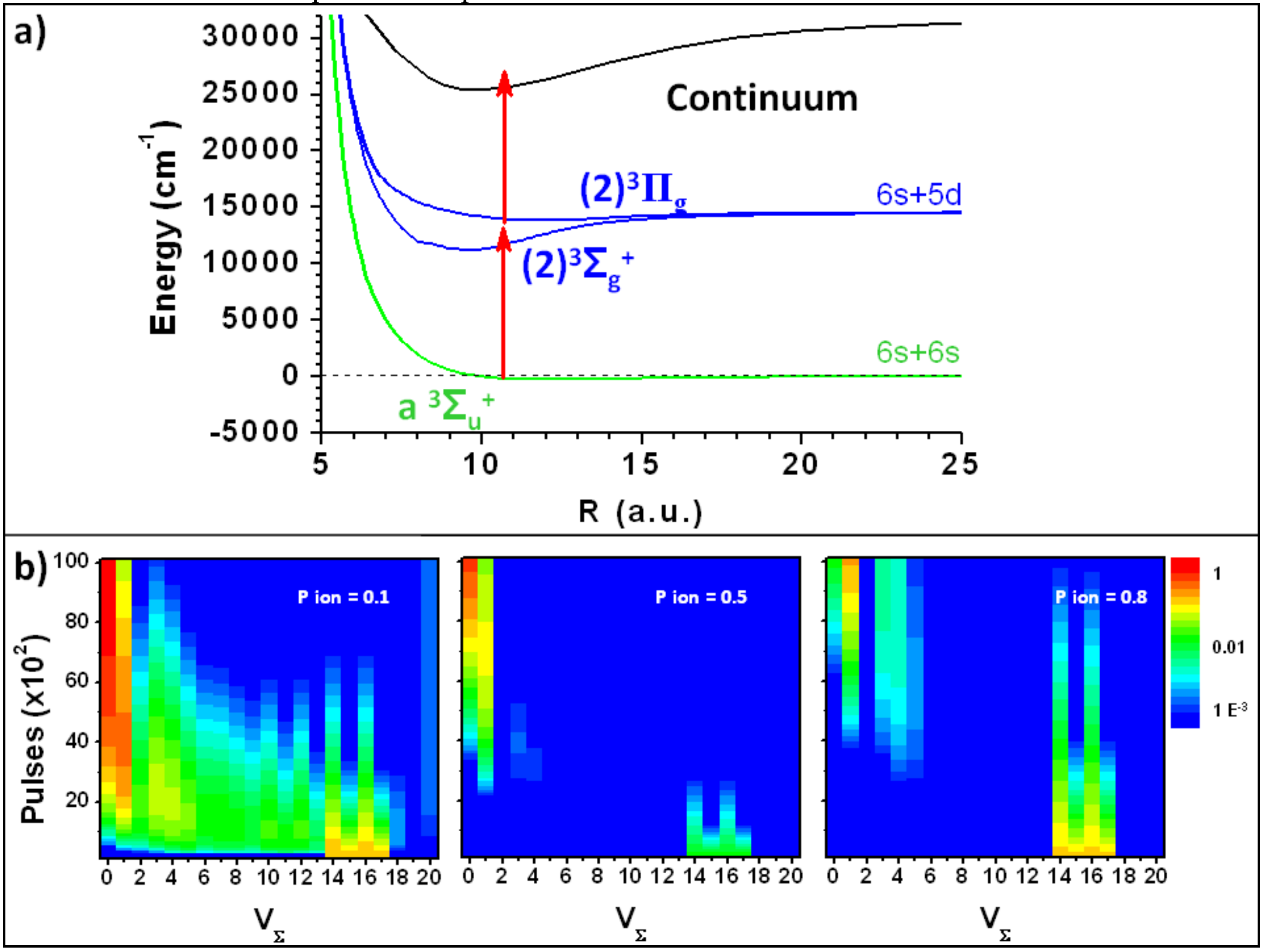

Fig. II.6.2.c.2: (a) Molecular potentials and ionization potential for the optical pumping scheme considered in this paragraph. As we see, the ~720 nm femtosecond photon can now connect the excited state to the continuum. (b) Simulations of the vibrational pumping scheme, where we consider the ionization (and thus loss) of the excited molecules with probability of 0.1, 0.5 and 0.8 respectively.

Coupling to the $(2)^3\Sigma_g$ potential

Even though ionization cannot explain the experimental results resumed in Fig. II.6.2.b.1, a similar loss channel perhaps could. It suffices to find a mechanism that removes molecular population after excitation and prevents any redistribution in the lower electronic state. In such a situation, a very small percentage of the initial molecular population is redistributed in the vibrational levels of the ground potential and no cooling can be observed.

As implied by Fig. II.6.2.a.1 were the molecular potentials are shown, a loss channel for the optical pumping between the $a^3\Sigma_u^+$ to $^3\Pi_g$ potentials can be considered to be the $(2)^3\Sigma_g^+$ potential. Indeed, the vibrational states corresponding to those two potentials are overlapping in energy for states with vibration higher than ~80 of the $(2)^3\Sigma_g^+$ potential.

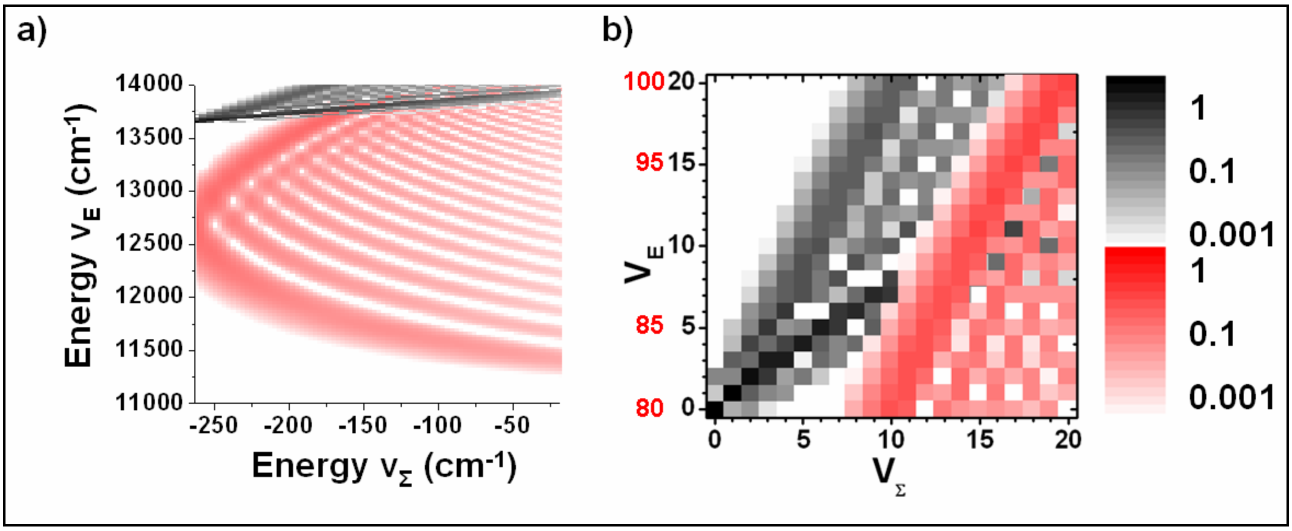

Fig. II.6.2.c.3: (a) The Franck-Condon coefficients corresponding to transitions from the $a^3\Sigma_u^+$ to the either the $(2)^3\Pi_g$ (black) or the $(2)^3\Sigma_g^+$ electronic potentials (red). The coefficients are here plotted against the energy of the transition to which they correspond. Plot of the Franck-Condon coefficients corresponding to transition from the $a^3\Sigma_u^+$ to the $(2)^3\Pi_u$ state along with the Franck-Condon parabola corresponding to transition from the $a^3\Sigma_u^+$ to the $(2)^3\Sigma_g^+$ state, for v_E greater than 80. The image intents to display the 'overlap' between those two electronic transitions.

In Fig. II.6.2.c.3 we see a plot of the Franck-Condon parabola corresponding to the $^3\Sigma^+$ to $^3\Pi_g$ transition and a plot of the Franck-Condon parabola corresponding to the $^3\Sigma^+$ to $^3\Sigma_g$ transition on top of each other. On the part (a), the Franck-Condon coefficients are plotted against energy, while in part (b) they are plotted agains vibrational number (red numbers on the vertical axis, correspond to vibration on the $(2)^3\Sigma_g^+$ potential). The aim of the picture is to express pictorially the fact that the femtosecond pulse can excite all these transitions. If we assume that the femtosecond pulse can excite molecules to both these potentials, we can consider that the part of the molecular population that was excited to the $^3\Sigma_g$ potential is lost if not at once, in few cycles. This is due to the form of the Franck-Condon parabola for the particular transition, displayed in Fig. II.6.2.a.2. It is evident that molecules excited to high vibrational levels of the $(2)^3\Sigma_g^+$ potential, will relax in the best case in v_Σ around ten, while an important part of the population will be spread to levels with $10 < v_\Sigma < 80$. The overall losses, that such a parasitic coupling can have in the overall optical pumping process, can be estimated if the excitation probability towards each excited potential is known. However, the values of the Franck-Condon parameters corresponding to the $a^3\Sigma_u^+ - (2)^3\Sigma_g^+$ transition are almost 10 times smaller than the values corresponding to the $a^3\Sigma_u^+ - (2)^3\Pi_g$ transition in similar excitation energies. Thus, if we assume almost equal probability for the excitation in the $(2)^3\Sigma_g^+$ and in the $(2)^3\Pi_g$ electronic state, we see that such a mechanism, even though could result to important losses, can not explain the total absence of vibrational population re-distribution exhibited in Fig. II.6.2.b.1.

Fine structure

The $^3\Pi_g$ potential, which is chosen as the excited potential for the optical pumping process is not a single potential, since the spin-orbit coupling 'brakes' it to four different potentials, named $^3\Pi_{0g\pm}$, $^3\Pi_{1g}$ and $^3\Pi_{2g\pm}$ respectively. This is displayed in Fig. II.6.2.c.4 were we see in (b) that the transitions to which a relatively high probability (Franck-Condon parameter) is corresponding, are separated by at least 100 cm^{-1}. This was a point that was taken into consideration before the beginning of our experimental activity; we are confident that the existence of multiple $^3\Pi_g$ potentials cannot insert problems to the optical pumping process as they are easily resolvable.

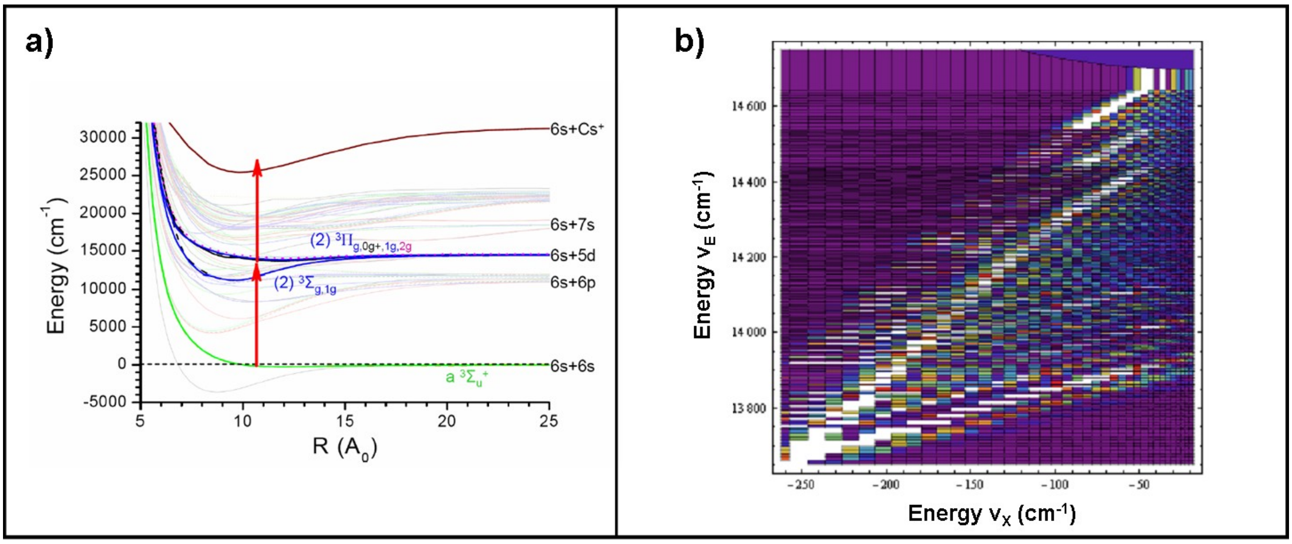

Fig. II.6.2.c.4: (a) Electronic potential involved in the optical pumping process of the experiment. We see that four (2)$^3\Pi_g$ potential could be involved, the 0g±, the 1g and 2g. (b) The Franck-Condon parameters corresponding to transitions from a$^3\Sigma_u^+$ towards any of these four potentials, traced versus transition energy. We see that the separation between the Franck-Condon parameters of relatively high value (white in this color scale) is in the order of some hundreds of cm^{-1}, and thus experimentally resolvable.

Losses due to spontaneous emission

In Fig. II.6.2.c.5 we see the potential energy curves related to our optical pumping scheme. If we suppose that spontaneous emission towards a potential different from the initial a$^3\Sigma_u^+$, is the reason for which our optical pumping scheme was not successful, this can be only towards one of the potentials emerging from the 6s+6p dissociation limit. We can consider three different cases for the spontaneous emission. One case is that the molecular population is transferred, through spontaneous emission, to a 'normal', bounding state, as the excited (2)$^3\Pi_g$ state. In this case, the molecular population can decay to the desired, ground triplet a$^3\Sigma_u^+$ state, via a second step of spontaneous emission; if these two steps can happen in relatively short time scales, the molecular population is not lost, and it is possible that the efficiency of the vibrational cooling is not severely affected. This is of course a very favorable case; to this we have to include the possibility that the molecular population relaxes towards any other level, or that the lifetime of the molecules in this intermediate state is large, and thus the molecular population is 'kept' away from the cooling cycles. As we see in Fig. II.6.2.c.5, such a possibility does not exist for our optical pumping scheme, since there is no state available.

Another possibility is that the molecular population is transferred, via spontaneous emission, to an 'anti-bounding', or dissociative state, as the one noted in Fig. II.6.2.c.5 with 'diss'. The molecular population that is transferred to these dissociating states is lost. The presence of the dissociating state shown in Fig. II.6.2.c.5 was noted when the experiment was considered, however, the small energetic distance between this state and the $(2)^3\Pi_g$ state, made us believe that the losses towards this state would not be severe.

Another interesting situation arises from the singlet-triplet complex, which is noted in Fig. II.6.2.c.5 as 'comp'. In this case, two of the potentials emerging from the 6s+6p dissociation limit are adiabatically coupled to give electronic states of mixed singlet – triplet character, and can be coupled via spontaneous emission from either singlet or triplet excited potentials. Moreover, population transferred to such a mixed potential can end up to the ground $X^1\Sigma_g^+$ singlet state via spontaneous emission, and not to the ground $a^3\Sigma_u^+$ triplet state. A realistic calculation for the probability of such a process is not going to presented here. This is the subject of a study that is now in progress [Bal09]; the preliminary results show that the probability of spontaneous emission towards one of these potentials is high (larger than 20%), a fact that would perfectly explain the experimental results summarized in Fig. II.6.2.b.1. Except of explaining the results of the experimental study of cooling Cs molecules in the $a^3\Sigma_u^+$ state, such a theoretical study finds motivation in the possibility of providing with a mechanism to transfer the large numbers of molecules initially created in the $a^3\Sigma_u^+$ potential by photoassociation, to the ground electronic $X^1\Sigma_g^+$ singlet state.

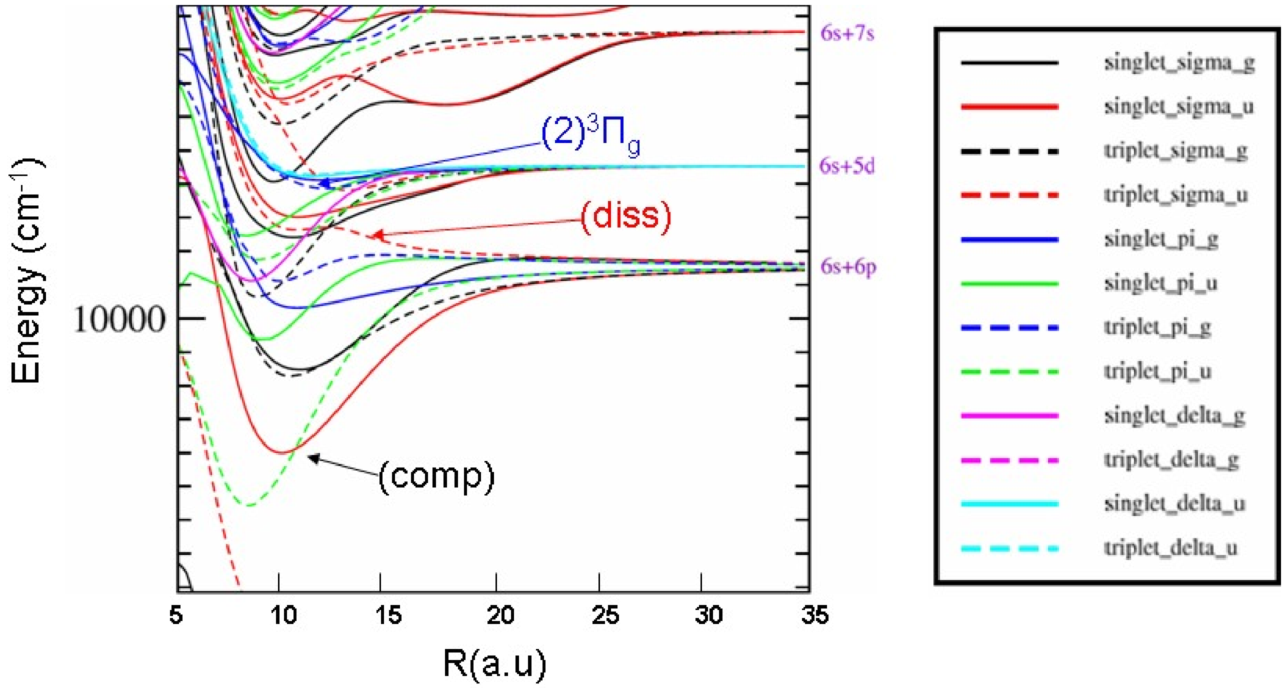

Fig. II.6.2.c.5: Potential energy curves (PECs) of the Cs_2 molecule, emerging from the 6s+6p, 6s+5d and the 6s+7s dissociation limit. The position of the $(2)^3\Pi_g$ PEC is noted, as well as the position of two important PEC cases, see text for details.

Summary

In this paragraph, I analyzed the various reasons that could result to the failure of the optical pumping considered for the cooling of $a^3\Sigma_u^+$ triplet state. Among the various reasons considered here, what it seems to be the explanation is the presence of a loss channel (spontaneous emission) towards an adiabatic potential emerging from the 6s+6p dissociation limit. Such a 'leak' in the optical pumping is enough to destroy process, as it would also do in the case of atoms, since the chosen transition would not be closed.

All the assumptions considered in this paragraph, can be useful for the understanding of the disagreement between the theoretical predictions resumed in Fig. II.6.2.c.1 and Fig. II.6.2.a.4 and the experimental results resumed in Fig. II.6.2.b.1. Moreover, they indicate that there are more parameters, apart from the Franck-Condon parabola, that can be proved determinant for the realization of vibrational cooling. Having this in mind, can be useful in the study of the generalization of the vibrational cooling technique towards heteronuclear molecules that follows.

II.6.3. Study of the applicability of vibrational cooling to heteronuclear molecules.

In this paragraph, I study the generalization of the vibrational cooling technique towards other molecular systems and in particular heteronuclear molecules. The molecule which I use as the example for this study is NaCs. The study is consisted in choosing the electronic transition for the optical pumping, based on the criteria outlined in the beginning of this chapter, producing the corresponding Franck-Condon parabola and using it in order to simulate the optical pumping process.

The choice the of NaCs molecule is mostly related to the availability of the molecular potentials and transition dipole moments, which were calculated by members of the theoretical group of Cold Molecules in the laboratory [Aym07]. The interest in heteronuclear molecules is very big, since they are promising candidates for a variety of exotic applications, such as the observation of large scale dipole blockade for quantum computation experiments, or as realizations of probes for the measurement of the permanent Electron Dipole Moment (EDM). In particular, NaCs is one of the most promising molecular systems, while it has been prepared in low ro-vibrational states and has been electrostatically trapped [Klei07b]. For these reasons, the NaCs molecule is the molecule studied in most detail, while the NaRb and NaK molecules are discussed for comparison. This study can be expanded to other, promising heteronuclear molecules, like LiCs or CsRb.

II.6.3.a. Choice of electronic transition

In Fig. II.6.3.a.1 we see the low singlet and triplet electronic states in the NaCs molecule [Doce04]. The objective here, is to try to find the most suitable transition for optical pumping, and eventually, for vibrational cooling, with the help of the argumentation developed in the first part of this chapter. We see that some of the most suitable states for the realization of vibrational cooling are the lower lying Π states, since the minimum of these potentials is relatively close to the minimum of the potential of the ground state. Having in mind the selection rules for optical transitions in molecules presented in Chapter I, we focus in the singlet Π potentials, in which we could excite efficiently molecular population originating from the fundamental state.

An important difference between the behavior that heteronuclear molecules exhibit with respect to the homonuclear ones, is the breakdown of the g → u symmetry selection rule (see Chapter II 1). This has as an effect that the excited state can now be coupled to much more states lying between this and the fundamental state, increasing dramatically the number of 'loss channels' for most of the cases.

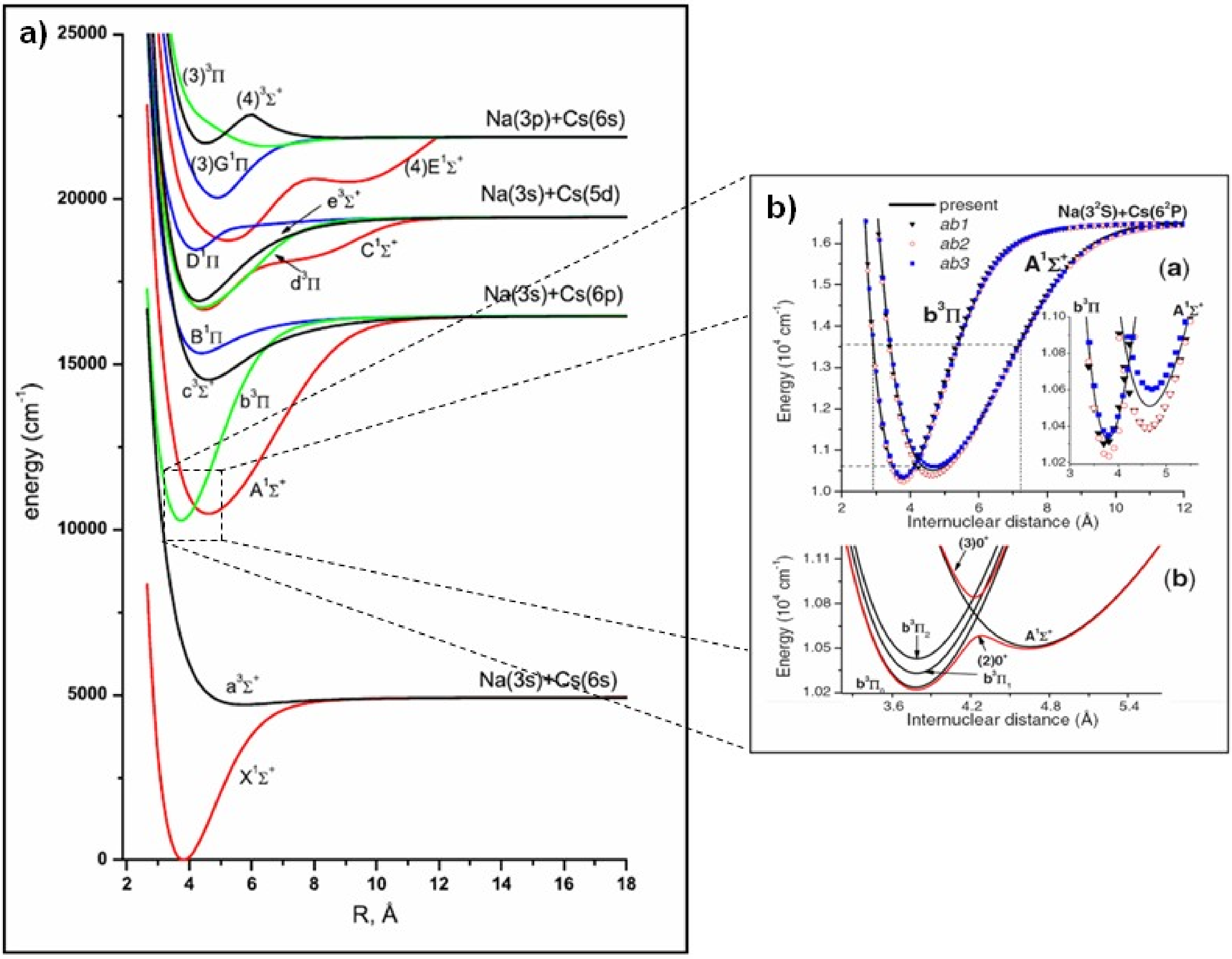

Fig. II.6.3.a.1: (a) Low singlet and triplet electronic states in NaCs. Figure adapted from [Doce04] (b) *upper graph*: The present empirical and available ab-initio PECs for the A $^1\Sigma^+$ and b $^3\Pi$ states. *lower graph*: The present diabatic PECs of the A $^1\Sigma^+$ and b $^3\Pi$ states and their adiabatic counterparts $(2,3)\Omega = 0^+$. Figure adapted by [Zaha09].

Let us start thinking on which of the potentials presented in Fig. II.6.3.a.1 could be useful in a vibrational cooling scheme. We focus our attention to singlet states; the triplet states are also shown since they could cause 'parasitic' coupling and lead to losses. This is the case of the $A^1\Sigma^+$ state for example. This state is strongly coupled to the nearby $b^3\Pi$ state, to the point that those two states form a 'complex', which has both singlet and triplet character. The situation is pictorially presented inFig. II.6.3.a.1.b, while the new potential energy curves (PECs) resulting from this coupling have been calculated in [Zaha09]. Thus, excitation to the $A^1\Sigma^+$ state would result to severe loss of population towards the $a^3\Sigma^+$ triplet state due to spontaneous emission. The remaining candidates are the singlet $^1\Pi$ states. As far as losses are concerned, the choice of the first $^1\Pi$ state is the most conservative. This state can relax towards the ground $X^1\Sigma^+$ state and the $b^3\Pi$- $A^1\Sigma^+$ complex, which is, of course a loss channel. However, these losses are expected to be minimized with the choice of the first $^1\Pi$ state with respect to the higher $^1\Pi$ states, especially due to the transition frequency which is smaller. In the following paragraph we will construct the FC-dipole parabolas for the first four $^1\Pi$ states, however, it is only with the first two that we will attempt simulations on vibrational cooling.

II.6.3.b. Production of the FC-dipole parabola

The study was made with the use of the Potential Energy Curves (PECs) and transition dipole moment information, which was provided by O.Dulieu and is shown in Fig. II.6.3.b.1. In part (a) we show the potential energy curves which correspond to the transition between the first $^1\Sigma^+$ ground state and the first $^1\Pi$ state. In part (b) we see the dipole moments which correspond to transitions between the 1 $^1\Sigma^+$ and the first five excited $^1\Pi$ states.

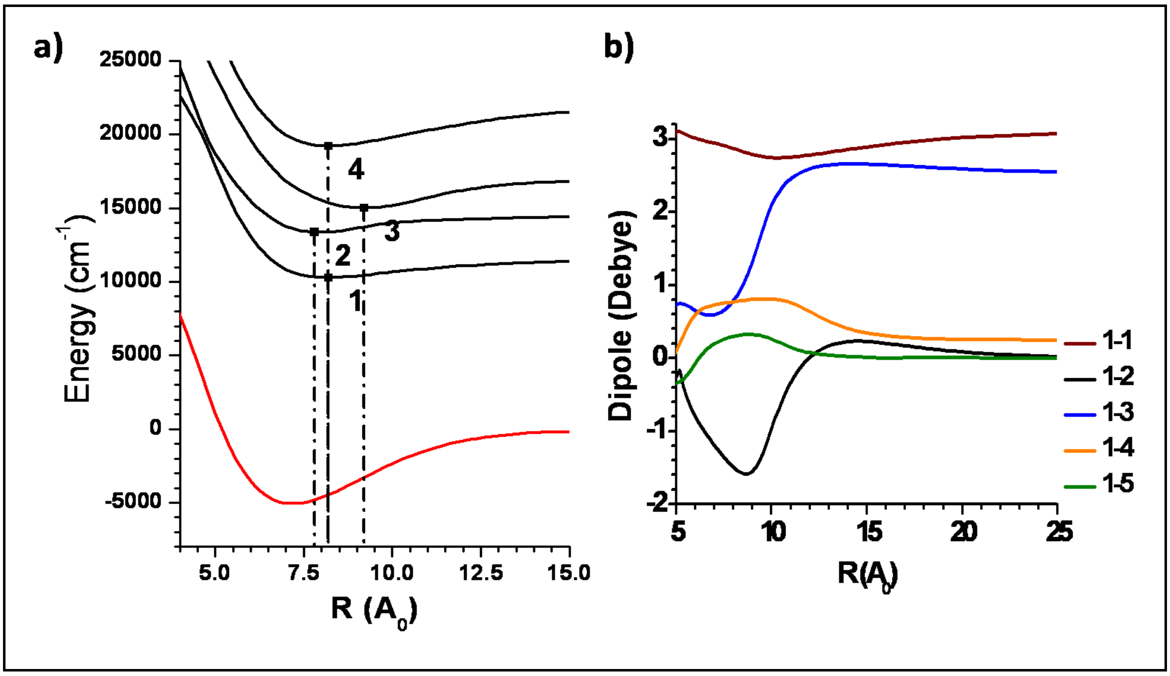

Fig. II.6.3.b.1: (a) Potential Energy Curves (PECs) of NaCs for the transitions between the first $^1\Sigma$ and the first four $^1\Pi$ states, while the corresponding transition dipole moments are shown in (b). Data available by [Aym07].

The variation of the dipole moment associated with the particular transition obliges to include it in the our calculations. The way this is done, is to include it in the calculation of the Franck-Condon parabola with the use of the OVERLAP[1] program. Strictly speaking, the Franck-Condon coefficients do not include dipole moment but are produced simply by the overlap of the vibrational wavefunctions. The Franck-Condon parabolas used in the following paragraphs are thus generalized and should be noted differently. Thus, I introduce the similar term FC-dipole parabola; both for convenience and to express its similar use for the description of the dynamics of optical pumping.

The potential energy curve corresponding to the transition between the first 1 $^1\Sigma^+$ ground state and the first excited $^1\Pi$ state, is shown in more detail in Fig. II.6.3.b.2 along with the corresponding energy levels and wavefunctions of the first five vibrational levels. As we see, the wavefunctions are centered in different internuclear distances, as expected by the large separation between the equilibrium distances of the two involved potentials, which we note that is not the smallest among the $^1\Pi$ potentials.

---

[1] OVARLAP is the name of the FORTRAN program used to calculate the overlap between the vibrational states and thus provide with the Franck-Condon coefficients. It uses as input numerical expressions for the vibrational wavefunctions of the involved potentials calculated by the GRID program. A brief description of this software is given in the Annex II2.

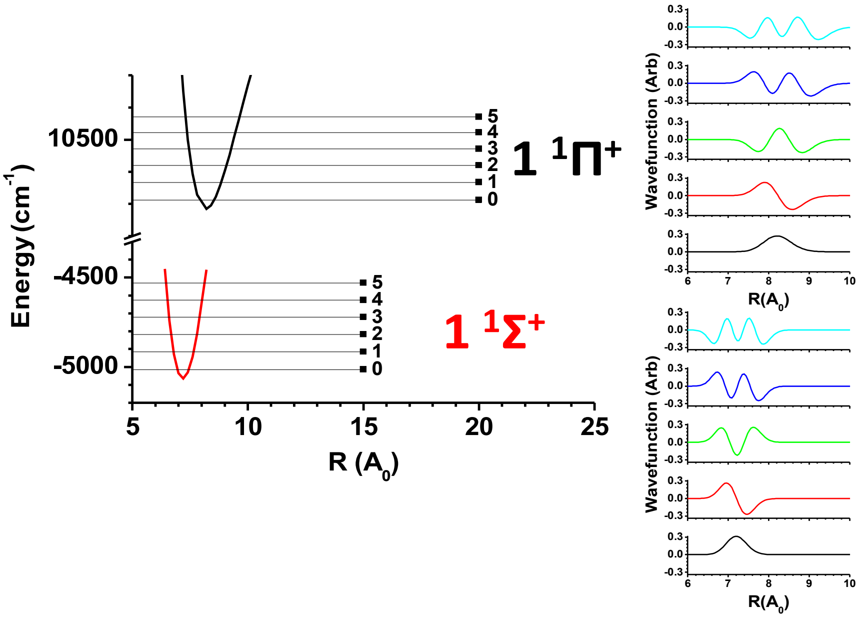

Fig. II.6.3.b.2: Potentials of the 1 $^1\Sigma$+ and 1 $^1\Pi$ states along with the corresponding energy levels and wavefunctions of the first five vibrational states.

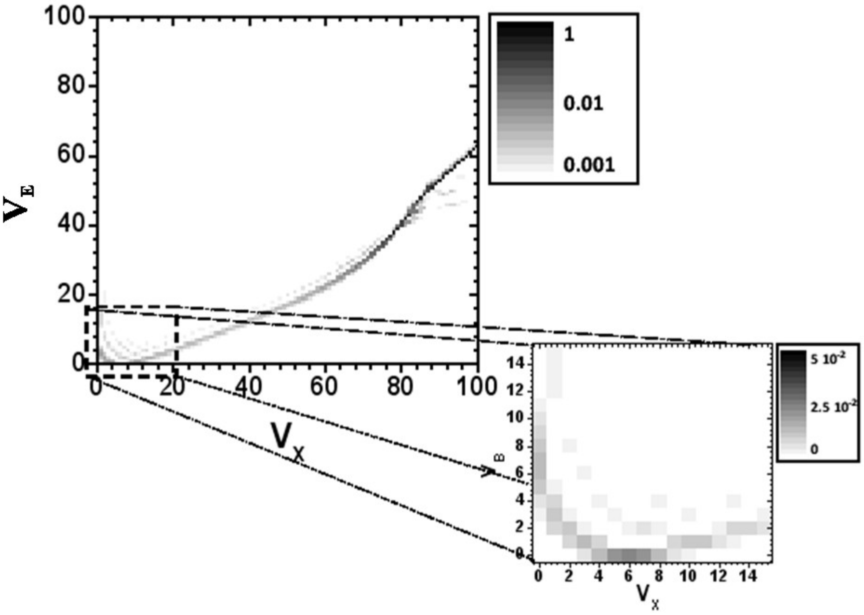

Fig. II.6.3.b.3: FC-dipole parabola corresponding to transition from the 1 $^1\Sigma^+$ to the 1 $^1\Pi$ state. In the upper part, we see the hole parabola for the first 100 states in a logarithmic scale, while in the lower left part, a zoom in the first 15 states, in a linear scale.

This important separation between the potential minima of almost one atomic unit is expected to lead to small overlap, and thus, to small Franck-Condon factors, at least between states of low vibration. Indeed, as seen in the lower right part of Fig. II.6.3.b.3 in the magnified part, the Franck-Condon factors corresponding to transitions from and towards $v < 2$ are very low. This makes population transfer to these states difficult, since it is difficult to connect them to other nearby states by optical pumping. The separation is reduced if the choice of the excited potential was the second $^1\Pi$ state. The lower part of this potential along with the ground $^1\Sigma^+$ potential and the corresponding energy levels and wavefunctions can be seen in Fig. II.6.3.b.4.

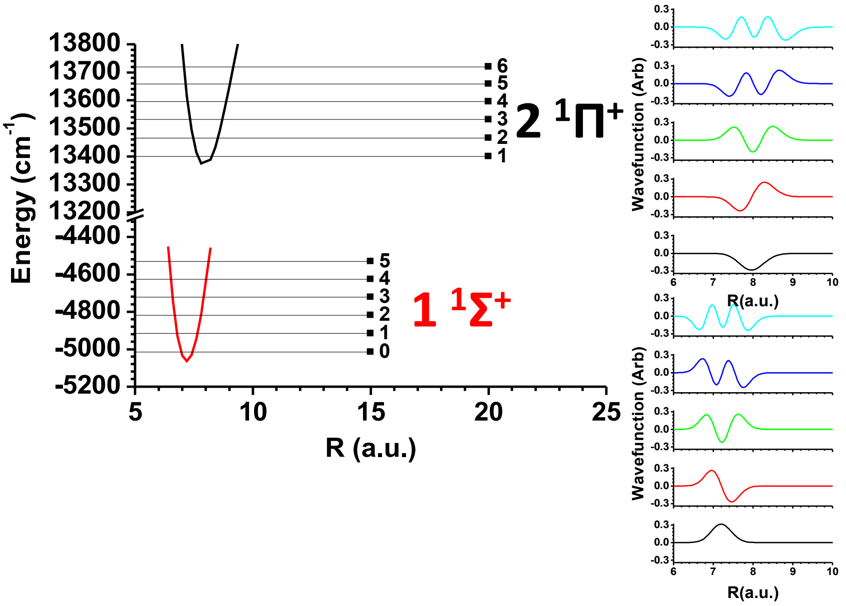

Fig. II.6.3.b.4:Potentials of the 1 $^1\Sigma^+$ and 2 $^1\Pi$ states along with the corresponding energy levels and wavefunctions of the first five vibrational states.

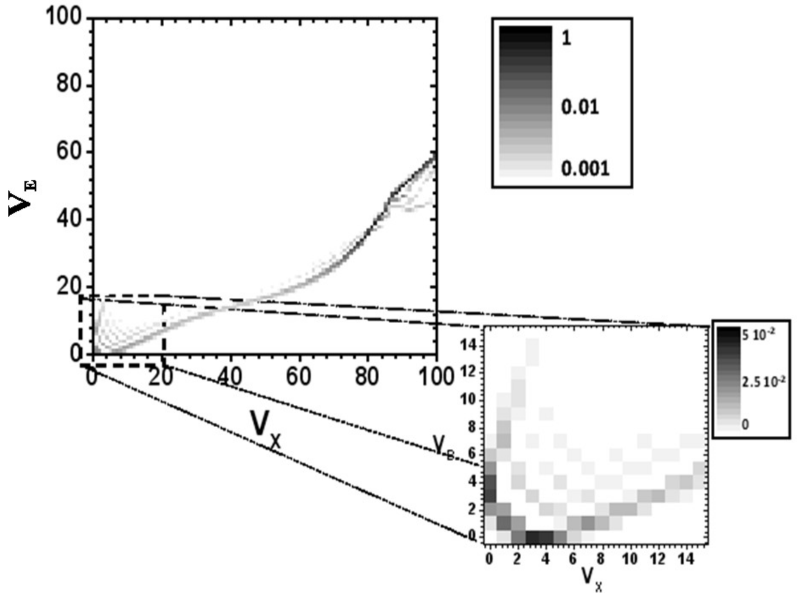

Fig. II.6.3.b.5: FC-dipole parabola corresponding to transition from the 1 $^1\Sigma^+$ to the 2 $^1\Pi$ state. In the upper part, the hole parabola for the first 100 states in a logarithmic scale, while in the lower left part, a zoom in the first 15 states, in a linear scale.

Note that this separation between the potential minima is the smallest between the ground $^1\Sigma^+$ potential and any $^1\Pi$ potentials. This has an impact in the wavefunctions, which now appear to be more closely centered than in the previous case. The corresponding FC-dipole parabola is shown in Fig. II.6.3.b.5. As we see, the 'hole' in the low vibration states in the FC-dipole parabola is reduced. Nevertheless, the ground vibrational levels of the two potentials hardly overlap resulting to a small Franck-Condon coefficient for the particular transition.

The two remaining choices among the $^1\Pi$ potentials shown in Fig. II.6.3.b.1.a, are expected to be less promising, due to the larger separation between their minima with respect the one of the ground state. This is shown in Fig. II.6.3.c.1(a), while the corresponding FC-dipole parabola are shown in (b). The even larger separation between the potential equilibrium distances, especially in the case of transition toward the 3 $^1\Pi$ potential, lead to very low Franck-Condon factors for the low lying vibrational states.

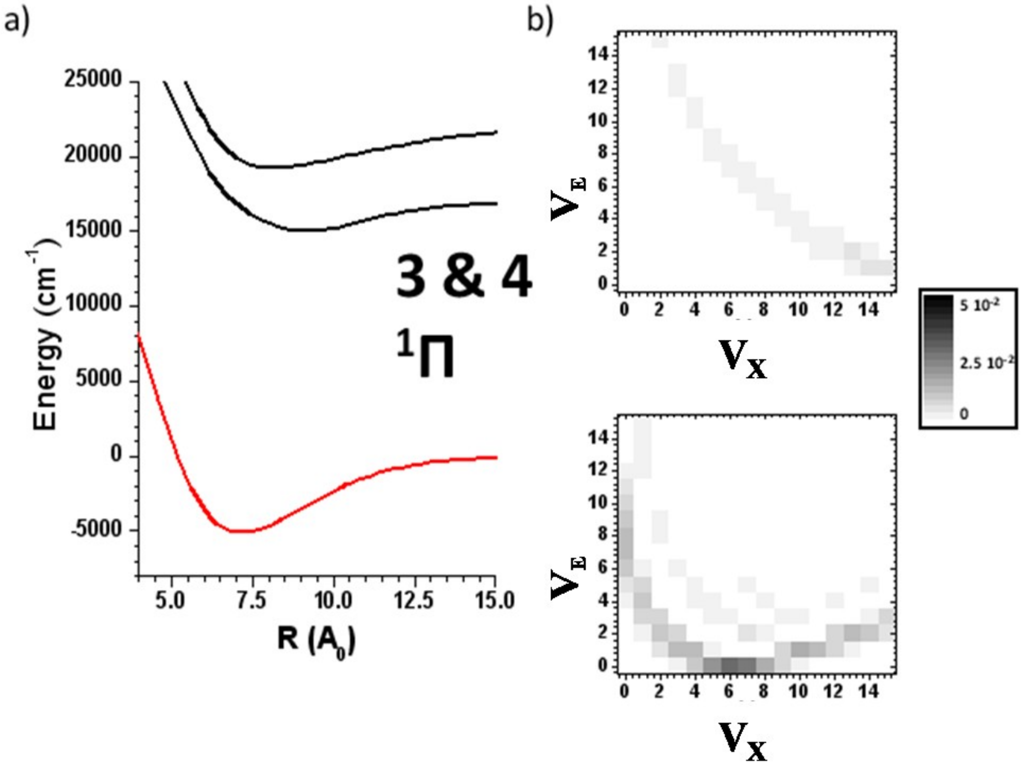

Fig. II.6.3.b.6: (a) Molecular potential curves of the $^1\Sigma^+$ ground state and the 3 and 4 $^1\Pi$ states. (b) FC-dipole parabola corresponding to transition from the $^1\Sigma^+$ ground state to the 3 $^1\Pi$ state (upper part) and the 4 $^1\Pi$ (lower part)

II.6.3.c. Simulations of optical pumping

We saw that the large separation between the equilibrium points of the ground $^1\Sigma^+$ potential and the excited $^1\Pi$ potentials, leads to reduced overlap between low vibrational states and thus to FC-dipole parabola with a 'hole' in the corresponding positions. This separation is reduced in the case where the 2 $^1\Pi$ potential is chosen as the excited state, and as it leads to a FC-dipole parabola which is more suitable for vibrational cooling. However, if we take into consideration coupling to other molecular potentials due to spontaneous emission, the choice of the first excited $^1\Pi$ state is more reasonable, since with such a choice we minimize the 'loss channels', and our optical pumping transition is as closed as possible.

Pumping with an unshaped pulse

As an initial step for the study of vibrational cooling in NaCs, we choose to simulate the excitation of the chosen $^1\Sigma^+ \rightarrow 1\ ^1\Pi$ transition by an unshaped, broadband pulse. This way, we can see if optical pumping is feasible; if this is not the case then vibrational cooling cannot be realized in this transition. In the simulations I consider a pulse with a bandwidth that is ~10 times bigger than the one used in the case of Cs_2. It is clear that bigger bandwidth leads to more efficient optical pumping (less population transferred to high vibrational states), as long as there are no frequency components that excite population to other, closely lying potentials. Radiation of such bandwidth can be available, for example by the use of super-continuum sources.

In the left column of Fig. II.6.3.c.1 we consider the effect of an unshaped pulse on the molecular population. In (a), we see the broadband radiation considered for this simulation. This radiation is also shown in (b), where with the red hatched squares I indicate which vibrational transitions are lying in the band where the Gaussian intensity has dropped to the 0.001 of its maximum value. The FC-dipole parabola of the $^1\Sigma^+ \rightarrow 1\ ^1\Pi$ transition is also shown.

In part (c) we see the result of the simulation. The molecular population is initially equally distributed in the first 10 vibrational levels (10% each). We see that the 'hole' of the FC-dipole parabola in the low lying vibrational states prevents efficient pumping prevents efficient excitation, and the molecular population of these states hardly changes. A part of the molecular population should be redistributed in lower vibrational states while a big part is transferred to high-lying vibrational states, which are out of the pumping radiation's spectra and thus exit the system. The simulation result should be a dynamic equilibrium between these processes.

Simple Shaping

The previous simulation, as well as shape of the Franck-Condon parabola in this particular transition, suggests that the simple shaping used in [Vit08] would not lead to efficient population transfer, as displayed in the middle column of Fig. II.6.3.c.1. As we see in this figure, removing the frequency components that can excite the $v_X = 0$ vibrational level hardly changes the result. This is easy to understand: The shaping that we introduce has the objective to make the $v_X = 0$ state a dark state of the system, so that it no longer interacts with the optical pumping radiation. However, this is already the case, since the small values of the Franck-Condon coefficients in the lower left part of the parabola have already isolated this and the nearby states.

Optimized shaping

In the previous examples, we saw that the particular shape of the FC-dipole parabola, does not allow realization of optical pumping with the use of simply shaped pulses. A different choice for the optical transition could perhaps lead to better results, but the restrictions indicated in the first paragraph of this chapter do not leave many other candidates for the excited potential.

However, the situation is improved if optimized pulses, like the ones described in chapter IV, are considered for the optical pumping. The use of such an optimized pulse is shown in the right column of Fig. II.6.3.c.1, however, the objective here is the transfer of all the molecular population in a particular vibrational state, not necessarily the fundamental one. The choice of the target state is here the state $v_X = 6$. One reason is that the value of the Franck-Condon coefficient is maximized for the $v_X = 6 \rightarrow v_X = 0$ transition. Additionally, the system seems to have a 'natural tendency' for accumulation in this state, as indicated by the form of the FC-dipole parabola.

The optimized pulse is shown in the right column of Fig. II.6.3.c.1.a. The idea behind this shaping is, as in Chapter IV, to try to excite these transitions that would favorably decay to the target or to nearby states. The transitions chosen be such a shaping are shown in part (b) and the result of the simulation in part (c). As we see, a big percentage of the initial molecular population (63,9%) is pumped to the target state, while an important part of the remaining population is left in the low lying states due to the small values of the corresponding Franck-Condon coefficients. In all cases, I consider that the shaping is done to a Gaussian pulse, thus I do not consider arbitrary power for each chosen transition. The ability to pump harder the states of low vibration could improve the overall result. Such a scheme manages to assemble the molecular population, that was initially spread over 10 vibrational states into a single one. From this point, population transfer to the ground vibrational state can be achieved, for example with the use of a single STIRAP step.

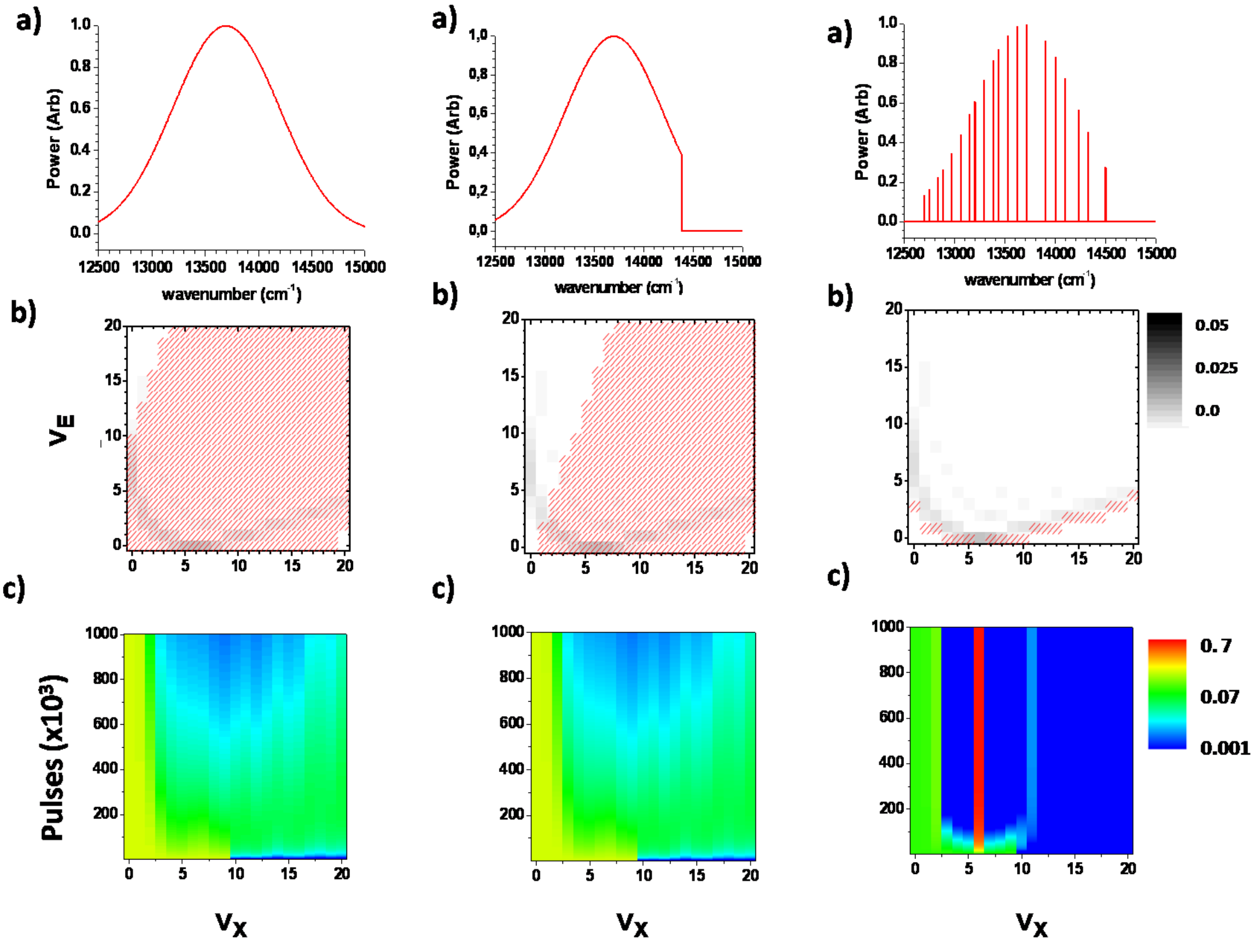

Fig. II.6.3.c.1: LEFT: (a) The pulse used in the simulation. (b) The FC-dipole parabola in a logarithmic gray-scale while the red squares correspond to transitions addressed by the pulse shown in (a). (c) Simulation with the initial molecular population equally distributed in states with $v_X = 0 - 9$. MIDDLE: (a) The pulse from which we simply remove any frequency equal or larger than the $v_X = 0 \rightarrow v_A = 0$ transition. (b) The FC-dipole parabola in a logarithmic gray-scale while the red squares correspond to transitions addressed by the pulse shown in (a). (c) Simulation with the initial molecular population equally distributed in states with $v_X = 0 - 9$. RIGHT: (a) The optimized pulse used in this simulation (b) The FC-dipole parabola in a logarithmic gray-scale while the red squares correspond to transitions addressed by the pulse shown in (a). (c) Simulation with the initial molecular population equally distributed in states with $v_X = 0 - 9$. The population transfer efficiency is predicted close to 64%.

Pumping through the (2)$^1\Pi$ state

In the previous paragraph, where the choice of the transition involved in the optical pumping process was discussed, we saw that the transition from the ground $^1\Sigma$ to the (2)$^1\Pi$ state is the most suitable for optical pumping, since the separation between the equilibrium positions is minimized for this choice of potentials. Until now, I chose to study in detail the possibility of optical pumping in the transition from the ground $^1\Sigma$ to the (1)$^1\Pi$ state, since I wanted to make a choice which would minimize the possibility of spontaneous emission destroying the optical pumping process, as it was most probably the case for the triplet Cs_2 experiment. The answer on whether spontaneous emission from the (2) to the $(1)^1\Pi$ state, as well as to the $b^3\Pi$- $A^1\Sigma^+$ complex is important, can be given by a calculation similar to one in progress for Cs_2 [Bal09], and should be included to the theoretical preparation of a vibrational cooling experiment of NaCs.

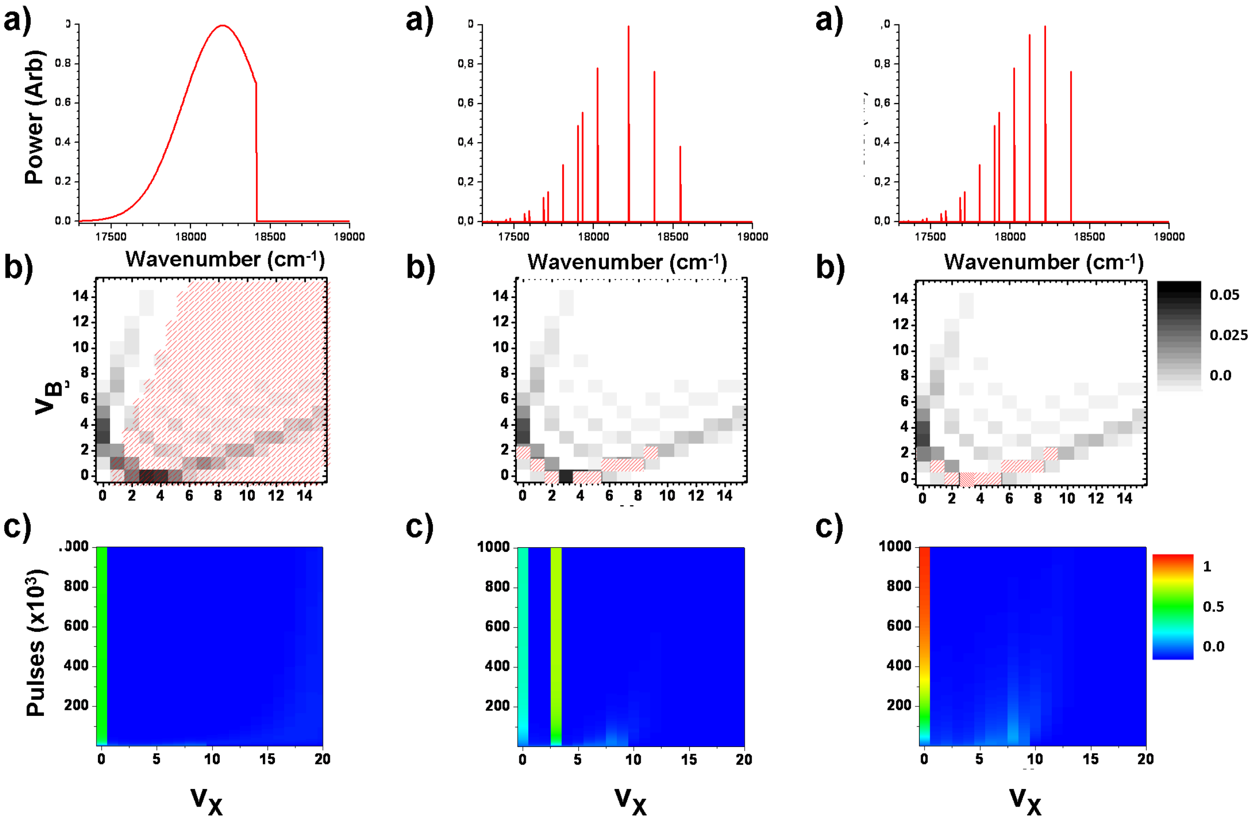

Fig. II.6.3.c.2: LEFT: (a) A simply shaped pulse is used in this simulation. All the frequency components that can excite the v_X=0 level are removed.(b) The FC-dipole parabola in a linear gray-scale while the red squares correspond to transitions addressed by the pulse shown in (a). (c) Simulation with the initial molecular population equally distributed in states with $v_X = 0 - 9$. After the vibrational cooling, the molecular population in the $v_X = 0$ level has risen from 10% to 51%. MIDDLE: (a) An optimized pulse to transfer the molecular population in the $v_X = 3$ level. (b) The FC-dipole parabola in a linear gray-scale while the red squares correspond to transitions addressed by the pulse shown in (a). (c) Simulation with the initial molecular population equally distributed in states with $v_X = 0 - 9$. The molecular population transferred to the $v_X = 3$ level is now equal to 66% of the total population. RIGHT: (a) The optimized pulse used in this simulation is the same as previously, only that now, $v_X = 3$ is not a dark state while $v_X = 0$ is (b) The FC-dipole parabola in a logarithmic gray-scale while the red squares correspond to transitions addressed by the pulse shown in (a). (c) Simulation with the initial molecular population equally distributed in states with $v_X = 0 - 9$. The population transfer to $v_X = 0$ is predicted close to 95%.

In Fig. II.6.3.c.2 we see the results of a simulation of vibrational cooling in NaCs, with the $(2)^1\Pi$ state as the excited state of the optical pumping process. The pulses have Gaussian shape and similar intensity as the ones considered in Fig. II.6.3.c.1, while the initial vibrational population distribution is the same. No spontaneous emission towards a potential other than the ground $^1\Sigma$ state is taken into consideration. In the left column, I consider cooling with a simply shaped pulse, where all the frequencies that can excite population in the $v_X = 0$ state have been removed. As we see in part (c) of this column, this pulse can transfer ~50% of the total molecular population to the ground vibrational level. If an optimized pulse like the one considered in the left column of Fig. II.6.3.c.1 is used, then an even higher percentage of ~66% can be transferred to the level with $v_X = 3$. This is now the level with the highest Franck-Condon coefficient, and the pulse considered here, follows the natural tendencies of the FC-dipole parabola, in a similar manner as the pulse of Fig. II.6.3.c.1, right, (a). A percentage of ~10% is left to the $v_X = 0$ state; the small value of the Franck-Condon coefficient corresponding to the $v_X = 0 \rightarrow v_B = 0$ transition does not permit to efficiently pump molecular population out of this state. However, the difference between this FC-dipole parabola and the one corresponding to the $(1)^1\Sigma \rightarrow (1)^1\Pi$ transition is that the $v_X = 0$ can be coupled to other vibrational states, since other Frack-Condon coefficients, like the ones connecting it to $v_B = 3$ or 4 have high values. This permits us to do the following trick displayed in the right column of Fig. II.6.3.c.2. Here we use a pulse which is identical to the one used in the middle column, except that the transition $v_X = 3 \rightarrow v_B = 0$ is now addressed, while the $v_X = 0 \rightarrow v_B = 2$ is not, and thus the $v_X = 0$ is now a dark state. This pulse is optimized to transfer molecular population to the $v_X = 3$ vibrational level; however, the frequency component addressing the $v_X = 3 \rightarrow v_B = 0$ transition manages to 'steal' the molecular population from this level and to bring it to the $v_X = 0$ dark state where it is accumulated. Such a pulse results to the transfer of ~95% of the total molecular population to the ground vibrational level.

II.6.4. *Conclusion & Perspectives*

In this paragraph, I consider the extension of the vibrational cooling technique to different choice of molecular potentials and eventually different molecular systems. This is done, on the one hand, in order to explain the results of the study of cooling molecules in the $^3\Sigma^+$ triplet state and, on the other, to discuss the technique's generalization to heteronuclear molecules, with the NaCs as principal example.

For the case of the experiment for the cooling of Cs_2 molecules in their ground triplet $^3\Sigma^+$ state, the experimental results showed that more parameters except for the Franck-Condon coefficients, have to be taken into consideration for successful optical pumping in molecules. Among these parameters, we find that losses due to spontaneous emission have to be responsible for the failure of the optical pumping scheme. A realistic estimation of spontaneous emission in this case, is beyond the scope of this chapter, and is currently under study [Bal09]. Similar considerations lead me to focus my studies of cooling vibration in the NaCs molecule, to the $(1)^1\Sigma \rightarrow (1)^1\Pi$ transition, since for this choice, the losses due to spontaneous emission are minimized. A calculation of the branching ratios like in [Bal09] is needed in order to make the final choice, and it is considered as a necessary element of the theoretical preparation of such an experiment. Depending on which electronic potential among the (1) and (2) $^1\Pi$ is used as the excited state of the optical pumping scheme, the desired population transfer can be realized either with a simply shaped either with an optimized pulse, with the total transferred population ranging from ~50% to ~95% depending on the choice of shaping and excited state potential.

We saw that the large separation between the equilibrium points of the involved potentials, leads to very small overlap between low vibrational states and thus to small corresponding Franck-Condon values. This effect imposes serious restrictions in the ability to use simply shaped pulses, where all frequencies are removed above a give threshold. However, vibrational cooling can be considered in the context of optimized pulses as the ones described in Chapter II 4. Perhaps, more convenient Franck-Condon-dipole parabolas could be found in the case were other combinations of potentials are considered for the optical pumping.

Leaving such, more complicated studies for a future work, we note a remarkable, common characteristic of the several heteronuclear molecules studied in [Aym07], the NaCs, NaRb and NaK molecules. We see, that the separation between the minimum of the ground state and the excited $^1\Pi$

states, is always important compared to the corresponding values for the homonuclear Cs dimer. These separations are listed in TABLE I. We note that the value corresponding to the Cs dimer is the one of the X ($^1\Sigma^+$) → B ($^2\Pi$) state. This difference is essentially zero if the C ($^2\Pi$) state is chosen for the role of the excited potential. This increase in the equilibrium point separation between the ground and the excited state, seems to be due to symmetry reasons, which for the time being, I have not managed to clarify. In discussions with Viatcheslav Kokoouline, Vladimir Akouline and Romaine Gouerout, it seems that the reason can be explained with the use of Local Density Approximation theory (LDA), with which the molecular potentials are usually calculated [Murr92]. I remain in the search for a more intuitive explanation for this equilibrium point separation increase, since it seems to have important consequences in the applicability of vibrational cooling to heteronuclear molecules.

Molecule	***(X→B) Cs_2**	**NaCs**	**NaRb**	**NaK**
Δrmin (a.u.)	9.2 - 8.7 = 0.5	7.8 – 7.2 = 0.6	8.2 – 6.8 = 1.4	7.8 – 6.4 = 1.4

Table 2: Minimum equilibrium point separation between the ground and any excited state. The Cs_2 is marked with a * since the value corresponds to transition to the B state while the real minimum is almost 0 for the C state.

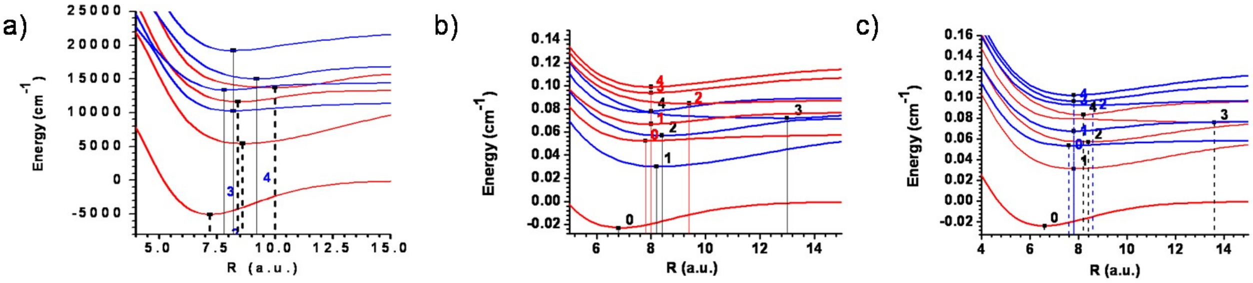

Fig. II.6.4.1: PEC of the first five $^1\Sigma$ (always red) and $^1\Pi$ (always blue) for the NaCs (a) the NaRb (b) and the NaK (c) taken by [Aym07]. The minima of the potential are noted with vertical lines.

CHAPTER II7: TOWARDS COOLING THE MOLECULAR ROTATION

II.7. TOWARDS COOLING THE MOLECULAR ROTATION

One of the most important generalizations of the vibrational pumping technique is cooling the molecular rotation. Such an extension can lead to laser cooling of molecules in their absolute ground state, and would be a major breakthrough in the field of Cold Molecules. In this chapter I discuss the various studies that took place during the last one and a half years in Laboratoire Aimé Cotton towards this direction. Due to the importance of this particular generalization of the vibrational cooling technique, it was the first generalization considered by the group. In most of the group's articles that discuss the vibrational cooling technique, there are studies of proposed schemes for the accomplishment of rotational cooling. As it is natural, the initial propositions eventually gave their place to new, more competitive schemes. However, the complete study of the various proposed schemes, gives an interesting point of view of our approach.

Thus, In this chapter I give the various approaches considered for rotational cooling in a semi-chronological order. This is a suitable choice, due to the fact that the conceptually simpler initial propositions were replaced by other, perhaps less intuitive approaches. In the first part I will discuss the initial rotational cooling schemes considered in [Vit08c, Vit09, Sof09]. These involve the use of broadband radiation, shaped with the required resolution in order to achieve rotational cooling. In these cases, the optical pumping is considered with the $C^1\Pi_u$ state as the excited state. After discussing the technical difficulties and limitations involved with these optical pumping schemes, we consider rotational cooling with the use of an initially narrow-band, but spectraly broadened laser radiation, via the $B^1\Pi_u$ state. Finally, I discuss the experimental study that is in progress, and which is aiming to investigate rotational cooling via the proposed schemes that include the use of broadened narrowband light. The starting point in our approach, is the acquisition of rotationally resolved spectra. For this purpose, a depletion spectroscopy similar to the one reported in [Del08] is being developed.

The study for the development of an rotational cooling technique has not terminated, on the contrary it is considered to be an ongoing objective for the laboratory. However, the theoretical analysis presented in this chapter, as well as the preliminary experimental results give already a nice overview of the project and can support a fruitful discussion in the perspectives of the proposed techniques.

II.7.1. Rotational cooling with broadband radiation

The initial proposition for rotational cooling by the group, considered optical pumping with broadband radiation via the $C^1\Pi_u$ state and is discussed in [Vit08c, Vit09, Sof09]. The main idea is similar to the one behind the vibrational cooling technique, and involves simultaneous excitation of all rovibrational levels of the ground electronic state $X^1\Sigma_g^+$. Shaping of the femtosecond pulse with a much better accuracy (stiffness of the frequency 'cut') is used in order to achieve the removal of only the frequencies that excite the absolute ground state of the system $v_X = J_X = 0$, and thus turning it to a dark state of the system.

A similar way to consider the problem is related to the P, Q and R transitions. We recall from the Chapter I that the Hönl-London factors allow only transitions for which the rotation is modified by 0, + 1 or -1. The so-called P branch corresponds to transitions with $\Delta J = -1$, the Q branch to $\Delta J = 0$ and the R branch to transitions with $\Delta J = +1$. In Fig. II.7.1.1 we see a plot of the energies which correspond to transitions between the vibrational levels $v_X = 0$ and $v_{B,C} = 0$ between the $X^1\Sigma^+$ ground electronic potential, and either the $B^1\Pi_u$ potential (a) or the $C^1\Pi_u$ potential (b). The P, Q and R branches are noted with black, blue and red color respectively, while we note that transition between $J_X = 0$ and $J_{B,C} = 0$ are not allowed by the Hönl-London selection rule. We see that, in the case of the $B^1\Pi_u$ potential considered in part (a), it is not possible to suppress uniquely the transitions starting $\Delta J = J_B - J_X = 0$ with a simple pulse shaping. The situation is different, if we no longer consider the state $B^1\Pi_u$, but the state $C^1\Pi_u$. In part (b), we see that the transitions $\Delta J = J_B - J_X = 0$ can now be suppressed. This explains why the $B^1\Pi_u$ potential, which was the usual choice for excited state in the vibrational cooling schemes, is now replaced by the $C^1\Pi_u$ potential[1].

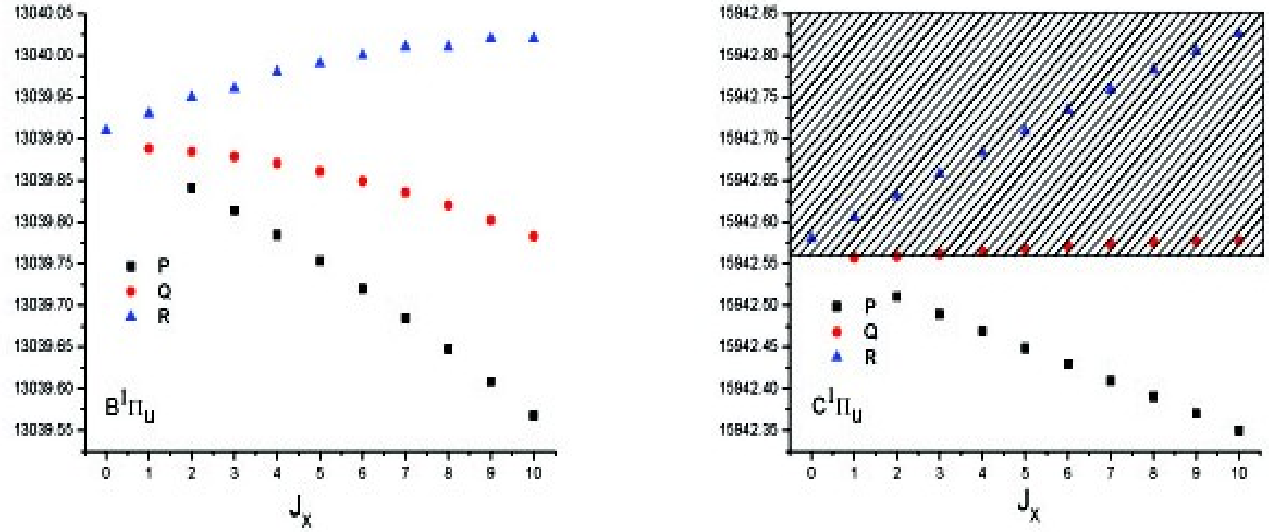

Fig. II.7.1.1: Energy of the different ro-vibrational transitions ($\Delta J = J_B - J_X = 0 \pm 1$ for the P, Q and R branches) (a) with the B state, (b) with the C state. The hatched areas represent the pulse shaping needed to realize rotational cooling.

A disadvantage related to the choice of the $C^1\Pi_u$ instead of the $B^1\Pi_u$ potential, is that vibrational cooling cannot be performed via this state. This is due to the fact that this state is 'shallow', that is, it can support few vibrational states (up to v = 12). As explained in the following paragraphs, rotational cooling has to be implemented together with vibrational cooling, otherwise the heating effect of the rotational cooling on the vibration leads to big losses. The application of two separate cooling pulses, one for the vibration and one for the rotation, each addressing a different electronic transition, can be considered. The two different cooling methods can, in principle, be applied simultaneously. However, the scheme considered here, vibrational cooling must be applied first, in order for the vibrational number to remain low during the rotational cooling process and for pre-dissociation in the $C^1\Pi_u$ state to be avoided. Figure Fig. II.7.1.2 shows the results of a simulation where the molecules are first vibrationally cooled by considering the excitation of the state $B^1\Pi_u$ (part (a)), and then rotationally cooled by considering the excitation of the state $C^1\Pi_u$ (part (b)). The simulation supposes equal power for the two laser fields.

---

[1] Rotational cooling is possible when except from the P branch, the Q branch is also excited, as we will see in the following paragraph. However, excitations of the Q branch transitions do not reduce rotation and thus reduce the cooling efficiency. Thus, in the initial schemes concerning broadband radiation, selective excitation of only the P branch transitions was considered.

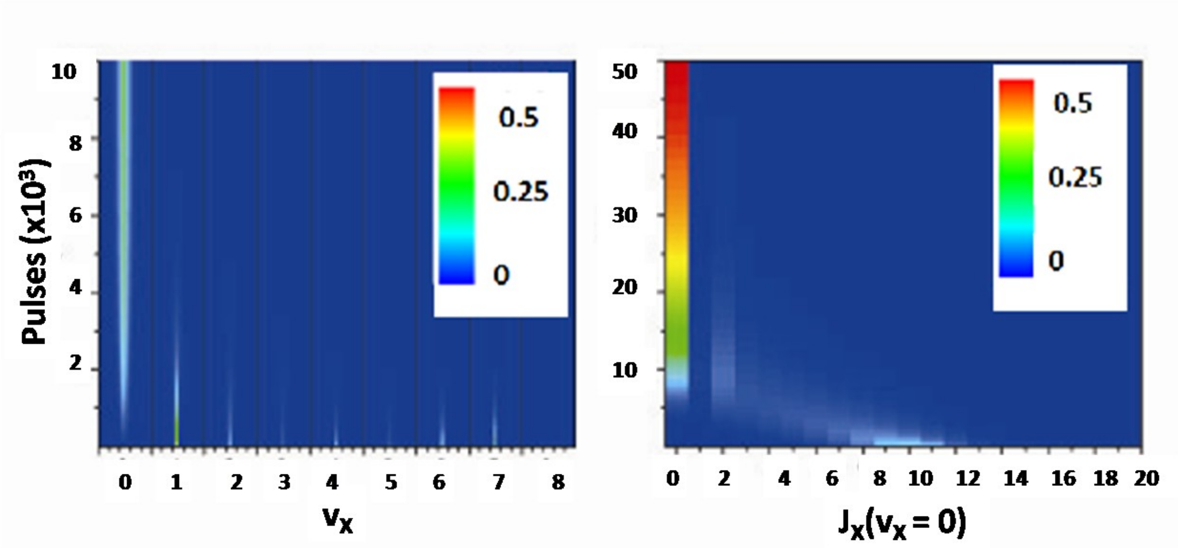

Fig. II.7.1.2: (a) Vibrational cooling via the B state. The plotting is now versus the rotational states, while the vibrational states are also noted, and the effect of the vibrational cooling in the rotational distribution is shown. Each vibrational level is considered to have 10 rotational levels, and they are separated between them with the dark lines. (b) Subsequent rotational cooling scheme. The initial distribution of the part (b) is the final distribution of the vibrational cooling process shown in part (a). The population transfer to the $v_X = J_X = 0$ is ~46%.

However, the shaping considered in such a simulation is very difficult to be achieved. As shown in Fig. II.7.1.1, the required resolution in order only for the P branch to be excited is in the order of 0.02 cm^{-1}(~600MHz). If we consider realization of the required shaping with a 4-f line like the one considered for vibrational cooling, the required width of the optical grating is more than one meter. Another complication comes from the fact that we want to perform vibrational and rotational cooling in temporary separated steps. This constrain could become important if the time we have in our disposal to perform our manipulations to the molecules, before they exit the MOT volume, is limited. For the case of cooling Cs_2 molecules, as displaced in Fig. II.7.1.2 the temporal evolution of the system is such that no problems arise. The overall optical pumping process requires 60 thousand pulses for the population transfer of ~65% of the initial population in the absolute ground state. The laser power, as for the case of vibrational cooling, is considered to be low (~700 mW/cm^2). If we take into account that the pulses are separated with each other by 12.5 ns then the total time required is 0.75 ms. However, if we consider application of the technique to a different molecular system, such a problem might exist, since a larger value for the lifetime of the excited state would lead to a much slower optical pumping process. As we will see in the next paragraph, more realistic optical pumping schemes can be considered, that do not require high resolution shaping, and permit simultaneous application of vibrational and rotational cooling.

II.7.2. Rotational cooling with narrowband radiation

In the previous paragraph, we saw that the initial considerations for rotational cooling with the use of shaped broadband radiation, is in on the one hand applicable, but on the other hand it is related to various problems, with the most important being the experimental difficulties associated with the required shaping resolution. However, the broadband approach described in the previous paragraph is not the only one that can be considered for rotational cooling of Cs dimers, neither optical pumping via the shallow $C^1\Pi_u$ is the only possibility. It is true that the relative position of the P, Q and R branches displayed in Fig. II.7.1.1a imposes serious restrictions, but given a second look, these restrictions do not seem completely unsurpassed.

After the demonstration of vibrational cooling with the use of the non coherent diode source, we know that femtosecond radiation is not the only possibility for optical pumping in molecules. A variety of different sources can be considered, as long as they can be accurately controlled in order to contain those frequency components that favor the cooling process. Other sources of radiation might allow different ways to modify their spectral characteristics, apart from the 4-f line, which if considered for the particular application, leads to unrealistic experimental set-ups. Such an alternative, as we will see in the following part of this paragraph, opens the possibility to perform rotational cooling via the $B^1\Pi_u$ state, which is very convenient, since rotation can be cooled in the same time as vibration and no pre-dissociating phenomena affects the technique's efficiency.

An alternative way to consider optical pumping for rotational cooling of molecules is with the use of narrow-band diode laser, which can be rapidly modulated in the frequency domain. A sufficiently narrowband laser, which would have a spectral width in the order of the rotational spacing (~0.02 cm^{-1}) can selectively excite a particular transition between specific ro-vibrational states.

Simplified example of rotational cooling with narrowband radiation

Let us imagine for simplicity a vibrationally cooled but rotationally hot molecular sample, with the molecular population distributed in the first six rotational states as displaced in Fig. II.7.2.1.a, in the histogram on the left part. By selectively addressing the $J_X = 5$ to $J_E = 4$ ($J_E \rightarrow J$ excited) transition with the narrowband laser (P branch transition), we can eventually pump population from the state with $J_X = 5$ to the state with $J_X = 4$. Of course, such an excitation would result to the transfer of molecular population to different vibrational states, but in an real experiment, this can be compensated with the simultaneous application of a vibrational cooling laser field. We can therefore omit any heating effects of the rotational cooling upon the vibration for this simple example and return to this subject in the following paragraph. Once all molecular population is pumped out of the state with $J_X = 5$, the frequency of the narrowband laser can be rapidly modulated to excite the $J_X = 5$ to $J_A = 4$ transition, as shown in part (b), and similarly until all molecular population is transferred in the state with $J_X = 0$ as shown in part (c).

Molecular population transfer in J = 8

In our experiments, photoassociation in 11730.12 cm^{-1}, initially provides with molecules in the J = 8 rotational level, a fact that is verified by the depletion spectroscopy discussed in the following paragraph. The subsequent, two step relaxation towards the $X^1\Sigma^+$ ground electronic potential, redistributes the molecular population symmetrically in the neighboring rotational levels, with the largest part of the population remaining in the initial J = 8 rotational state. This gives the idea to consider an optical pumping process which could pump all population back to the initial J = 8 level. Such an optical pumping scheme in displayed in the part (a) of Fig. II.7.2.2. The idea is, similarly to the simplified example considered before, to selectively address those transitions which could pump population to the J = 8 level. The choice of J = 8 as the target state, reduces considerably the number of transitions that have to be addressed, with respect to the choice of the fundamental J = 0 state as the target state. In part (b) of Fig. II.7.2.2, we see the rotational distribution that results the photoassociation process (with the subsequent relaxation steps). The highest populated rotational level is the one which has J = 10 and the lowest has J = 6, as a consequence of the Hönl-London selection rule.

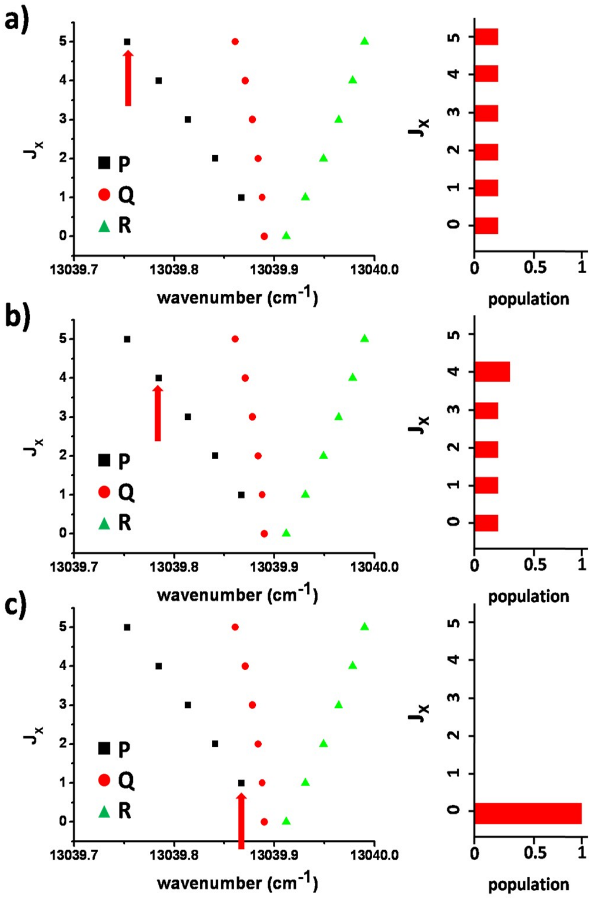

Fig. II.7.2.1: Simplified example of rotational cooling with narrowband radiation. The positions of the P, Q and R branches correspond to the ones of the $v_X = 0 \rightarrow v_E = 0$ transition in Cs_2, however, any effect on vibration is omitted. In part (a), the narrowband radiation is addressing the $J_X = 5 \rightarrow J_A = 4$ transition. Once all molecular population is removed from the $J_X = 5$ state, the laser is rapidly modulated to excite the $J_X = 4 \rightarrow J_A = 3$ transition (b), a process which can be repeated until all population is pumped into the $J_X = O$ state (c).

If we consider simultaneous vibrational cooling on the Cs molecules, the effect of the vibrational cooling pulse in the rotational distribution has to be taken into consideration as well. A typical, simply shaped pulse, as the ones discussed in Chapter III, would result to the broadening of this distribution, as displaced in Fig. II.7.2.2.b. Finally, in the part (c) of Fig. II.7.2.2, we see the effect of the optical pumping scheme displayed schematically in part (a) upon the rotational distribution. We see that this way, we can achieve transfer of all the molecular potential back to the initial J = 8 level as shown in part (d) of Fig. II.7.2.2.

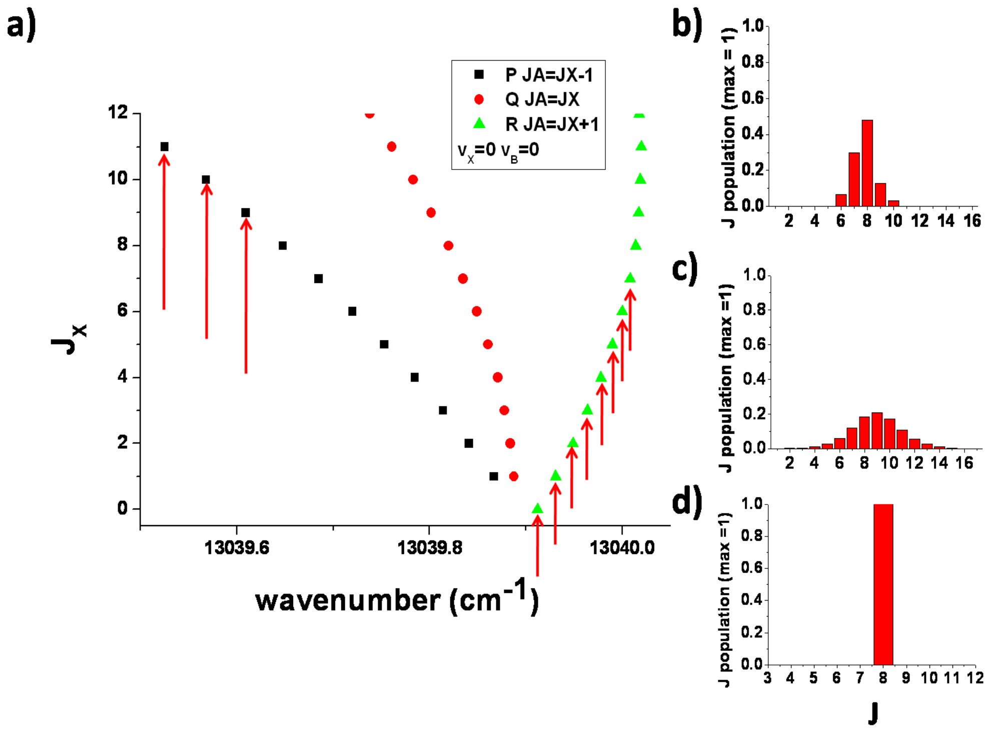

Fig. II.7.2.2: (a) Optical pumping scheme for the molecular population transfer to the J = 8 level. (b) Rotational distribution of Cs molecules prepared by photoassociation at 11730.12 cm^{-1}. (c) Effect of vibrational cooling in the rotational distribution of part (b). (d) Rotational distribution after the application of the optical pumping scheme displayed in (a).

Population transfer in the J = 0 ground state

As it was previously noted, vibrational and rotational cooling can be applied simultaneously in this narrowband approach. Each method concerning the cooling of each degree of freedom (vibration and rotation) has a heating effect in the other, the amount of which depends on the forms of the Franck-Condon parabola and on the relative intensities of the cooling fields. Thus, in a realistic situation, these laser intensities have to be accurately balanced in order for the maximum efficiency to be achieved.

At this point, it would be useful to discuss the feasibility of the above proposed rotation cooling scheme, and more specifically, the availability of narrowband sources suitable for rotational cooling. As we show in the previous paragraph, the required spectral resolution in order to address an individual rotational state is in the order of some hundreds MHz, depending on the choice of the addressed vibrational transition. This is achievable by DFB diode lasers which have a spectral width of some MHz. The rotational states that have to be addressed are those with $J_X<14$, since J = 14 is the level with the highest J which is populated. This means, that the diode's central wavelength has to be modified for ~0.5 cm^{-1} while the exact numbers again depends on the choice of the vibrational transition. The narrowband source available to us is an Eagleyard DFB diode laser in ~13040 cm^{-1}. This wavelength corresponds to transitions between the $v_X = 0$ and $v_A = 0$ states, and thus, the discussed schemes for rotational cooling concern this transition. Any choice of the vibrational transition can be considered, as long as Cs molecules can be transferred there efficiently, for example with the optical pumping technique discussed in Chapter II 4.

We saw that vibrational cooling has to be applied in the same time with rotational cooling for efficient population transfer. This is because each optical pumping technique applied to cool one of the two separate degrees of freedom, the rotation or the vibration, is heating the other if applied alone. Vibrational cooling could be demonstrated without the need of rotational cooling, simply because the heating inserted in the rotation was small, and all populated rotational states could be excited and detected simultaneously by the 0.1 cm^{-1} spectraly broad dye laser. The heating induced by the vibrational cooling in the rotational degrees of freedom is indicated in Fig. II.7.2.3, where we see the usual vibrational cooling scheme via optical pumping between the $X^1\Sigma_g^+$ and $B^1\Pi_u$ states. In part (a) we see the Franck-Condon parabola for this case while the spectrum of the femtosecond pulse used is shown in the inlet. In part (b) we see the evolution of the vibrational state population distribution under the influence of 10 000 pulses. We see that all molecular population is transferred in the v_X=0 ground vibrational level, but, as shown in (c), this population is symmetrically distributed in rotational levels ranging from 4 up to 11. However, this does not influence the observation of vibrational cooling since all rotational states are simultaneously detected.

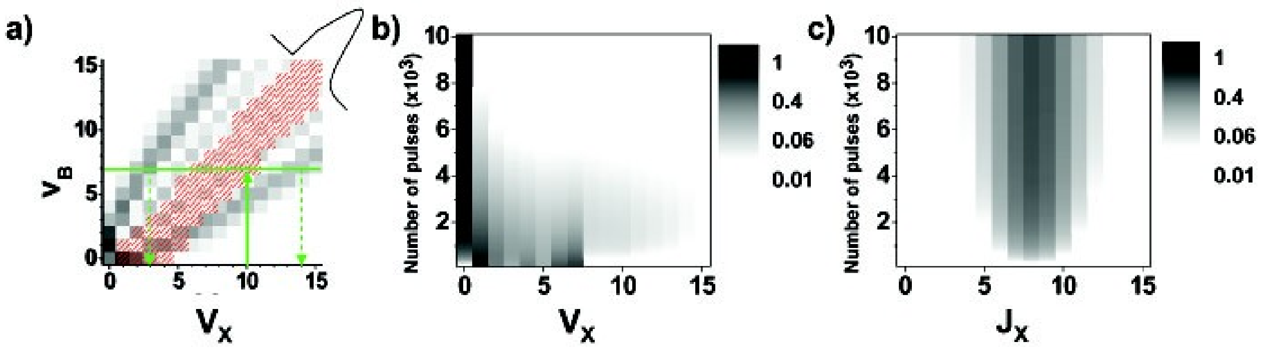

Fig. II.7.2.3: Simulation for the ro-vibrational cooling with a truncated spectrum through the excited B state: a) FC factors for the X - B transitions (gray levels), the (red) dashes indicate the energy range covered by the truncated (allowed frequencies ν ≤ 13000 cm−1) laser spectrum with an intensity above 10% of maximum, b) temporal evolution of the vibrational population when using the pulse in a); c) temporal evolution of the rotational population of the $v_X = 0$ level.

This is not the case for the rotational cooling scheme, since the redistribution it causes among vibrational states prohibits their simultaneous detection. In other words, we are in position to detect simultaneously many rotational states, and yet been selective as far as vibration is concerned, while we cannot selectively detect rotation of molecules distributed in various vibrational states. However, if the number of molecules redistributed to different vibrational states was small, we could try to detect rotational cooling in the remaining molecules.

The most usual case, for which the rotational cooling leads to significant vibrational heating is shown in Fig. II.7.2.4. In part (a) we see the spectrum for the laser field chosen for the rotational pumping. This laser has a top hat form and is extended between 13039.50 and 13039.86 cm^{-1}, which means that addresses excitation from the $v_X = 0$ to $v_B = 3$ vibrational levels. This field can cool the rotation of Cs_2 molecules, as well as they can be simultaneously overtake sufficiently efficient vibrational cooling, since the laser frequencies excite the P and Q branches and not the R branch. This is enough to achieve rotational cooling, since the fact that $J_X = 0$ can be excited only via the R branch and it is a dark state. We note that this scheme is less efficient than the scheme of via the $C^1\Pi_u$ state discussed in the previous paragraph, since here we are obliged to tolerate excitation of the Q branch. Without simultaneous vibrational cooling, the biggest part of the molecular population is quickly pumped towards several of vibrational states under the influence of this laser field as shown in (b). The remaining population in the $v_X = 0$ level shown in (c) is not cooled rotationally, since it has not been 'cycled' by the rotational cooling field.

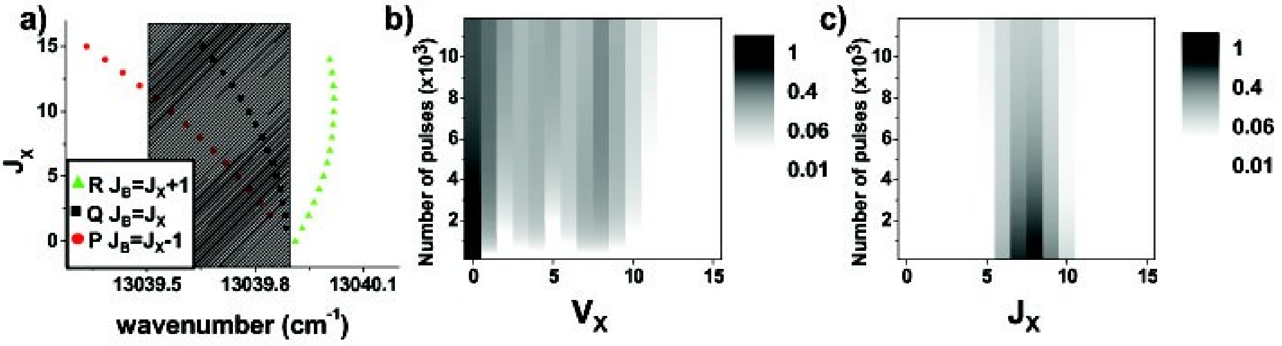

Fig. II.7.2.4: Energies of the allowed transitions from the X to the B state. We see the three different P, Q and R branches. The laser that can cool the rotation has to be zero for energies higher or equal to 13039.912 cm^{-1}, the frequency of the $J_X = 0$ to $J_B = 1$ transition. b) Evolution of the vibration state population distribution under the influence of the laser spectrum shown in the gray area in (a). We see that without simultaneous vibrational cooling the population is redistributed among various vibrational levels. c) Evolution of the rotation state population distribution of the $v_X = 0$ for the same laser spectrum. The rotational distribution is not narrowed since molecules are redistributed to other vibrational levels rather than accumulated in the ground state.

A top-hat a laser field like the one shown in Fig. II.7.2.4.a can result to the rotational cooling of Cs dimers, as long as its heating effect in the vibration can be efficiently compensated. The required vibrational cooling efficiency for the rotational cooling scheme considered here is increased due to the participation of the Q branch in the optical pumping. By the term vibrational cooling efficiency, we mean here the maximum cooling effect for the minimum number of absorbed photons.

Let us consider the Honl-London coefficients, in which the relative probability of transitions between rotational states is depended (see eq. 1.12). The probability for the rotation to be increased or decreased during a transition is ~0.25 and 0.5 to remain constant. However, if we consider excitation from the field considered in Fig. II.7.2.4, since the R branched is not addressed, the probabilities have to be re-normalized, yielding to ~0.33 and ~0.66 respectively. The possibility of an increase in rotation has to be considered however in the relaxation step. In any case, for one absorption-emission circle the probability for the rotation to be decreased by one is around 0.25, which means that we could estimate that this decrease requires the absorption of ~4 photons in order to decrease J by one (we do not consider the possibility of decreasing rotation by two for simplicity).

The absorption of a photon of the rotational cooling field, pumps population out of the initial vibrational level with a probability propositional to $(1 - FC_{trans})$, where FC_{trans} is the value of the Franck-Condon coefficient of the transition chosen for the rotational cooling. This means that rotational cooling is easier when applied to vibrational transitions with a large Franck-Condon coefficient. The necessary condition is that the Franck-Condon coefficients are such that do not allow for an important part of the population to relax to high lying vibrational levels, from which they would need several absorption-emission step of vibrational cooling in order to return to the target level.

In the our case, where the target state is the absolute ground state of the system $X^1\Sigma_g^+$ with $v = J = 0$, and the transition chosen for the vibrational cooling is $v_X = 0 \rightarrow v_B = 3$, as the one discussed in the previous picture. The relative value of the Franck-Condon coefficient is ~0.319. If we aim to the transfer of the maximum possible percentage of the molecular population in the absolute ground state, then we need a very efficient vibrational cooling scheme, as the ones considered in the context of the optimized vibrational cooling pulses discussed in Chapter II 4. In Fig. II.7.2.5(a), we see such a vibrational cooling pulse, combined to the ~100 times more powerful rotational cooling field, similar to the one shown in Fig. II.7.2.4.a. As we see, the use of such a system permits the accumulation of all the molecular population in the ground vibrational state, with the 55% of them being in the zero rotation state as well. An increased final percentage can be achieved, either by improving the vibrational cooling efficiency, in terms of the number of photon required, or even more easily, by choosing a final target state with higher Franck-Condon coefficient, as the $v_X = 1$ for example.

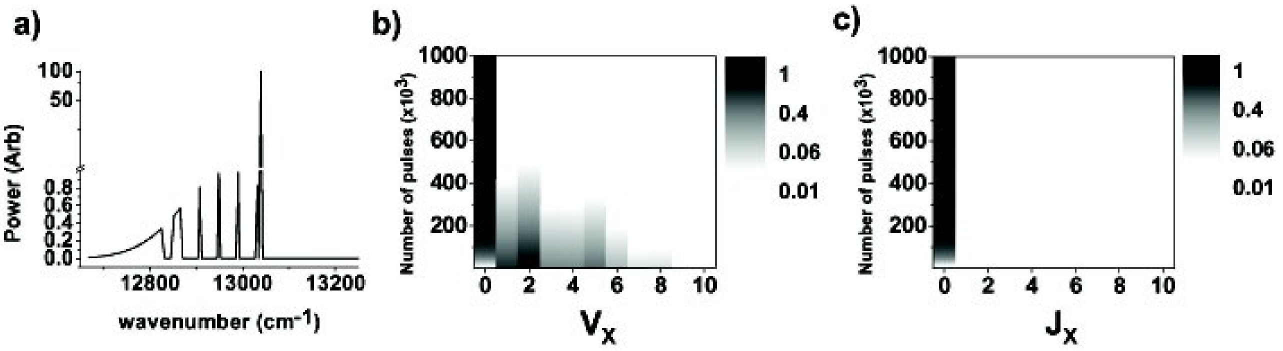

Fig. II.7.2.5: a) spectrum of the fs pulse optimized for vibrational cooling to the $v_X = 0$ state (FWHM = 100 cm^{-1}) plus that of the rotational cooling of Fig. II.7.2.4,(a) (laser power is out of scale as $P_{cw} = 100P_{fs}$) b) Evolution of the vibrational state population distribution under the influence of the laser spectrum shown in (a). c) Evolution of the rotation state population distribution of the $v_X = 0$ level for the same laser spectrum. We see that the optimized pulse can cool the vibration faster than this is heated by the cw laser resulting in the accumulation of 55% of the initial molecular population into the $v_X = 0$, $J_X = 0$ ground level.

II.7.3. Preliminary experiments and depletion spectroscopy

In the previous paragraph, we saw that narrowband lasers can be considered in for cooling of the molecular rotation. However, the successful implementation of the technique requires accurate knowledge the rotational transitions, in order to position the narrowband laser's frequency correctly. Actually, it is not the absolute position of the rotational transitions that is required, but their position with respect to the value of the diode driving current, so that this can be adjusted in the various optical pumping steps. Thus, the point from which our experimental activity towards molecular cooling with the use of narrowband radiation was started, was the realization of a rotationally resolved spectroscopic technique.

The method was to insert a narrow-band, cw light, available by the same narrowband Eagleyard DFB diode considered for rotational cooling, in the molecular cloud before their detection via REMPI. The molecules are previously cooled to the $v_X = 0$ state with the use of the shaped femtosecond laser radiation. As we see in Fig. II.7.2.4, the narrowband radiation quickly pumps the molecular population out of the initial vibrational level, depleting the REMPI signal; that's why the technique is known as 'depletion spectroscopy' In each measurement, the vibrational cooling which proceeds the application of the depletion field is at some point stopped and the diode radiation is applied for ~1 ms. If the depletion laser's frequency is modified in each measurement, while its wavelength is monitored by the optical fiber lambdameter, we can acquire depletion spectra like the one shown in Fig. II.7.3.2.

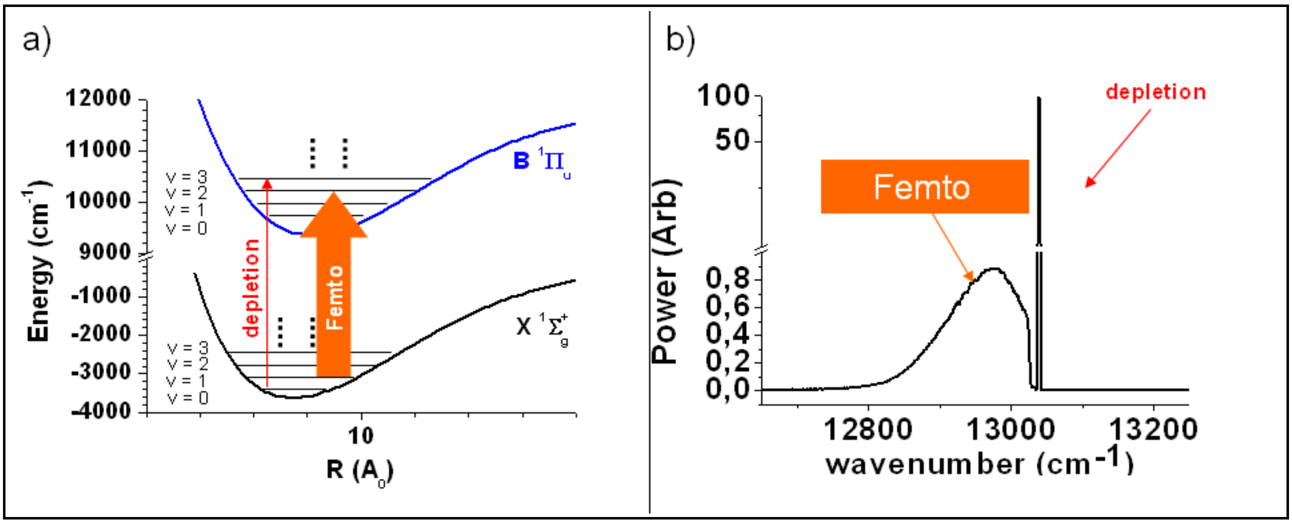

Fig. II.7.3.1: (a) The schematic representation of the transition involved in performing the vibrational pumping and the rotational depletion spectroscopy. For clarity only the vibrational levels are shown. (b) The spectrum of the two lasers used for these operations.

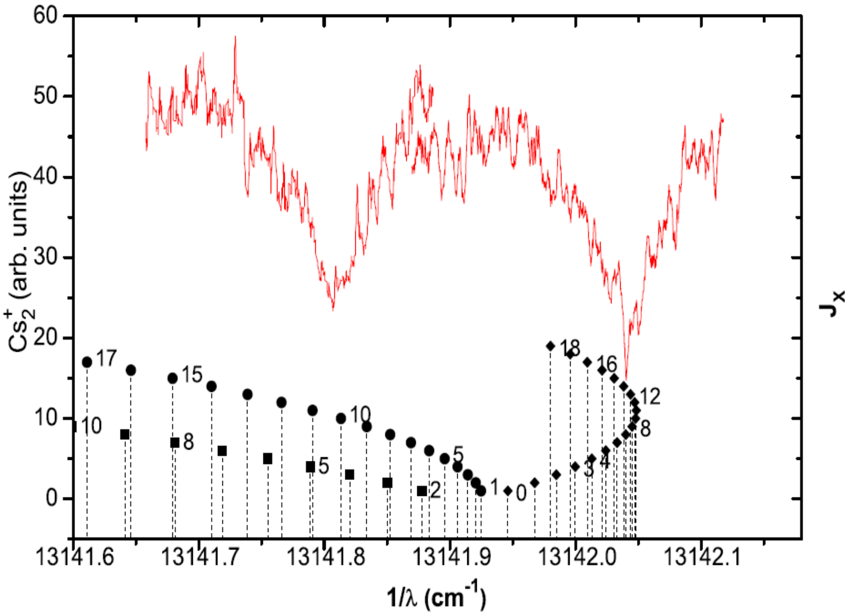

Fig. II.7.3.2: In red, depletion spectrum of ground state $v_X = 0$ level. The depletion laser is scanned on the X, $v_X = 0$ to B, $v_X = 3$ transition. In black, the calculated transitions (shown as vertical lines with associated J_X values) for the P (squares), Q (circles) and R (diamond) branches are based on experimental data from (Tow95, Dal99).

In this depletion spectra, we see two broad lines which, as shown by comparison to the position of rotational transitions indicated below, correspond to excitation of several rotational levels simultaneously. The depletion spectra does not offer the required resolution for the experimental determination of the rotational distribution. However, it is evident that the maximum of the rotational distribution is indeed in the J = 8 level. Moreover, this scan can be used in order to 'calibrate' our narrowband laser with respect to the rotational transitions, and thus be useful for the preparation of the future rotational cooling experiments.

II.7.4. Conclusions

In this paragraph I discussed the possibility of extending the vibrational cooling technique to include rotation. The theoretical studies presented in this paragraph have been discussed in [Vit08c, Vit09, Sof09], while the preliminary depletion rotation data have been demonstrated in [Fio09]. The initial considerations for rotational cooling of Cs dimers via optical pumping was done in the context of femtosecond lasers and shaping with the use of 4-f line. A femtosecond pulse exciting only the P branch of the transition between the $X^1\Sigma_g^+$ and $B^1\Pi_u$ states can result to molecular population transfer to the absolute ground state $v_X = J_X = 0$. However, the required resolution imposed by the Cs rotational spacing makes the experimental demonstration of this scheme unrealistic.

Another possibility is considered with the use of a rapidly modulated DFB diode. In any case, rotational cooling has to be accompanied by simultaneous application of vibrational cooling, in order for an important percentage of the total molecular population to be transferred in the target state. Moreover, this has to be an optimized vibrational cooling technique, if cooling the rotation to the absolute ground state is considered with the use of the DFB diode at 1314 cm^{-1}. However, more schemes can be considered for simpler demonstrations of rotational cooling. For example, if the first excited vibrational level, which benefits the highest value of Franck-Condon coefficient for the electronic transition is considered, an optimally shaped pulse is not longer necessary for vibrational cooling. Simpler demonstrations of rotational cooling can also be considered, such as cooling to $J_X = 8$, which would not correspond to the reduction of the average rotation of the molecules, but to their redistribution to a single rotational state.

Finally, the preliminary experiments concerning rotational cooling are discussed. The initial point is the implementation of a rotationally resolved, depletion spectroscopy technique. The spectra acquired with the use of this spectroscopic study, do not have yet the required resolution in order to determine the rotational distribution. However, they can be useful in 'calibrating' the narrowband diode with respect to the rotational transitions, and thus to contribute in the preparation of the future rotational cooling experiments.

II.8. CONCLUSION& PERSPECTIVES

In this part of my thesis I described my experimental activity in the field of cold molecules, and in particular, in the study of the recently developed vibrational cooling technique and the various generalizations and simplifications considered. The first three chapters are introductory. The first chapter is a general introduction, along with some useful elements of molecular physics theory. The second chapter is dedicated in the general description of the field of cold molecules. The most important techniques for the study of cold molecular systems are presented, along with a description of some important, recent developments in the field. In the third chapter, I discuss the vibrational cooling technique which is the main subject of my thesis. In this chapter, I discussed the experiments that led to the demonstration of this technique in Laboratoire Aimé Cotton, and which are the subject of [Vit08c] and I describe the experimental set-up used in the cold molecule experiment.

In the fourth chapter, I discuss the extension of the technique that I implemented to achieve population transfer to any pre-selected vibrational level. The experimental demonstration included advanced femtosecond shaping, which was performed with the use of a spatial light modulator provided by the group of Beatrice Chatel. In this experiment, we introduced an optimization process for the shaped pulses, that provides with more efficient vibrational cooling, as far as the final number of transferred molecules is considered, but as far as the total number of photons absorbed as well.

The vibrational cooling technique is also demonstrated with the use of a non-coherent, diode based source in the fifth chapter. The simplicity of this experimental setup, can make this technique very attractive since the cost is significantly reduced with respect to the previous experiments, which involved a femtosecond laser and/or a spatial light modulator. The use of a photo-mask eliminates the problem of the non perfect extinction ratio that existed in the spatial light modulator setup. Also, the fact that cooling was performed with the diode laser operating below threshold, shows that coherence related effects are not relative to this process. Additional advances can be foreseen with the use of such a method, like the use of shaped broadband diode to create a 'molecular repumper' in a scheme for direct laser cooling of molecules. The relatively low cost and the simplicity of such a set up allows for the use of more than one diode laser sources if needed, for instance each of them addressing transitions between different vibrational states or even different electronic states.

A study of the generalization of the vibrational cooling technique via different optical pumping schemes is discussed in the sixth chapter. An attempt to apply the vibrational cooling technique to cool molecules in the $a^3\Sigma_u^+$ has been considered theoretically and experimentally in the first part. The interest for such a study is due to two main reasons: One aim is to demonstrate the generality of the vibrational cooling technique in another electronic transition, even though in the same molecular system. The other, is to have the ability to perform our experiments with $a^3\Sigma_u^+$ molecules, which can be produced in large numbers by the so called 'giant' rates. I attempt to understand the reasons why our experimental approach did not led to any interesting results via a more detailed theoretical study. Most probably, the experimental results are related to 'parasiting' coupling of the molecular population in an additional electronic potential, other than the one considered as the excited state of the optical pumping scheme. As noted in the end of the corresponding paragraph, these experimental results have raised a big discussion within the Cold Molecule group in LAC, thus the most probable reasons are under itheoretical investigation by members of the team [Bal09].

In the second part of Chapter II6, I discuss the applicability of the vibrational cooling technique in heteronuclear molecules and in particular in NaCs. I discuss the particular difficulties, that are introduced both in the search for a 'closed' transition for the realization of optical pumping and in the demonstration of vibrational cooling. The poor performance of the simply shaped pulses, like the ones considered in [Vit08c], can be largely improved with the use of optimized pulses, like the ones considered in Chapter II 4. These optimized pulses permit us to 'follow' the transition's natural tendency to accumulate molecular population in a particular vibrational level, which is the one with the highest Franck-Condon coefficient. The fact that for the transitions considered in the case of Cs_2, this is a deeply bound vibrational level ($v_X = 1$), makes the use of simply shaped pulses in this case applicable. This is not true for the case of NaCs. However, optimized pulses can collect the largest part of the molecular population in a single vibrational level. From there it is fairly simple to populate another, desired vibrational state, which is usually the fundamental vibrational state.

Finally, the extension of the vibrational cooling technique to rotation has been theoretically considered. A variety of cooling schemes are discussed for the demonstration of rotational cooling, involving broadband or narrowband radiation. In any case, rotational cooling has to be accompanied by simultaneous application of vibrational cooling, in order for an important percentage of the total molecular population to be transferred in the target state, since vibrational cooling heats rotation and vice-versa. However, the initial point of the experimental approach of rotational cooling is the accurate determination of the rotational transitions involved in the optical pumping scheme. Thus, the preliminary data presented here, concern the implementation of a, rotationally resolve, depletion spectroscopy, which can be proved useful in future experiments towards rotational cooling.

III. GENERAL CONCLUSION

In this thesis I describe two different lines of experiments, the experiments involving a dipole trap of Cs atoms, and the experiments of preparation and manipulation of Cs_2 molecules created in a MOT. Although these two different experimental activities are different, they are both included in the long term objectives of the group of cold molecules in LAC.

The long term objectives of the group are mostly related to the creation of cold molecules, with neither vibration nor rotation, in the largest possible quantity. The preparation of an experimental set up, in which atoms of Cs can be trapped in ultra-low temperature, which was the aim of the dipole trap experiment, is justified in this context for a variety of reasons. A first reason is, that the technique of photoassociation, which is the main tool used for the preparation of molecules in our group, has increased efficiency for low temperature. Additionally, in a conservative trap, photoassociation can be applied repeatedly, in order for cold molecules to be accumulated [Zahz06, Vanh02].

As mentioned in the previous chapters, our efforts towards the efficient loading of a dipole trap were never completed. The whole study involved loading a dipole trap from an atomic 'reservoir' obtained by various traps (magnetic, Dark-SPOT, C-MOT), as well as comparison to several instantaneous loading techniques. We can say that, the study showed that the reservoir loading method could not be the simplest way to reach this target. The fact is that the work of [Hung08] provided with a very attractive method based in Raman-Sideband Cooling. Additionally, the improvement shown in our own preliminary results that we obtained combining Raman-Sideband Cooling and shallow trapping potentials, implies that this approach towards ultra-cold Cs is very difficult to be 'beaten'.

On the same time, the demonstration of the vibrational cooling technique [Vit08], showed that the development of an ultra-cold Cs atom experiment is not the only way to approach the group's long term objectives. First, the technique already manages to cool molecular vibration and potentially rotation. This means, that molecules can be prepared in their absolute ground state, in large numbers, if repeatable preparation-cooling cycles are considered. There are not many obvious reasons why such a trapped, molecular sample cannot be cooled down further, by means of evaporating cooling. Additionally, if the production mechanism of the cold Cs molecules, i.e. the photoassociation and stabilization, are given a second look, we see that the quantity of the produced molecules could be increased by stimulating one of the two spontaneous emission steps that occur (see Fig. II.3.1.a.1).

My work in the cold molecule experiment did not deal explicitly with the number of cold molecules created, and was mostly related to the extensions of the vibrational cooling technique. However, the general targets remained the same. If we take a good look in the experiments described in the second half of my thesis, we can see that all of them can be placed in the framework of the long term objectives of the LAC cold molecule group. In particular, the experiment concerned molecular population transfer to a pre-selected vibrational level, and is described in Chapter II4. Furthermore, through this work, it was made possible to consider and realize an additional, optimized pulse shaping for the optical pumping. The diode-based cooling, described in Chapter II5, provides with a new, flexible set-up, and also reinforces our considerations on the vibrational cooling operating principle. Both these generalizations might be of high value in the future of the particular field, since they could lead to directly laser cool molecules. In Chapter II6, the generalizations to cool the Cs triplet molecules and the NaCs molecules are discussed. A successful cooling of the Cs molecules in their triplet state, would already raise the number of molecules without vibration created in our laboratory by at least an order of magnitude, and thus it is directly linked to the group's long term objectives. Finally, the rotational cooling considered in Chapter II7, is a necessary step, towards creating large samples of ultra-cold molecules in their absolute ground state.

The demonstration of optical pumping in molecules with the use of a broadband laser, opened new perspectives for the manipulation of cold molecules. Moreover, the work presented in this thesis, widens the technique's perspectives even further, towards applications that are, according to our opinion, very important for the field. One important point, is that optical pumping offers the ability to 'play' with the molecular vibration, by choosing the vibrational level in which molecular population can be accumulated. A second point, concerns more complicated shaping of the spectrally broadened light, through which, molecular population transfer can be optimized. Such optimized optical pumping schemes can be especially useful in the application of vibrational cooling in heteronuclear molecules, like for example NaCs. Finally, the experimental generalization of using incoherent broadband light instead of femtosecond laser radiation, allows the consideration of sophisticated optical pumping schemes for the realization of more complicated processes.

By summarizing the work presented in my thesis, I consider to have contributed to the group's long term objectives by two different ways: the dipole trap experiment and the molecular cooling techniques. Those two different ways were not equal, neither in difficulty nor in productivity, a fact which becomes more evident by looking at the time invested in each field. However, I think that this is a general characteristic in research, but also in life, thus I believe that during my work in Laboratoire Aimé Cotton, I had a good, realistic look of what future is going to be for me, as I continue my effort of becoming a scientist.

ANNEX I.1

Data analysis in the dipole trap's lifetime

As I mentioned in the Chapter I5, I initially intended to devote a large part of the analysis of the experimental results in the study of the lifetime of the dipole traps prepared. Indeed, the lifetime of every trap prepared in the lab was measured, while I have made several attempts to fit the most characteristic ones with theory discussed in [Web03]. However, I soon abandoned this idea for two reasons. The data analysis discussed in [Web03] was performed in atomic samples of much smaller temperature, were the collisional process are less complicated. Our methods of preparing a hot and dense dipole trap was not at all compatible to this analysis.

Moreover, the dipole traps prepared with with the methods discussed in this thesis had lifetimes shorter than half second, with the exception of the traps loaded by the RSC method described in I.4.5.c. and the single arm dipole traps. In Fig. 1 we see the study of the lifetime of a single armed dipole trap loaded by a C-MOT according to I.4.3. and the waist is 137 μm and the dipole laser's power ~50 W. The lifetime is found to be 2.7 s, a value much higher than the usual crossed dipole traps loaded by these conditions. Evaporation of this trap was not efficient due to small oscillation frequency in the longitude direction (parallel to the propagation of the trapping beam). Single armed dipole traps like this could be useful to an alternative loading approach, in which evaporation in the existing arm is performed while the second arm is simultaneously turned on in an adiabatic fashion. Similar methods were useful in [Pfau07, Beau08] in the case of Chromium, and were luckily to result to improved loading for our case as well. However, the technical possibility to perform such a loading strategy, although was realizable, it was not initially available. Realization of a loading strategy with these characteristics was in our plans, however, Raman-Sideband cooling sounded more promising and was preferred. As far as data analysis is concerned, this is simplified in the case of crossed rather than in the case of single armed dipole traps, since the configuration of the VISION software is made for crossed dipole traps.

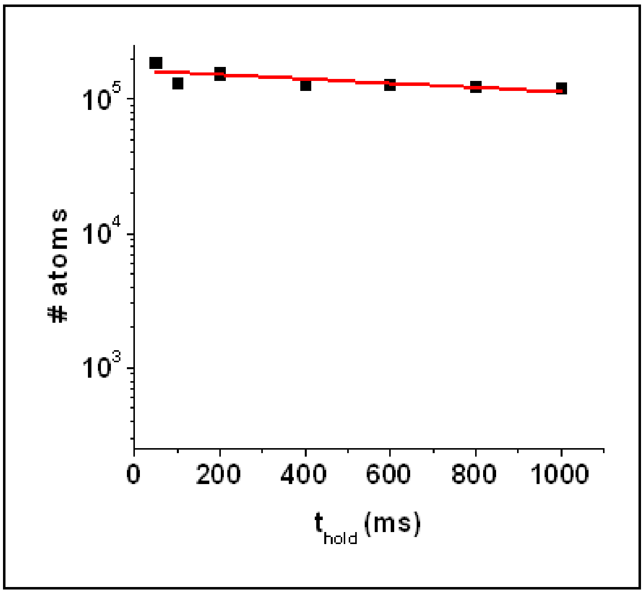

Fig. 1: Evolution of the number of atoms in a single arm dipole trap with a waist equal to 137 and a power of 50 W. The dipole trap lifetime in these conditions was equal to 2.7 s.

The usual data analysis performed in the lifetime of a dipole trap's, which is the evolution of the atom number and temperature in the dipole trap without modification of its power, consists in the determination of the rate of the corresponding losses and associating heating. In particular, the analysis performed in [Web03] was aiming to determine the three body recombination rate and the associated heating. I performed a simplified analysis in the lifetime of various dipole traps with the aim to conclude if the notorious three body recombination rate, than had so much affected the experiments [Boir98, Web03], had anything to do with the performance of my experiment. However, the lifetimes observed for traps obtained in our experiment were too short, resulting to sometimes unreasonably high numbers for the relative coefficients.

An example of such simplified analysis is the one performed in a 137 μm dipole trap prepared by C-MOT loading as discussed in I.4.4. and which is shown in Fig. 2. The lifetime of the dipole trap was found to be 400 ms, a characteristic value for the dipole traps in these dimensions. The evolution of the number of atoms in a dipole trap of constant power, as well as their temperatures, can be fitted according to the following equations [Web03]:

$$\frac{\partial N}{\partial t}=-\alpha_R N-\gamma\frac{N^3}{T^3} \tag{1}$$

$$\frac{\partial T}{\partial t}=-\gamma\frac{N^2(T+T_h)}{3T^3} \tag{2}$$

where $\gamma=L_3 m\bar{\omega}/2\sqrt{27}\pi k_B$ the three body recombination rate, related to L_3 the associated three body loss coefficient. The average frequency of the oscillating atoms in the crossed dipole trap is symbolized by $\bar{\omega}$ and its value is automatically calculated by VISION to be equal 343 Hz. The parameter α_R is the residual gas collision rate, and T_h the heating associated to three body recombination. Equations 1 and 2 consist a set of coupled differential equations without analytic solutions. In the analysis performed in [Web03], initially the temperature is considered to be steady in Eq.1, while the number evolution in the dipole trap is plotted. The extracted value is inserted to Eq.2 which fits the experimental data for the temperature evolution, and when the heating rate is calculated *T* is substituted in Eq.1 by *T(t)* and the atom number evolution in the dipole trap is fitted again.

In the simplified analysis performed here, the term proportional to the residual gas collisions is omitted, since the residual gas lifetime is measured to exceed 15 seconds, a value which is considered vary large compared to the 400 ms of the dipole trap's lifetime. Moreover, we treat only the data for the evolution of the number of atoms in the dipole trap, with Eq. 1 and with the average (now) temperature equal to 80 μK. This method is considerably simplified with respect to the one performed in [Web03], while it suffices for a first estimation of the three body recombination rate. Equation (1) has now an analytical solution which is

$$N(t)=\frac{1}{\sqrt{2\frac{\gamma}{T^3}t+\frac{1}{N(0)^2}}} \tag{3}$$

This equation should be fitted in an interval in which the reduction of the atom number in the dipole trap indeed depends on the three body recombination, since it is sure that an initial, more violent decrease should be explained by 'spilling'. As seen by Eq. 3, the evolution of the number of atoms under the influence of three body recombination is proportional to the inverted square root of the time. Thus, a 'safe' area for Eq. 3 to be applied, should be one in which the inverse square of the number of atoms is evolved linearly with respect to the time. Such an area is the one between 250 and 600 ms shown in Fig 3(b). In Fig 3(c) we see the fit of Eq. 1 to the evolution of the number of atoms in this period, realized with Igor Pro.6.5.

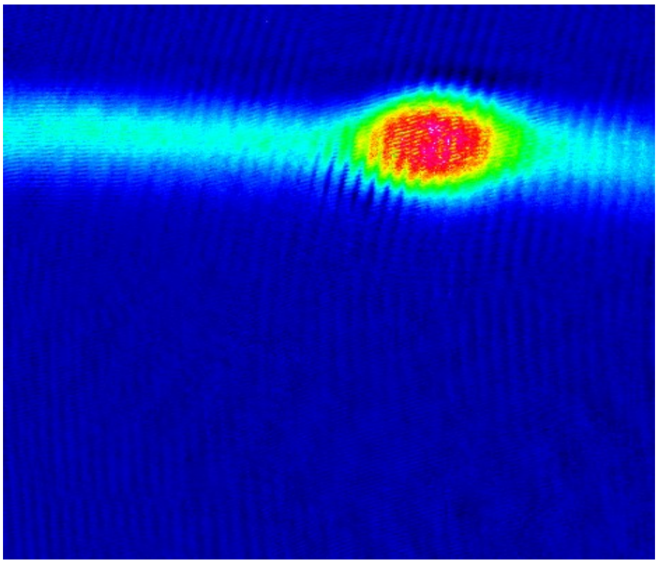

Fig. 2: Absorption image of a crossed dipole trap of ~137 μm loaded by C-MOT.

The resulting value of the fit shown in Fig 3(b) for the three body recombination length, was found to be $L_3 = 6.98\ 10^{-21}\ \mathrm{cm}^6/\mathrm{s}$. This parameter is connected to the s-wave scattering length a by the relation [Grimm00]

$$L_3 = n_l C \frac{\hbar}{m} a^4 \tag{4}$$

where the product $n_l C$ equals to 225. This results to a value for the scattering length of ~10000α_0, which is more than 3 times larger than the value predicted in these temperature conditions [D'Inc04].

The large difference observed between the dipole trap's lifetime when this is realized by a single beam and when this is realized by two beams in a crossed configuration is not totally unexpected. We have already explained that the temperature of the atoms in the dipole trap is mostly depended on the trap's depth rather than in anything else. Thus, the single-arm dipole traps are expected to have much colder molecules, and more over, the η parameter, which is the ratio of the temperature of the atoms upon the trap's depth in Kelvin, is expected to be much smaller, leading to completely different 'spilling' behavior. This means that a single arm dipole trap can have a larger lifetime, without necessarily implying that whenever the lifetime is small it has to be due to interatomic collisions.

The conclusion from this analysis is actually the opposite. I believe, that despite the linear dependence of the inverse square of the number of atoms on the time shown in Fig 3 (b), the reason for the atom decrease should not be searched in the three body recombination, which is expected to be much lower and should be visible with this method only with dipole trap's with lifetimes of several seconds.

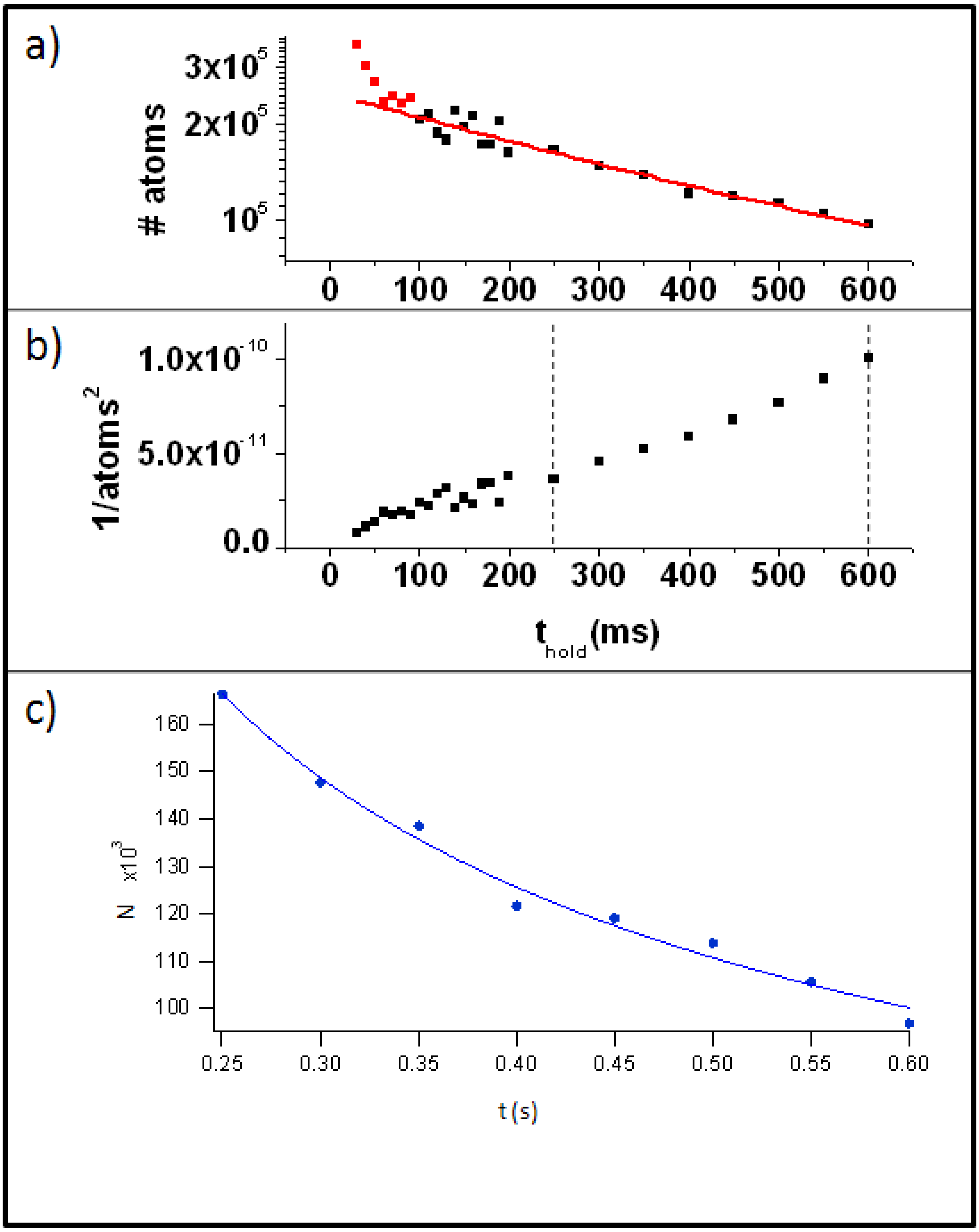

Fig. 3: (a) Evolution of the number of atoms for a constant power of the dipole trap presented in Fig 2. The dipole trap's lifetime, which is the time it takes for the number of atoms in it to be decreased ti the 1/e of the initial value, results form the exponential fit shown in by the red curve, and is found to be ~400 ms. Not all the points are taken into consideration during this fit, as the first seven are considered as the results of 'spilling'. (b) The evolution of the inverse square of the trapped atom's number. The linear area between 250 and 600 ms is considered to be appropriate for the fitting shown in part (c) according to Eq. (3).

ANNEX I.2

Evaporation and waist compression of the crossed dipole trap

As mentioned in the introduction of Chapter I5, a big part of our experimental activity had to do with the evaporation process. We have realized numerous efforts to perform evaporating cooling, by various methods that involved magnetic expulsion or real-time modification of the dipole trap's dimensions. Our goal at the time was the observation of a phase space density increase as a preliminary evaporation study. Additionally, we were hopping that a temperature decrease in our dipole trap, resulting a successful evaporation sequence, would somehow stabilize our traps, leading to longer lifetimes and in general in easier manipulation. The results of these studies were very haze and no important increase in the phase space density was observed. That's why I decide not to discuss evaporation studies in the main text; the results of the most characteristic of them are presented in this Annex, along with results on the real time compression of the dipole trap.

A reason for the failure of the evaporation cooling in our experiment is the very short lifetime of the dipole traps we managed to prepare. Indeed, the dipole trap's detection was possible for less than a second, a time in which the dipole trap's is mostly characterized by 'spilling', a process that is difficult to be theoretically treated. An important parameter for the theoretical study of the evaporation process is the ratio between the dipole potential's depth (expressed in μK) and the temperature of the trapped atoms, noted as η. The theoretical analysis discussed in chapter I.2. and in [Comp06] is not valid for values of η smaller than 4, and different analysis has to be followed [deCar04].

The fact that in our experiment the ratio η was smaller than 4 did not only affect the theoretical treatment of the evaporation data produced in our studies, but the experimental sequences used to produce them as well. Our initial strategy for the production of successful evaporation sequences involved optimization of the evaporation steps (decrease of the dipole potential versus time) according to theory related to the analysis of Chapter I2. The evaporation sequence would consist of several steps where the power of the dipole trap laser would be decreased in the amount that would optimize the phase space density increase, while each step would be delayed with respect to the previous one as much as it takes for the dipole trap to be thermalised.

Thus, our experimental study consisted of two different approaches. The first was to try to use the evaporation sequence produced by the theory discussed in Chapter I2 by inserting for η a value higher than four, and thus compatible to the theory. The hope in this case was that the drop in the temperature of the trapped atoms caused by this, non-optimized evaporation sequence, would gradually increase η, making the evaporation ramp more and more suitable. The second approach was a more practical experimental approach. In this case, the evaporation sequence was 'cut' in several parts with a pre-defined duration. The power was linearly decreased to a final value. This final value varied between several repetitions of the sequence, and the value that corresponded to the highest space density was chosen for this evaporation step.

In addition to these studies, we performed various studies of the real-time compression of the dipole trap's dimensions. In Chapter I2, we discussed how real-time compression of the dipole trap can result to an increase of the phase space density and to the acceleration of the evaporation process towards the BEC. The ability to modify the dimensions of the dipole trap in real time was discussed in Chapter I3. We studied the effect of modification of the dipole trap's dimensions in two different ways. Initially, modification of the dipole trap's dimensions was considered to take place simultaneously with the evaporation in order to accelerate it. These studies were performed, but they did not result to an increase of the phase space density that would bring our experiment closer to Cs condensation. The analysis of these results is problematic due to the fact that the theory described in Chapter I2 is not valid, neither for the evaporation nor for the modification of the dipole trap's dimensions. A different study aimed to see the effect of the dipole trap compression alone on the number and the temperature of the trapped atoms. The remarkably high number of atoms that remain in the trap after compression under specific conditions, make us think that the ability to modify the dipole trap's dimensions in real time would indeed be a useful tool for the preparation of a Cs BEC, as long as the evaporation sequence could be prepared to work successfully.

a) Evaporation in the crossed dipole trap

i. 'Theoretically optimized' ramp.

The first approaches to evaporation where connected to the theoretical analysis discussed in I.2. The experimental approach consisted of calculating the optimum power decrease and the minimum time in which the power should remain constant, in order for the overall process to adiabatic. In order to derive the equations with which the evaporation ramps are going to be produced we need to choose a strategy for the evaporation cooling. By the term strategy, we mean the aim which the evaporation equations are going to have and which determines the way the dipole potential will be lowered. For example, the evaporation can be considered in such a way, that the dipole potential is lowered while the oscillating frequency of the atoms in the dipole trap is kept constant. Another strategy aims in keeping constant the factor $\eta = U/kT$ during the evaporation process. In [Comp06], the theoretical study of the evaporation process in a crossed dipole trap showed that a strategy which aims in keeping constant the factor η, leads to optimization of the final atom number in the condensate, while other strategies lead to minimization of the evaporation duration. We choose to present the experimental study of such a conservative evaporation process, even though our set up enabled us to study various evaporation processes and indeed, various have been studied in the lab.

The energy change experienced by the trapped atoms during the evaporation process can be written as [O'Ha01]

$$\dot{E}=\dot{N}\,(U+\alpha k T)+\frac{\dot{U}}{U}\frac{E}{2} \tag{1}$$

where U is the trapping potential, N the number of trapped atoms, $E = 3NkT$ the total energy of the trapped gas and $\alpha = (\eta - 5)/(\eta - 4)$ for any trap which is harmonic near its center. Solving equation (1) for a fixed ratio $U/kT = \eta$ we find

$$\frac{N}{N_i}=\left(\frac{U}{U_i}\right)^{3/[2(\eta'-3)]} \tag{2}$$

where $\eta' = \eta + \alpha$. By differentiating (2) we obtain

$$P=P_{\mathrm{i}}\,(1-\alpha_{ev}\gamma_{ev}\Delta t)^{\frac{-\alpha_p}{\alpha_{ev}}} \tag{3}$$

$$w=w_{\mathrm{in}}\,(1-\alpha_{ev}\gamma_{ev}\Delta t)^{\frac{-\alpha_{w_0}}{\alpha_{ev}}} \tag{4}$$

where we express the trapping potential in terms of laser power and waist. Here P_i is the power in the beginning of the evaporation sequence, w_i is the waist and Δt the duration of the each of the ramps steps. We see that the initial step's duration is proportional to the inverse product of α_p and γ_{ev}, where $\gamma_{ev}=(\Gamma_{el}\,e^{-\eta}(\eta-4))/\sqrt{2}$ and $\alpha_p=-2\alpha_w$ while it is decreased for later steps by a factor which depends in the previous step's duration, to γ_{ev} and to $\alpha_{ev}=(-\eta+1)/3$. The parameter α_w is a parameter characteristic of the ramp, and results from the optimization of the evaporation sequence with respect to the ratio η [Comp06].

In order to realize the evaporation ramps with the use of equations (3) and (4) we need to determine the duration of the ramps steps. The change in the trapping potential has to be compatible with the adiabaticity criteria. We demand that

$$\frac{dU}{U} \ll 1 \text{ or } \frac{dU}{U} = \frac{1}{10} \tag{5}$$

By inserting equation (3) in (4) we find

$$\Delta t = \frac{10\,\alpha_p \gamma_{ev}}{1 - \alpha_{ev} \gamma_{ev} \Delta t_{prev}} \tag{6}$$

Applying these theoretically optimized ramps in our experiment was problematic due to the small η observed in the dipole traps we were able to create. The ambiguity of the small η values was initially lifted by inserting a 'by hand' an acceptable value for η equal to 4.7. The resulting value for the parameter α_{ev} is 0.3 and the corresponding evaporation ramp is shown in Fig. 1, while the related parameters are shown in the table below.

P_{in} (W)	P_{fin} (W)	waist (μm)	η	Γ_{el}	α_{ev}
33	14,52	136,9	4,7	300	0,3

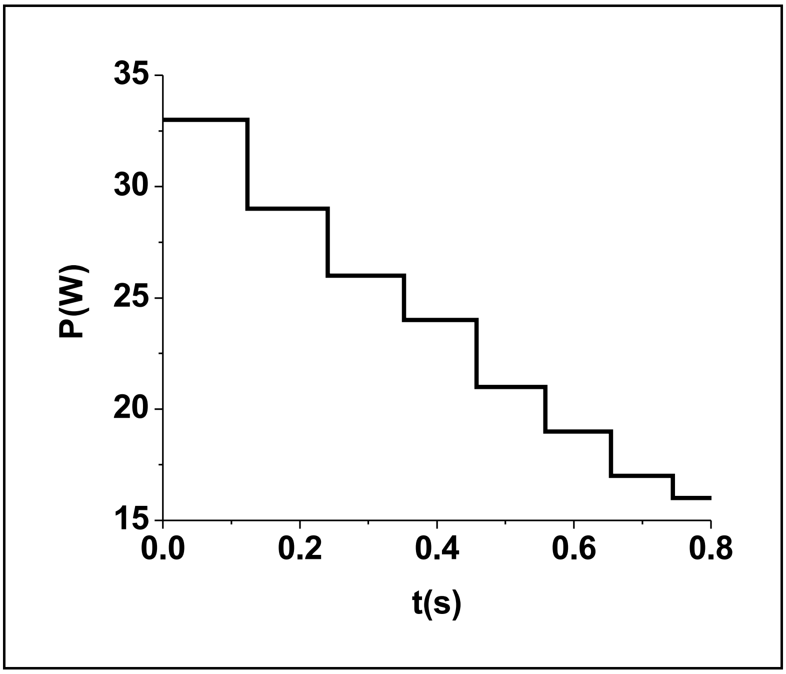

Fig. 1: Evolution of the power of the crossed dipole trap during the evaporation ramp.

This evaporation sequence was repeatedly realized and the dipole trap was detected by means of absorption imaging every 100 μs for times up to a second. In Fig. 2 we see the evolution of the number of atoms in the dipole trap during the evaporation ramp presented in Fig. 1. These results are compared to the theoretical prediction according to the theory developed in Chapter I2 (Eqs. 2.22 and 2.23).

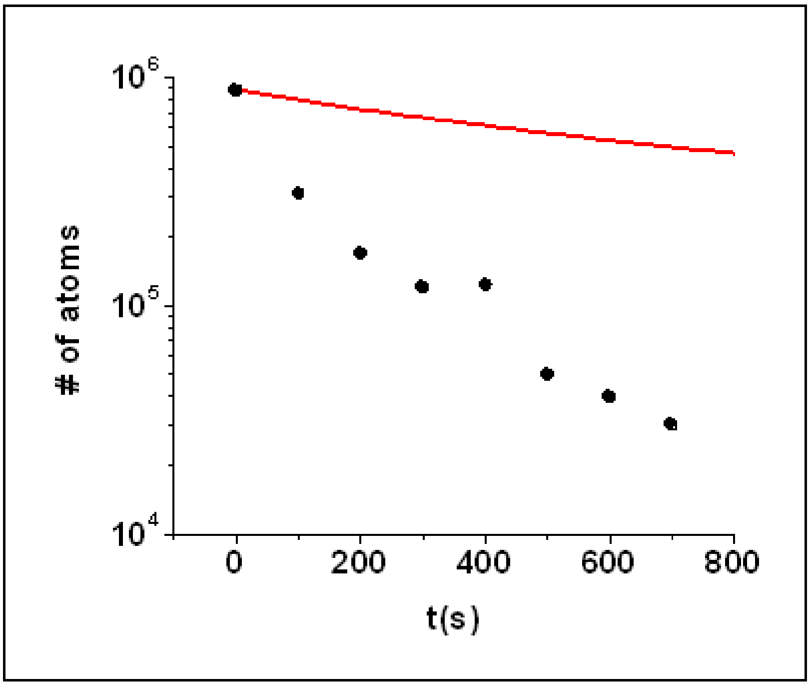

Fig. 2: Evolution of the number of atoms in the dipole trap during the evaporation sequence shown in Fig. 1. (Power ~60 W, waist ~167 µm) The red line corresponds to the theoretical prediction for the number of atoms according to Eqs. 2.23 and 2.24.

In Fig. 3 we see the evolution of the temperature of the trapped atoms during the same evaporation sequence, again compared to the theoretical prediction of Eqs. 2.22 and 2.23 for the same initial conditions. We see that the evolution of the trapped atoms temperature, although initially (first 500 µs) decreases much faster than the theoretical predictions, its final value does not lie too far away from the theoretically predicted value of ~12 µK. This is not the case for the atom number where the number of atoms detected in the end of the evaporation sequence is is almost 150 times lower than the value theoretically predicted. This large decrease in the trapped atom number, is probably explained due to the small η values, which suggest that the dipole trap's dynamics is mostly determined by spilling processes rather than evaporation. This decrease in the number of atoms perhaps suggested that the evaporation ramp presented in Fig. 1 was insufficient, and a different approach had to be used.

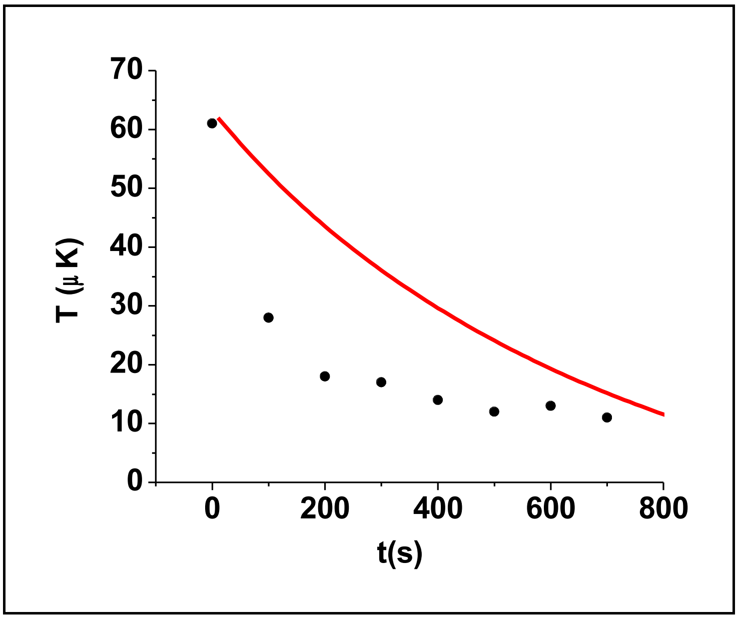

Fig. 3: Evolution of the temperature of the trapped atoms in the dipole trap during the evaporation sequence shown in Fig. 1. The red line corresponds to the theoretical prediction according to Eqs. 2.23 and 2.24.

The performance of the evaporation ramp was attempted to be improved by an different evaporation approach. In a conceptual level, the low η values inserted a big uncertainty in the preparation of the evaporation ramp, especially via the α_{ev} parameter, which is more strongly depended in η. In the alternative approach, we chose to fix the values of γ_{ev} while the value of the α_{ev} parameter was varied. Each resulting ramp was detected and the results of this study are shown in Fig. 4. We see that the value used in the previous study corresponding to the previous study was very far from optimized, while the best value for the α_{ev} parameters was found to be closer to five. The result of his study suggested that the theoretical approach of Chapter I2 is not applicable here due to the ambiguity inserted by the low η values.

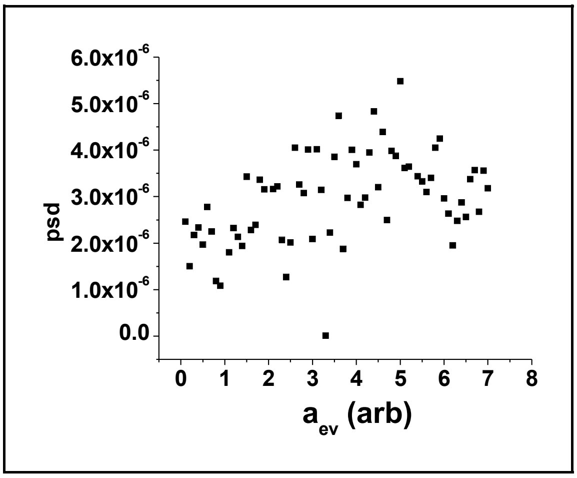

Fig. 4: Phase space density of the atoms remaining in the dipole trap for different values of the α_{ev} parameter.

ii. 'Experimentally optimized' ramp

In the previous paragraph, I discussed an approach for the evaporation cooling where the modulation of the dipole trap power is optimized according to several parameters of the dipole trap and the resulting evaporation 'ramp' is experimentally studied. Since the results of the evaporation cooling were poor, probably due to the low η values of the experimentally achieved dipole trap, an alternative approach for the realization of a successful evaporation ramp was tested. The approach was based in the capabilities of the experimental set up to generate repeatedly a particular experimental sequence, with a parameter varied form an initial to a final value, and on the same time to detect and store the temperature and number of atoms remaining at the dipole trap in the end of the experimental sequence. An example of such an optimization sequence is the previously shown Fig. 4, were an experimental parameter (α_{ev}) is varied between an initial and a final value and the final phase space density is displayed. Nevertheless, in this study, the optimization process is used in order to 'cover' the weakness inserted in the determination of α_{ev} due to the small values of η. We could go a step forward and try a much simpler optimization process, were the evaporation ramp is constructed step by step, by a similar optimization process.

A simple approach consist in considering an evaporation ramp of a given duration, where the crossed dipole trap power is varied linearly from an initial to a final value. The optimization of the ramp consists of repeating the evaporation sequence for different values of the final power and selecting the the value which corresponds to the higher phase space density observed. The optimized evaporation ramps produced by the theoretic approach of the previous chapter were never linear, a fact which suggests that a linear dependence on the power versus the time would not be able to provide with an optimized evaporation ramp. However, the evaporation ramp can be 'broken' in several steps, and the optimization process presented here can be applied in each step separately, permitting for more complicated time dependencies to result form this evaporation process.

In the period where this experimental study was conducted, the IPG fiber laser was out of use due to a technical problem[1]. We had always the alternative to use a 20 W Yag laser at 1064 nm.; This laser was used extensively for various studies, as well as for studies of evaporation. The difference between all previous studies was the lower dipole laser power (~12 W) which permitted the use of a normal AOM, but restricted us to the study of traps of much smaller dimensions (~40 μm). However, the phase space densities achieved with these kinds of traps where not much smaller than the ones achieved by the IPG laser with waists ~3 times larger, and most importantly for the evaporation studies, the lifetimes of these traps were similarly close to 0.5 s. Analogous experimental studies of the optimization of the evaporation ramps were made by the IPG laser as well, however, the study presented here was the first of its kind, and was never repeated in better detail, thus the data presented here are the most detailed study of the experimental optimization of the evaporation ramp available.

In Fig. 5 we see an example of the experimentally optimized evaporation ramp. The evaporation sequence is cut in five 'parts' of 100 ms duration each. In part (a) we see the optimization process which leads to the choice for the dipole trap's power according to the phase space densities achieved. In part (b) we see the resulting evaporation ramp and in part (c) we see pictures of the dipole trap in the end of each of the ramp's 'parts' with the use of absorption imaging.

---

[1] The special, high power AOM which controlled this laser was out of order

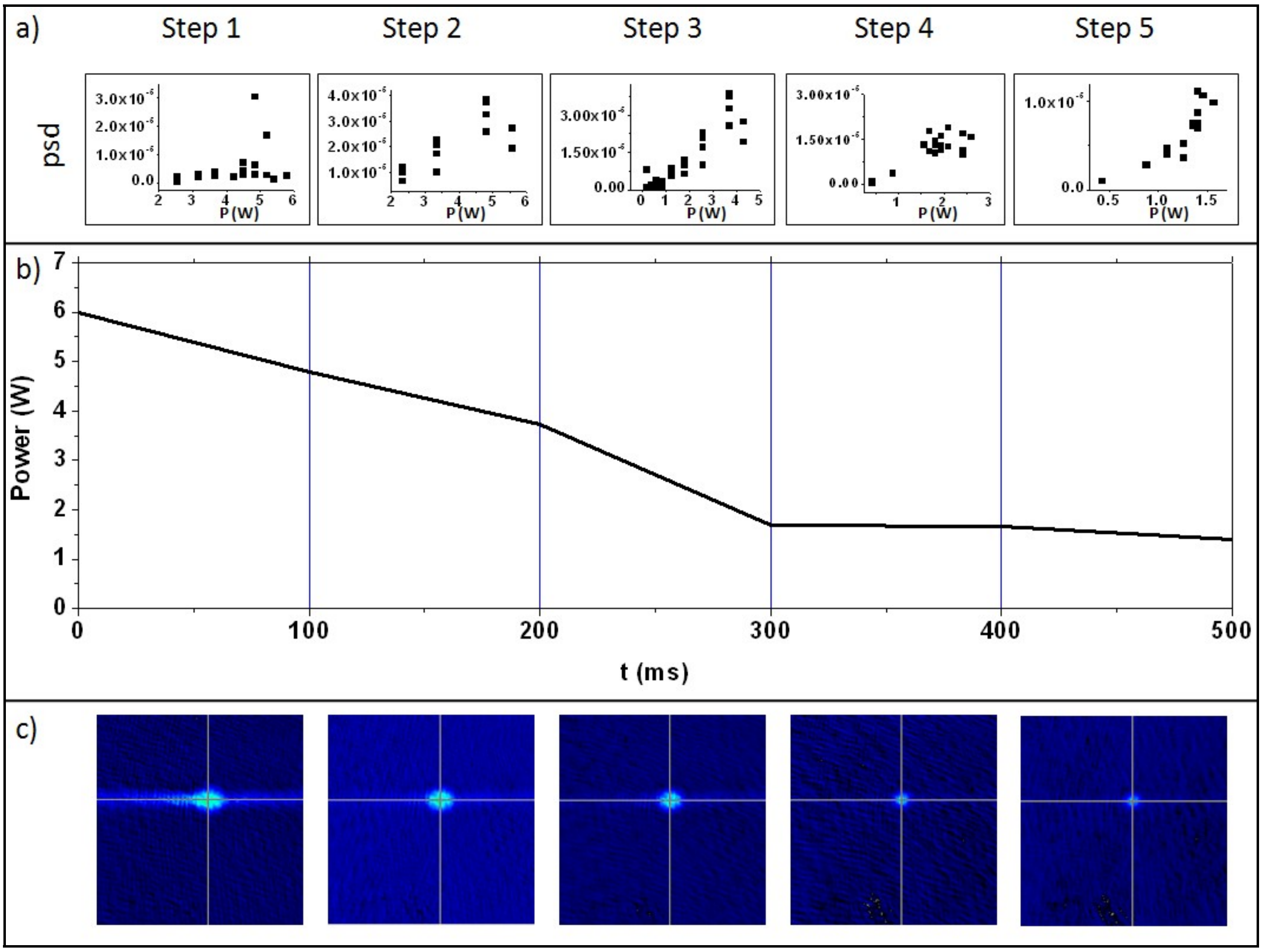

Fig. 5: Experimentally optimized evaporation ramp. The ramp, which has a total duration of 500 ms, is divided into five equal steps. The final power of the linear ramps of each optimization step is chosen according to the phase space density of the atoms in the dipole trap. In part (a) we see the phase space densities achieved for each different choice of the final power. In part (b) we see the resulting evaporation ramp and in (c) absorption images of the atoms remaining in the dipole trap in the end of each step.

In Fig. 6 we see the evolution of the *N(t)/N(0)* and *T(t)/T(0)* ratios during the ramp presented in Fig. 5(b), were *N(t)* and *T(t)* the number of atoms and temperature of the atoms in the crossed dipole trap. We see that the number of atoms do not exhibit the fast decay as in Fig. 2, however this low decrease (~0.5) is not accompanied by a sufficient decrease of the temperature. The study could not continue for larger times, since the density of atoms in the dipole trap was too low for the absorption imaging results to be trustworthy. Studies of the evaporation as the ones described in this annex were often repeated, as we were hopping to observe temperature decreases that could result to a more long lived and, in general, better behaved trap. The results were always similar: the evaporation process never resulted to an important increase of the phase space density of the trapped atoms, and their lifetime in the trap was never improved.

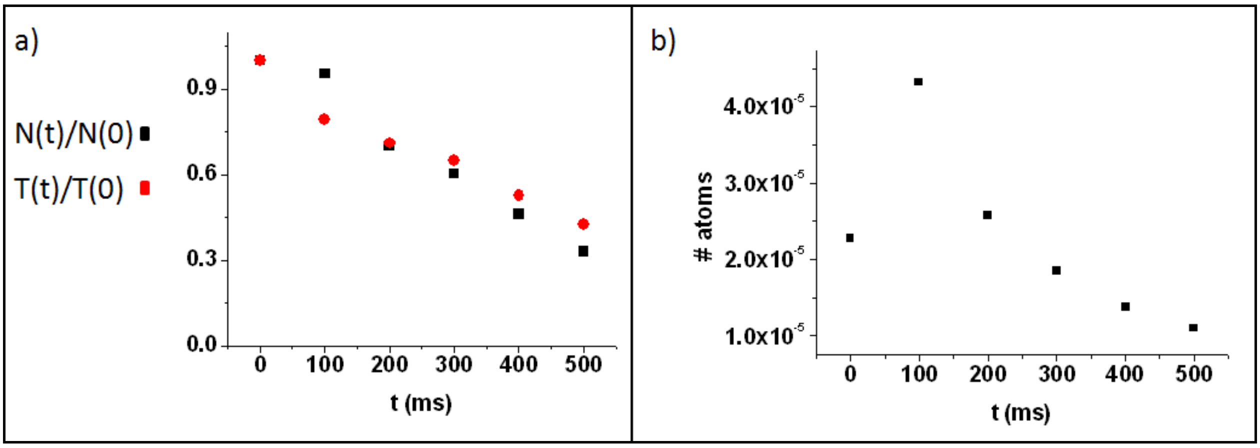

Fig. 6: a) Evolution of the ratios N(t)/N(0) and T(t)/T(0) during and evolution of the phase – space density (b) the ramp presented in Fig. 5(b).

b) Compression of the crossed dipole trap

In Chapter I2 we considered real time modification of the dipole trap's waist during the evaporation process in order to increase the evaporation efficiency. We predicted that reducing the trap's dimensions could improve the evaporation process, leading to smaller duration of the evaporation ramp necessary to produce a Cs condensation. When evaporation is performed in dipole traps simply by reducing the trapping laser's power, as considered here, the frequency of the oscillation of the atoms in the dipole trap is reduced, a fact which decreases the ramp's efficiency and leads to larger thermalisation times. The ability to control the dipole laser's waist allows to keep this frequency constant, or even increase it during the evaporation sequence, leading to increased overall evaporation efficiency. Decreasing the dipole trap's dimensions has a heating effect in the trapped atoms, however this is easily compensated by the evaporation cooling for appropriate choice of parameters, provided of course, that evaporating cooling is successful.

Compression of the dipole trap was experimentally studied, since this ability was provided by the piezoelectric-driven zoom discussed in Chapter I3. The hope at that time was that we would be able to load large number of atoms in large trap dimensions and conserve a big part of them to a much more confined trapping potential, where evaporation could be much more efficient than observed. For this reason, we prepared a crossed dipole trap of 137 μm waist and loaded it by a CMOT as described in paragraph I.4.3.

The compression was studied with and without simultaneously reducing the dipole laser's power. Optimized ramps for the waist and for the power of the dipole laser can be provided by an optimization similar to the theoretical optimization discussed in the previous paragraph. In this case the waist has to evolve according to

$$w = w_{\text{in}}(1-\alpha_{ev}\gamma_{ev}\Delta t)^{\frac{-\alpha_{w_0}}{\alpha_{ev}}} \tag{7}$$

but now the time Δt is more generally calculated to be

$$\Delta t = \left(\frac{10\alpha_p\gamma_{ev}}{1-\alpha_{ev}\gamma_{ev}\Delta t_{prev}} + \frac{2\alpha_{w_0}\gamma_{ev}}{1-\alpha_{ev}\gamma_{ev}\Delta t_{prev}}\right)^{-1} \tag{8}$$

where α_{w0} is a parameter that depends on the optimization process. We have practically tested the compression for several final waists and several compression velocities (meaning the velocity with which we move the zoom's lens, and which is practically linearly connected to the waist minimization in the trap's region). We observed that the compression leads to loss of almost all the atoms in the dipole trap for compression velocities higher than 20 mm/s, while the best results were observed with velocities of 10 mm/s. With such velocities we were able to compress the dipole trap almost to the half of its initial size within 250 ms, while further decrease of it's dimensions lead to larger losses. This compression speed corresponds, for the dipole trap of 137 μm waist and 66 W total power discussed here, to an α_{w0} equal to 0.9, which results to the evaporation and waist ramp shown in Fig. 7. In part (a) we see the optimized ramp calculated by Eqs. 3 and 6 while the waist ramp, shown in part (b) is calculated according to Eqs. 7 and 8. Since we choose to modify the waist linearly, the actual waist ramp is the linear approximation of the theoretically predicted one shown by the red curve. The piezoelectric translation stage gives us the possibility to create more complicated waist ramps, since, except for the initial and final zoom position and velocity, we can choose the acceleration (or deceleration) of the zoom's motion. Moreover, we can update these parameters during the ramp duration, and thus create almost arbitrary compression curves. However, this was not considered to be necessary, since the simple compression used here should suffice if the overall process is successful.

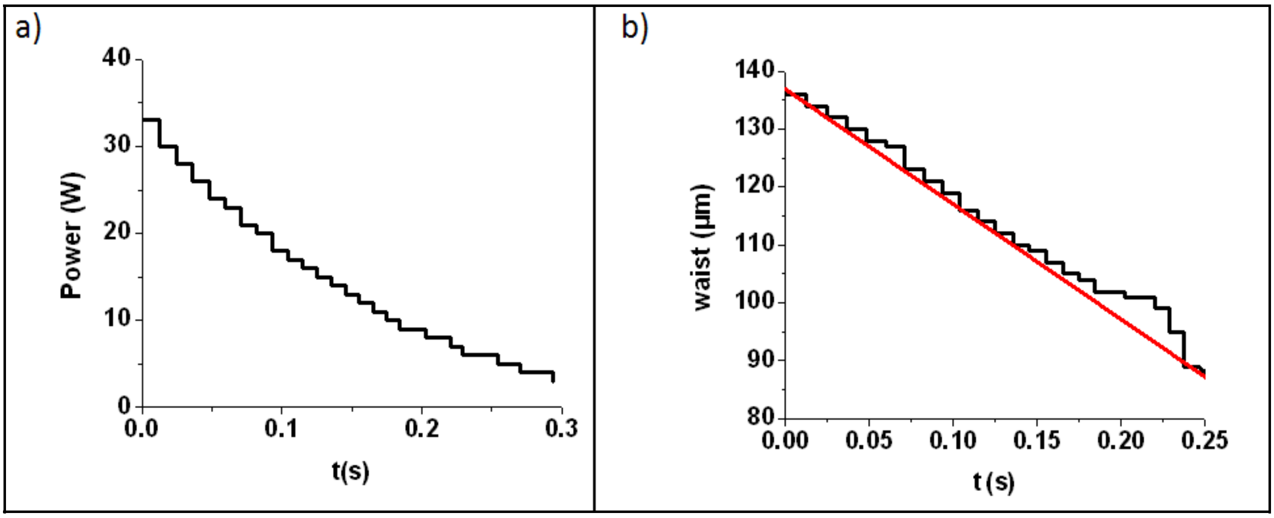

Fig. 7: Theoretically optimized evaporation (a) and waist (b) ramps. The waist ramp actually used corresponds to the red curve shown in part (b).

In Fig. 8 we show the dipole trap compressed from an initial waist of 137 μm to 87 μm, with the 'waist ramp' shown in Fig. 7(b), with (ii) and without (i) the modification of the dipole laser's power shown in Fig. 7(a). In part (i.a) we see the dipole trap detected before any compression. The trap contains ~4.5 10^5 atoms in a temperature of 260 μK. In part (i.b) we see an image of the same dipole trap observed after 250 ms, without any modification of the dipole laser's dimensions or power. In part (i.c) we see the trap after only its waist is modified according to the red curve in Fig. 7(b). In part (ii.a) the same trap is detected with a slightly bigger atom number and temperature. In part (ii.b) the trap is observed after the passage of 250 ms while it's power alone is modified as shown in Fig. 7(a). In part (ii.c) the power and waist are simultaneously modified as shown in Fig. 7.

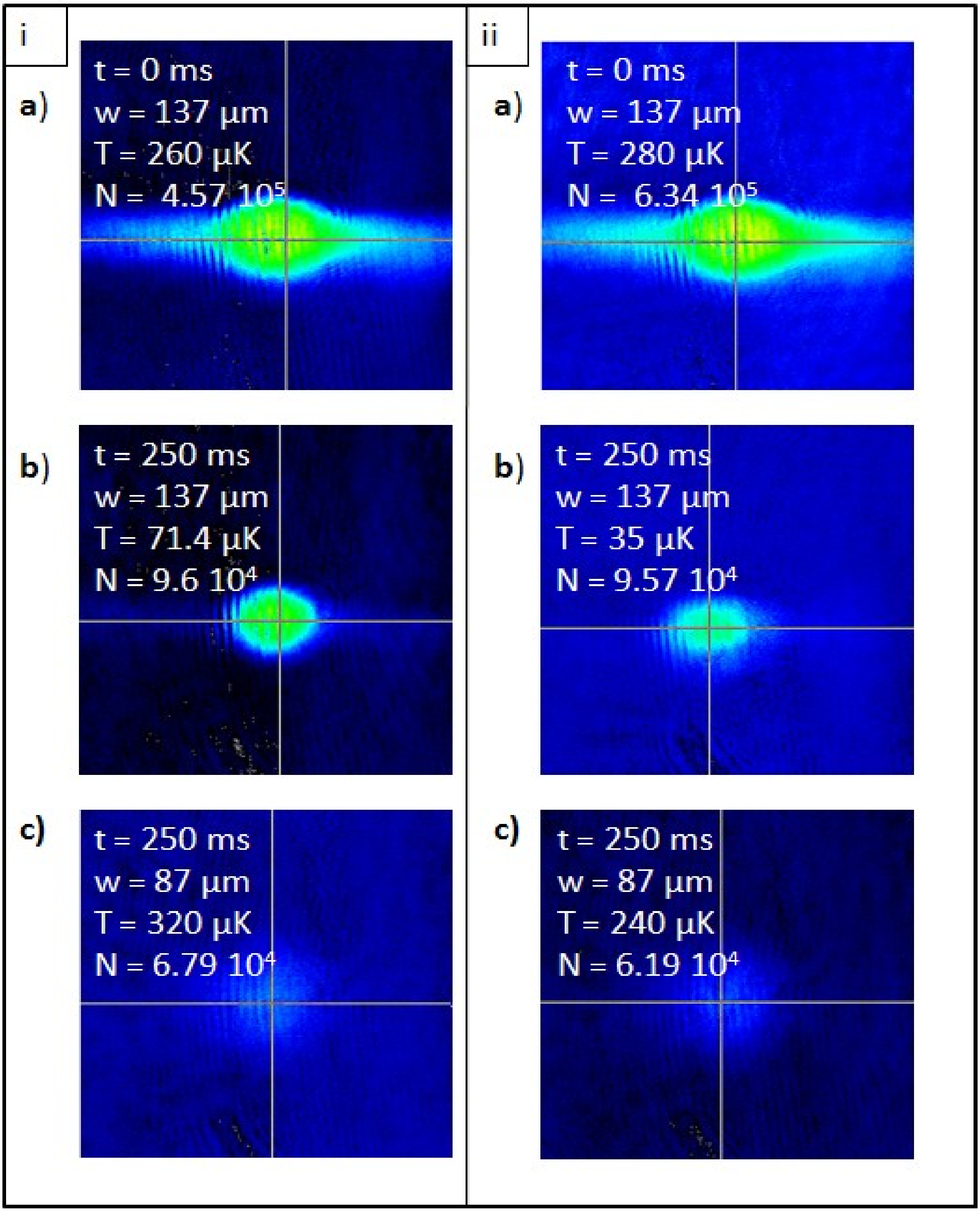

Fig. 8: Compression of the crossed dipole trap. On the left (I) a dipole trap of waist of 137 µm, containing 4.57 10^5 atoms in a temperature of 260 µK (a) is compressed to 87 µm (c) with no simultaneous decrease of the dipole laser's power. The waist is decreased linearly within 250 ms. In (b) the same dipole trap is observed after 250 ms without any waist compression for comparison. On the right (II) the same compression is realized with simultaneously applying an evaporation ramp in the dipole laser's power. In (a) the trap is observed before compression and evaporation are applied, in (b) the trap is observed after 250 ms, without any waist compression or power modification while in (c) it is observed after compressing to 87 µm and decreasing the power according to Fig. 7(a).

We were surprised to see that such a modification of the trap's dimensions hardly modified the number of atoms in the dipole trap. However, the accompanied temperature rise was not compensated by the power ramp, a fact that can be attributed in the overall poor performance of the evaporation. Similar studies where performed for various traps. One of these studies is shown in Fig. 9. The waist has been compressed from the initial value of 320 μm to a final value of 180 μm with a the dipole laser power kept constant. We see that this compression is accompanied with a decrease of more than an order of magnitude in the atoms number and by a doubling of the atoms' temperature.

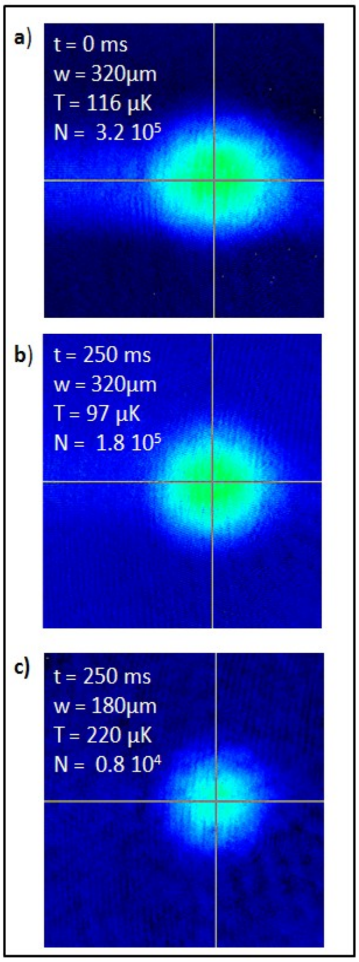

Fig. 9: Compressing the dipole trap from ~320 μm to ~180 μm with no simultaneous modification of the dipole laser's power. In part (a) the dipole trap is detected before any modification in the dimensions and the power of the dipole laser. In part (b) the trap is detected after 250 ms and in (c) after modifying in the dimensions but not the power of the dipole laser.

In general, we could say that compression of the dipole trap gave promising results, however, they were not accompanied by an satisfactory performance of the evaporation cooling. The reason for the failure of the evaporation process has to be related with the small lifetimes of the dipole traps prepared, which has to be related to the η parameter in the dipole trap after the loading, no matter which loading strategy was followed. Compression had a relatively positive performance, although its results cannot be easily analyzed and, in any case, it was not enough in order to provide with improved dipole traps and to bring our experiment closer to the achievement of Cs condensation.

ANNEX I.3

Experimental tests on the quality of the dipole trapping potential

In this paragraph I present a series of simple experimental test realized in order to verify that the dipole trapping potential corresponds to the one described in [Comp06] and Chapter I2. The first experimental test is related to the intensity profile of the trapping laser. The usual Gaussian profile can be alternated by various reasons such as insufficient scattering in the AOM, absorption by dust accumulated in the various optics or misalignment in one of them. The second test aims to exclude the possibility of interference between the two crossed dipole beams. These studies are chosen to be shown in order to reduce the possible causes of inconsistency between the theoretical prediction and the experimental studies.

a) Verification of the intensity profile of the dipole laser along the various elements

The ability to inspect the intensity profile of the dipole trap laser was provided by the use of a WinCamD^{TM} CCD camera, which was constructed by DataRay Inc. and borrowed to us by the Cold Atom group in Laboratoire Aimé Cotton (L. Pruvost). This camera in combination with the DataRay v600G10 software gives the ability to visualize the intensity profile of CW or a pulsed laser. The way such a camera is used is that the beam is inserted to it after having pass for a number of reflections, so that the power is sufficiently reduced. Since an intensity of more than some mW/cm^2 saturate the camera, and since reflection in uncoated glass in ~90° results to ~10% of the incoming power to be reflected, we need to insert the beam in the camera after having reflected it 5-6 times if we want to visualize it's intensity profile in maximum power. The way this is realized is by using thick peaces of uncoated glass, and collecting the 3rd of 4th internal reflection. This is done in angles larger than 45°, a fact that increases the attenuation of the laser power and contributed to the safety of the equipment during the measurement. Since the visualization of the intensity profile is done in arbitrary units the exact attenuation factor is not required to be known

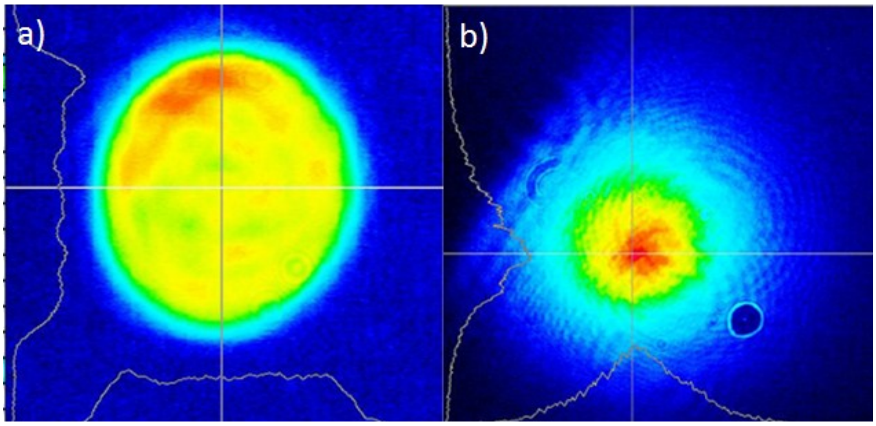

Fig. 10: Intensity profile of the dipole laser after passing the AOM with a waist of (a) 500 μm and (b) 2 mm. In the first case the intensity profile is deformed due to insufficient diffraction.

It is relatively easy for the intensity profile of the dipole laser to be alternated, since a number of experimental imperfections can lead to a modification, especially when the power is high. In Fig. 10(a), we see the intensity profile of the dipole laser beam after passing the AOM with a waist of ~500 μm. Such a waist is smaller than the minimum waist required by the AOM's specifications. Passing the dipole laser in these dimensions by the AOM was an error that resulted from the confusion among multiple definitions of the Gaussian laser waist, involving or not a 2 factor. The result of this error was that the photon diffraction in the acoustic crystal becomes insufficient for high intensity, so that the central, more intense part of the beam is only partially diffracted, and the observed 1st diffraction order has a top hat, rather than a Gaussian shape. As shown in Fig. 10(b), as soon as the laser waist is set to 2 mm, the intensity profile is much closer to a normal Gaussian.

Such a study of the intensity profile of the laser beam was performed more than once between all the elements of the dipole trap. Except for the error reveled in the AOM set up once, none other important intensity profile modification was reveled, even when the laser power was set to its maximum value of 100 W, a value rarely used in the experiment. Thus, the conclusion of this paragraph is that the a possible error on quality of the dipole laser profile can not explain our experimental results.

b) A study of interference between the two crossed dipole beams

Interference between the crossed dipole beams is possible if the coherence length of the laser is larger than the separation between the two arms. Interference can result to a trapping potential very far away from the Gaussian shaped potential considered in Chapter I2 and shown in Fig.2.2, since a series of local potential minima and maxima are created in the areas where interference is constructive or destructive respectively. Furthermore, the position and the depth of these local minima depends in the exact position and polarization of the dipole laser beams. If we assume that the dipole laser beam's position is always modified due to vibrations in the various optics (for example mirrors), the potential created by interference is much more sensitive than the potential created by the simple overlap of the potential of two Gaussian beams.

For light with a Lorentzian optical spectrum, the coherence length can be calculated as

$$L=\frac{c}{\pi \Delta \nu} \tag{1}$$

where c is the speed of the light, and $\Delta\nu$ the spectral width of the source. The spectral bandwidth of the dipole laser was measured (several months later) with the use of a Avantes AvaSpec-128 Fiber Optic spectrometer for various values of its power as shown in Fig. 11. From the spectra shown in Fig. 11 and Eq. 1 the coherence length is found to be inferior to a mm (~0.3 mm) .

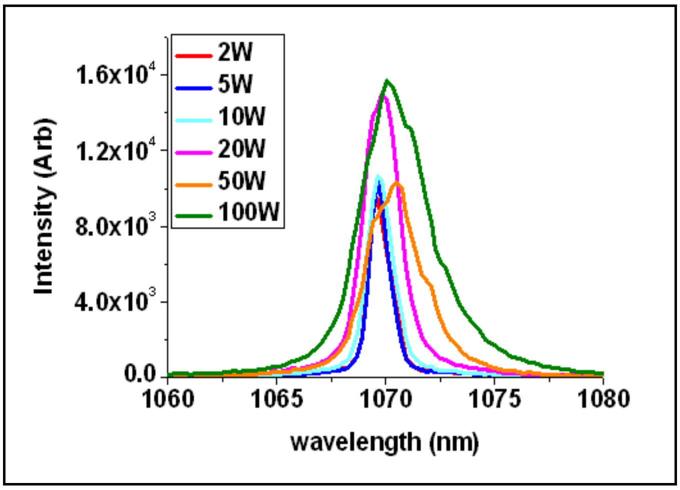

Fig. 11: Spectra of the IPG fiber laser for various values of the power as indicated in the inlet.

Nevertheless, in a period where all the experiment components where examined in order for the reduced loading efficiency to be explained, the possibility of interference in the crossed beam was also studied. This possibility was relatively easy to be examined by the following test. The polarization of one of the dipole trap's beams was rotated so that the angle between the polarization vectors of the two beams is varied from 0° to 90°. The number of atoms loaded in the dipole trap was observed after the passage of ~1 ms after the end of the loading process (C-MOT loading here). If interference effects are present, their effect should strongly vary with respect to this polarization angle, so the number of atoms should have some dependence on it. In the case that such a dependence was found, the polarization angle would be fixed in the value for which the maximum number of atoms would be observed, in order to minimize interference.

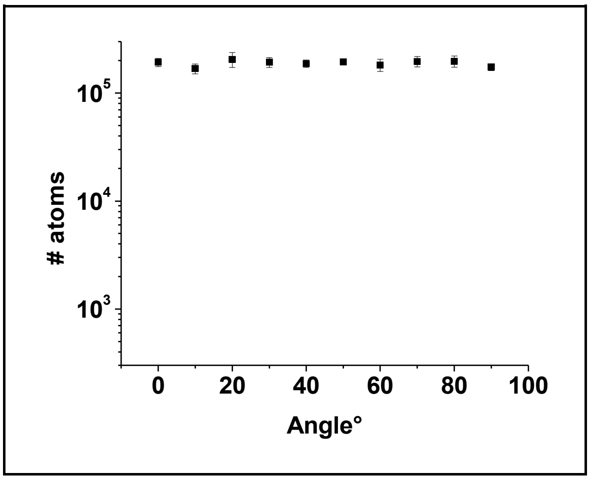

Fig. 12: Results of the experimental test performed to detect possible interference between the dipole trap's crossed beams. The number of atoms loaded in the crossed dipole trap is plotted versus the angle of the polarization of the crossed dipole trap.

As shown in Fig. 12, where the number of detected atoms is plotted versus this polarization angle, no clear dependence is found, while the small variation of the atom number is probably due to atom number fluctuations between the subsequent loading sequences. In each point the number of atoms was detected five times and averaged and the standard deviation was used in the error bars. Thus interference effects were no longer considered and the polarization elements used for this study were removed.

ANNEX II.1

Rate equations for the simulation of the vibrational cooling method

In this Annex I describe the process of describing the optical pumping process in our experiments with the use of rate equations. The simulation is based on the information for the Potential Energy Curves (PECs) for the particular molecular system. For the case of Cs, this information was provided by calculations of Olivier Dulieu and Nadia Balufa.

Using the known X and B potential curves and their rotational constants, we can calculate the ro-vibrational energy levels as well as the Frank-Condon (FC) factors for the transitions. With this information, the optical pumping process can be simulated and the efficiency of the vibrational cooling method can be predicted. These simulations are proved valuable, since on the one hand, they can be used for the estimation of parameters which cannot be experimentally determined, with the most important being the overall efficiency of the vibrational cooling technique. On the other hand, these simulations have been widely used for the preparation of various experiments, especially of these ones described in the current chapter, since they allow the optimization of several important experimental parameters.

Our simulations are based in the rate equations for the system molecule – shaped pulse, a choice, which simplifies considerably the corresponding C++ programs. This choice is justified by the fact that the average laser intensity is very low during our experiments, and that coherent effects do not seem to be important. Thus, we could assume that the excitation probability is simply proportional to the laser spectral density at the transition frequencies, to the FC factor, the transition dipole moment, and to the Hönl-London factor. The rate equations used are simplified according to simple considerations that are explained in the following. Thus, they are solved analytically, and these solutions consist the kernel of our simulating program. If needed, any set of rate equations can be solved using for instance Kinetic Monte Carlo modeling [Cho08].

There are two rate equation sets that used for the realization of the vibrational cooling simulations, one concerning the excitation by the laser field, and another concerning spontaneous emission.

Let us begin our description with the, conceptually simpler, spontaneous emission step. Here, the only possibility for the population exchange between the ground X and the excited A state, is via the spontaneous emission. The rate equations that describe such a situation are:

$$\frac{dN_{v_A}(t)}{dt} = -\sum_{v_X} \Gamma_{v_A \to v_X} N_{v_A}(t) \tag{1}$$

$$\frac{dN_{v_X}(t)}{dt} = \sum_{v_A} \Gamma_{v_A \to v_X} N_{v_A}(t) \tag{2}$$

where with $N_{X,A}$ we symbolize the number of atoms in the ground and in the excited level respectively, and with $\Gamma_{vA \to vX}$ we symbolize the transition rate from the state with v_A to the state with v_X. This rate, as we recall from the first chapter, is proportional to

$$\Gamma_{v_A \to v_X} \propto FC[v_X][v_A](D[v_X][v_A])^2 \omega^3_{A \to X} \tag{3}$$

where with $FC[v_X][v_A]$ and with $D[v_X][v_A]$ we symbolize the Franck-Condon coefficient and the dipole moment of the associated transition, while with $\omega_{A \to X}$ the transition frequency. Solving equation 4.1 results to the following expression for $N_{vA}(t)$

$$N_{v_A}(t) = N_{v_A}(0)\, e^{-\sum_{v_{X'}} \Gamma_{v_A \to v_{X'}} t} \tag{4}$$

By substituting 4.4 to 4.2 and integrating from t = 0 to t = ∞ we result to

$$N_{v_X}(\infty)-N_{v_X}(0)=\frac{1}{\sum_{v_{X'}}\Gamma_{v_A\to v_{X'}}}\sum_{v_A}\Gamma_{v_A\to v_X}N_{v_A}(0) \tag{5}$$

Integration to infinity is a first approximation that we insert to our calculations. In the conditions of our experiment, the end of the spontaneous emission process is not in infinite time, but ~12,5 ns after excitation. We assume that during this time, all molecular population has relax and thus, each arriving pulse finds the excited state empty.

This relation can be re-written for the molecular population, a choice which is more convenient when considering the simulation program. If we define $p_{vA}(t) = N_{vA}(t)/N_{tot}$ and $p_{vB}(t) = N_{vB}(t)/N_{tot}$, with N_{tot} the initial total molecular population, then Eq. 5 can be written as

$$p_{v_X}-p_{v_X}(0)=\frac{1}{\sum_{v_X}\Gamma_{v_{A'}\to v_X}}\sum_{v_A}\Gamma_{v_A\to v_X}p_{v_A}(0) \tag{6}$$

while the approximation indicated previously means that

$$p_{v_A}=0 \tag{7}$$

Considering the excitation step, the rate equations are

$$\frac{dN_{v_A}(t)}{dt}=-\sum_{v_X}\Gamma_{v_A\to v_X}N_{v_A}(t)+\sum_{v_X}\Gamma_{v_X\to v_A}N_{v_X}(t) \tag{8}$$

$$\frac{dN_{v_X}(t)}{dt}=\sum_{v_A}\Gamma_{v_A\to v_X}N_{v_A}(t)-\sum_{v_A}\Gamma_{v_X\to v_A}N_{v_X}(t) \tag{9}$$

where with $\Gamma_{vX\to vA}$ we symbolize the transition rate from the state with v_X to the state v_A and which now is (10)

$$\Gamma_{v_A\to v_X}\propto FC[v_X][v_A](D[v_X][v_A])^2\omega_{A\to X}^3 I_{laser}[v_X][v_A]$$

which is similar to equation 4.3 except for the inclusion of the excitation laser's intensity.

Equations 8 and 9 include two terms each, since now we have to include both absorption and spontaneous emission. In equations 8 and 9, we neglect spontaneous emission due to the small laser's intensity. However, since we are considering absorption of pulse of duration of less than 100 fs, the terms describing spontaneous emission in equations 8 and 9 can be omitted, since the spontaneous emission in such small time intervals is negligible. In this case, the rate equations are approximated by

$$\frac{dN_{v_A}(t)}{dt}=\sum_{v_X}\Gamma_{v_X\to v_A}N_{v_X}(t) \tag{11}$$

$$\frac{dN_{v_X}(t)}{dt}=-\sum_{v_A}\Gamma_{v_X\to v_A}N_{v_X}(t) \tag{12}$$

Similarly as before, we solve Eq.8 to find $N_{vX}(t)$

$$N_{v_X}(t)=N_{v_X}(0)e^{-\sum_{v_A}\Gamma_{v_X\to v_A}t} \tag{13}$$

and we substitute to Eq. 9 to take

$$\frac{d\,N_{v_A}(t)}{dt}=\sum_{v_X}\Gamma_{v_X\to v_A}N_{v_X}(0)e^{-\sum_{v_A}\Gamma_{v_X\to v_A}t} \tag{14}$$

Integrating Eq.14 from t = 0 to t = 100 fs (the pulse duration) gives

$$N_{v_A}(\tau)-N_{v_A}(0)=\sum_{v_X}\Gamma_{v_X\to v_A}N_{v_X}(0)\left(\frac{1-e^{-\sum_{v_A}\Gamma_{v_{X'}\to v_A}\tau}}{\sum_{v_A}\Gamma_{v_{X'}\to v_A}}\right) \tag{15}$$

Since the pulse duration, which should be inferior to hundred femtoseconds, is small, we can do the following approximation

$$e^{-\sum_{v_A} \Gamma_{v_X{}' \to v_A} \tau} \approx 1 - \sum_{v_A} \Gamma_{v_X{}' \to v_A} + \left(\sum_{v_A} \Gamma_{v_{X'} \to v_A}\right)^2 \approx 1 - \sum_{v_A} \Gamma_{v_{X'} \to v_A} \tag{16}$$

¿

Dividing with N_{tot} to take the expressions for the populations p_{vX} and p_{vA}, and taking into consideration that $p_{vA} = 0$ we have

$$p_{v_A}(\tau) = \sum_{v_X} \Gamma_{v_X \to v_A} p_{v_X}(0) \tag{17}$$

while for the population of the ground state, we have from Eq. 13

$$N_{v_X}(\tau) = N_{v_X}(0) e^{-\sum_{v_A} \Gamma_{v_X \to v_A} \tau} \tag{18}$$

and by applying approximation 16 and dividing with N_{tot}, we take

$$p_{v_X}(\tau) = p_{v_X}(0)\left(1 - \sum_{v_A} \Gamma_{v_X \to v_A}\right) \tag{19}$$

Equations 17 and 19 describe the femtosecond laser absorption, like Eqs. 6 and 7 describe spontaneous emission in our system, and are found in the kernel of the C++ program that simulates the optical pumping process.

ANNEX II.2

In this Annex I will briefly describe the operating principle of the GRID and OVERLAP programs used for the calculation of the Franck-Condon and FC-dipole parabolas shown throughout this thesis. The material for this description was found in references [Kokoo99, Kokoo99b], where the reader could search a more detailed description. Calculation of the Franck-Condon factors was not a trivial task to me, and I was in position to perform it only with the help of members of the theoretical group 'Molecules froides' of Laboratoire Aimé Cotton. In particular, the calculations were performed with the use of the programs GRID and OVARLAP, written in FORTRAN by Viatcheslav Kokoouline [Kokoo99]. Besides the help of Viatcheslav, I also counted upon the guidance of Nadia Bouloufa and Olivier Dulieu, while I acknowledge discussions on the general subject of cold molecules with Vladimir Akouline and Romaine Gouerout. I also had the luck to accept the valuable help of Manabendra Bera, who was familiar with the use of the OVERLAP software and contributed to a long 'debugging' process.

The GRID program is actually solving the Schrödinger equation numerically, and provides with the energy levels of the vibrational states as well as the wavefunctions that correspond to each one of them. It is based in the Fourier Grid Representation (FGR) method which is considered to be one of the most effective methods for the solution of this type of differential equations. The scheme presented here was developed mainly by R. Kosloff in the period 1983-1993. The calculations are performed employing a discrete grid, the wave function is represented on a finite set of grid points. The Schrödinger for an eigenvalue problem can be written as

$$[T+V(R)]\Psi(R)=E\Psi(R) \tag{1}$$

We consider the grid to have points that are equally spaced in *R*, which is the internuclear distance. Thus, we define the grid as R_i, (i =1,N). We can introduce a set of functions defined at the grid points

$$\phi_i(R_j)=\delta(R_i-R_j),(i,j=1,N) \tag{2}$$

With this functions we can define a basis in which the Hamiltonian of Eq. 1 can be represented by an rectangular matrix of dimension *N*. The potential energy operator *V(R)* is diagonal in this coordinate representation. We can pass to an analogous representation in the momentum space with a simple Fourier transformation. In this case it is the kinetic energy operator *T* which would be diagonal. The elements of the operator *T* can be written as a function of the number of grid points *N* and the total length of the grid *L*

$$T_{i,i}=\frac{\pi^2}{\mu L^2}\frac{N^2+2}{6} \tag{3}$$

$$T_{i,j}=(-1)^{i-j}\frac{\pi^2}{\mu L^2}\frac{1}{\sin^2[(i-j)\pi/N]} \tag{4}$$

where μ is the reduced mass of the (molecular) system. The eigenenergies of the system can be directly calculated by diagonalization of the composite T + V matrix. In the particular case of the GRID program used here, this is done with the use of the LAPAC library.

An approximation of the wavefunction $\Psi(R)$ can be a finite set of *N* analytical, linear independent functions $g_n(R)$:

$$\Psi(R)\approx\bar{\Psi}(R)=\sum_{n=1}^{N}a_n g_n(R) \tag{5}$$

or in the matrix form by

$$\Psi=Ga \tag{6}$$

where Ψ and a are *N*-component vectors and G is a rectangular matrix with dimension *N*. The grid points are chosen so that the expansion functions obey the orthogonality relation:

$$\sum_{n=1}^{N} g_n^*(R_i)\, g_n(R_j) = \delta_{i,j} \tag{7}$$

Thus, the coefficients a_n are calculated by

$$a_n = \sum_{j=1}^{N} \Psi_n^*(R_j)\, g_n(R_j) \tag{8}$$

There are various choices for the definition of the functions g_n. In [Kokoo99], an exponential basis is chosen

$$g_k = \frac{1}{\sqrt{N}} e^{i2\pi kR/L} \tag{9}$$

where k is an index 'running' from *-(N/2 -1)* up to *N/2*. This is called the coordinate basis since it is the coordinate R which is found in the function's argument. An additional definition is used in [Kokoo99b]:

$$\Psi_q = \sum_{j=1}^{N} \Psi(q_j)\, sinc\left(\frac{\pi(q - q_j)}{\Delta q}\right) \tag{10}$$

where q_j is a working uniform grid, q is any intermediate point, Δq is a grid step, and we have defined the function *sinc(z)=sin(z)/z*.

The OVERLAP program takes as an input the vibrational wavefunctions as well as the dipole of the transition calculated on the grid points. The resulting Franck-Condon (or FC-dipole)coefficients are just the point-by-point multiplication of the above on the grid.

When the vibrational motion extends at very long range, like for example in the long-range molecules created by photoassociation, the grid length L has to be large, and the overall computation becomes very heavy. A way to go around such a problem is the Mapped FGR method. There, the points of the grid are not set in equal distances, but vary according to the shape of the molecular potential. In particular, the grid points are more dense in areas that are important for the calculation and less dense in areas is which the results of the calculation are not so sensitive. This mapping is also useful when the shape of the potential curves is complicated (like for example in complexes as the one shown in Fig. II.6.3.a.1. However, I have not used such a procedure, since the molecular potentials I used were relatively simple and the calculation of highly excited vibrational states was not required. In Fig.1, we see a schematic representation of the mapping, for more details on the subject the reader should defer to [Kokoo99].

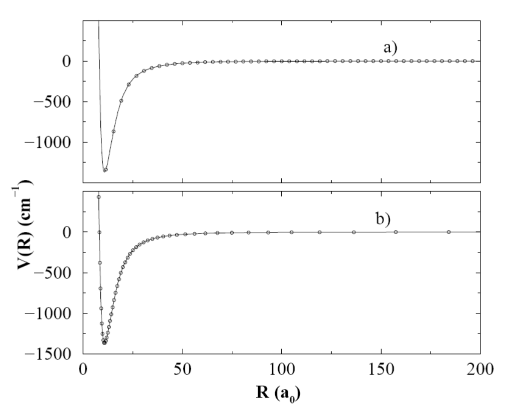

Fig. 1: Schematic example of the mapping. In (a) we see the simple case were the grid points are considered to be equidistant, while in (b) the advance mapping is used.

Knoo08 : S. Knoop, F. Ferlaino, M. Mark, M. Berninger, H. Schoebel, H.-C. Naegerl, R. Grimm, 'Observation of an Efimov-like resonance in ultracold atom-dimer scattering' arXiv:0807.3306v1

Kast66 : A. Kastler Nobel Lectures, Physics, 1966.

Sof09c : D. Sofikitis, A. Fioretti, S. Weber, M. Viteau, A. Chotia, R. Horchani, M. Allegrini, B. Chatel, D. Comparat and P. Pillet ' Broadband Vibrational Cooling of Cold cesium Molecules: Theory and Experiments ' *Chin. J. Chem. Phys.* **22** No 2 (April 2009) 149-156

Knoo08 : S. Knoop, F. Ferlaino, M. Mark, M. Berninger, H. Schoebel, H.-C. Naegerl, R. Grimm, 'Observation of an Efimov-like resonance in ultracold atom-dimer scattering' arXiv:0807.3306v1

Kast66 : A. Kastler Nobel Lectures, Physics, 1966.

Sof09c : D. Sofikitis, A. Fioretti, S. Weber, M. Viteau, A. Chotia, R. Horchani, M. Allegrini, B. Chatel, D. Comparat and P. Pillet ' Broadband Vibrational Cooling of Cold cesium Molecules: Theory and Experiments ' *Chin. J. Chem. Phys.* **22** No 2 (April 2009) 149-156

Perr98 : H. Perron, 'Refroidissement d'atomes de césium confines dans un piège dipolaire très désaccorde' Thesis LKB – Paris VI, (1998).

Web03 : T. Weber, J. Herbig, M. Mark, H.-C. Nägerl and R. Grimm, 'Bose-Einstein Condensation of cesium', *Science* **299**, **232**, (2003).

Thom04 : A.M. Thomas, 'Ultra-cold Collisions and Evaporative Cooling of Caesium in a Magnetic Trap', Ph.D Thesis, Jesus College, Oxford University, (2004).

Hung08 : C.L. Hung, X. Zhang, N. Gemelke and C. Chin, 'Fast, Runaway Evaporative Cooling to Bose-Einstein Condensation in Optical Traps', *Phys. Rev. A* **78**, 011604, (2008).

Comp06 : D. Comparat, A. Fioretti, G. Stern, E. Dimova, B. Laburthe Tolra and P. Pillet, 'Optimized production of large Bose-Einstein condensates', *Phys. Rev. A* **73**, 043410 (2006).

Stern08 : Stratégies pour le chargement d'un piège-dipolaire d'atomes froides de césium et le refroidissement évaporatif', Ph.D Thesis. Université Paris 11, Laboratoire Aimé Cotton, (2008).

Vit08 : M. Viteau, A. Chotia, M. Allegrini, N. Bouloufa, O. Dulieu, D. Comparat, and P. Pillet, 'Optical Pumping and Vibrational Cooling of Molecules', *Science* **321: 232-234,** [DOI: 10.1126/science.1159496], (2008).

Herb03 : J. Herbig, T. Kraemer, M. Mark, T. Weber, C. Chin, H.-C.Nägerl, and R. Grimm, 'Preparation of a Pure Molecular QuantumGas', *Science* **301**, **1510**, published online 21 Aug. 2003 (doi:10.1126/science.1088876), (2003).

Lee07 :M.D. Lee, T. Köhler and P. Julienne, 'Excited Thomas-Efimov levels in ultracold gases', *Phys. Rev. A* **76**, 012720, (2007).

Vit08 : M. Viteau, A. Chotia, M. Allegrini, N. Bouloufa, O. Dulieu, D. Comparat, and P. Pillet, 'Optical Pumping and Vibrational Cooling of Molecules', *Science* **321: 232-234,** [DOI: 10.1126/science.1159496], (2008).

Deng99 : L. Deng, E. Hagley, J. Wen, M. Trippenbach, Y. Band, P. Julienne, J. Simsarian, K. Helmerson, S. Rolston and W. Phillips, 'Four-wave mixing with matter waves', *Nature* **398** (6724): 218–220, (1999).

Den00 : J. Denschlag, J. Simsarian, D. Feder, C. Clark, L. Collins, J. Cubizolles, L. Deng, E. Hagley, K. Helmerson, W. Reinhardt, S. Rolston, B. Schneider and W. Phillips, 'Generating solitons by phase engineering of a Bose-Einstein condensate', *Science* **287** (5450): 97– 101, (2000).

Grein02 : M. Greiner, O. Mandel, T. Esslinger, T. Hansch and I. Bloch, 'Quantum phase transition from a superfluid to a Mott insulator in a gas of ultracold atoms', *Nature* **415** (6867): 39–44, (2002).

Abo01 : J.R. Abo-Shaeer, C. Raman, J.M. Vogels and W. Ketterle, 'Observation of Vortex Lattices in Bose-Einstein Condensates', *Science* **292**, **476** (2001).

Gret06 : G.K. Campbell, J. Mun, M. Boyd, P. Medley, A.E. Leanhardt, L.G. Marcassa, D.E. Pritchard and W. Ketterle, 'Imaging the Mott Insulator Shells by Using Atomic Clock Shifts', *Science* **313: 649-652** (2006).

Billy08 : J. Billy, V. Josse, Z. Zuo, A. Bernard , B. Hambrecht, P. Lugan, D. Clément, L. Sanchez-Palencia, P. Bouye, A. Aspect, 'Direct observation of Anderson localization of matter- waves in a controlled disorder', *Nature* **453**, 891 – 894, (2008).

Corn02 : E. Cornell and C. Wieman: Nobel Lecture, 'Bose-Einstein condensation in a dilute gas, the first 70 years and some recent experiments', *Rev. of Mod. Phys.,* **74** (3): 875– 893, (2002).

And97 : M.R. Andrews, C.G. Townsend, H.J. Miesner, D.S. Durfee, D.M. Kurn and W. Ketterle, 'Observation of Interference Between Two Bose Condensates', *Science* **275, 589** (1997).

Kohl07 : Th. Kohler, 'Feshbach resonances in Ultracold Quantum Gases', *Notes in the Onassis lectures in BECs,* (2007).

Peth02 : C.J. Pethick and H. Smith, 'Bose-Einstein Condensation in Dilute Gases', *Cambridge University Press,* (2002).

Fried98 : D.G. Fried, T.C. Killian, L. Willmann, D. Landhuis, S.C. Moss, D. Kleppner and T.J. Greytak, 'Bose-Einstein Condensation of Atomic Hydrogen', *Phys. Rev. Lett.* **81**, 3811, (1998).

Kasp06 : J. Kasprzak, M. Richard, S. Kundermann, A. Baas, P. Jeambrun, J. Keeling, F. Marchetti, M. Szymaska, R. André, J. Staehli,V. Savona, P.B. Littlewood, B. Deveaud and L.S. Dang: 'Bose-Einstein condensation of exciton polaritons', *Nature* **443 :409**, (2006).

Metc99 :H. J. Metcalf, P. van der Straten, 'Laser Cooling and Trapping' Springer-Verlag', New York (1999).

Boir98: D. Boiron, 'Étude de refroidissement et de piégeage d’atomes de césium dans des structures lumineuses a faible taux de diffusion', Thesis LKB – Paris VI, (1998).

Nago86 : W. Nagourney, J. Sandberg and H. Dehmelt, 'Shelved optical electron amplifier: Observation of quantum jumps', *Phys. Rev. Lett.* **56**, 2797 - 2799 (1986).

Treut01 : Ph. Treutlein, K.Y. Chung and St. Chu, 'High-brightness atom source for atomic fountains' *Phys. Rev. A* **63**, 051401~R!

Kerm00 : A.J. Kerman, V. Vuletic, C. Chin and St. Chu, 'Beyond Optical Molasses: 3D Raman Sideband Cooling of Atomic cesium to High Phase-Space Density', *Phys. Rev. Lett.* **84**, 3 439, (2000).

Wing84 : W. Wing, 'On Neutral Particle Trapping in Quasielectrostatic ElectromagneticFields', *Prog. Quant. Elect.* **8**, **181** (1984).

Steck02 : D.A. Steck, 'cesium D Line Data', *http://steck.us/alkalidata* , Revision 1.5, (2002).

Fio98 : A. Fioretti, D. Comparat, A. Crubellier, O. Dulieu, F. Masnou-Seeuws, and P. Pillet, 'Formation of Cs2 cold molecules through photoassociation', *Phys. Rev. Lett.* **80**: 4402, (1998).

Herb03 : J. Herbig, T. Kraemer, M. Mark, T. Weber, C. Chin, H.-C.Nägerl, and R. Grimm, 'Preparation of a Pure Molecular QuantumGas', *Science* **301**, **1510**, published online 21 Aug. 2003 (doi:10.1126/science.1088876), (2003).

Fio99 : A. Fioretti et al, 'Long-Range Forces between Cold Atoms', *Phys. Rev. Lett.* **82**, 1839 (1999).

Vanh02 : N. Vanhaecke, W. de Souza Melo, B.L. Tolra, D. Comparat and P. Pillet, 'Accumulation of cold cesium molecules via photoassociation in a mixed atomic and molecular trap', *Phys. Rev. Lett*. **89**:063001, (2002).

Ties93 :E. Tiesinga, B.J. Verhaar, and H.T.C. Stoof, 'Threshold and resonance phenomena in ultracold ground-state collisions', *Phys. Rev. A* **47**, 4114 (1993).

Inou98 : S. Inouye, M.R. Andrews, J. Stenger, H.J. Miesner, D.M. Stamper-Kurn, W.K., 'Observation of Feshbach resonances in a Bose–Einste in condensate', *Nature* **392** (1998).

Ing07 : M. Inguscio, W. Ketterle, C. Salomon: 'Ultra-cold Fermi Gases', *Società italiana di fisica*, IOS Press, ISBN 158603846X, 9781586038465, (2007).

Herb03: J. Herbig, T. Kraemer, M. Mark, T. Weber, C. Chin, H.-C.Nägerl and R. Grimm, 'Preparation of a Pure Molecular QuantumGas', *Science* **301**, 1510, published online 21 Aug. (doi:10.1126/science.1088876), (2003).

Zwie05 : M.W. Zwierlein, J.R. Abo-Shaeer, A. Schirotzek, C.H. Schunck, W. Ketterle, 'Vortices and superfluidity in a strongly interacting Fermi gas', *Nature* **435**, 1047-1051 (2005).

Efi70 : V. Efimov, 'Energy levels arising from resonant two-body forces in a three-body system', *Physics Letters* B, Volume 33, Issue 8 , 21 December, Pages 563-564, (1970).

Niel99 : E. Nielsen and J.H. Macek, 'Low-Energy Recombination of Identical Bosons by Three- Body Collisions', PRL **83**, 1566 (1999).

Krae06 : T. Kraemer et al., *Nature* **440, 315-318** (16 March 2006)

Lee07 : M.D. Lee, T. Köhler and P. Julienne, 'Excit ed Thomas-Efimov levels in ultracold gases', *Phys. Rev.* **A** 76, 012720 (2007).

Sod98 : J. Söding, D. Guéry-Odelin, P. Desbiolles, G. Ferrari, and J. Dalibard, 'Giant Spin Relaxation of an Ultracold cesium Gas', *Phys. Rev. Lett.* **80**, 1869 (1998).

Gue98 : D. Guéry-Odelin, J. Söding, P. Desbiolles and J. Dalibard, 'Strong evaporative cooling of a trapped cesium gas', *Optics Express* **2** (1998).

Leo98 : P.J. Leo, E. Tiesinga, P. S. Julienne, D. K. Walter, S. Kadlecek and T. G. Walker, 'Elastic and Inelastic Collisions of Cold Spin-Polarized ^{133}Cs Atoms', *Phys. Rev. Lett.* **81**, 1389 (1998).

Leo00 : P.J. Leo, C.J. Williams and P.S. Julienne, 'Collision Properties of Ultracold ^{133}Cs Atoms', *Phys. Rev. Lett.* **85**, 2721 (2000).

Thom03 : A.M. Thomas, S. Hopkins, S.L. Cornish, and C.J. Foot, 'Strong evaporative cooling towards Bose-Einstein condensation of a magnetically trapped caesium gas', *J. Opt.* **B**: Quantum Semiclass. *Opt.* **5**, S107 (2003).

Wing84 : W. Wing, 'On Neutral Particle Trapping in Quasielectrostatic ElectromagneticFields', *Prog. Quant. Elect.* **8**, 181 (1984).

Corn91 : E.A. Cornell, C. Monroe, C. E. Wieman, 'Multiply loaded ac magnetic trap for neutral atoms', *Phys. Rev. Lett.* **67** .2439 (1991).

Zahz06 : N. Zahzam, T. Vogt, M. Mudrich, D. Comparat and P. Pillet, 'Atom-Molecule Collisions in an Optically Trapped Gas', *Phys. Rev. Lett.*, **96**(2) :023202 (2006).

Bouss04 : S. Boussen, N. Hoang, N. Zahzam, S. Guibal, L. Pruvost, D. Marescaux, J. Pinard, P. Pillet, *Eur. Phys. J. D* **28** 259 (2004)

.

Hung08 : C.L. Hung, X. Zhang, N. Gemelke and C. Chin, 'Fast, Runaway Evaporative Cooling to Bose-Einstein Condensation in Optical Traps', *Phys. Rev. A* **78**, 011604 (2008).

Grim00 : R. Grimm, M. Weidemüller, and Y. Ovchinnik ov, 'Optical dipole traps for neutral atoms', *Adv. At. Mol. Opt. Phys.* **42**, 95, arXiv:physics/9902072, (2000),

Web03b : T. Weber : Bose-Einstein Condensation of Optically Trapped cesium. Ph.D thesis Institut für Experimentalphysik, Innsbruck Austria

Web03b : T. Weber : Bose-Einstein Condensation of Optically Trapped cesium. Ph.D thesis Institut für Experimentalphysik, Innsbruck Austria

Kett96 : W. Ketterle / N. J. van Druten, 'Bose-Einstein condensation of a finite number of particles trapped in one or three dimensions', *Physical Review A*, **54** (1), p.656-660, doi:10.1103/ Phys. Rev. A.54.656, (1996).

Gue98 : D. Guéry-Odelin, J. Söding, P. Desbiolles and J. Dalibard, 'Strong evaporative cooling of a trapped cesium gas', *Optics Express* **2** (1998).

Web03c : T. Weber, J. Herbig, M. Mark, H. Nägerl, and R. Grimm : “Three-body recombination at large scattering lengths in an ultracold atomic gas ” *Phys. Rev. Lett.* 91, 123201 2003.

Hoa02 : N. Hoang, 'Développement d’un piège atomique lumineux et magnétique : étude duregime de collisions, perspectives pour la condensation de Bose-Eintein du césium', *Ph.D. Thesis*, Université Paris XI, (2002).

Bouss04 : S. Boussen, N. Hoang, N. Zahzam, S. Guibal, L. Pruvost, D. Marescaux, J. Pinard, P. Pillet, *Eur. Phys. J. D* **28** 259, (2004).

Dim02 : E. Dimova, O. Morizot, G. Stern, C. L. Garrido Alzar, A. Fioretti, V. Lorent, D. Comparat, H. Perrin and P. Pillet, 'Continuous transfer and laser guiding between two cold atom traps', *Eur. Phys. J. D* **42**, 299–308, (2007).

Phill82 : W. Phillips and H. Metcalf, 'Laser decelaration of an atomic beam', *Phys. Rev. Lett.*, 596 :596, (1982).

.

Prod85 : J. Prodan, A. Migdall, W. Phillips, H. Metcalf and J. Dalibard, 'Stopping atoms with laser light', *Phys. Rev. Lett.* **54** :992, (1985).

Roos02 : C. F. Roos, P. Cren, T. Lahaye, J. Dalibard and D. Guuery-Odelin, 'Injection of a cold atomic beam into a magnetic guide', *Laser Physics,* proceedings LPHYS'02, Bratislava, (2002).

Sav97 : T.A. Savard, K.M. O’Hara and J.E. Thomas, 'Laser-noise-induced heating in far-off resonance optical traps', *Phys. Rev. A* **56** (2) :1095, August (1997).

Dal99 : J. Dalibard, 'Collisional dynamics of ultra-cold atomic gases', IOS Press, (1999).

Tow95 : C.G. Towsend et al., 'Phase-space density in the magneto-optical trap', *Phys. Rev. A*, **52**(2) :1423, (Aug. 1995).

Lap07 : Yannis Laplace : réalisation d'un système d'imagerie non destructive d'un nuage d'atomes froids. Stage expérimental et de traitement de données. Université Pierre et Marie Curie & laboratoire Aimé Cotton (2007)

Turn04 : L. Turner "Holographic imaging of cold atoms", Ph.D thesis, University of Melbourne, 2004

.

Turn05 : L.D. Turner, K.F.E.M. Domen & R.E. Scholten, 'Diffraction-contrast imaging of cold atoms', *Phys. Rev.* A, (15 Septembre 2005).

Pfau07 : Cooling Chromium: a dipolar quantum gas', *Notes in the Onassis lectures in BECs,* (2007).

Beau08 : Q. Beaufilset al., *Phys.Rev.* A **77,** 061601(R), (2008).

Szcze09 : I. Szczepkowicz et all: 'Optimal geometry for efficient loading of an optical dipole trap' Phys. Rev. A **79**, 013408 (2009).

Kett93 : W. Ketterle, K. B. Davis, M. A. Joffe, A. Martin and D. E. Pritchard, 'High densities of cold atoms in a dark spontaneous-force optical trap', *Phys. Rev. Lett.*, 70:2253–2256, (April 1993).

And95 : M.H. Anderson, J.R. Ensher, M.R. Matthews, C.E. Wieman, and E.A. Cornell, *Science* **269**, **198** (1995).

Dav95 : K.B. Davis, M.O. Mewes, M.R. Andrews, N.J. van Druten, D.S. Durfee, D.M. Kurn and W. Ketterle, *Phys. Rev. Lett.* **75**, 3969 (1995).

Kim01 : J.Y. Kim and D. Cho, 'Dark-Spot Magneto-Optical Trap of cesium Atoms Journal', *Korean Physical Society*, Vol. **39**, No. **5**, pp. 864868, (November 2001).

Dumk06 : R. Dumke, M. Johanning, E. Gomez, J.D. Weinstein, K.M. Jones and P.D. Lett, 'All-optical generation and photoassociative probing of sodium Bose-Einstein condensates', *New J. Phys.* **8**, 64 doi:10.1088/1367-2630/8/5/06, (2006).

Clem09 : J.F. Clement, J.P. Brantut, M. Robert de Saint Vincent, R.A. Nyman, A. Aspect, T. Bourdel and P. Bouyer, 'All-optical runaway evaporation to Bose-Einstein condensation', arXiv:0903.2745v1, (2006).

Kupp00 : S.J.M. Kuppens, K.L. Corwin, K.W. Miller, T.E. Chupp, and C.E. Wieman, 'Loading an optical dipole trap', *Phys. Rev.* A, **62**, 013406, (2006).

Boir96 : D. Boiron, A. Michaud, P.Lemonde, Y.Castin and C. Salomon, 'Laser cooling of cesium atoms in gray optical molasses down to 1.1 μK', *Phys. Rev. A* **53**, R3734 – R3737, (1996).

Treut01 : Ph. Treutlein, K.Y. Chung and St. Chu, 'High-brightness atom source for atomic fountains' *Phys. Rev. A* **63**, 051401~R!

Kais91 : R. Kaiser, N. Vansteenkiste, A. Aspect, E. Arimondo and C. Cohen-Tannoudji, 'Mechanical Hanle effect', Zeitschrift für Physik D Atoms, Molecules and Clusters, Vol. **18**, Issue **1**, pp.17-24

Stern08 : G.Stern, 'Stratégies pour le chargement d'un piège dipolaire des atomes de froids césium et le refroidissement évaporatif', Thesis LAC – Paris XI (1998).

deCar04 : R. de Carvalho and J. Doyle, 'Evaporative cooling at low trap depth' *Phys. Rev. A* **70**, 053409 (2004).

Vit08 : M. Viteau, A. Chotia, M. Allegrini, N. Bouloufa, O. Dulieu, D. Comparat and P. Pillet, 'Optical Pumping and Vibrational Cooling of Molecules', *Science*, 321:232–234, (July 2008).

Vit08c : M. Viteau, 'Pompage optique et refroidissement laser de la vibration de molécules froides', Thesis LAC – Paris XI, (2008).

Vit08c : M. Viteau, 'Pompage optique et refroidissement laser de la vibration de molécules froides', Thesis LAC – Paris XI, (2008).

Huts06 : J.M. Hutson, 'Molecule formation in ultracold atomic gases', *Intern. Rev. in Phys. Chem.*, **Vol. 25**, Issue 4, (Oct-Dec 2006).

Doy04 Editorial: J. Doyle, B. Friedrich, R.V. Krems and F. Masnou-Seeuws, 'Quo vadis, cold molecules?' *Eur. Phys. J. D* **31**, 149–164, (2004).

Krem05 : R.V. Krems, 'Molecules near absolute zero and external field control of atomic and molecular dynamics', Intern. Rev. in Phys. Chem., **Vol. 24**, No. 1, Jan.–Mar. 2005, 99–118.

Jon06 : Kevin M. Jones Eite Tiesinga, Paul D. Lett, and Paul S. Julienne, 'Ultracold photoassociation spectroscopy: Long-range molecules and atomic scattering', Rev. of Mod. Phys., **vol. 78**, (april-june 2006).

Dul06 : O. Dulieu, M. Raoult and E. Tiemann, 'Cold Molecules: a chemistry kitchen for physicists?', J. Phys. B: At. Mol. Opt. Phys. **39** (2006).

Bart93 : A. Bartana, R. Kosloff, and D. J. Tannor, J. *Chem. Phys.***99**, 196 (1993).

Tann99 : D. J. Tannor, R. Kosloff, and A. Bartana, Faraday Discuss **113**, 365 (1999).

Bart01 : : A. Bartana, R. Kosloff, and D. J. Tannor, *Chem. Phys.* **267**, 195 (2001).

Schi00 :S. G. Schirmer, *Phys. Rev.* A **63**, 013407 (2000).

Voge02 : I. S. Vogelius, L. B. Madsen, and M. Drewsen, *Phys. Rev. Lett.* **89**, 173003 (2002), arXiv:quant-ph/0206132.

Dem98 : Wolfgang Demtröder, Molecular Physics – Theoretical Principles and Experimental Methods, WILEY-VCH, Verlag GmbH & Co. KgaA

Comp99 :D. Comparat, 'Formation de molécules froides par photoassociation d'atomes de césium froids. Mise en évidence de forces à longue portée entre atomes froids excités de césium', Ph.D thesis, Université d'Orsay Paris XI, (1999).

McCleO6 : J.J. McClelland and J.L. Hanssen, 'Laser Cooling Without Repumping: A Magneto-Optical Trap for Erbium Atoms', *Phys. Rev. Lett.* **96**(14), 143005 (2006).

McCleO6 : J.J. McClelland and J.L. Hanssen, 'Laser Cooling Without Repumping: A Magneto-Optical Trap for Erbium Atoms', *Phys. Rev. Lett.* **96**(14), 143005 (2006).

Niko00 : A.N. Nikolov, J.R. Ensher, E.E. Eyler, H. Wang, W.C. Stwalley and P. L Gould., 'Efficient Production of Ground-State Potassium Molecules at Sub-mK Temperatures by Two-Step Photoassociation', *Phys. Rev. Lett.*, **84** :246249, (2000).

Sage05 : J.M. Sage, S. Sainis, T. Bergeman, and D. Demille, 'Optical Production of Ultracold Polar Molecules', *Phys. Rev. Lett.*, **94**(20) :20300, (2005).

Danzl08 : J.G. Danzl, E. Haller, M. Gustavsson, M.J. Mark, R. Hart, N. Bouloufa, O. Dulieu, H. Ritsch and H.C. Naegerl, 'Quantum Gas of Deeply Bound Ground State Molecules', ArXiv e-prints, 806, (2008).

Bert99 : H. L. Bethlem, G. Berden and G. Meijer, 'Decelerating neutral dipolar molecules', *Phys. Rev. Lett.*, **83** :1558, (1999).

Wein98 : J.D. Weinstein, R. de Carvalho, T.G.B. Friedrich, and J.M. Doyle, 'Magnetic trapping of calcium monohydride molecules at millikelvin temperatures', *Nature*, 395 :148, (1998).

Bert99 : H. L. Bethlem, G. Berden and G. Meijer, 'Decelerating neutral dipolar molecules', *Phys. Rev. Lett.*, **83** :1558, (1999).

Pro03 : S. Procter, Y. Yamakita, F. Merkt and T. Softley, 'Controlling the motion of hydrogen molecules', *Chem. Phys. Lett.*, **374** :667675, (2003).

Vanh07 : N. Vanhaecke, U. Meier, M. Andrist, B. H. Meier and F. Merkt, 'Multistage Zeeman deceleration of hydrogen atoms', *Phys. Rev. A*, **75**(3) :031402+, (2007).

Nar08 : E. Narevicius, A. Libson, C. G. Parthey, I. Chavez, J. Narevicius, U. Even, and M. G. Raizen, 'Stopping supersonic oxygen with a series of pulsed electromagnetic coils : A molecular coilgun', *Phys. Rev. A*, **77**(5) :051401(2008).

Rang03 : S.A. Rangwala, T. Junglen, T. Rieger, P.W. Pinkse and G. Rempe, 'Continuous source of translationally cold dipolar molecules', *Phys. Rev. A*, **67**(4) :043406 (2003).

Gup99 : M. Gupta and D. Herschbach, 'A mechanical means to produce intense beams of slow molecules', *J. Phys. Chem. A*, **103** :10670, (1999).

Eli03 : M.S. Elio, J. J. Valentini and D.W. Chandler, 'Subkelvin Cooling NO Molecules via Billiard-like Collisions with Argon', *Science*, **302** :19401943, (2003).

Tann99 **:** D.J. Tannor, R. Koslo and A. Bartana, 'Laser cooling of internal degrees of freedom of molecules by dynamically trapped states', *Faraday Discuss* **113**, 365È383, (1999).

Pe'Er07 : A. Pe'Er, E.A. Shapiro, M.C. Stowe, M. Shapiro and J. Ye, 'Precise Control of Molecular Dynamics with a Femtosecond Frequency Comb', *Phys. Rev. Lett.*, **98**(11) :113004, (2007).

Saph07 : E.A. Shapiro, V. Milner, C. Menzel-Jones and M. Shapiro, 'Piecewise Adiabatic Passage with a Series of Femtosecond Pulses', *Phys. Rev. Lett.*, **99**(3) :033002+, (2007).

Ooi03 : H. Raymond Ooi, K.-P. Marzlin and J. Audretsch, 'Laser cooling of molecules via single spontaneous emission', *Eur. Phys. J. D* **22,** 259–267, DOI: 10.1140/epjd/e2002-00227-7, (2003).

Mor07 : G. Morigi, P.W. H. Pinkse, M. Kowalewski and R. de Vivie-Riedle, *Phys. Rev. Lett.* **99**, 073001 (2007).

Vul00 : V.Vuletic and S. Chu, 'Laser Cooling of Atoms, Ions, or Molecules by Coherent Scattering', *Phys. Rev. Lett.* **84**, 3787 – 3790, (2000).

Tann99 : D. J. Tannor, R. Kosloff. and A. Bartana. “Laser cooling of internal degrees of freedom of molecules by dynamically trapped states” *Faraday Discuss.*, 1999, **113**, 365È383

Bart00 : A. Bartana, R. Kosloff and D; J. Tannor : “Laser Cooling of molecules by dynamically trapped states” *Chem. Phys.* **262** 195-207 (2000)

Berg98 : K. Bergmann, H. Theuer and B. W. Shore, *Rev. Mod. Phys.*, 1998, **70**, 1003.

Kett07 : W. Ketterle, 'Condensation and Superfluidity in Bosonic and fermionic Gases', *Notes in the Onassis lectures in BECs,* (2007).

Sal07 :C. Salomon, 'Tuninginteractions in ultracoldBose and Fermi gases', *Notes in the Onassis lectures in BECs,* (2007).

Web03 : T. Weber, J. Herbig, M. Mark, H.-C. Nägerl and R. Grimm, 'Bose-Einstein Condensation of cesium', *Science* **299**, **232**, (2003).

Herb03 : J. Herbig, T. Kraemer, M. Mark, T. Weber, C. Chin, H.-C.Nägerl, and R. Grimm, 'Preparation of a Pure Molecular QuantumGas', *Science* **301**, **1510**, published online 21 Aug. 2003 (doi:10.1126/science.1088876), (2003).

Comp99 : D. Comparat, 'Formation de molécules froides par photoassociation d'atomes de césium froids. Mise en évidence de forces à longue portée entre atomes froids excités de césium', Ph.D thesis, Université d'Orsay Paris XI, (1999).

Drag 00 : : C. Drag, 'Photoassociation d'atomes de césium froids. Formation et caractérisation d'un nuage froid de molécules diatomiques de césium.', Ph.D thesis, Université Paris XI, (2000).

Tho87 : H.R. Thorsheim, J. Weiner and P.S. Julienne, 'Laser induced photoassociation of ultracold sodium atoms', *Phys. Rev. Lett.*, **58** :2420, (1987).

Lett93 : P.D. Lett, K. Helmerson, W.D. Philips, L.P. Ratli, S.L. Rolston and M.E. Wagshul, 'Spectroscopy of Na2 by photoassociation of laser-cooledNa'. *Phys. Rev. Lett.*, 71 :2200, (1993).

Mill93 : J.D. Miller, R.A. Cline and D.J. Heinzen, 'Photoassociation spectrum of ultracold Rb atoms', *Phys. Rev. Lett.*, **71** :2204, (1993).

McAl95 : W. I. McAlexander, E.R.I. Abraham, N.W.M. Ritchie, C.J. Williams, H.T.C. Stoof and R.G. Hulet, 'Precise atomic radiative lifetime via photoassociative spectroscopy of ultracold lithium', *Phys. Rev. A*, **51** :871, (1995).

Wang96 : H. Wang, P.L. Gould and W. Stwalley, 'Photoassociative spectroscopy of ultracold 39 K atoms in a highdensity vapor-cell magneto-optical trap', *Phys. Rev. A*, **53** :R1216, (1996).

Fio98 : A. Fioretti, D. Comparat, A. Crubellier, O. Dulieu, F. Masnou-Seeuws, and P. Pillet, 'Formation of Cs2 cold molecules through photoassociation', *Phys. Rev. Lett.* **80**: 4402, (1998).

Vanh02 : N. Vanhaecke, W. de Souza Melo, B.L. Tolra, D. Comparat and P. Pillet, 'Accumulation of cold cesium molecules via photoassociation in a mixed atomic and molecular trap', *Phys. Rev. Lett*. **89**:063001, (2002).

Zahz06 : N. Zahzam, T. Vogt, M. Mudrich, D. Comparat and P. Pillet, 'Atom-Molecule Collisions in an Optically Trapped Gas', *Phys. Rev. Lett.*, **96**(2) :023202 (2006).

Vit08 : M. Viteau, A. Chotia, M. Allegrini, N. Bouloufa, O. Dulieu, D. Comparat and P. Pillet, 'Optical Pumping and Vibrational Cooling of Molecules', *Science*, **321**:232–234, (July 2008).

Dion01 : C.M. Dion, C. Drag, O. Dulieu, B. Laburthe Tolra, F. Masnou-Seeuws and P. Pillet, 'Resonant Coupling in the Formation of Ultracold Ground State Molecules via Photoassociation', *Phys. Rev. Lett.*, **86** :22532256, (2001).

Nik00 : A.N. Nikolov, J.R. Ensher, E.E. Eyler, H. Wang, W.C. Stwalley and P. L Gould., 'Efficient Production of Ground-State Potassium Molecules at Sub-mK Temperatures by Two-Step Photoassociation', *Phys. Rev. Lett.*, **84** :246249, (2000).

Sag05 : J.M. Sage, S. Sainis, T. Bergeman, and D. Demille, 'Optical Production of Ultracold Polar Molecules', *Phys. Rev. Lett.*, **94**(20) :20300, (2005).

Del08 : J. Deiglmayr, A. Grochola, M. Repp, K. Mörtlbauer, C. Glück, J. Lange, O. Dulieu, R. Wester and M. Weidemüller, 'Formation of ultracold polar molecules in the rovibrational ground state', ArXiv e-prints, 807, (2008).

Haim04 : C. Haimberger, J. Kleinert, M. Bhattacharya and N.P. Bigelow, 'Formation and detection of ultracold ground-state polar molecules', *Phys. Rev. A* **70** 021402(R), (2004).

Haim06 : C. Haimberger, J. Kleinert, O. Dulieu and N.P. Bigelow, 'Processes in the formation of ultracold NaCs', *J. Phys. B*: At. Mol. Opt. Phys. **39** S957–S963, (2006).

Klei07 : J. Kleinert, C. Haimberger, P.J. Zabawa and N.P. Bigelow, 'Trapping of Ultracold Polar Molecules with a Thin-Wire Electrostatic Trap', *Phys. Rev. Lett.* **99,** 143002, (2007).

Klei07b : J. Kleinert, C. Haimberger, P.J. Zabawa and N.P. Bigelow, 'Manufacturing a thin wire electrostatic trap for ultracold polar molecules', Rev. of Scient. Instr. **78**, 113108, (2007).

Danz08 : J.G. Danzl, E. Haller, M. Gustavsson, M.J. Mark, R. Hart, N. Bouloufa, O. Dulieu, H. Ritsch and H.C. Naegerl, 'Quantum Gas of Deeply Bound Ground State Molecules', ArXiv e-prints, 806, (2008).

Vit09b : M. Viteau, A. Chotia, M. Allegrini, N. Bouloufa, O. Dulieu, D. Comparat, and P. Pillet, *Phys. Rev. A* **79**, 021402 (2009), 0809.4991.

Diem89 : U. Diemer, R. Duchowicz, M. Ertel, E. Mehdizadeh and W. Demtr€oder, *Chem. Phys. Lett.*, , **164**, 419–426, (1989).

Wei85 : W. Weickenmeier, U. Diemer, M. Wahl, M. Raab, W. Demtreoder and W.Meuller, *J. Chem. Phys.* **82**, 5354–5363, (1985).

Mon05 : Monmayrant, A. (2005). Façonnage et caractérisation d'impulsions ultracourtes. Contrôle cohérent des systèmes simples. PhD thesis, Université Paul Sabatier, Toulouse III.

Dan89 : M.B. Danailov and I.P. Christov, 'Time-space Shaping of Light Pulses by Fourier Optical Processing', *Journal of Modern Optics,* **36** :725 731, (1989).

Raa82 : M. Raab, G. Höning, W. Demtröder and C.R. Vidal, 'High resolution laser spectroscopy of Cs2. II. Doppler-free polarization spectroscopy of the $X^1\Sigma_g^+$ C1Πu system', *J. Chem. Phys.,* **76** :43704386, (1982).

Vata99 :M. Vatasescu, 'Étude théorique de la réaction de photoassociation entre deux atomes de césium froids : Mise en évidence d'un eet tunnel et traitement dépendant du temps', Ph.D thesis, Université Paris XI, (1999).

Sof09 : D. Sofikitis, S. Weber, A. Fioretti, R. Horchani, M. Allegrini, B. Chatel, D. Comparat and P. Pillet 'Molecular vibrational cooling by optical pumping with shaped femtosecond pulses', *New J. Phys.* **11** No **5,** 055037 (17pp), (May 2009).

Mon04 : A. Monmayrant and B. Chatel. 'A new phase and amplitude high resolution pulse shaper', *Rev. Sci. Instr.*, **75**:2668, (2004).

Sto01 : G. Stobrawa, M. Hacker, T. Feurer, D. Zeidler, M. Motzkus and F. Reichel, 'A new high-resolution femtosecond pulse shaper', *Appl. Phys. B*, **72**(5):627, (2001).

Bah96 : J.T. Bahns, W.C. Stwalley, and P.L. Gould, 'Laser cooling of molecules: A sequential scheme for rotation, translation, and vibration', *J. Chem. Phys.* , **104**:9689–9697, (June 1996).

DiRo04 : M.D. di Rosa, 'Laser-cooling molecules', *European Physical Journal D*, **31**:395–402, (2004).

Sof09b *:* D. Sofikitis, R. Horchani, X. Li, M. Pichler, A. Fioretti, M. Alegrini, D. Comparat and P. Pillet, 'Simple, non-coherent, selective population transfer in cold cesium dimers', *(Submitted)*

Stand99 : J. M. Standard and B. K. Clark “The Franck–Condon Principle and Condon Parabolas in a Physical Chemistry or Quantum Physics Course” *Journal of Chemical Education* **76** 10 (1999)

Aym07 : M. Aymar and O. Dulieu: 'Calculations of transition and permanent dipole moments of heteronuclear alkali dimers NaK, NaRb and NaCs' . *Molecular Physics*, Vol. **105**, Nos. 11–12, 10 June–20 June 2007, 1733–1742

Stand99 : J. M. Standard and B. K. Clark “The Franck–Condon Principle and Condon Parabolas in a Physical Chemistry or Quantum Physics Course” *Journal of Chemical Education* **76** 10 (1999)

Diem91: U. Diemer, J. Gress and W. Demtroder “The 2 $^3\Pi_g \leftarrow$ x $^3\Sigma_u$ triplet system of Cs_2” *Chem. Phys. Lett.* **178** 2,3 (1991)

Kim93 : B. Kim and K. Yoshihara “Triplet-triplet transition of Cs_2 studied by multiphoton ionization spectroscopy in very cold pulsed molecular beam” *Chem. Phys Lett.* **204** 5,6 (1993)

Dion02: C.M. Dion, O. Dulieu, D. Comparat, W. de Souza Melo, N. Vanhaecke, P. Pillet, R. Beuc, S. Milosevic, and G. Pichler “Photoionization and detection of ultracold Cs2 molecules through diffuse bands” Eur. Phys. J. D 18, 365{370 (2002) DOI: 10.1140/epjd/e20020042

Doce04 : O. Docenko, M. Tamanis, R. Ferber, A. Pashov, H. Kn¨ockel, and E. Tiemann Spectroscopic studies of NaCs for the ground state asymptote of Na + Cs pairs Eur. Phys. J. D **31**, 205–211 (2004)

Zaha09 : J. Zaharova, M. Tamanis, R. Ferber, A. N. Drozdova, E. A. Pazyuk, and A. V. Stolyarov “Solution of the fully-mixed-state problem: Direct deperturbation analysis of the *A* 1+–*b* 3 complex in a NaCs dimer” *Phys. Rev. A.* **79**, 012508 (2009)

Murr92 : J. S. Murray, J. M. Seminario, M. C. Concha and P. Politzer “An analysis of molecular electrostatic potentials obtained by a local density functional approach“ *International journal of quantum chemistry* **44**, 2.113-122 (1992)

Vit09 : Matthieu Viteau, Amodsen Chotia, Dimitris Sofikitis, Maria Allegrini, Nadia Bouloufa, Olivier Dulieu, Daniel Comparat and Pierre Pillet, Broadband lasers to detect and cool the vibration of cold molecules *Faraday Discuss.*, 2009 DOI: 10.1039/b819697d

Vit09 : Matthieu Viteau, Amodsen Chotia, Dimitris Sofikitis, Maria Allegrini, Nadia Bouloufa, Olivier Dulieu, Daniel Comparat and Pierre Pillet, Broadband lasers to detect and cool the vibration of cold molecules *Faraday Discuss.*, 2009 DOI: 10.1039/b819697d

Vit09 : Matthieu Viteau, Amodsen Chotia, Dimitris Sofikitis, Maria Allegrini, Nadia Bouloufa, Olivier

Dulieu, Daniel Comparat and Pierre Pillet, Broadband lasers to detect and cool the vibration of cold molecules *Faraday Discuss.*, 2009 DOI: 10.1039/b819697d

Fio09 : A. Fioretti, A. Sofikitis, X. Horchani, R.and Li, M. Pichler, S. Weber, M. Allegrini, B. Chatel, D.Comparat, and P. Pillet, *Journal of Modern Optics* (2009), Submitted.

Bal09 : N. Balufa, M. Pichler and O. Dulieu (work in preparation)
Grimm00: R. Grimm, M. Weidemüller and Y. Ovchinnikov, 'Optical dipole traps for neutral atoms', *Adv. At. Mol. Opt. Phys.* **42**, **95**, arXiv:physics/9902072, (2000).

D'Inc04 : J.P. D'Incao, H. Suno, and B.D. Esry, 'Limits on universality in ultracold three-boson recombination', *Phys. Rev. Lett.*, **93**(12) :123201, (September 2004).

O'Ha01: K.M. O'Hara, M.E. Gehm, S.R. Granade and J.E. Thomas, 'Scaling laws for evaporative cooling in time-dependent optical traps', *Phys. Rev. A* **64** 051403(R)

Cho08 : A. Chotia, M. Viteau, T. Vogt, D. Comparat and P. Pillet. 'Kinetic Monte Carlo modeling of dipole blockade in Rydberg excitation experiment', *New Journal of Physics*, **10**(4):045031 (April 2008).

Kokoo99b : V. Kokoouline, O. Dulieu, R. Kosloff and F. Masnou-Seews. "Mapped Fourier methods for long range molecules: Application to perturbations in the Rb2 (0u0) photoassociation spectrum'. *J. Chem. Phys.* **110**, 20, 9865 (1999)

Kokoo99 : V. Kokoouline, 'Theoretical approach to cold molecules: developpment of numerical methods' Ph.D Thesis. Univertité Paris XI.